EFFICIENT FILTER DESIGN AND IMPLEMENTATION APPROACHES FOR MULTI-CHANNEL CONSTRAINED ACTIVE SOUND CONTROL

by

Yongjie Zhuang

A Dissertation

Submitted to the Faculty of Purdue University

In Partial Fulfillment of the Requirements for the degree of

Doctor of Philosophy



School of Mechanical Engineering

West Lafayette, Indiana

August 2023

THE PURDUE UNIVERSITY GRADUATE SCHOOL
STATEMENT OF COMMITTEE APPROVAL

Dr. Yangfan Liu, Chair

School of Mechanical Engineering

Dr. J. Stuart Bolton

School of Mechanical Engineering

Dr. Jianghai Hu

School of Electrical and Computer Engineering

Dr. George T. Chiu

School of Mechanical Engineering

Approved by:

Dr. Nicole Key

ACKNOWLEDGMENTS

During my PhD journey, I have been fortunate to receive support, guidance, and inspiration from numerous individuals who have played an important role in my academic development. I am profoundly grateful for their unwavering dedication and commitment.

First and foremost, I express my deepest gratitude to my advisor, Dr. Yangfan Liu, whose invaluable advice and guidance have shaped my graduate life. He fostered my interest in math-intensive research, always encouraging and respecting my research ideas. Engaging in research discussions with him has been an immensely enjoyable and enlightening experience. Dr. Liu provided me with numerous opportunities for career development and has been a supportive and inclusive mentor. From him, I have learned invaluable skills in research, teaching, mentoring, and communication.

I would also like to extend my sincere thanks to my dissertation committee members: Dr. J. Stuart Bolton, Dr. Jianghai Hu, and Dr. George T. Chiu. Their guidance and insights have significantly contributed to my research journey. Dr. Bolton's door was always open to address any questions I had. His acoustics courses not only provided me with technical knowledge but also taught me how to present technical content in an engaging and enjoyable manner. His thorough reviews of my written work, from application materials to research proposals, have been invaluable to me. Dr. Liu and Dr. Bolton also generously supported me in enhancing my teaching skills during the time I taught a noise control course in my final year. Dr. Hu's suggestions for addressing various optimization challenges encountered during my research projects are valuable. He suggested I consider alternative formulation when I met the numerical issues in my research project which eventually became a crucial section in my dissertation. Dr. Chiu's control course imparted invaluable insights into control problems. His suggestions following the multiple rejections of my initial journal publication were pivotal in improving my paper-writing skills.

My gratitude also extends to Dr. Patricia Davies for making the math-intensive signal processing course so attractive and this course formed a crucial technical background for my PhD study. Her suggestions on my presentation skills, writing, and application materials

have been invaluable. I am also grateful to Dr. Kai Ming Li for his guidance and collaboration on our outdoor sound prediction project.

I also thank Beijing Ancsonic Technology Co. Ltd for providing financial support and help with the experimental system setup and data collection, which played a vital role in the majority of my work presented in this dissertation. I would like to express special appreciation to Yinhai Xu, the co-founder, COO, and CTO of Ancsonic, for actively applying my developed methods to various prototypes and providing valuable feedback on the testing results. His involvement has greatly contributed to the improvement of my proposed method.

I want to thank my parents for their support despite the significant time I had to spend away from them while pursuing my degree. Additionally, I want to thank my friends for their companionship and help throughout my graduate life. In alphabetical order, I express my appreciation to Zhengpu Chen, Wei Ding, Jianxiong Feng, Haitian Hao, Zechao Lu, Jiacheng Ma, Zhuang Mo, Weijing Qiu, Guochenhao Song, Xuchen Wang, Yiming Wang, Pengcheng Xia, Yujian Xu, Jinming Zhang, and many others. Their presence and support have made my academic pursuit more enjoyable and meaningful.

TABLE OF CONTENTS

LIST OF TABLES 9

LIST OF FIGURES 10

LIST OF SYMBOLS 16

ABBREVIATIONS 19

ABSTRACT 20

1 INTRODUCTION 22

1.1 A Brief History of Active Noise Control 23

1.2 Classification of Active Noise Control Methods 24

1.3 Motivations and Objectives 27

1.3.1 Current challenges in constrained filter design methods 27

1.3.2 Current challenges in filter implementations 29

1.4 Dissertation Outline 32

2 REVIEW OF ACTIVE SOUND CONTROL FILTER DESIGN AND IMPLEMENTATION APPROACHES 33

2.1 Filter Design Approaches 33

2.1.1 Control system description 33

2.1.2 Wiener filter and FxLMS algorithm 35

2.1.3 Regularization parameter method and leaky FxLMS algorithm 36

2.1.4 Constrained optimization method using H_2/H_∞ formulation 38

2.2 Filter Implementation Approaches 42

2.2.1 Polyphase filter implementation structure 42

2.2.2 Stable IIR filter fitting methods 44

2.3 Convex Optimization 48

2.3.1 Convex sets, functions, and duality properties 48

2.3.2 Cone programming problem and its dual form 50

2.3.3 Warmstarting strategies 53

3 EFFICIENT MULTI-CHANNEL CONSTRAINED OPTIMAL ACTIVE SOUND CONTROL FILTER DESIGN 57

3.1 Convexification and Reformulation 57

3.1.1 Convexification of the stability constraint 58

3.1.2 Reformulation of the objective function and other constraint functions 60

3.1.3 Summary of the convexified formulation 62

3.2 Cone Programming Reformulation 63

3.2.1 Conic formulation using the conventional reformulation procedure . . 64

3.2.2 Proposed conic formulation using the duality properties 66

3.2.3 Obtaining filter coefficients from the proposed conic formulation . . . 68

3.2.4 Analysis of the proposed conic formulation 70

3.3 Constraint Modifications for the Warmstarting Strategy 71

3.4 Singular Vector Filtering Method for the Noise Amplification Constraint . . 73

3.5 Experimental Results and Discussions 78

3.5.1 Description of the experimental setup 78

3.5.2 Comparison between the regularization parameter method and the proposed conic method 80

3.5.3 Comparison between the traditional constrained optimization method and the proposed conic method 82

3.5.4 Other characteristics of the proposed conic method 86

3.5.5 Comparison between the conventional conic formulation and the proposed conic formulation using duality 88

3.5.6 Investigation of the warmstarting strategy 92

3.5.7 Investigation of the singular vector filtering method 98

3.6 Summary 103

4 ACTIVE SOUND CONTROL APPLICATIONS USING THE PROPOSED CONIC FORMULATION 107

4.1 Adaptive Constrained Active Noise Control Filter Design Method 107

4.1.1 Control system description . . . 107
4.1.2 Experimental results and discussions . . . 108
4.2 A Constrained Room Equalization Filter Design Method . . . 114
4.2.1 Control system description . . . 115
4.2.2 The efficient room equalization filter design formulation . . . 117
4.2.3 A reduced order technique . . . 120
4.2.4 Simulation results and discussions . . . 121
4.2.5 Experimental results and discussions . . . 127
4.3 A Constrained Optimal Hear-Through Filter Design Approach for Earphones 133
4.3.1 Control system description . . . 134
4.3.2 Experimental results and discussions . . . 135
4.4 Summary . . . 140

5 EFFICIENT ACTIVE SOUND CONTROL FILTER IMPLEMENTATION APPROACHES . . . 142
5.1 Delayless Polyphase Method for Efficient Filter Implementation at High Sampling Rate . . . 142
5.1.1 Delayless polyphase implementation structure . . . 143
5.1.2 Causal filter decomposition method . . . 147
5.1.3 Experimental results and discussions . . . 149
5.2 A Stable IIR Filter Fitting Method for High-Order Active Sound Control . . 155
5.2.1 Improvements in weighted least-square approximation method . . . 156
5.2.2 Experimental results and discussions . . . 157
5.3 Summary . . . 164

6 SUMMARY . . . 166

REFERENCES . . . 168

A DETAILED DERIVATION IN CONVEX AND CONE PROGRAMMING REFORMULATION . . . 182

A.1 Reformulation of the Objective Function to a Standard Convex Quadratic Function 182
A.2 Second Order Cone Reformulation 183
A.3 Positive Semidefinite Cone Reformulation 187
A.4 Analytical Expressions for Matrix Inversions in the Proposed Conic Formulation 190

VITA 193

PUBLICATIONS 194

LIST OF TABLES

3.1 Comparison of problem dimensions using different conic formulations. 71

3.2 Comparison of the computational time using the traditional constrained optimization methods and the proposed conic method. 83

3.3 Computational time of different numbers of frequency points used in the objective function by using the proposed conic method when FIR filter length is 128. . . . 87

3.4 Required iterations of different filter lengths of the "$4N_r2N_s4N_e$" system when using proposed method. 88

4.1 Comparison of the number of design parameters using the traditional least-squares optimization method and the proposed method in small room case. . . . 124

4.2 Comparison of the number of design parameters using the traditional least-squares optimization method and the proposed method in large room case. . . . 124

4.3 Comparison of the number of design parameters using the traditional least-squares optimization method and the proposed method in the experimental setup. 129

5.1 A comparison of real-time multiplications per second for different traditional methods and the proposed method. 146

5.2 A comparison of real-time multiplications per second for different traditional methods and the proposed method in the experimental setup. 154

LIST OF FIGURES

1.1 An illustration of active sound control systems. 22

1.2 Classification of active noise control systems based on the control region size and channel counts. 24

1.3 Classification of active noise control systems based on the targeted bandwidth and attainable time-advanced information. 25

2.1 Block diagram of the multi-channel feedforward controllers (a) with the acoustic feedback path and internal model control structure, (b) in a standard feedforward form when assuming internal model control structure perfectly cancels the acoustic feedback path effect. 34

2.2 Block diagram of the commonly used implementation of ANC (non-adaptive) digital controllers. 42

2.3 Block diagrams of (a) a typical multi-rate system, (b) a multi-rate system after applying polyphase filter structures. 43

2.4 An illustration of the challenges of applying a direct warmstarting strategy to cone programming problems using the primal-dual interior-point methods. . . . 53

2.5 An illustration of the reviewed warmstarting strategy. 55

3.1 A flow chart showing the procedure of implementing the conventional CP method (conic formulation using standard procedure) and the proposed CP method. . . 70

3.2 An intuitive illustration of the modification from original frequency responses of singular vectors to the modified frequency responses that are to be fitted. 77

3.3 The picture of the experimental setup and individual components. 79

3.4 The dimensions in the experiment setup (unit: mm). 79

3.5 The comparison of the regularization parameters method and the proposed conic method using an FIR order of 128 in each control filter channel in a $4N_r2N_s4N_e$ system for (a) noise control performance and (b) stability behavior at 3000 Hz sampling rate, (c) noise control performance and (d) stability behavior at 8000 Hz sampling rate. 81

3.6 The comparison of the traditional constrained optimization method and the proposed conic method of $4N_r2N_s4N_e$ case in 8000 Hz sampling rate for (a) noise control performance and (b) stability behavior of FIR length of 8 in each channel, (c) noise control performance and (d) stability behavior of FIR length of 16 in each channel. 85

3.7 Comparison of ANC performance in the "$4N_r2N_s4N_e$" system with different choices of filter lengths N_t designed by the proposed conic method. 86

3.8 The duality gap before numerical issues occur when using (a) 56 frequencies (60 Hz frequency interval), (b) 83 frequencies (40 Hz frequency interval), and (c) 111 frequencies (30 Hz frequency interval) for stability and robustness constraints. . 90

3.9 The comparison of ANC performance using 96-point FIR filters when 111 frequencies (30 Hz frequency interval) are used for the stability and robustness constraints. 91

3.10 The computational time when using (a) 56 frequencies (60 Hz frequency interval), (b) 83 frequencies (40 Hz frequency interval), and (c) 111 frequencies (30 Hz frequency interval) for stability and robustness constraints. 92

3.11 The comparison of noise control performance between the originally used PSDCs robust stability constraints, relaxed SOC robust stability constraints using the maximum norm, and relaxed SOC robust stability constraints using the Frobenius norm. 93

3.12 The comparison of the value of stability constraint function values when using the originally used PSDCs robust stability constraints, relaxed SOC robust stability constraints using the maximum norm, and relaxed SOC robust stability constraints using the Frobenius norm. The ϵ_s is set to be 0.01 and thus the value should be less than 0.99 to be considered stable. 94

3.13 The comparison of the warmstart performance when perturbing $\mathbf{S}_{xx}$ using (a) SOCs only formulation, (b) mixed SOCs and PSDCs formulation; perturbing $\mathbf{G}_{\mathrm{e}}$ using (c) SOCs only formulation, (d) mixed SOCs and PSDCs formulation; perturbing $\mathbf{G}_s$ using (e) SOCs only formulation, (f) mixed SOCs and PSDCs formulation. 96

3.14 The experimental setup for investigating the singular vector filtering method. . . 98

3.15 Frequency responses of singular vectors of auto-correlation matrix associated with (a) the 1st input and 1st output channel, (b) the 2nd input and 1st output channel, (c) the 1st input and 2nd output channel, and (d) the 2nd input and 2nd output channel. 99

3.16 Comparison of averaged sound pressure at the error microphones for truncated SVD method and proposed singular vector filtering method. 100

3.17 Comparison of total frequency responses of singular vectors indexed from 120 to 350 for the original response, target response, and filtered response associated with: (a) the 1st input and 1st output channel, (b) the 2nd input and 1st output channel, (c) the 1st input and 2nd output channel, and (d) the 2nd input and 2nd output channel. 101

3.18 Comparison of averaged sound pressure at the error microphones for regularization method and proposed singular vector filtering method. 102

3.19 Comparison of averaged sound pressure at the error microphones for two different singular vector filtering methods. 103

4.1 Block diagram of the proposed multi-channel adaptive constrained ANC filter design method. 107

4.2 A flowchart of the proposed multi-channel adaptive constrained ANC filter design method. 108

4.3 A picture of the experimental setup. 109

4.4 The measured frequency responses of (a) secondary paths $\mathbf{G}_e$, and (b) acoustic feedback paths $\mathbf{G}_s$. "SC1" and "SC2" represent two control speakers; "ERR1" and "ERR2" represent two error microphones; "REF1" and "REF2" represent two reference microphones. 110

4.5 The designed frequency responses of (a) full-band case: digital filter passband is from 100 Hz to 1450 Hz, and (b) half-band case: one digital filter passband is from 100 Hz to 950 Hz and another digital filter passband is from 600 Hz to 1450 Hz. 111

4.6 The comparison of ANC performance in the time domain using the traditional leaky FxLMS method and the proposed conic method. The power is normalized by the total error signal power at full-band noise sources case without using an ANC system. 112

4.7 The comparison of steady-state ANC performance in the frequency domain when both the traditional leaky FxLMS and the proposed conic method converge for (a) full-band case, and (b) half-band case. 113

4.8 Block diagram for designing constrained equalization filter (a) in a full band filter structure, (b) in a subfilters structure. 116

4.9 An illustration of dividing an equalization filter into two subfilters with different impulse response lengths and sampling frequencies. 120

4.10 An illustration of setups for simulating (a) the small room and (b) the large room. The stars represent the source and the circles represent the listening location. (Unit: meters) 122

4.11 Impulse responses and frequency responses of the room response (the path from the speaker input to the listening location). (a): impulse responses in the small room case; (b): impulse responses in the large room case; (c): frequency responses in the small room case; (d): frequency responses in the large room case. 123

4.12 The comparison of the designed equalization filter using the frequency-domain deconvolution (denoted as "FDD" in the plot) and the proposed method in time and frequency domain. (a): time domain for the small room case; (b): time domain for the large room case; (c): frequency domain for the small room case; (d): frequency domain for the large room case. 125

4.13 The comparison of the convolution result of impulse responses and the multiplication of frequency responses of the designed equalization filters and room responses using the frequency-domain deconvolution (denoted as "FDD" in the plot) and the proposed method. (a): impulse responses in the small room case; (b): impulse responses in the large room case; (c): frequency responses in the small room case; (d): frequency responses in the large room case. 126

4.14 Comparison of power spectral density (PSD) of reproduced signal and desired signal at listening location for simulated (a) small room and (b) large room cases. 127

4.15 (a) Layout of the experimental setup, (b) picture of the listening location. . . . 128

4.16 (a) Impulse responses and (b) frequency responses of the room response (the path from the speaker input to the listening location). 129

4.17 The comparison of the designed equalization filter using the frequency-domain deconvolution (denoted as "FDD" in the plot) and the proposed method in (a) time and (b) frequency domain. 130

4.18 The comparison of (a) the convolution result of impulse responses and (b) the multiplication of frequency responses of the designed equalization filters and room responses using the frequency-domain deconvolution (denoted as "FDD" in the plot) and the proposed method. 131

4.19 Comparison of simulated power spectral density (PSD) of reproduced signal and desired signal at the listening location. 131

4.20 Comparison of experimentally measured sound pressure level (SPL) of reproduced signal and desired signal at (a) listening location and location 10 cm to the (b) left of, (c) right of, and (d) behind the listening location. 132

4.21 Block diagram of a hear-through filter structure: (a) system with an acoustic feedback path and an internal model control structure, (b) an equivalent feedforward system when assuming a perfect cancellation of the acoustic feedback path effect. 135

4.22 Pictures of the earphone mounted on AWA6162 (IEC711) for experimental data collection. 136

4.23 Frequency response of (a) G_{e}, (b) $G_{\mathrm{e}}W_x$, where W_x is designed using direct inverse filter method. 137

4.24 Comparison of (a) hear-through performance in normalized PSD, and (b) impulse response for direct inverse filter design method and the proposed conic method. 138

4.25 (a) Comparison of hear-through filter performance with and without applying stability constraint. (b) The frequency response of G_s. 139

4.26 The Nyquist plot (i.e., the frequency response of open loop W_xG_s) for hear-through filter W_x designed (a) without applying stability constraint, and (b) with stability constraints. 139

5.1 Block diagrams of (a) a proposed ANC filter structure that $H(z)$ is replaced by $A(z)$ and $B(z)$ and no $W_x(z)$ is required, (b) a proposed ANC filter structure after applying polyphase filter structures. 144

5.2 Block diagram of the ANC controllers when using the proposed delayless polyphase implementation. 145

5.3 A flow chart showing the traditional filter implementation methods and the proposed ANC filter implementation method using delayless polyphase implementation. 149

5.4 A picture of the experimental setup. 150

5.5 The total electronic delay including group delay of anti-aliasing and reconstruction filter, and one-sample delay for the processing in controllers for two different sampling rate. 151

5.6 (a) Magnitude of the frequency responses of $A(z)$ and $B(z)$ for the whole frequency band to show they are well attenuated above 2 kHz, (b) comparison of magnitude and phase of the frequency responses of $W_x(z)$ and $A(z)B(z)$ for the desired noise control frequency band (below 2 kHz). 152

5.7 The comparison of noise control performance for traditionally used high sampling rate method using the original IRD and the proposed delayless polyphase implementation method at the desired noise control frequency band. 153

5.8 The comparison of noise control performance for the traditional high sampling rate method using shorter IRD, the low sampling rate method, and the proposed delayless polyphase implementation method at the desired noise control frequency band. 155

5.9 A picture of the experimental setup showing an earphone mounted on an artificial ear for experimental data collection. 159

5.10 The frequency responses of measured secondary path $\mathbf{G}_e$. The reference value for the dB scale is 1. 160

5.11 The nominal noise control performance of designed noise control filter using FIR filter structure with different filter lengths: (a) showing the full frequency band: from 0 Hz to 24 kHz; (b) showing the zoomed-in frequency band: from 100 Hz to 800 Hz. 161

5.12 The (a) impulse response and the (b) frequency response of designed optimal control filter using FIR filter structure using 7200 time-domain coefficients . . . 162

5.13 The comparison of pre-designed FIR filter frequency responses and the fitted IIR filter frequency responses using different methods and filter orders: (a) showing the full frequency band: from 0 Hz to 24 kHz; (b) showing the zoomed-in frequency band: from 100 Hz to 800 Hz. 162

5.14 The comparison of nominal noise control performance using the traditional method and the proposed method: (a) showing the full frequency band: from 0 Hz to 24 kHz; (b) showing the desired noise control frequency band: from 0 Hz to 3 kHz. 163

5.15 Zoomed-in frequency band: from 100 Hz to 800 Hz for the comparison of nominal noise control performance using the traditional method and the proposed method.. 164

LIST OF SYMBOLS

$\bullet(t)$	Represents the value of physical quantity $\bullet$ in the continuous time domain at time instance t
$\bullet(n)$	Represents the value of physical quantity $\bullet$ in the discrete time domain at index n
$\bullet(f)$	Represents the value of physical quantity $\bullet$ in the continuous frequency domain at frequency f
$\bullet(f_k)$	Represents the value of physical quantity $\bullet$ in the discrete frequency domain at frequency f_k
$A_{\mathrm{e}}(f_k)$	A constant scalar or a frequency-dependent scalar that is specified as the upper bound of the amplification ratio of error signals at frequency f_k for the noise amplification (disturbance enhancement) constraint
$\mathbf{A}_s(f_k)$	The open-loop response of ANC controller and estimated acoustic feedback path, $-\mathbf{W}_x(f_k)\hat{\mathbf{G}}_s(f_k)$
$B(f_k)$	The upper bound on the output multiplicative plant uncertainty at frequency f_k for the robustness constraint
$C_{i,j}(f_k)$	The applied upper bound on the amplitude of the designed filter frequency response of i-th output and j-th input channel at frequency f_k for the controller response magnitude constraint
$\mathbf{d}$	The primary signals at error sensor locations
$\mathbf{e}$	The error signals, i.e., the sum of primary and secondary sound fields at error sensor locations
f_i	The i-th frequency
f_c	Cut-off frequency for lowpass filter
f_s	Sampling frequency
$\mathbf{F}_z(f)$	A Fourier vector used for transforming the time-domain coefficients to the frequency-domain value at frequency f defined in Eq. (2.9)
$g_{i,j,l}$	The i-th output, j-th input channel, and l-th coefficient in that channel of the discretized impulse response of the secondary path $\mathbf{G}_{\mathrm{e}}$

$\mathbf{G}_e$	The acoustical responses matrix of secondary paths from the secondary sources to the error sensor positions
$\mathbf{G}_s$	The acoustic feedback path matrix represents the acoustic responses of secondary sources at the reference sensors
$\hat{\mathbf{G}}_s$	A model of the physical acoustic feedback path, i.e., the estimate of $\mathbf{G}_s$
$\bullet^{\mathrm{H}}$	Complex conjugate transpose operation on a matrix $\bullet$
j	Either a complex number $\sqrt{-1}$ or an index depending on the context
n	The discrete-time index
N_e	The number of error sensors
N_r	The number of reference sensors (i.e., the controller input channels)
N_s	The number of secondary actuators (i.e., the controller output channels)
N_t	The number of FIR filter coefficients in each channel, i.e., taps
N_f	The number of discretized frequency points
$\mathbf{r}$	The signals measured by the reference sensors when the active sound control system is activated including sound from both the primary sources and the secondary sources
$\mathbf{R}$	The set of real numbers
Re()	Denotes the real part of a complex number or matrix
$\mathbf{S}_{xx}(f_k)$	The cross-spectral density matrices of reference signals $\mathbf{x}$ at frequency f_k
$\mathbf{S}_{dd}(f_k)$	The cross-spectral density matrices of disturbance signals $\mathbf{d}$ at frequency f_k
$\mathbf{S}_{xd}(f_k)$	The cross-spectral density matrix between the primary noise signals $\mathbf{x}$ and the disturbance signals $\mathbf{d}$ at frequency f_k, which is defined as $\mathbf{S}_{xd} = \lim_{T\to\infty} \frac{1}{T}\mathrm{E}[\mathcal{F}(\mathbf{x})\mathcal{F}(\mathbf{d})^{\mathrm{H}}]$ where $\mathcal{F}$ denotes the Fourier transform
t	The continuous-time index
$\bullet^{\mathrm{T}}$	Transpose operation on a matrix $\bullet$
$\mathbf{w}$	A vector containing filter coefficients from all channels whose sequence is more suitable for the cost function formulated in the proposed method and is defined in Eq. (3.9)

$\mathbf{w}_{i,j}$	A vector containing the time-domain coefficients of the designed i-th output and j-th input channel of the control filter and $\mathbf{w}_{i,j}(l)$ denotes the l-th coefficient
$\mathbf{w}_{w\mathrm{i}}$	A vector containing filter coefficients from all channels whose sequence is more suitable for the cost function formulated in the time domain (such as Wiener filter design) and is defined in Eq. (2.1)
$\mathbf{W}_x$	The response matrix of the multi-channel control filters (usually in Fourier transform domain defined in Eq. (2.10))
$\mathbf{x}$	The primary signals from the primary sources measured at reference sensor locations, or a vector of variables in optimization problem depending on the context
$\hat{\mathbf{x}}$	The estimated primary signals at reference sensor locations, i.e., the estimate of $\mathbf{x}$
$\tilde{x}_{i,j,k}$	The filtered reference signal (i.e., the result of filtering reference signal by the estimated secondary path filter) associated with i-th error sensor, j-th control actuator, and k-th reference sensor. It is defined in Eq. (2.1)
$\mathbf{y}$	The output of the controller, or a vector of variables in optimization problem depending on the context
$\mathbf{Z}$	The set of integers
$\bullet^*$	Complex conjugate on every element in a matrix $\bullet$ or a scalar $\bullet$
α	The step length in the filtered-x least mean square (FxLMS) method
β	The regularization parameter in the regularization parameter method, which is also the leakage factor in the leaky FxLMS method
γ	The warm ratio used in the warmstarting method defined in Eq. (2.54)
ϵ_s	A small positive constant introduced to ensure the strict stability in Eq. (3.8)
$\lambda()$	Denotes the eigenvalues of a matrix
$\sigma()$	Denotes the singular values of a matrix

ABBREVIATIONS

ADC	analog to digital converter
ANC	active noise control
ASC	active sound control
CP	cone program
DAC	digital to analog converter
FDD	frequency domain deconvolution
FIR	finite impulse response
FPGA	field programmable gate array
FxLMS	filtered-x least mean square
HVAC	Heating, ventilation, and air conditioning
IIR	infinite impulse response
IPM	interior-point method
IMC	internal model control
IRD	impulse response duration
KKT	Karush-Kuhn-Tucker (conditions)
LMS	least mean square
LP	linear program
MRI	magnetic resonance imaging
PD-IPM	primal-dual interior-point method
PSDC	positive semidefinite cone
PSD	power spectral density
SOC	second-order cone
SPL	sound pressure level
SQP	sequential quadratic programming
SVD	singular value decomposition

ABSTRACT

In many practical multi-channel active sound control (ASC) applications, such as active noise control (ANC), various constraints need to be satisfied, such as the robust stability constraint, noise amplification constraint, controller output power constraints, etc. One way to enforce these constraints is to add a regularization term to the Wiener filter formulation, which, by tuning only a single parameter, can over-satisfy many constraints and degrade the ANC performance. Another approach for non-adaptive ANC filter design that can produce better ANC performance is to directly solve the constrained optimization problem formulated based on the H_2/H_∞ control framework. However, such a formulation does not result in a convex optimization problem and its practicality can be limited by the significant computation time required in the solving process. In this dissertation, the traditional H_2/H_∞ formulation is convexified and a global minimum is guaranteed. It is then further reformulated into a cone programming formulation and simplified by exploiting the problem structure in its dual form to obtain a more numerically efficient and stable formulation. A warmstarting strategy is also proposed to further reduce the required iterations. Results show that, compared with the traditional methods, the proposed method is more reliable and the computation time can be reduced from the order of days to seconds. When the acoustic feedback path is not strong enough to cause instability, then only constraints that prevent noise amplification outside the desired noise control band are needed. A singular vector filtering method is proposed to maintain satisfactory noise control performance in the desired noise reduction bands while mitigating noise amplification.

The proposed convex conic formulation can be used for a wide range of ASC applications. For example, the improvement in numerical efficiency and stability makes it possible to apply the proposed method to adaptive ANC filter design. Results also show that compared with the conventional constrained adaptive ANC method (leaky FxLMS), the proposed method can achieve a faster convergence rate and better steady-state noise control performance. The proposed conic method can also be used to design the room equalization filter for sound field reproduction and the hear-through filter design for earphones.

Besides efficient filter design methods, efficient filter implementation methods are also developed to reduce real-time computations in implementing designed control filters. A polyphase-structure-based filter design and implementation method is developed for ANC systems that can reduce the computation load for high sampling rate real-time filter implementation but does not introduce an additional time delay. Results show that, compared with various traditional low sampling rate implementations, the proposed method can significantly improve the noise control performance. Compared with the non-polyphase high-sampling rate method, the real-time computations that increase with the sampling rate are improved from quadratically to linearly. Another efficient filter implementation method is to use the infinite impulse response (IIR) filter structure instead of the finite impulse response (FIR) filter structure. A stable IIR filter design approach that does not need the computation and relocation of poles is improved to be applicable in the ANC applications. The result demonstrated that the proposed method can achieve better fitting accuracy and noise control performance in high-order applications.

1. INTRODUCTION

Active sound control (ASC) uses electroacoustic transducers such as loudspeakers to control a sound field [1]. Fig. 1.1 shows an illustration of ASC systems. The reference sensors such as microphones are used to collect the original sound signals. The transfer path from the sound source to the desired locations is called the primary path. Error sensors can be placed at those desired locations to monitor the sound control performance. The sound produced by the control speakers (i.e., secondary speakers) will propagate to the desired locations through the secondary path, and also back to the reference sensors through the acoustic feedback path. This closed loop formed by the controller and acoustic feedback path imposes a greater challenge to ASC problems.

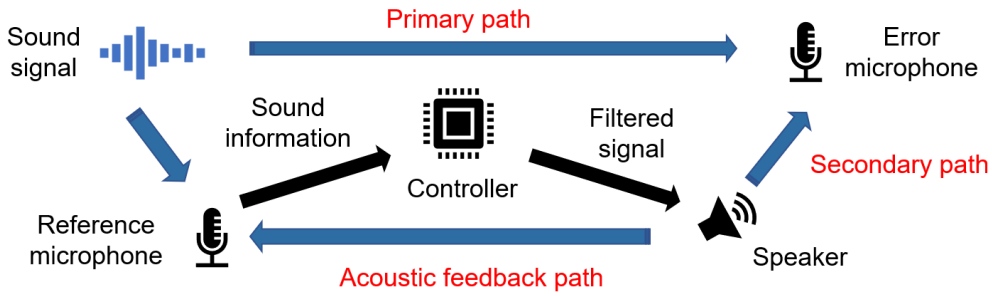


Figure 1.1. An illustration of active sound control systems.

Active noise control (ANC), which is one of the most common applications of ASC, designs control filters that drive secondary sources to produce anti-noise waves and interfere with the primary noise waves destructively. Compared with passive noise control, ANC is more effective in reducing noise at a low-frequency range [2]. Thus, it allows a lightweight and highly configurable engineering treatment in various applications. Another promising advantage of ANC is its capability to manipulate the sound field spectra conveniently instead of only reducing the total noise power. This makes it possible to use ANC technologies in various other ASC applications, e.g., improving human-perceived acoustic comfort or sound quality [3]–[6], spatial audio reproduction [7], etc. The hear-through filter is another type of ASC filter that shares a similar control diagram to the ANC filter. Instead of attenuating the primary sound wave, a hear-through filter compensates for the distorted sound caused

by barriers in the sound propagation path. Hear-through filters are used in many earphone applications, providing a more natural hearing experience of the exterior sound, which is also known as transparent mode, or ambient mode [8]–[11]. Many equalization filter design applications such as room equalization filter design can also be formulated similarly to a simplified ANC problem [12]. Thus, ANC filter design and implementation methods will be focused on in this dissertation and their applications in either hear-through filters or room equalization filters will also be investigated.

1.1 A Brief History of Active Noise Control

The ANC technology can be traced back to Leug's patent in 1936 [13]. In 1953, Olson and May's published the first academic paper [14] in the ANC field where they proposed an analog circuit design whose impedance can be adjusted to achieve noise control performance. Conover later addressed the application of ANC in reducing transformer noise, identifying employing a self-adjusting system (i.e., adaptive control) for time-varying transformer noise as a major challenge [15].

In the 1970s, ANC research primarily focused on theoretical development with a preliminary experimental setup. For example, Jessel et al. [16] obtained a general theory for active absorption and applied it to sound waves in an air duct. Mangiante proposed a general theory of ANC for three-dimensional sound wave propagation and highlighted the challenges of extending the frequency range and achieving complete automation [17]. More details of the ANC development can be referred to in Elliott and Nelson's work [18].

In recent decades, because of the development of inexpensive and robust electronic speakers, microphones, and computing devices such as the digital signal processor and field programmable gate array (FPGA), ANC technologies were successfully applied to a wide range of applications, e.g., headphones [19]–[21], headrests [22]–[27], interior noise in vehicles [1], [28], [29], aircraft cabins [30]–[32], motorcycle helmet [2], [33], magnetic resonance imaging (MRI) noise [2], [34], [35], etc. Without blocking the sound propagation path using passive materials, ANC is also preferable in applications where air ventilation is required, e.g., in air-conditioners [36] and open window applications [37]–[39]. To expand the ANC applica-

tions, efficient filter design and implementation methods are essential to further reduce time and resource expenses, which is the main topic of this dissertation.

1.2 Classification of Active Noise Control Methods

ANC technologies can be classified into various categories according to different criteria. ANC can be classified into local control and global (or spatial) control depending on the size of the control region as shown in Fig. 1.2. Local control is usually applied to applications requiring a small quiet zone around 1/10 the wavelength [40], [41] such as noise-canceling earphones targeting the eardrum region. Global control is preferable when the required quiet zone is large such as the interior noise control of vehicles [42]. To achieve global ANC performance, a multi-channel system is usually required and is more challenging compared with a single-channel system due to the coupling between channels and the increase in computational complexity.

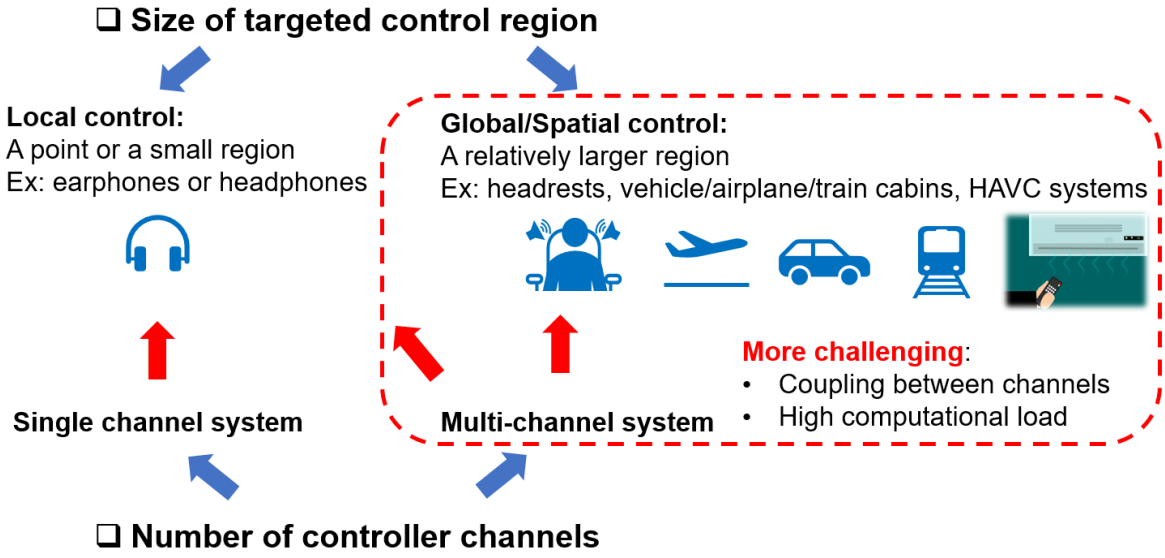


Figure 1.2. Classification of active noise control systems based on the control region size and channel counts.

ANC can target either narrowband noises or broadband noises as shown in Fig. 1.3. Pure feedback control lacks time-advanced information and is usually suitable for attenuating narrowband (tonal/periodic) noises only such as rotating machinery noises. In contrast,

feedforward control requires time-advanced information for the random noise signals and can usually achieve broadband noise reduction. Compared with narrowband ANC, broadband ANC is usually more challenging because the noise is random and more difficult to be predicted, which requires time-advanced information and makes the system performance inversely impacted by the introduced delay in the signal path when using electronic devices [43]. And, a longer filter length and more frequency points are usually required which significantly increases the computational load in the filter design and implementation stages.

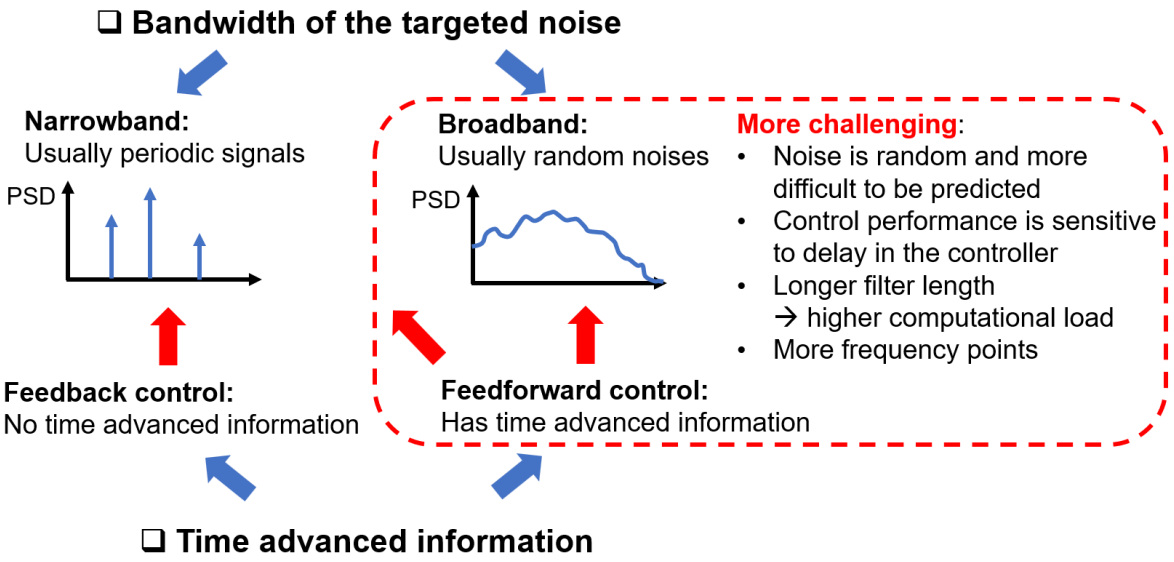


Figure 1.3. Classification of active noise control systems based on the targeted bandwidth and attainable time-advanced information.

Depending on whether the control parameters will be updated in real time, ANC can be classified into non-adaptive control and adaptive control. Non-adaptive control strategies usually design the control filter offline and then the set of fixed filter coefficients is implemented in the real-time controller. Adaptive control usually updates the filter coefficients in real time using the updated system responses. The filter coefficients can be updated in each sampling interval or after several sampling intervals. Adaptive control requires more real-time computational effort but is preferred if the control environment is time-varying. Sometimes, adaptive control performance can be achieved in time-varying environments using the non-adaptive control method. For example, different pre-trained fixed-coefficient

filters are selected in real time when the environment is changing (also known as the selective fixed-filter ANC) [44], or the filter coefficients can be re-designed continuously using the updated system responses in real time [45]. Convergence and convergence rate are two important considerations if an adaptive controller is designed.

ANC can also be classified into unconstrained ANC and constrained ANC according to whether some practical constraints on control filters are required [46]. One of the most important controller constraints is the robust stability constraint because the acoustic feedback path will form a closed loop when the active controller is used [45], [47], [48]. Another common constraint is the controller output power constraint to ensure the loudspeakers operate in their linear response ranges and to limit the system power consumption [49]–[53]. Sometimes, the noise amplification constraints (also called disturbance enhancement constraint) are required to prevent noise amplification outside the main noise control frequency band [54]–[57]. Constrained ANC is usually much more difficult to be designed compared with unconstrained ANC, especially when multiple constraints are required simultaneously [36], [58]–[60].

Different ANC categories can be combined and form greater challenges. When constraints are required in multi-channel systems, the constraint functions will change from scalar functions to matrix functions which further complicates the formulations. When constraints are required in broadband ANC, the number of frequency-dependent constraint functions (i.e., the computational load) will be increased by several orders. When adaptive controllers are used in multi-channel systems, the convergence rate will be lower due to the inter-channel coupling [61], [62]. When adaptive controllers are used for broadband noises, the convergence rate will be lower because of the wide spread of eigenvalues associated with the reference signal covariance matrix [63], [64]. In this dissertation, the multi-channel constrained ANC systems for broadband noise will be focused on targeting the above-mentioned combined challenges. Both non-adaptive and adaptive controller designs will be investigated.

1.3 Motivations and Objectives

The challenges of current multi-channel constrained ANC filter design methods targeting broadband noises and the goals of this dissertation in developing filter design methods are first discussed in this section. Then, two topics in filter implementation challenges are analyzed and the associated goals of this dissertation in developing filter implementation methods are listed.

1.3.1 Current challenges in constrained filter design methods

In many practical applications, various above-mentioned constraints, are essential. An illustrating practical example of these constraint concerns is a multi-channel ANC system to control the in-duct noise of a central air handling system with a relatively large wind channel where waves with multiple cross-sectional modes can propagate. In this practical application, considerations from industrial design and cost of deployment aspects usually require the in-duct upstream ANC reference microphones to be placed close to the secondary control loudspeakers. An unconstrained optimal Wiener filter is likely to result in an unstable system due to the strong acoustic feedback path (which is confirmed by results reported in reference [36] and Section 3.5.3). Thus, stability and robustness constraints are necessary for the ANC filter design process. In addition, a frequency-dependent constraint on the magnitude of the controller output signal is also necessary to ensure the loudspeaker response is within its linear region, and a noise amplification (disturbance enhancement) constraint is required to avoid the phenomenon that the overall noise power is attenuated but significant sound level enhancement occurs in some frequency bands.

One commonly used approach to ensure the satisfaction of those constraints simultaneously is to introduce a regularization term in the filter coefficients optimization process [46]. Instead of minimizing the power of error signals only, it minimizes a weighted sum of error signal power and the power of the ANC filter response. This approach is also known as the leaky filtered-x least mean square (FxLMS) method when implemented in an adaptive filter design process. The previous research usually focuses on tuning the parameter for one type of constraint: robust stability constraint [47], [48], controller output power constraint

[49]–[53], or noise amplification constraints [54], [55]. Since only a single parameter is used to enforce multiple frequency-dependent constraints, the satisfaction of one constraint usually leads to an over-satisfaction of others which, in turn, degrades the ANC performance. This phenomenon is also verified by reference [36] and Section 3.5.3 and 4.1.2.

A potentially better ANC filter design approach is to directly solve a constrained optimization problem with multiple constraints formulated under the H_2/H_∞ control framework in the frequency domain [27], [65]–[68]. However, one issue with this H_2/H_∞ based ANC filter design method (such as in a recent study [29]) is that the stability constraint expression, which involves obtaining the real part of a frequency response matrixs eigenvalues, is not a convex function of the filter coefficients. This, mathematically, makes the whole optimization problem non-convex, so that no global minimum solution is guaranteed (sometimes, the numerical method may not even converge to a local minimum solution due to numerical issues [36]). Practically, it means that this filter design method may not be reliable in a wide range of applications and the ANC performance may be sacrificed because a global minimum solution is not achieved in the numerical solving process.

In addition to the above-mentioned non-convexity issue, the long computation time required in the solving process also leads to limitations in the practical implementation of this method. In principle, this H_2/H_∞ based filter design method can be applied to slow time-varying systems by continuously repeating the filter optimization process using the most recent measurements of reference and disturbance signals, and then updating the filter coefficients. However, since, in all previous applications of this H_2/H_∞ based ANC filter design method, the constrained optimization problem is solved by sequential quadratic programming (SQP) or similar algorithms [29], [69], [70], it requires a computation time on the order of hours or days, depending on the filter order, channel count, as well as frequency range, which makes it impossible for this filter design method to be implemented in practical applications requiring filter adaptation. In the air handling unit example mentioned earlier, if the filter design computation time can be shortened to the order of seconds or minutes, a simple continuous repetition of this filter design calculation can extend the ANC application from systems with fixed fan speeds to systems that pair with variable speed air conditioners (since variable-speed HVAC equipment does not usually change speed within

several minutes). Another practical advantage of shortening the computation time is that, if the selective fixed-filter ANC [44] is used in constrained ANC applications, significant time can be saved in the pre-training stage when a large set of ANC filters are pre-designed. Even for a non-adaptive ANC system, it can accelerate the product development cycle in the commercialization of the ANC technique, since many design parameters, such as geometry, sensor/transducer locations, etc., need to be optimized and several filter design processes are to be conducted in the performance evaluation of each design trial. Thus, one main objective of this dissertation is to propose an efficient multi-channel constrained ANC filter design method for broadband noises.

Here are the objectives of this dissertation in the filter design part:

- Propose an efficient multi-channel constrained ANC filter design method for broadband noises
- Investigate the noise control performance and design efficiency of the proposed method in time-invariant systems
- Apply the proposed efficient method to the time-varying environment by solving the filter coefficients in real time using updated measurements
- Apply the proposed filter design method in various other ASC applications including room equalization filter design and the hear-through filter design

1.3.2 Current challenges in filter implementations

In addition to improved filter design methods, enhanced noise control performance can also be achieved through superior filter implementation techniques. Most practical ANC systems are realized by digital devices. When digital control systems are implemented, an electronic delay will be introduced into the signal path because of the anti-aliasing and reconstruction filters in the analog-to-digital converters (ADC) and digital-to-analog converters (DAC) [71]–[73]. As mentioned in Section 1.2, achieving effective broadband noise control performance relies on the availability of time-advanced information. Consequently, the delay

introduced by electronic devices adversely impacts the noise control performance [43], and even causes causality problems in filter design [74].

Increasing the sampling rate of the digital system [43], [72] is an effective and common way to reduce electronic delay. The group delay in anti-aliasing and reconstruction filters can be reduced or even removed [71] if the cut-off frequency is much higher [43], [75]. Also, for sigma-delta type ADC, there will be a delay of a fixed number of samples and a higher sampling rate will result in a shorter time delay. However, increasing the sampling rate will significantly increase the computational complexity when the digital filters are implemented in real time. The required order of control filters will be increased proportionally to the sampling rate if the filters' effective time lengths, i.e., the impulse response duration (IRD) in time are kept the same. Also, each output signal sample needs to be computed in a shorter sampling interval for a higher sampling rate. Thus, the required real-time multiplications per second will usually increase quadratically with the sampling rate.

One commonly used approach to improving the real-time computational efficiency of high sampling rate ANC systems is to use a multi-rate system with a polyphase filter structure so that the sampling rate for implementing control filters is relatively lower than the sampling rate of the input and output signals [64], [76]–[78]. However, the use of a multi-rate system requires additional lowpass filters (anti-aliasing and reconstruction filters) which also introduce additional delay in real-time implementation. Thus, in ANC applications, the multi-rate techniques with polyphase structures were only applied in the filter adaption process instead of the real-time filtering process, e.g., the subband ANC method [64], [76]. This additional lowpass filter-induced delay contradicts the purpose of using a high sampling rate to reduce the electronic delay, thus, the traditional delayless subband ANC techniques cannot be used to improve the real-time computational efficiency in the real-time active noise control filtering process. An efficient real-time filter implementation structure should be developed to reduce the introduced delay in digital devices without excessively increasing the required real-time computations.

The filter can be implemented in a real-time controller using usually either a finite impulse response (FIR) filter structure or an infinite impulse response (IIR) filter structure. The use of an FIR filter structure can be more beneficial in the design phase because the filter

response will be a linear function of the FIR filter coefficients to be designed and it simplifies the filter design problem formulation. However, compared with the IIR filter, the FIR filter usually requires a longer filter length, thus, a higher real-time computational power. In many commercial ANC applications, a high sampling rate may be chosen for multiple reasons [74]: e.g., to reduce the electronic delay to improve the noise control performance [43], to achieve a wider frequency band [79], to be compatible with the sampling rate in audio applications, etc. The use of a high sampling rate in ANC systems significantly increases the required order of control filters if an FIR filter structure is used [74], [79]. Thus, an IIR filter structure will be preferred in high-sampling cases to reduce the real-time computations at the sacrifice of simplicity in the filter design phase.

To combine the benefits of both FIR and IIR filter structures, an IIR filter can be fitted from pre-designed FIR filter coefficients (or the desired frequency responses). The most challenging part of using this approach is that the designed IIR filter should be stable. Many traditional IIR filter fitting methods cannot ensure stability directly, such as the prony's method [80], stmcb method [81], [82], the least-square approximation in the frequency domain using equation error method [83] or damped Gauss-Newton method [84]. To ensure stability, most of the methods compute the poles and map the unstable poles to the inside of the unit circle in the z-transform domain at each iteration. However, for high-order cases, numerically computing the poles (i.e., computing the roots of a high-order polynomial) can be difficult [85], [86], which makes many traditional stable IIR filter approximation approaches not suitable to be used in high sampling rate ANC applications. Thus, a stable IIR approximation approach for high sampling rate ANC applications should be developed.

Here are the objectives of this dissertation in the filter implementation part:

- Propose an efficient real-time filter implementation structure that reduces the introduced delay in digital devices without excessively increasing the required real-time computations.

- Propose a stable IIR approximation approach for high sampling rate (i.e., high FIR filter order) ANC applications.

1.4 Dissertation Outline

In Chapter 2, the commonly used filter design and implementation methods for ANC systems are reviewed. The main contribution of this dissertation involves many convex optimization techniques which are also reviewed in this chapter.

In Chapter 3, the proposed multi-channel constrained ANC filter design approach based on the traditional constrained optimization approach is presented, which is the main contribution of this dissertation. First, the traditional constrained optimization ANC problem is convexified and reformulated into a convex optimization problem. Then an improved conic formulation derived from this convex formulation is proposed using the duality properties. This proposed conic formulation can improve the computational time from the order of days to seconds and it is numerically stable and reliable. Some constraint modifications are investigated to enable the warmstarting strategy for the proposed conic formulation to reduce the required iteration counts. A singular vector filtering method is also proposed for cases where only the noise amplification constraint is required.

The proposed conic formulation is then applied to three ASC applications in Chapter 4. The first application is to use the proposed conic formulation to design an adaptive constrained ANC filter. Another demonstrated application is the design of the room equalization filter using the proposed conic formulation combined with a proposed reduced-order technique. The proposed conic formulation can also be used to design a constrained hear-through filter which is one of the most popular functions in modern earphones.

Besides the efficient filter design methods, efficient filter implementation methods are also developed. In Chapter 5, a delayless polyphase method is proposed to achieve an efficient filter implementation for high sampling rate delay-sensitive ASC systems. A stable IIR fitting method is also proposed for high sampling rate (high-order) ASC systems.

The summary of this document is written in Chapter 6.

Some parts of the results of this dissertation were published in *The Journal of the Acoustical Society of America* and reproduced from [36], [58] with the permission of AIP Publishing, and published in *Noise Control Engineering Journal* [56]. Some parts of the results were presented in several conferences [8], [45], [57], [59], [60], [87]–[90].

2. REVIEW OF ACTIVE SOUND CONTROL FILTER DESIGN AND IMPLEMENTATION APPROACHES

The Wiener filter method, considered the most fundamental approach, is initially reviewed. The filtered-x least mean square (FxLMS) method can then be derived by iteratively solving the Wiener filter solution, which has gained significant prominence as the prevailing adaptive algorithm in ANC applications. The regularization parameter method and leaky FxLMS method are derived by modifying the Wiener filter method and FxLMS method, respectively, and are commonly selected for constrained ANC applications. Another type of constrained ANC technique, the constrained optimization method based on H_2/H_∞ formulation, is then reviewed, serving as the foundation for the proposed method in this dissertation. Besides filter design methods, two conventional filter implementation techniques, specifically the polyphase filter structures and IIR filter fitting methods, are reviewed.

In addition to traditional filter design and implementation methods, this section further provides a review of convex optimization and cone programming which is a key topic closely tied to the proposed filter design method in Chapter 3.

2.1 Filter Design Approaches

Traditional filter design approaches are reviewed in this section based on the general ANC system diagram. A number of other ASC applications either employ similar system diagrams or utilize simplified versions of this general ANC diagram, which will be demonstrated in Chapter 4.

2.1.1 Control system description

The system block diagram of a typical multi-channel ANC feedforward controller is shown in Fig. 2.1 (a). This ANC system includes N_r microphones as reference sensors, N_s loudspeakers as secondary sources, and N_e microphones as error sensors. In the diagram, $\mathbf{x}$ denotes the noise signals from the primary noise sources measured at reference sensor locations. Elements in vector $\mathbf{r}$ are signals measured by the reference microphones when the

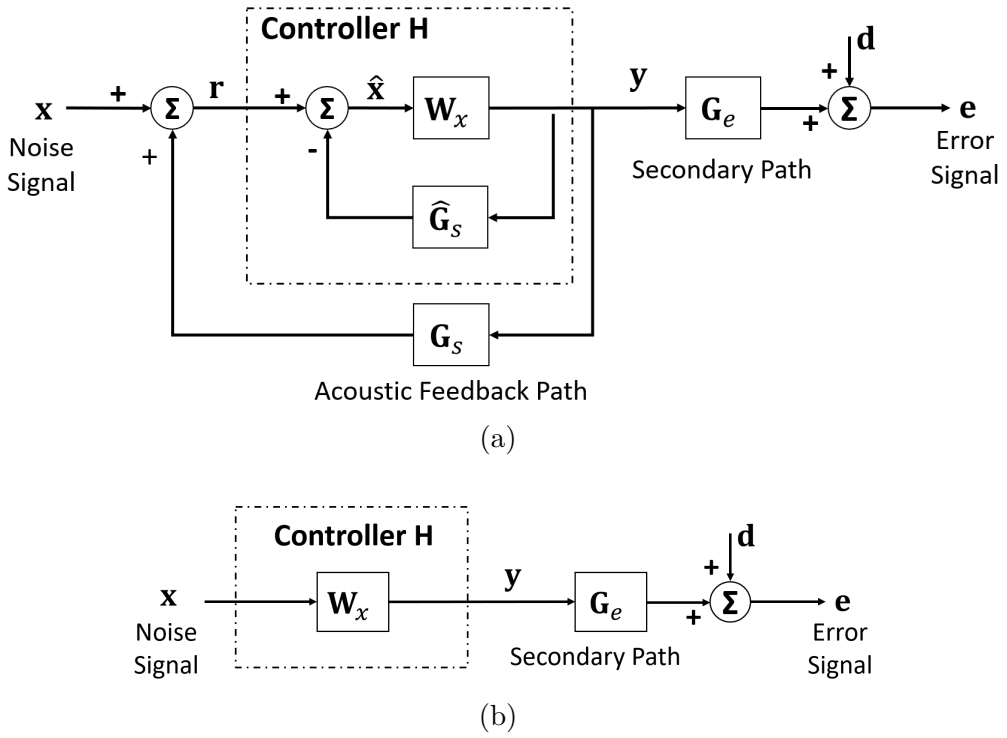


Figure 2.1. Block diagram of the multi-channel feedforward controllers (a) with the acoustic feedback path and internal model control structure, (b) in a standard feedforward form when assuming internal model control structure perfectly cancels the acoustic feedback path effect.

ANC system is activated, thus it includes sound from both the primary sources and the secondary sources. $\mathbf{y}$ is the output of the controller. $\mathbf{d}$ denotes the disturbance signals (i.e., the primary noise at error sensor locations) that is correlated with $\mathbf{x}$. $\mathbf{e}$ denotes the error signals, the sum of primary and secondary sound fields at error sensor locations. The total power of error signals is to be attenuated by the ANC system.

$\mathbf{G}_s$ is the acoustic feedback path matrix that represents the acoustic responses of secondary sources at the reference sensors. It is noted that the reference signals $\mathbf{r}$ is the combination of primary noise signals $\mathbf{x}$ and the signals from the acoustic feedback path $\mathbf{G}_s$. To estimate the primary noise signals $\mathbf{x}$ from reference signals $\mathbf{r}$, an internal model control (IMC) structure is applied to cancel the acoustic feedback path effect [27], [29], [46]. In the controller $\mathbf{H}$, the $\hat{\mathbf{G}}_s$ is a model of the physical acoustic feedback path, $\mathbf{G}_s$. It is usually

assumed that $\hat{\mathbf{G}}_s$ is a perfect model in the nominal operating condition, i.e., $\hat{\mathbf{G}}_s = \mathbf{G}_s$. The estimated noise signals $\hat{\mathbf{x}}$ will then be the same as the true primary noise signals $\mathbf{x}$ and this system becomes a standard feedforward system in Fig. 2.1 (b). The possible acoustic feedback path modeling error in practice is considered a model uncertainty in the robustness constraints applied on controllers. $\mathbf{G}_{\mathrm{e}}$ represents the acoustical responses matrix of the secondary sources at the error sensor positions.

$\mathbf{W}_x$ is the frequency response matrix of the multi-channel ANC FIR filters whose coefficients, denoted as $\mathbf{w}_{i,j}(l)$ which is a vector containing the time-domain coefficients of the designed i-th output, j-th input channel, and the l-th coefficient in that channel of the control filter. The optimal coefficients $\mathbf{w}_{i,j}(l)$ obtained by solving the filter design problem can be directly implemented in the real-time signal processing controller via time-domain filtering. Note that N_t is used to denote the number of FIR filter coefficients in each channel which is also known as taps.

2.1.2 Wiener filter and FxLMS algorithm

The basic conventional approach to calculate control filter parameters is to minimize the total power of the error signal in the time domain, $\mathbf{e}(n)$, when the ANC system is activated. The cost function of this optimization problem can be expressed as [65]

$$\mathrm{E}\left[\mathbf{e}^{\mathrm{T}}(n)\mathbf{e}(n)\right] = \mathbf{w}_{w\mathrm{i}}^{\mathrm{T}}\mathbf{A}_{w\mathrm{i}}\mathbf{w}_{w\mathrm{i}} + 2\mathbf{b}_{w\mathrm{i}}^{\mathrm{T}}\mathbf{w}_{w\mathrm{i}} + c_{w\mathrm{i}}, \tag{2.1}$$

where,
$$\mathbf{A}_{w\mathrm{i}} = \mathrm{E}\left[\mathbf{R}^{\mathrm{T}}(n)\mathbf{R}(n)\right], \quad \mathbf{b}_{w\mathrm{i}} = \mathrm{E}\left[\mathbf{R}^{\mathrm{T}}(n)\mathbf{d}(n)\right], \quad c_{w\mathrm{i}} = \mathrm{E}\left[\mathbf{d}^{\mathrm{T}}(n)\mathbf{d}(n)\right],$$
$$\mathbf{w}_{w\mathrm{i}} = \begin{bmatrix}\mathbf{w}_{1,1}(0) & \mathbf{w}_{1,2}(0) & \dots & \mathbf{w}_{1,N_r}(0) & \dots & \mathbf{w}_{N_s,N_r}(0) & \dots & \mathbf{w}_{N_s,N_r}(N_t-1)\end{bmatrix}^{\mathrm{T}},$$
$$\mathbf{R}(n) = \begin{bmatrix}\tilde{\mathbf{x}}_1^{\mathrm{T}}(n) & \tilde{\mathbf{x}}_1^{\mathrm{T}}(n-1) & \dots & \tilde{\mathbf{x}}_1^{\mathrm{T}}(n-N_t+1) \\ \vdots & \vdots & \ddots & \vdots \\ \tilde{\mathbf{x}}_{N_{\mathrm{e}}}^{\mathrm{T}}(n) & \tilde{\mathbf{x}}_{N_{\mathrm{e}}}^{\mathrm{T}}(n-1) & \dots & \tilde{\mathbf{x}}_{N_{\mathrm{e}}}^{\mathrm{T}}(n-N_t+1)\end{bmatrix},$$
$$\tilde{\mathbf{x}}_q(n) = \begin{bmatrix}\tilde{x}_{q,1,1}(n) & \tilde{x}_{q,1,2}(n) & \dots & \tilde{x}_{q,1,N_r}(n) & \tilde{x}_{q,2,1}(n) & \dots & \tilde{x}_{q,N_s,N_r}(n)\end{bmatrix}^{\mathrm{T}},$$
$$\tilde{x}_{i,j,k}(n) = \sum_{l=0}^{\infty} g_{i,j,l}\, x_k(n-l),$$

and E is the expectation operator, T represents the matrix transpose, $g_{i,j,l}$ denotes the i-th output, j-th input channel, and l-th coefficient in that channel of the discretized impulse response of the secondary path $\mathbf{G}_{\mathrm{e}}$; $x_k(n)$ is the k-th channel of reference signals collected from the k-th reference sensor. The optimal solution that minimize Eq. (2.1) (i.e., the Wiener filter) is [65]

$$\mathbf{w}_{w\mathrm{i},opt} = -\mathbf{A}_{w\mathrm{i}}^{-1}\mathbf{b}_{w\mathrm{i}}. \tag{2.2}$$

The Wiener filter design by Eq. (2.2) can be implemented as a non-adaptive filter via time-domain filtering. If the adaptive filters are desired, the Wiener filter can be extended to the FxLMS algorithm by the stochastic gradient descent method. The gradient of the cost function can be estimated by instantaneous signal [65], i.e.,

$$\begin{aligned}\frac{d\left[\mathbf{e}^{\mathrm{T}}(n)\mathbf{e}(n)\right]}{d\mathbf{w}_{w\mathrm{i}}} &= 2\mathrm{E}\left[\mathbf{R}^{\mathrm{T}}(n)\mathbf{R}(n)\right]\mathbf{w}_{w\mathrm{i}} + 2\mathrm{E}\left[\mathbf{R}^{\mathrm{T}}(n)\mathbf{d}(n)\right] \\ &\approx 2\mathbf{R}^{\mathrm{T}}(n)\left(\mathbf{R}(n)\mathbf{w}_{w\mathrm{i}} + \mathbf{d}(n)\right) \\ &\approx 2\hat{\mathbf{R}}^{\mathrm{T}}(n)\mathbf{e}(n),\end{aligned} \tag{2.3}$$

where $\hat{\mathbf{R}}$ is an estimate of the true $\mathbf{R}$. By choosing an appropriate step length α, the control filter parameters can be updated by

$$\mathbf{w}_{w\mathrm{i}}^{(n+1)} = \mathbf{w}_{w\mathrm{i}}^{(n)} - \alpha\hat{\mathbf{R}}^{\mathrm{T}}(n)\mathbf{e}(n). \tag{2.4}$$

The Eq. (2.4) can be written channel by channel as

$$\mathbf{w}_{i,j}(l)^{(n+1)} = \mathbf{w}_{i,j}(l)^{(n)} - \alpha\sum_{q=1}^{N_{\mathrm{e}}}\tilde{x}_{q,i,j}(n-l)\mathrm{e}_q(n). \tag{2.5}$$

where $e_q(n)$ is the q-th channel of error signals collected by the q-th error sensor.

2.1.3 Regularization parameter method and leaky FxLMS algorithm

Although the Wiener filter design reviewed in Section 2.1.2 provides an optimal control filter for ANC systems, it is not robust in practical applications. For example, the matrix

$\mathbf{A}_{w\mathrm{i}}$ in Eq. (2.2) may be near singular due to strong correlation in different reference signals or secondary paths. Some of those constraints discussed in Section 1.2 and 1.3.1 are required in practical applications, i.e., the robust stability, noise amplification, and filter output power constraints, which may not be satisfied by the Wiener filter. To resolve these concerns, the regularization parameter method was used. The regularization parameter approach is briefly described here. More details can be found in studies of the leaky FxLMS [50], [55], [91] and in Elliott's work on robust controller design [46], [92].

For the regularization parameter method, instead of the total signal power at the error sensors, the objective function being minimized is

$$\mathrm{E}\left[\mathbf{e}^{\mathrm{T}}(n)\mathbf{e}(n)+\beta\sum_{\mathrm{i}=1}^{N_s}\sum_{\mathrm{j}=1}^{N_r}\mathbf{w}_{i,j}^{\mathrm{T}}\mathbf{w}_{i,j}\right], \tag{2.6}$$

where β is the regularization parameter. Note that each $\mathbf{w}_{i,j}$ is a column vector that is composed of the ANC filter coefficients associated with the channel pair specified by output i and input j. β needs to be tuned to satisfy the non-singular condition or required constraints. By minimizing the objective function Eq. (2.6), the optimal filter can be written as:

$$\mathbf{w}_{reg,opt}=-(\mathbf{A}_{w\mathrm{i}}+\beta\mathbf{I}_{N_rN_sN_t})^{-1}\mathbf{b}_{w\mathrm{i}}, \tag{2.7}$$

where $\mathbf{I}_{N_rN_sN_t}$ is a square identity matrix with a dimension of $N_rN_sN_t$ by $N_rN_sN_t$. When β increases, all the required constraints will be gradually satisfied but it can cause an over satisfaction of many constraints and thus results in a sacrifice of noise control performance.

The regularization parameter method can also be extended to an adaptive algorithm (leaky FxLMS) by the stochastic gradient descent method. The control filter coefficients can be updated as

$$\begin{aligned}\mathbf{w}_{i,j}(l)^{(n+1)}&=\mathbf{w}_{i,j}(l)^{(n)}-\alpha\left(\sum_{q=1}^{N_\mathrm{e}}\tilde{x}_{q,i,j}(n-l)\mathrm{e}_q(n)+\beta\mathbf{w}_{i,j}(l)^{(n)}\right)\\&=(1-\alpha\beta)\mathbf{w}_{i,j}(l)^{(n)}-\alpha\sum_{q=1}^{N_\mathrm{e}}\tilde{x}_{q,i,j}(n-l)\mathrm{e}_q(n).\end{aligned} \tag{2.8}$$

Thus, the regularization parameter β is also called the leakage factor in the leaky FxLMS method. The leaky FxLMS method can also be improved by considering the frequency weighting [47], [55] or the required output power constraints [50].

2.1.4 Constrained optimization method using H_2/H_∞ formulation

An alternative constrained ANC filter design method is to formulate and solve a constrained optimization problem. In this section, all the formulations are presented in the context of feedforward control. It is noted that they can be directly applied to feedback ANC as well, because, if an IMC structure is used, a feedback controller can be designed using an identical way as that for a feedforward controller [29]. It is also noted that, compared with the time-domain methods reviewed in Section 2.1.2 and 2.1.3, the formulation in this section is based on the frequency domain but the design variables are still time-domain filter coefficients which can be applied directly in real-time controllers using time-domain filtering.

The previous work of Cheer and Elliott [29] was presented here to introduce the traditional H_2/H_∞ approach. Firstly, the frequency response of an FIR ANC filter can be expressed as:

$$\mathbf{W}_{x_{i,j}}(f) = \mathbf{F}_z^{\mathrm{T}}(f)\mathbf{w}_{i,j}, \tag{2.9}$$

where

$$\mathbf{F}_z(f) = \begin{bmatrix} 1 & \mathrm{e}^{-\mathrm{j}2\pi f\frac{1}{f_s}} & \mathrm{e}^{-\mathrm{j}2\pi f\frac{2}{f_s}} & \dots & \mathrm{e}^{-\mathrm{j}2\pi f\frac{N_t-1}{f_s}} \end{bmatrix}^{\mathrm{T}};$$

f denotes the frequency; f_s denotes the sampling frequency. $\mathbf{W}_{x_{\mathrm{i,j}}}$ means the i-th row and j-th column of frequency response matrix of the ANC filter $\mathbf{W}_x$. Thus, $\mathbf{W}_{x_{i,j}}(f_k)$ denotes the frequency response of the channel of ANC filter associated with the i-th control actuator and j-th reference sensor at frequency f_k:

$$\mathbf{W}_x(f_k) = \begin{bmatrix} \mathbf{W}_{x_{1,1}}(f_k) & \mathbf{W}_{x_{1,2}}(f_k) & \dots & \mathbf{W}_{x_{1,N_r}}(f_k) \\ \mathbf{W}_{x_{2,1}}(f_k) & \mathbf{W}_{x_{2,2}}(f_k) & \dots & \mathbf{W}_{x_{2,N_r}}(f_k) \\ \vdots & \vdots & \ddots & \vdots \\ \mathbf{W}_{x_{Ns,1}}(f_k) & \mathbf{W}_{x_{N_s,2}}(f_k) & \dots & \mathbf{W}_{x_{N_s,N_r}}(f_k) \end{bmatrix}. \tag{2.10}$$

The objective function J_0 to be minimized is the total power of error signals across all desired frequencies:

$$J_0 = \sum_{k=1}^{N_f} J(f_k), \tag{2.11}$$

where the $J(f_k)$ is the power of error signal at k-th frequency f_k. N_f denotes the total number of frequency points in the desired noise attenuation band. Following the work of Cheer and Elliott [29], $J(f_k)$ can be expressed as:

$$\begin{aligned} J(f_k) &= \mathrm{tr}\Big\{ \mathrm{E}\left[\mathbf{e}(f_k)\mathbf{e}^{\mathrm{H}}(f_k)\right] \Big\} \\ &= \mathrm{tr}\Big\{ \mathrm{E}\left[\left(\mathbf{d}(f_k) + \mathbf{G}_{\mathrm{e}}(f_k)\mathbf{W}_x(f_k)\mathbf{x}(f_k)\right)\left(\mathbf{d}(f_k) + \mathbf{G}_{\mathrm{e}}(f_k)\mathbf{W}_x(f_k)\mathbf{x}(f_k)\right)^{\mathrm{H}}\right] \Big\} \\ &= \mathrm{tr}\Big\{ \mathbf{G}_{\mathrm{e}}(f_k)\mathbf{W}_x(f_k)\mathbf{S}_{xx}(f_k)\mathbf{W}_x^{\mathrm{H}}(f_k)\mathbf{G}_{\mathrm{e}}^{\mathrm{H}}(f_k) \\ &\quad + \mathbf{G}_{\mathrm{e}}(f_k)\mathbf{W}_x(f_k)\mathbf{S}_{xd}(f_k) + \mathbf{S}_{xd}^{\mathrm{H}}(f_k)\mathbf{W}_x^{\mathrm{H}}(f_k)\mathbf{G}_{\mathrm{e}}^{\mathrm{H}}(f_k) + \mathbf{S}_{dd}(f_k) \Big\}, \end{aligned} \tag{2.12}$$

where H denotes the conjugate transpose of a matrix; $\mathbf{S}_{xx}(f_k)$ and $\mathbf{S}_{dd}(f_k)$ are the cross spectral density matrices of $\mathbf{x}$ and $\mathbf{d}$ respectively at frequency f_k; $\mathbf{S}_{xd}(f_k)$ is the cross spectral density matrix between the primary noise signals $\mathbf{x}$ and the disturbance signals $\mathbf{d}$ at frequency f_k, which is defined as $\mathbf{S}_{xd} = \lim_{T\to\infty} \frac{1}{T}\mathrm{E}[\mathcal{F}(\mathbf{x})\mathcal{F}(\mathbf{d})^{\mathrm{H}}]$ where $\mathcal{F}$ denotes the Fourier transform.

In practical applications, noise amplification (disturbance enhancement) constraints are added to prevent large amplification inside or outside of the desired frequency bands [29], [46]. In Cheer and Elliott's work, they applied a constraint to the normalized power of each error channel. A simplified version is used in this dissertation, i.e., applying the constraint to the normalized total power of all error signals:

$$J(f_k) \leq A_{\mathrm{e}}(f_k)\mathbf{S}_{dd}(f_k), \tag{2.13}$$

where $A_{\mathrm{e}}(f_k)$ is a constant or a frequency-dependent value that is specified as the upper bound of the amplification ratio of error signals at frequency f_k.

A constraint on the amplitude of the ANC filter response, $\mathbf{W}_{x_{\mathrm{i,j}}}(f_k)$, is usually needed [27], [49]–[53] to ensure that the loudspeakers always operate in their linear response range,

especially at very low frequencies. Also, in some applications such as ANC systems using batteries, the power consumption of the loudspeakers needs to be limited. This constraint can be achieved by enforcing a specified spectral limit on the controller. The filter response amplitude constraint can be expressed as:

$$|\mathbf{W}_{x_{i,j}}(f_k)| \leq C_{i,j}(f_k) \tag{2.14}$$

where $C_{i,j}(f_k)$ is the applied upper bound on the amplitude of the designed filter frequency response of i-th output and j-th input channel at frequency f_k. Note that, if $C_{\mathrm{i,j}}(f_k)$ is small enough and Eq. (2.14) is satisfied at some frequencies, Eq. (2.13) mentioned above, and Eqs. (2.15), (2.16) for robust stability constraints discussed below are also automatically satisfied at those frequencies. So for those frequency bands where $C_{\mathrm{i,j}}(f_k)$ is small, Eq. (2.14) can be used to replace Eqs. (2.13), (2.15), (2.16) to reduce the calculation effort of solving the optimization problem. Also, it is found that when the energy of the disturbance signal is small at some frequency bands, e.g., near Nyquist frequency due to anti-aliasing filtering, the use of response limits, Eq. (2.14), to replace Eqs. (2.13), (2.15), (2.16) on these frequency bands can help improve the numerical behavior during solving the optimization problem.

Even if a feedforward controller is used targeting the broadband noises, the stability and robustness constraints are still required because of the acoustic feedback cancellation path $\hat{\mathbf{G}}_s$ in the controller. The controller stability can be ensured by limiting the open-loop response trajectory of controller $\mathbf{H}$ (i.e., the eigenvalues of the open-loop frequency response matrix) to be at the right-hand side of the Nyquist point in the Laplace domain [29], [46], which can be expressed as:

$$\min\left(\mathrm{Re}\left(\lambda\left(\mathbf{W}_x(f_k)\hat{\mathbf{G}}_s(f_k)\right)\right)\right) > -1 \tag{2.15}$$

where $\lambda()$ denotes the eigenvalues of a matrix; Re() denotes the real part of a complex number. Note that, compared with Cheer and Elliott's work [29], $\hat{\mathbf{G}}_s(f_k)\mathbf{W}_x(f_k)$ is changed to $\mathbf{W}_x(f_k)\hat{\mathbf{G}}_s(f_k)$ since this will not change the values of non-zero eigenvalues. The size of $\hat{\mathbf{G}}_s(f_k)\mathbf{W}_x(f_k)$ is N_r by N_r, and the size of $\mathbf{W}_x(f_k)\hat{\mathbf{G}}_s(f_k)$ is N_s by N_s. For most ANC appli-

cations, the number of secondary sources N_s is smaller than the number of reference sensors N_r, which makes $\mathbf{W}_x(f_k)\hat{\mathbf{G}}_s(f_k)$ result in smaller problem size. However, for applications where N_s is greater than N_r, a formulation with $\hat{\mathbf{G}}_s(f_k)\mathbf{W}_x(f_k)$ is preferred.

For robustness constraints, with the **M-Δ** structure and the small-gain theory applied [29], [46], they can be expressed as:

$$\max\left(\sigma\left(\mathbf{W}_x(f_k)\hat{\mathbf{G}}_s(f_k)\right)\right)B(f_k) \leq 1 \tag{2.16}$$

where $\sigma()$ denotes the singular values of a matrix; $B(f_k)$ is the upper bound on the output multiplicative plant uncertainty at frequency f_k. To reduce the problem size, as explained in the stability constraint Eq. (2.15), $\mathbf{W}_x(f_k)\hat{\mathbf{G}}_s(f_k)$ is used instead of $\hat{\mathbf{G}}_s(f_k)\mathbf{W}_x(f_k)$.

As a summary of the H_2/H_∞ formulation of ANC applications, an optimization problem for the multi-channel ANC filter design can be constructed by using Eq. (2.11) as the objective function, and Eqs. (2.13), (2.14), (2.15), (2.16) as constraints:

$$\begin{aligned}
\text{minimize} \quad & \sum_{k=1}^{N_f} J(f_k) \\
\text{subject to} \quad & J(f_k) \leq A_{\mathrm{e}}(f_k)\mathbf{S}_{dd}(f_k), \quad \text{for all } f_k, \\
& |\mathbf{W}_{x_{i,j}}(f_k)| \leq C_{i,j}(f_k), \quad \text{for all } f_k,\ i,\ \text{and } j, \\
& \min\left(\mathrm{Re}\left(\lambda\left(\mathbf{W}_x(f_k)\hat{\mathbf{G}}_s(f_k)\right)\right)\right) > -1, \quad \text{for all } f_k, \\
& \max\left(\sigma\left(\mathbf{W}_x(f_k)\hat{\mathbf{G}}_s(f_k)\right)\right)B(f_k) \leq 1, \quad \text{for all } f_k.
\end{aligned} \tag{2.17}$$

Cheer and Elliott proposed to solve this optimization problem Eq. (2.17) by sequential quadratic programming (SQP). But the problem-solving process can be quite time-consuming since it involves complicated non-smooth constraints, especially for high-order multi-channel filters and a large number of frequency components. Also, the SQP cannot guarantee to converge to the global optimal solution for such a general problem. To overcome these difficulties, modifications, and reformulations of Eq. (2.17) are proposed and discussed in Chapter 3.

2.2 Filter Implementation Approaches

Two traditional efficient implementation approaches are reviewed in this section: the polyphase filter implementation structure, and the IIR filter fitting method. It is noted that those filter implementation methods are discussed based on a single-channel system. The extension to the multi-channel case is trivial because the method discussed in this section can be directly applied channel by channel.

2.2.1 Polyphase filter implementation structure

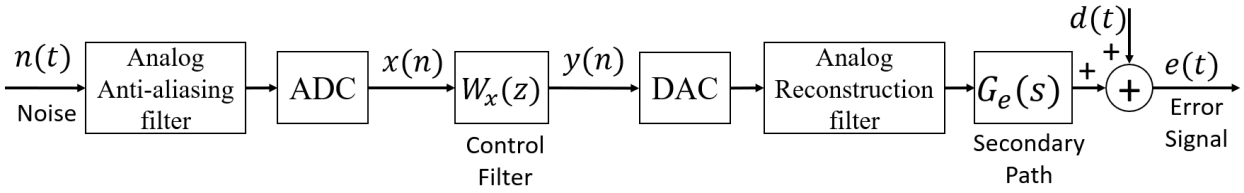


Figure 2.2. Block diagram of the commonly used implementation of ANC (non-adaptive) digital controllers.

The system block diagram of a typical ANC controller considering the ADC and DAC is shown in Fig. 2.2. $n(t)$ represents the analog noise signal from noise sources. $x(n)$ represents the sampled reference signal. $W_x(z)$ is the designed digital ANC FIR filter. $y(n)$ is the digital output signal. The secondary path $G_{\mathrm{e}}(s)$ represents the acoustical responses of the secondary source at the error sensor positions. $d(t)$ is the disturbance signal to be controlled by the signal produced by the secondary source. e(t) is the error signal whose power is to be minimized when designing the control filter coefficients.

In many applications, $X(z)$ in Fig 2.2 is sampled at a high sampling rate for various reasons: e.g., to reduce the delay introduced by anti-aliasing and reconstruction filters, ADC, and DAC; to be compatible with the sampling rate in audio applications, etc. However, the desired sound control band is still at the low-frequency band. To reduce the real-time computations, a multi-rate system can be applied. In Fig. 2.3 (a), a block diagram of a commonly used multi-rate system is shown. $X(z)$ is the digital signal sampled at a sampling rate of f_s. $H(z)$ is a lowpass filter with a cutoff frequency at f_c. If $H(z)$ is assumed to be

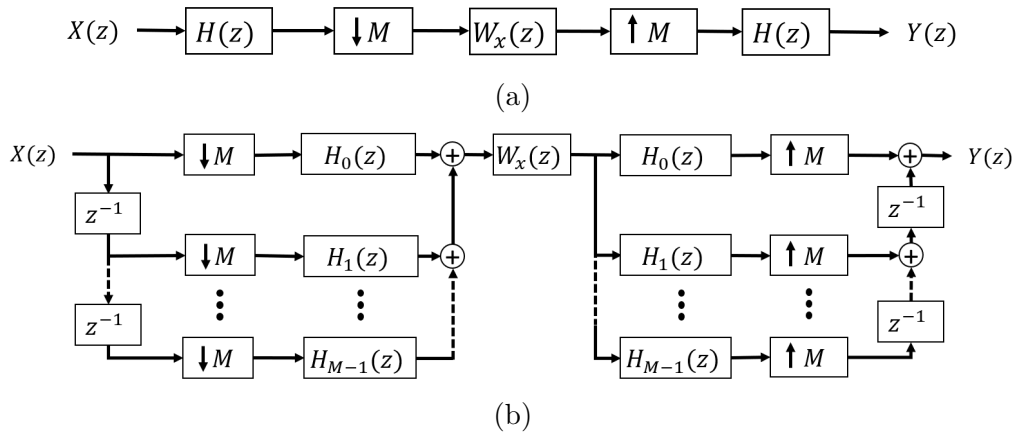


Figure 2.3. Block diagrams of (a) a typical multi-rate system, (b) a multi-rate system after applying polyphase filter structures.

an ideal lowpass filter and $f_s/f_c > 2M$, then a downsampling with a decimation factor of M can be achieved without aliasing. $W(z)$ is a digital filter (the designed ANC filter) that will be implemented with a sampling rate of f_s/M. Compared with implementing the filter at a sampling rate of f_s, the real-time computations in $W(z)$ will then be reduced to $1/M$ of the computations and the same impulse response duration can be maintained.

One disadvantage of the multi-rate system in Fig. 2.3 (a) is that the lowpass filter $H(z)$ is still operating at the higher sampling rate, f_s. To further reduce the real-time computations in implementing $H(z)$, polyphase implementation can be applied. In Fig. 2.3 (b), the traditional use of a polyphase filter structure is illustrated. $H(z)$ can be expressed as

$$H(z) = h_0 + h_1 z^{-1} + h_2 z^{-2} + \ \ldots \ + h_{L-1} z^{-L+1}. \tag{2.18}$$

If a proper choice of filter length or zero-padding of the filter length is applied, it is always possible to have the ratio of the filter length to decimation factor, $P = L/M$, to be an integer. Then the lowpass filter $H(z)$ can be split into multiple filter phases, $H_m(z)$:

$$H_m(z) = \sum_{n=0}^{P-1} h_{nM+m} z^{-n}. \tag{2.19}$$

According to the first and second noble identities [93], if $X(z)$ are the same for the two filter structures in Fig. 2.3 (a) and (b), $Y(z)$ will also be the same for the two filter structures. Compared with Fig. 2.3 (a), the filter structure in Fig. 2.3 (b) performs the downsampling operation before any filters are applied and performs the upsampling operation after all filters are applied. Thus, the filter structure in Fig. 2.3 (b) reduces the real-time computations in both $H_m(z)$ (or essentially the $H(z)$) and $W(z)$. Similarly, the lowpass filter $H(z)$ can be replaced by other band-limited sub-band filters so that signal content in each associated frequency band can be processed separately. More details of multi-rate polyphase filter structure can be referred to in Chapter 11 in Proakis and Manolakis' book [93].

The use of a multi-rate system with polyphase filter structure implementation can reduce the high real-time computations caused by a high sampling rate. And this high sampling rate in input signal $X(z)$ and output signal $Y(z)$ will allow a lower delay in the analog anti-aliasing and reconstruction filters as well as ADC and DAC hardware. However, because of the real-time downsampling and upsampling operations, two real-time lowpass filters $H(z)$ are always required, which inevitably introduce additional time delay to the system compromising the performance if the application is delay sensitive (e.g. ANC application).

2.2.2 Stable IIR filter fitting methods

In this section, the commonly used traditional stable IIR filter fitting approach is first reviewed. Then, the method proposed by Brandenstein and Unbehauen [94], [95] is reviewed. Only FIR and IIR filters with real time-domain coefficients are considered in this section.

Let the transfer function of the FIR filter that needs to be approximated be

$$F(z) = \sum_{n=0}^{L} f_n z^{-n}. \tag{2.20}$$

And the transfer function of a causal and stable IIR filter is expressed as

$$H(z) = \frac{P(z)}{Q(z)}, \tag{2.21}$$

where, the numerator polynomial $P(z)$ is

$$P(z) = \sum_{\mu=0}^{M} p_\mu z^{-\mu}, \tag{2.22}$$

and the denominator polynomial $Q(z)$ is

$$Q(z) = 1 + \sum_{\nu=1}^{N} q_\nu z^{-\nu}. \tag{2.23}$$

The objective of fitting an FIR filter using IIR filter structure is to minimize the approximation error

$$E = \left(\frac{1}{2\pi} \int_{-\pi}^{\pi} W(\mathrm{e}^{\mathrm{j}\Omega}) |F(\mathrm{e}^{\mathrm{j}\Omega}) - H(\mathrm{e}^{\mathrm{j}\Omega})|^2 d\Omega \right)^{\frac{1}{2}}, \tag{2.24}$$

with respect to p_μ (μ = 0, 1, ..., M) and q_ν (ν = 1, 2, ..., N), where $W(\mathrm{e}^{\mathrm{j}\Omega})$ denotes the weighting function and $W(\mathrm{e}^{-\mathrm{j}\Omega}) = W(\mathrm{e}^{\mathrm{j}\Omega})$ if the fitted FIR filter has only real coefficients.

One commonly used traditional stable IIR filter fitting method is reviewed here. For this traditional method, instead of the objective function value E used in Eq. (2.24), a discrete form of fitting error is formulated for numerical computation:

$$E_s = \sum^{\mathrm{i}} W(\mathrm{e}^{\mathrm{j}\Omega_\mathrm{i}}) |F(\mathrm{e}^{\mathrm{j}\Omega_\mathrm{i}}) - H(\mathrm{e}^{\mathrm{j}\Omega_\mathrm{i}})|^2, \tag{2.25}$$

where Ω_i is the i-th sampled frequency. If the total number of frequencies is chosen to be sufficiently large, then minimizing E_s in Eq. (2.25) can lead to approximately the same optimal filter coefficients compared with minimizing E in Eq. (2.24). The optimal IIR filter coefficients. To find the optimal filter coefficients that minimize E_s in Eq. (2.25), some iterative search algorithms can be implemented: e.g., the damped Gauss-Newton method [84]. The initial point for the iterative search algorithms can be chosen using the optimal coefficients solved by minimizing the equation error formulation [83]:

$$E_l = \sum^{\mathrm{i}} W(\mathrm{e}^{\mathrm{j}\Omega_\mathrm{i}}) |F(\mathrm{e}^{\mathrm{j}\Omega_\mathrm{i}}) Q(\mathrm{e}^{\mathrm{j}\Omega_\mathrm{i}}) - P(\mathrm{e}^{\mathrm{j}\Omega_\mathrm{i}})|^2. \tag{2.26}$$

To ensure stability, at each iteration, the roots of the polynomial $Q(z)$, i.e., the poles, should be computed and checked. If some roots z_{i} are outside the unit circle in the z-transform domain (i.e., $|z_{\mathrm{i}}| > 1$), they should be stabilized by replacing z_{i} with $1/z_{\mathrm{i}}^*$ where z_{i}^* is the complex conjugate of z_{i}. This traditional method is used in many IIR filter fitting toolboxes such as the invfreqz() function in Matlab R2022b.

The challenge of using this traditional method for high-order IIR filter cases is that computing the roots of a high-order polynomial can be difficult [85], [86] and there is no guarantee that the traditional method can converge when the pole stabilizing process is applied.

Besides the above traditional method, a least-square method for approximating FIR filter using IIR filter structure that guarantees the fitted IIR filter is stable without mapping unstable poles inside the unit circle was proposed by Brandenstein and Unbehauen [94] and then extended to its weighted version [95]. Since no computation and mapping of poles are required, it is applicable even in cases where the IIR filter length is large [94], [95]. Another advantage of their proposed method is that the optimal denominator coefficients can be firstly determined without involving the numerator coefficients. The optimal numerator coefficients can be determined after the optimal denominators are determined. For simplicity, their original proposed method is referred to as the "BU's method" in this dissertation. Their method is briefly summarized as follows (See Brandenstein and Unbehauen's work for more details [94], [95]).

Assume that a maximum phase function $G(z)$ with order K satisfies $|G(\mathrm{e}^{\mathrm{j}\Omega})|^2 = W(\mathrm{e}^{\mathrm{j}\Omega})$, then a function $X(z)$ can be defined as

$$X(z) = z^{-K} G_*(z^{-1}) z^{-L} F_*(z^{-1}), \tag{2.27}$$

where $G_*(z)$ denotes the polynomial which is obtained from $G(z)$ by replacing each coefficient with its conjugate complex counterpart, and $F_*(z)$ is defined in a similar way. By using $X(z)$,

starting from initial guess $Q^0(z) = 1$, the optimal $Q(z)$ can be solved iteratively [94], [95]. More specifically, suppose at the k-th iteration, $X^{(k)}(z)$ is defined as

$$X^{(k)}(z) = \frac{X(z)}{Q^{(k-1)}(z)}, \tag{2.28}$$

where $Q^{(k-1)}(z)$ is the $Q(z)$ obtained in $(k-1)$-th iteration. Then $Q^{(k)}(z)$ can be obtained by solving the set of equations

$$A^{(k)}q^{(k)} = b^{(k)}, \tag{2.29}$$

in least-square sense, where

$$A^{(k)} = \begin{bmatrix} x^{(k)}(0) & 0 & \dots & 0 \\ x^{(k)}(1) & x^{(k)}(0) & \dots & 0 \\ \vdots & \vdots & \ddots & 0 \\ x^{(k)}(N-1) & x^{(k)}(N-1) & \dots & x^{(k)}(0) \\ x^{(k)}(L+N-M-1) & x^{(k)}(L+N-M-2) & \dots & x^{(k)}(L-M) \end{bmatrix}, \tag{2.30}$$

$$b^{(k)} = -\begin{bmatrix} 0 & \dots & 0 & x^{(k)}(0) & \dots & x^{(k)}(L-M-1) \end{bmatrix}^{\mathrm{T}}, \tag{2.31}$$

and $x^{(k)}(n)$ is the sequence obtained by the inverse z-transform of $X^{(k)}(z)$. The solved $q^{(k)}$ consists of the coefficients of $Q^{(k)}(z)$:

$$q^{(k)} = \begin{bmatrix} q_N^{(k)} & q_{N-1}^{(k)} & \dots & q_1^{(k)} \end{bmatrix}^{\mathrm{T}}. \tag{2.32}$$

The approximation error norm at k-th iteration is defined as

$$E^{(k)} = \sum_{n=0}^{L+N-M-1} u^{(k)}(n)^2, \tag{2.33}$$

where $u^{(k)}(n)$ is the sequence obtained by the inverse z-transform of $U^{(k)}(z)$ and

$$U^{(k)}(z) = z^{-N}Q^{(k)}(z^{-1})X^{(k)}(z). \tag{2.34}$$

After the optimal $Q(z)$ is obtained, the optimal $P(z)$ can be obtained by solving the $M+1$ linear equations

$$\sum_{\mu=0}^{M} c(\lambda-\mu)p_\mu = b(\lambda), \tag{2.35}$$

for $\lambda = 0, 1, \ldots, M$, where

$$c(n) = \frac{1}{2\pi}\int_{-\pi}^{\pi} \frac{W(e^{j\Omega})}{|Q(e^{j\Omega})|^2} e^{jn\Omega} d\Omega \tag{2.36}$$

$$b(n) = \frac{1}{2\pi}\int_{-\pi}^{\pi} W(e^{j\Omega}) \frac{F(e^{j\Omega})}{[Q(e^{j\Omega})]^*} e^{jn\Omega} d\Omega \tag{2.37}$$

Some improvements will be given in Section 5.2 so this method is applicable in ASC applications.

2.3 Convex Optimization

In this section, an overview of the definitions and theories pertaining to convex optimization topics is provided. To maintain clarity and ease of reference, the variables introduced and utilized in this section are confined solely to this section.

2.3.1 Convex sets, functions, and duality properties

A brief review of convex sets, functions, and duality properties that are used to derive methods proposed in this dissertation is given here. More details about these topics can be referred to in reference [96].

Definition 2.3.1. *A set C is convex if for any two points $\mathbf{x}$, $\mathbf{y} \in C$, and any $0 \le \theta \le 1$, we have [96]*

$$\theta\mathbf{x} + (1-\theta)\mathbf{y} \in C. \tag{2.38}$$

The convexity of sets is preserved under various operations on sets. For example, the sets that are intersection, affine functions, linear-fractional functions, or perspective functions of other convex sets are also convex. [96]

Definition 2.3.2. *A function f: $\mathbf{R}^n \to \mathbf{R}$ is convex if the domain of f is a convex set and if for all points $\mathbf{x}$ and $\mathbf{y}$ in the domain, and $0 \leq \theta \leq 1$, we have [96]*

$$f\left(\theta\mathbf{x} + (1-\theta)\mathbf{y}\right) \leq \theta f(\mathbf{x}) + (1-\theta) f(\mathbf{y}). \tag{2.39}$$

The convexity of functions is preserved under various operations on functions. For example, nonnegative weighted sums, composition with an affine mapping, pointwise maximum and supremum, composition, minimization, and perspective functions. [96]

Definition 2.3.3. *An optimization problem*

$$\begin{aligned} \text{minimize} \quad & f_0(\mathbf{x}) \\ \text{subject to} \quad & f_{\mathrm{i}}(\mathbf{x}) \leq 0, \quad \mathrm{i} = 1, ..., m \\ & \mathbf{A}\mathbf{x} = \mathbf{b}, \end{aligned} \tag{2.40}$$

is called a convex optimization problem if $f_0(\mathbf{x})$ and $f_{\mathrm{i}}(\mathbf{x})$ are all convex functions, and $\mathbf{A}$ and $\mathbf{b}$ are constant matrix and vector. [96]

An example of a convex optimization problem is a linear program (LP), which is considered to be one type of convex optimization problem that can be solved efficiently.

Definition 2.3.4. *A general LP has the form*

$$\begin{aligned} \text{minimize} \quad & \mathbf{c}^{\mathrm{T}}\mathbf{x} \\ \text{subject to} \quad & \mathbf{G}\mathbf{x} \preceq \mathbf{h} \\ & \mathbf{A}\mathbf{x} = \mathbf{b}, \end{aligned} \tag{2.41}$$

where the general inequality $\preceq$ means $\mathbf{G}\mathbf{x}$ is less or equal to $\mathbf{h}$ on an element-wise basis.

For the convex optimization problem defined in Eq. (2.40), the Lagrangian L can be defined as below.

Definition 2.3.5. *The Lagrangian L associated with the problem Eq. (2.40) is defined as*

$$L(\mathbf{x}, \lambda, \mu) = f_0(\mathbf{x}) + \sum_{\mathrm{i}=1}^{m} \lambda_{\mathrm{i}} f_{\mathrm{i}}(\mathbf{x}) + \sum_{\mathrm{i}=1}^{p} \mu_{\mathrm{i}} h_{\mathrm{i}}(\mathbf{x}), \tag{2.42}$$

where λ_{i} *and* μ_{j} *are Lagrange multipliers associated with the* i*-th inequality constraint and* j*-th equality constraint. The vectors* λ *and* μ *are also called dual variables or Lagrange multiplier vectors.*

Definition 2.3.6. *The (Lagrange) dual function* g *associated with the problem Eq. (2.40) can then be defined as*

$$g(\lambda, \mu) = \inf_{\mathbf{x} \in D} L(\mathbf{x}, \lambda, \mu) = \inf_{\mathbf{x} \in D} \left(f_0(\mathbf{x}) + \sum_{\mathrm{i}=1}^{m} \lambda_{\mathrm{i}} f_{\mathrm{i}}(\mathbf{x}) + \sum_{\mathrm{i}=1}^{p} \mu_{\mathrm{i}} h_{\mathrm{i}}(\mathbf{x}) \right), \tag{2.43}$$

where D *is the domain of variable* $\mathbf{x}$*, and* inf *denotes the infimum.*

Definition 2.3.7. *The (Lagrange) dual problem associated with the problem Eq. (2.40) can be given as*

$$\begin{aligned} \text{maximize} \quad & g(\lambda, \mu) \\ \text{subject to} \quad & \lambda \succeq 0, \end{aligned} \tag{2.44}$$

where $\lambda \succeq 0$ *means each element in* λ *is larger than or equal to 0.*

The optimal duality gap is defined as the difference between the optimal primal and dual objective function values. For a convex optimization problem, if Slater's condition holds (i.e., there is at least one strict feasible point), the optimal objective function values of both primal and dual problems are the same which is also called strong duality (i.e., the optimal duality gap is 0) [96]. For constrained optimization algorithms, the Karush-Kuhn-Tucker (KKT) conditions are the first-order necessary conditions for a solution to be optimal. And the KKT conditions are closely related to the primal and dual problems.

2.3.2 Cone programming problem and its dual form

Definition 2.3.8. *A set* K *is called a cone, or nonnegative homogeneous, if for every* $\mathbf{x} \in K$*, and* $\theta \geq 0$*, we have* $\theta \mathbf{x} \in K$*. A set* K *is a convex cone if it is convex and a cone. [96]*

Definition 2.3.9. *A cone* $K \subseteq \mathbf{R}^n$ *is called a proper cone, if it satisfies the following: [96]*

- K *is convex*

- *K is closed, which means it contains all of its boundary points*
- *K is solid, which means it has nonempty interior*
- *K is pointed, which means if $\mathbf{x} \in K$, then $-\mathbf{x} \notin K$ unless $\mathbf{x} = 0$*

For convenience, the term "cone" consistently refers to a "proper cone" throughout this dissertation. An example of such proper cones is a norm cone associated with the vector or matrix norm $\|\cdot\|$ [96]

$$K = \{(\mathbf{x}, t) \subseteq \mathbf{R}^{n+1} \mid \|\mathbf{x}\| \leq t\} \tag{2.45}$$

One of the commonly seen norm cones is the second-order cone (SOC) associated with L^2 norm (it is also called the Lorentz cone)

$$K = \{(\mathbf{x}, t) \subseteq \mathbf{R}^{n+1} \mid \|\mathbf{x}\|_2 \leq t\} \tag{2.46}$$

Another example of cone is the positive semidefinite cone (PSDC)

$$\mathbf{S}_+^n = \{\mathbf{X} \in \mathbf{S}^n \mid \mathbf{X} \text{ is positive semidefinite}\} \tag{2.47}$$

where $\mathbf{S}^n$ denotes the set of n-by-n symmetric matrices.

Definition 2.3.10. *A proper cone K can be used to define a generalized inequality*

$$\mathbf{x} \preceq_K \mathbf{y} \;\Leftrightarrow\; \mathbf{y} - \mathbf{x} \in K. \tag{2.48}$$

Using the generalized inequality, we can modify the LP defined in Eq. (2.41) as

$$\begin{aligned} \text{minimize} \quad & \mathbf{c}^{\mathrm{T}}\mathbf{x} \\ \text{subject to} \quad & \mathbf{G}\mathbf{x} \preceq_K \mathbf{h} \\ & \mathbf{A}\mathbf{x} = \mathbf{b}, \end{aligned} \tag{2.49}$$

where the general inequality $\preceq$ now means $\mathbf{h} - \mathbf{G}\mathbf{x} \in K$. When K is the nonnegative orthant, this equation becomes an LP. The above-defined problem formulation is called a

cone program (CP). The cone programming problem can be viewed as the extension of linear programming by replacing the element-wise inequality as generalized inequality with respect to convex cones [96], [97]. The key properties of linear programming are preserved by cone programmings, such as reflexivity, antisymmetry, transitivity, and compatibility with linear operations, which allows some well-developed linear programming algorithms to be extended to cone programming so that the problem can be solved efficiently [97]. Usually, a more compact general form is used to express CP.

Definition 2.3.11. *A general CP has the form*

$$\begin{aligned} \text{minimize} \quad & \mathbf{c}^{\mathrm{T}}\mathbf{x} \\ \text{subject to} \quad & \mathbf{A}\mathbf{x} = \mathbf{b} \\ & \mathbf{x} \in K, \end{aligned} \tag{2.50}$$

where K is a Cartesian product of various proper cones.

Definition 2.3.12. *For a cone K, the dual cone of K can be defined as*

$$K_d = \{\mathbf{y} | \mathbf{x}^{\mathrm{T}}\mathbf{y} \geq 0 \text{ for all } \mathbf{x} \in K\}. \tag{2.51}$$

Definition 2.3.13. *A dual problem of the CP defined in Eq. (2.50) is*

$$\begin{aligned} \text{maximize} \quad & \mathbf{b}^{\mathrm{T}}\mathbf{y} \\ \text{subject to} \quad & \mathbf{A}^{\mathrm{T}}\mathbf{y} + \mathbf{s} = \mathbf{c} \\ & \mathbf{s} \in K_d, \end{aligned} \tag{2.52}$$

where $\mathbf{y}$ and $\mathbf{s}$ are dual variables associated with equality constraints and inequality constraints.

In this dissertation, one type of cone is particularly focused on, i.e., the self-dual cones.

Definition 2.3.14. *A cone K is called self-dual if its dual cone is the same set, i.e., $K_d = K$.*

If all cones in K in Eq. (2.50) are self-dual, the K_d in Eq. (2.52) can be changed to K. The efficient filter design method proposed in this dissertation (Chapter 3) heavily relies on the theory of self-dual CP reviewed in this section.

2.3.3 Warmstarting strategies

An initial point is required for solving the cone programming formulation Eq. (2.50) (2.52) due to the iterative nature of solving constrained optimization problems. Cold start means no a priori information of the optimization problem is considered while choosing the initial point. For example, starting from points well centered at the feasible set when using constrained optimization method [98], [99]. If some information such as the approximate location of the optimal solution point is known, the initial guess can be selected based on a priori information which is called the warmstarting method.

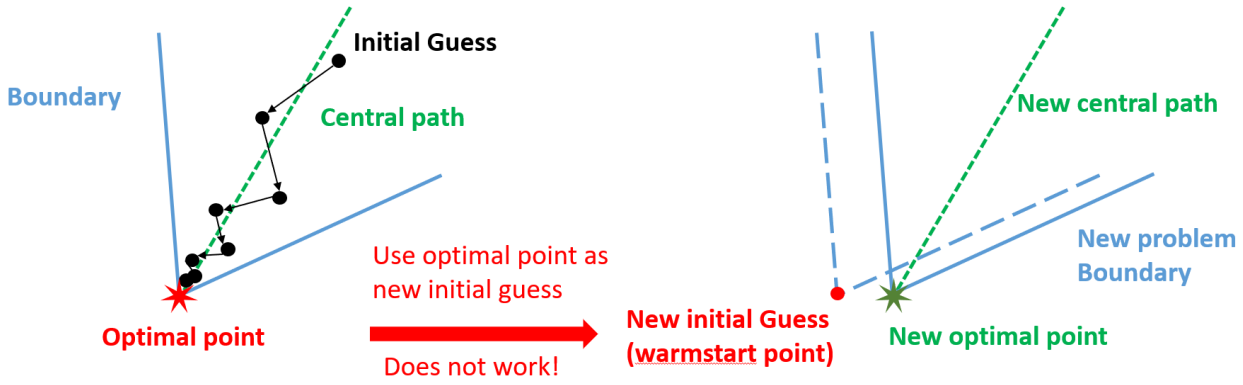


Figure 2.4. An illustration of the challenges of applying a direct warmstarting strategy to cone programming problems using the primal-dual interior-point methods.

The CP usually uses the primal-dual interior-point methods (PD-IPM) where applying warmstarting strategies is difficult as illustrated in Fig. 2.4. In Fig. 2.4, suppose an optimal solution is obtained for an optimization problem on the left side. A new optimization problem on the right side which has the solid line as feasible set boundaries is a perturbation of the optimization problem on the left side (with the dashed line as the original feasible set boundaries). The optimal solution is always at the feasible boundaries because of the linear

cost function in CP Eq. (2.50) (2.52). An initial point should be away from the boundaries and inside the feasible set, i.e., fall near the central path shown in Fig. 2.4. Using the original problem's optimal solution as the initial guess for the perturbed problem may lead to numerical issues if it is too close to or outside the feasible set boundaries [99].

In previous studies, the warmstarting strategies for PD-IPM have been investigated. Xia [100] proposed a warmstart strategy based on semismooth Newtons method, which requires the complementary conditions to be transformed into equations. In Gondzio and Grotheys work [101], a method leading the iterations back to a feasible region was proposed, which relies on sensitivity analysis on the Newton step. Skajaa et al. [102], [103] proposed a concise strategy with a convex combination of the cold start point of the current problem and the optimal solution of a similar problem. The warmstarting strategy for homogeneous and self-dual IPM proposed by Skajaa et al. [103] is reviewed in the following.

To solve the standard convex conic formulation Eq. (2.50) (along with Eq. (2.52)), a homogeneous and self-dual model is formulated as [103]

$$\begin{aligned}
\text{minimize} \quad & \theta\mu(z^0) \\
\text{subject to} \quad & \mathbf{A}\mathbf{x} - \mathbf{b}\tau = \theta r_p(z^0) \\
& -\mathbf{A}^{\mathrm{T}}\mathbf{y} - \mathbf{s} + \mathbf{c}\tau = \theta r_d(z^0) \\
& \mathbf{b}^{\mathrm{T}}\mathbf{y} - \mathbf{c}^{\mathrm{T}}\mathbf{x} - \kappa = \theta r_g(z^0) \\
& r_p(z^0)^{\mathrm{T}}\mathbf{y} - r_d(z^0)^{\mathrm{T}}\mathbf{x} + r_g(z^0)\tau = \mu(z^0) \\
& (\mathbf{x}, \tau) \geq 0, (\mathbf{s}, \kappa) \geq 0, (\mathbf{y}, \theta) \text{ free},
\end{aligned} \tag{2.53}$$

where $\mathbf{z} = (\mathbf{x}, \tau, \mathbf{y}, \mathbf{s}, \kappa)$ are the variables (τ and κ are two additional variables to make the formulation self-dual), $\mathbf{z}^0 = (\mathbf{x}^0, \tau^0, \mathbf{y}^0, \mathbf{s}^0, \kappa^0)$ are the initial points, and

$$\begin{aligned}
r_p(z) &= \mathbf{A}\mathbf{x} - \mathbf{b}\tau \\
r_d(z) &= -\mathbf{A}^{\mathrm{T}}\mathbf{y} - \mathbf{s} + \mathbf{c}\tau \\
r_g(z) &= \mathbf{b}^{\mathrm{T}}\mathbf{y} - \mathbf{c}^{\mathrm{T}}\mathbf{x} - \kappa \\
\mu(z) &= (\mathbf{x}^{\mathrm{T}}\mathbf{s} + \tau\kappa)/(\nu + 1),
\end{aligned}$$

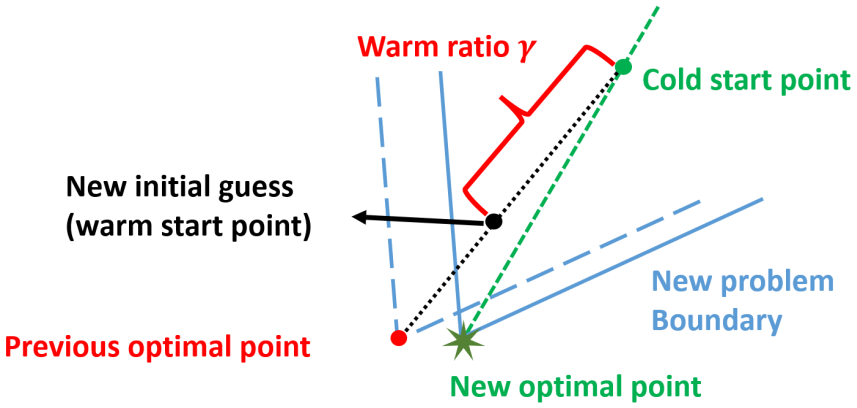


Figure 2.5. An illustration of the reviewed warmstarting strategy.

We can denote the commonly used cold start point as z^c. In this dissertation, $z^c = (\mathbf{x}^c, \tau^c, \mathbf{y}^c, \mathbf{s}^c, \kappa^c)$ is chosen using the same strategy in SDPT3 [104] which is a point well centered in the feasible set. Then the warmstarting point proposed is [103]:

$$\begin{aligned}
\mathbf{x}^0 &= \gamma\ \mathbf{x}_{opt} + (1-\gamma)\ \mathbf{x}^c \\
\mathbf{s}^0 &= \gamma\ \mathbf{s}_{opt} + (1-\gamma)\ \mathbf{s}^c \\
\mathbf{y}^0 &= \gamma\ \mathbf{y}_{opt} \\
\tau^0 &= \tau^c \\
\kappa^0 &= \mathbf{x}^{0\ \mathrm{T}}\mathbf{s}^0/N,
\end{aligned} \tag{2.54}$$

where $\mathbf{x}_{opt}$, $\mathbf{s}_{opt}$, and $\mathbf{y}_{opt}$ are known optimal solutions (i.e., the priori information) of a similar (or perturbed) optimization problem. $0 \leq \gamma \leq 1$ is the warm ratio representing the relative location of the warmstarting point between the optimal solution of a similar optimization problem and the cold start point of the current optimization problem. N is the dimension of the variables $\mathbf{x}$ or $\mathbf{s}$. A graphical illustration of this warmstarting is shown in Fig. 2.5. The warm ratio essentially interpolates a point in between the cold start point and the optimal point from a similar optimization problem such that it falls inside the feasible set and is near the central path to prevent numerical issues, while the interpolated point (warmstart point) is also closer to the new optimal point to reduce the required iterations. One advantage of this warmstarting method is that the required computational effort is small, and no iterative

process is involved. Thus, this warmstarting strategy has good numerical efficiency and stability.

One challenge of their proposed warmstarting method is that it cannot work properly for PSDCs which are illustrated in reference [89] and Chapter 3. Soon it will be demonstrated that ANC formulation will naturally have PSDCs because of the stability constraint Eq. (2.15) and robustness constraints Eq. (2.16). Constraint modifications will be proposed in Section 3.3 so this warmstarting method can be applied.

3. EFFICIENT MULTI-CHANNEL CONSTRAINED OPTIMAL ACTIVE SOUND CONTROL FILTER DESIGN

As reviewed in Section 2.1, the regularization parameter (or the leaky FxLMS) can be over-conservative and sacrifice the control performance because it satisfies multiple constraints simultaneously by tuning just one regularization parameter (or the leakage factor). The constrained optimization method can achieve better control performance but the computational load is significant. In this chapter, an efficient multi-channel constrained optimal ASC filter design method is proposed based on the traditional constrained optimization method. It is noted that the proposed formulation in this chapter is discussed based on the non-adaptive ANC applications. The application of the proposed method on other ASC applications such as adaptive ANC, room equalization filter design, or hear-through filter design can be found in Chapter 4.

3.1 Convexification and Reformulation

In this section, the original optimization problem, Eq. (2.17), is convexified and reformulated into a convex optimization problem. Thus, the global optimal solution can be found [96]. Computationally efficient algorithms can also be applied to the convex problem.

As reviewed in Section 2.3, a convex optimization problem requires the objective function and all inequality constraint functions to be convex. Eq. (2.17) does not meet this requirement since the functions in the inequalities for stability constraints are not convex (which can easily be shown by checking the Definition 2.3.2 of convex functions). Some convexification is proposed to reformulate the stability constraint in Section 3.1.1. All the other constraints and the objective function listed in Eq. (2.17) are already convex. For the benefit of analyzing the convexity of the optimization problem and describing further reformulations in later sections, some simplifications to Eq. (2.17) are also introduced in section 3.1.2 and it will be soon shown that theses simplified formulations, although equivalent to the original formulation, are essential to improve the efficiency of the proposed method.

3.1.1 Convexification of the stability constraint

Since the stability constraint is the only constraint that is not convex, only this constraint needs to be relaxed to accomplish the problem convexification. Eq. (2.15) can first be reformulated as:

$$\max\left(\mathrm{Re}\left(\lambda\left(-\mathbf{W}_x(f_k)\hat{\mathbf{G}}_s(f_k)\right)\right)\right) < 1. \tag{3.1}$$

It is noted that the operation of taking the real part of eigenvalues is not convex. For brevity, $\mathbf{A}_s(f_k)$ is used to represent $-\mathbf{W}_x(f_k)\hat{\mathbf{G}}_s(f_k)$ in the following modification process. And $\lambda_1\left(\mathbf{A}_s(f_k)\right)$ denotes the eigenvalue of $-\mathbf{W}_x(f_k)\hat{\mathbf{G}}_s(f_k)$ with the largest real part. Then, Eq. (3.1) can be expressed as:

$$\mathrm{Re}\left(\lambda_1\left(\mathbf{A}_s(f_k)\right)\right) = \frac{\lambda_1\left(\mathbf{A}_s(f_k)\right) + \lambda_1\left(\mathbf{A}_s(f_k)\right)^*}{2} < 1, \tag{3.2}$$

where $*$ denotes the complex conjugate of a complex number. Now suppose $\boldsymbol{\nu}_1$ is an eigenvector associated with $\lambda_1\left(\mathbf{A}_s(f_k)\right)$, so $\lambda_1\left(\mathbf{A}_s(f_k)\right) = \frac{\boldsymbol{\nu}_1^{\mathrm{H}}\mathbf{A}_s(f_k)\boldsymbol{\nu}_1}{\|\boldsymbol{\nu}_1\|_2^2}$. Then Eq. (3.2) becomes:

$$\mathrm{Re}\left(\lambda_1\left(\mathbf{A}_s(f_k)\right)\right) = \frac{\boldsymbol{\nu}_1^{\mathrm{H}}\left(\frac{\mathbf{A}_s(f_k)+\mathbf{A}_s(f_k)^{\mathrm{H}}}{2}\right)\boldsymbol{\nu}_1}{\|\boldsymbol{\nu}_1\|_2^2} < 1. \tag{3.3}$$

Now in order to achieve convexity, Eq. (3.3) can be relaxed by enforcing it to be satisfied not only for $\boldsymbol{\nu}_1$, but for any arbitrary vectors, which is equivalent to:

$$\max\left(\lambda\left(\frac{\mathbf{A}_s(f_k) + \mathbf{A}_s(f_k)^{\mathrm{H}}}{2}\right)\right) < 1. \tag{3.4}$$

Since Eq. (3.4) is obtained by relaxing Eq. (3.3), it serves as an upper bound for Eq. (3.1), i.e., a more restricted stability constraint. This constraint function is convex because it takes the largest eigenvalue of a Hermitian matrix [96] and this matrix is obtained by the linear transform of design variables, $\mathbf{w}_{i,j}$. It is noted that the use of Eq. (3.4) is still a less conservative stability constraint compared with some other constraints used in previous studies. For example, sometimes controller stability is ensured by limiting the eigenvalues of $\mathbf{W}_x(f_k)\hat{\mathbf{G}}_s(f_k)$ to be inside the unit circle [46], which is not convex either. There are

some other stability constraints used in some studies that are indeed convex, e.g., limiting the multiplication of the largest singular value of $\mathbf{W}_x(f_k)$ and the largest singular value of $\hat{\mathbf{G}}_s(f_k)$ to be less than 1 [46]:

$$\|\mathbf{W}_x(f_k)\|_2\|\hat{\mathbf{G}}_s(f_k)\|_2 < 1, \tag{3.5}$$

where $\| \bullet \|_2$ denotes the spectral norm (the maximum singular value) of a matrix. Or sometimes a slightly less conservative but still convex constraint was used in previous studies:

$$\|\mathbf{W}_x(f_k)\hat{\mathbf{G}}_s(f_k)\|_2 = \|\mathbf{A}_s(f_k)\|_2 < 1. \tag{3.6}$$

It can also be demonstrated that the proposed stability constraint (expressed in Eq. (3.4)) is less conservative than the ones expressed in Eq. (3.5) or Eq. (3.6). Thus, the associated ANC performance resulting from the proposed method can, in principle, be better. To show that Eq. (3.4) is less conservative, it can be first shown that:

$$\begin{aligned}
\max\left(\lambda\left(\frac{\mathbf{A}_s(f_k)+\mathbf{A}_s(f_k)^{\mathrm{H}}}{2}\right)\right) &\leq \left\|\frac{\mathbf{A}_s(f_k)+\mathbf{A}_s(f_k)^{\mathrm{H}}}{2}\right\|_2 \\
&\leq \frac{\|\mathbf{A}_s(f_k)\|_2 + \left\|\mathbf{A}_s(f_k)^{\mathrm{H}}\right\|_2}{2} \\
&= \|\mathbf{A}_s(f_k)\|_2 \\
&\leq \|\mathbf{W}_x(f_k)\|_2\|\hat{\mathbf{G}}_s(f_k)\|_2,
\end{aligned} \tag{3.7}$$

where the first inequality comes from the fact that the maximum eigenvalue of a matrix is always smaller or equal to its spectral norm; the second and fourth inequalities come from the triangle property and sub-multiplicativity properties of the spectral norm. Eq. (3.7) demonstrated that if either Eq. (3.5) or Eq. (3.6) is satisfied, then Eq. (3.4) will be satisfied. But neither Eq. (3.5) nor Eq. (3.6) is equivalent to Eq. (3.4) because it is easy to find matrices, $\mathbf{A}_s(f_k)$, such that the strict inequalities hold in Eq. (3.7). This proves that Eq. (3.4) is less conservative compared with Eq. (3.5) or Eq. (3.6).

In a convex optimization problem, the inequality constraints need to be non-strict. So a very small positive constant ϵ_s is introduced to ensure strict stability when expressed as a non-strict constraint. Eq. (3.4) can now become:

$$\max\left(\lambda\left(\frac{\mathbf{A}_s(f_k)+\mathbf{A}_s(f_k)^{\mathrm{H}}}{2}\right)\right)-(1-\epsilon_s)\leq 0. \tag{3.8}$$

Equation (3.8) can be used to replace Eq. (2.15) as the stability constraint so the ANC filter design problem is convex. The effectiveness of the proposed stability constraint is illustrated in experimental results shown in Section 3.5.2 and 3.5.3.

3.1.2 Reformulation of the objective function and other constraint functions

The objective function, Eq. (2.11), is the total power of the error signal which is convex in nature. For the benefit of applying optimization algorithms, it is simplified into a standard quadratic form. Firstly, Eq. (2.12) can be simplified to a standard quadratic form as (See Appendix A.1 for detail):

$$J(f_k)=\mathbf{w}^{\mathrm{T}}\mathbf{A}_J(f_k)\mathbf{w}+\mathbf{b}_J^{\mathrm{T}}(f_k)\mathbf{w}+c_J(f_k), \tag{3.9}$$

where

$$\begin{aligned}
&\mathbf{A}_J(f_k)=\mathrm{Re}\Big\{\Big(\mathbf{G}_{\mathrm{e}}^{\mathrm{H}}(f_k)\mathbf{G}_{\mathrm{e}}(f_k)\Big)\otimes\mathbf{S}_{xx}^{\mathrm{T}}(f_k)\otimes\Big(\mathbf{F}_z^{*}(f_k)\mathbf{F}_z^{\mathrm{T}}(f_k)\Big)\Big\},\\
&\mathbf{b}_J(f_k)=2\,\mathrm{Re}\Big\{\mathrm{vec}\Big[\,(\mathbf{S}_{xd}(f_k)\mathbf{G}_{\mathrm{e}}(f_k))\otimes\mathbf{F}_z(f_k)\Big]\Big\},\\
&c_J(f_k)=\mathrm{tr}\left(\mathbf{S}_{dd}(f_k)\right),\\
&\mathbf{w}=\Big[\mathbf{w}_{1,1}^{\mathrm{T}},\ \ \ldots,\ \ \mathbf{w}_{1,N_r}^{\mathrm{T}},\ \ \mathbf{w}_{2,1}^{\mathrm{T}},\ \ \ldots,\ \ \mathbf{w}_{N_s,N_r}^{\mathrm{T}}\Big]^{\mathrm{T}},
\end{aligned}$$

vec() converts a matrix to a vector by stacking the columns [105] and $\otimes$ denotes Kronecker product. To show that $J(f_k)$ is a convex function of filter coefficients [96], it is noted that in Eq. (3.9), the Hessian of quadratic function $J(f_k)$ is $2\mathbf{A}_J(f_k)$, and that $\mathbf{G}_{\mathrm{e}}^{\mathrm{H}}(f_k)\mathbf{G}_{\mathrm{e}}(f_k)$, $\mathbf{F}_z^{*}(f_k)\mathbf{F}^{\mathrm{T}}(f_k)$ and $\mathbf{S}_{xx}^{\mathrm{T}}(f_k)$ are always positive semidefinite by their definitions. So $\mathbf{A}_J(f_k)$ is positive semidefinite because of the Kronecker product properties. The original objective function Eq. (2.11) can be simplified firstly by using Eq. (3.9) and then dropping the constant

term $\mathbf{c}_J(f_k)$, which will not affect the resulting optimal solution. The simplified objective function can be expressed as:

$$J_0 = \mathbf{w}^{\mathrm{T}} \left(\sum_{k=1}^{N_f} \mathbf{A}_J(f_k) \right) \mathbf{w} + \sum_{k=1}^{N_f} \mathbf{b}_J^{\mathrm{T}}(f_k)\ \mathbf{w}. \tag{3.10}$$

It is noted that J_0 in Eq. (3.10) is also a convex function because the Hessian matrix of J_0, i.e., $2\sum_{k=1}^{N_f} \mathbf{A}_J(f_k)$, is positive semidefinite since it is a summation of positive semidefinite matrices. Also, the dimension of the objective function is independent of the number of frequencies after this simplification. This mathematical property provides an advantage of this formulation that even if a fine frequency resolution is chosen in the objective function expression, it will not increase the computational complexity, which will be illustrated in experimental results shown in Section 3.5.4.

For the noise amplification (disturbance enhancement) constraint, Eq. (2.13), it can also be simplified by using Eq. (3.9), which results in:

$$\mathbf{w}^{\mathrm{T}} \mathbf{A}_J(f_k) \mathbf{w} + \mathbf{b}_J^{\mathrm{T}}(f_k)\ \mathbf{w} + \tilde{c}_J(f_k) \leq 0, \tag{3.11}$$

where

$$\tilde{c}_J(f_k) = c_J(f_k)(1 - A_{\mathrm{e}}(f_k)) = \mathrm{tr}\left(\mathbf{S}_{dd}(f_k)\right)(1 - A_{\mathrm{e}}(f_k)).$$

The proof of convexity of this constraint function (Eq. (3.11)) is similar to the proof for Eq. (3.9).

For control filter response magnitude constraint, Eq. (2.14), by using Eq. (2.9), it can be expressed as:

$$\|\mathbf{F}_z^{\mathrm{T}}(f_k)\mathbf{w}_{i,j}\|_2 - C_{i,j}(f_k) \leq 0, \tag{3.12}$$

which is convex because it is the $\mathbf{L}_2$ norm of a vector obtained by linear transforms of the optimization variables [96].

For robustness constraint, Eq. (2.16), it can be simply expressed as:

$$\max\left(\sigma\left(\mathbf{A}_s(f_k)\right)\right) B(f_k) - 1 \leq 0. \tag{3.13}$$

Eq. (3.13) is already in a convex form because the maximum singular value is a matrix norm, and each matrix element is obtained by a linear transform of variables $\mathbf{w}$ [96].

3.1.3 Summary of the convexified formulation

Now, the convex formulation of designing multi-channel constrained optimal ANC filter can be constructed by using Eq. (3.10) as objective function and Eqs. (3.11), (3.12), (3.8), (3.13) as constraints:

$$
\begin{aligned}
\underset{\mathbf{w}}{\text{minimize}} \quad & \mathbf{w}^{\mathrm{T}} \left(\sum_{k=1}^{N_f} \mathbf{A}_J(f_k) \right) \mathbf{w} + \sum_{k=1}^{N_f} \mathbf{b}_J^{\mathrm{T}}(f_k)\ \mathbf{w}, \\
\text{subject to} \quad & \mathbf{w}^{\mathrm{T}} \mathbf{A}_J(f_k) \mathbf{w} + \mathbf{b}_J^{\mathrm{T}}(f_k)\ \mathbf{w} + \tilde{c}_J(f_k) \leq 0, \quad \text{for all } f_k, \\
& \|\mathbf{F}_z^{\mathrm{T}}(f_k) \mathbf{w}_{i,j}\|_2 - C_{i,j}(f_k) \leq 0, \quad \text{for all } f_k,\ i,\ \text{and } j, \\
& \max\left(\lambda \left(\frac{\mathbf{A}_s(f_k) + \mathbf{A}_s(f_k)^{\mathrm{H}}}{2} \right) \right) - (1 - \epsilon_s) \leq 0, \quad \text{for all } f_k, \\
& \max\left(\sigma\left(\mathbf{A}_s(f_k) \right) \right) B(f_k) - 1 \leq 0, \quad \text{for all } f_k.
\end{aligned}
\tag{3.14}
$$

Because of the convexity, a global optimal solution of this optimization problem Eq. (3.14) can always be found by using a gradient-based algorithm if the problem is feasible [96].

This simplified convex formulation Eq. (3.14) can also provide useful insights into ANC system design. For example, if no constraints are applied, it is usually preferred that the Hessian of the objective function is strict positive-definite so that the global minimum is unique and the convergence rate of the optimization algorithm is fast [96]. If the Hessian matrix of the objective is singular, the resulting optimal filter coefficients may not be unique and tend to be unnecessarily large without proper further constraints. By observing the Hessian matrix of J_0 (i.e., $2\sum_{k=1}^{N_f} \mathbf{A}_J(f_k)$), the strict positive definiteness preference implies that it is preferred:

- The number of frequencies in the objective function is larger than the number of filter coefficients ($\mathbf{A}_J(f_k)$ is a rank-one matrix due to the fact that $\mathbf{F}_z$ is a vector).
- Different channels of reference signals are uncorrelated and have similar power (i.e., $\mathbf{S}_{xx}$ is close to identity).

- The number of secondary sources is not larger than the number of error sensors (otherwise $\mathbf{G}_{\mathrm{e}}^{\mathrm{H}}(f_k)\mathbf{G}_{\mathrm{e}}(f_k)$ will be singular).

However, even if the above-mentioned conditions are not satisfied, with the help of constraints in Eqs. (3.8), (3.11), (3.13), and (3.12), appropriate control filters can still be found.

Some convex toolboxes can be used to solve this problem Eq. (3.14), e.g., the CVX toolbox [106], [107]. This toolbox reformulates the general disciplined convex optimization problem into a cone programming problem and uses cone programming solvers to solve it. To save time on reformulation in the CVX toolbox, this reformulation to cone programming can also be done analytically and use cone programming solvers directly, e.g., SDPT3 [98], [108], [109], SeDuMi [99], [110], or MOSEK [111], where primal-dual interior-point methods designed specifically for cone programming is implemented. Those algorithms can process non-differentiable constraints in Eq. (3.14) efficiently.

3.2 Cone Programming Reformulation

In this section, the proposed convex formulation, Eq. (3.14), is reformulated explicitly to a cone programming problem. As reviewed in Section 2.3, the objective function should be a linear function, the equality constraints should be affine functions, and the inequality constraints should be expressed as nonnegative constraints, SOCs, or PSDCs.

The reason for reformulating the proposed convex formulation Eq. (3.14) is:

- Although the time complexity of solving a general convex optimization problem can be polynomially bounded for appropriate algorithms [112], it does not mean that all convex optimization problems can always be solved quickly in practice. As reviewed in Section 2.3, cone programming is considered as one of the problem types that can be solved efficiently.

- Equation (3.14) involves nondifferentiable functions which add difficulties to solving them numerically. While by formulating the cone programming problems, it can be solved by specifically designed algorithms where special treatments are available to handle the nondifferentiable problems [113].

3.2.1 Conic formulation using the conventional reformulation procedure

The goal of this section is to reformulate Eq. (3.14) to a standard semidefinite-quadratic-linear programming (SQLP) problem [98] (sometimes also referred to as a mixed semidefinite and second order cone optimization problem [99]). One common cone programming formulation is shown in Eq. (2.50), where, in the proposed formulation, K should be a Cartesian product of SOCs defined in Eq. (2.46) and PSDCs defined in Eq. (2.47).

The objective function, filter response magnitude constraint, and noise amplification constraint are reformulated into SOCs because they are quadratic functions in essence. Those quadratic functions are firstly linearized by replacing the second-order terms with introduced additional variables. To ensure equivalence, the introduced variables are constrained by SOCs related to the second-order terms in original quadratic functions. The reformulated functions are further rearranged into the standard form as in Eqs. (A.13), (A.16), and (A.19) (A detailed description of this reformulation process can be found in Appendix A.2). One thing to note is that a better expression is proposed when obtaining Eq. (A.14) during the noise amplification constraint reformulation instead of using a conventional method. Compared with the conventional method (brutal force matrix square root operation on $\mathbf{A}_J(f_k)$), two significant advantages of using the proposed Eq. (A.14) are (use an example of 2-input-2-output ANC system with 64 filter coefficients in each channel)

- The resulting dimension is N_t times smaller (i.e., 64 times smaller in this example) which greatly improves the algorithm efficiency.
- The dimensions in the required numerical matrix square operation are N_r by N_r and N_s by N_s (i.e., 2 by 2 in this example), instead of $N_rN_sN_t$ by $N_rN_sN_t$ (i.e., 256 by 256 in this example), which makes the proposed formulation more numerical efficient and reliable.

The stability constraint and the robustness constraint are reformulated into PSDCs because they involve constraining the maximum eigenvalues or singular values of some matrices. Those reformulations are also equivalent and the reformulated functions are further

rearranged into the standard form as Eqs. (A.26), and (A.27) (A detailed description of this reformulation process can be found in Appendix A.3).

Finally, the constrained multi-channel ANC filter design optimization problem, Eq. (3.14), can be reformulated in a standard form by combining Eqs. (A.13), (A.16), (A.19), (A.26), (A.27):

$$\begin{aligned} \underset{\mathbf{w},\ \mathbf{x}}{\text{minimize}} \quad & \begin{bmatrix} (\mathbf{c}_w)^{\mathrm{T}} & (\mathbf{c}_x)^{\mathrm{T}} \end{bmatrix} \begin{bmatrix} \mathbf{w} \\ \mathbf{x} \end{bmatrix} \\ \text{subject to} \quad & \begin{bmatrix} \mathbf{A} & \mathbf{B} \end{bmatrix} \begin{bmatrix} \mathbf{w} \\ \mathbf{x} \end{bmatrix} = \mathbf{b} \\ & \mathbf{w} \in \mathbf{R}^{N_r N_s N_t} \\ & \mathbf{x} \in K, \end{aligned} \tag{3.15}$$

where $\mathbf{x}$ is a concatenation of $\mathbf{x}_0$ in Eq. (A.13), $\mathbf{x}_{1,k}$ in Eq. (A.16), $\mathbf{x}_{2,l,k}$ in Eq. (A.19), $\mathbf{x}_{3,k}$ in Eq. (A.26), and $\mathbf{x}_{4,k}$ in Eq. (A.27) for all k and l, $\mathbf{c}_x$ is a sparse vector whose first element is the only non-zero element with value 1, $\mathbf{A}$ is obtained by vertically concatenating $\mathbf{A}_0$, $\mathbf{A}_{1,k}$, $\mathbf{A}_{2,l,k}$, $\mathbf{A}_{3,k}$, and $\mathbf{A}_{4,k}$ for all k and l, $\mathbf{B}$ is a sparse block diagonal matrix obtained by diagonally concatenating $\mathbf{B}_0$, $\mathbf{B}_{1,k}$, $\mathbf{B}_{2,l,k}$, $\mathbf{B}_{3,k}$, and $\mathbf{B}_{4,k}$ for all k and l, $\mathbf{b}$ is obtained by vertically concatenating $\mathbf{b}_0$, $\mathbf{b}_{1,k}$, $\mathbf{b}_{2,l,k}$, $\mathbf{b}_{3,k}$, and $\mathbf{b}_{4,k}$ for all k and l, K is a Cartesian product of all associated cones (A detailed expression for these constant matrices and vectors can be found in Appendix A.2 and A.3).

The cone programming problem specified in Eq. (3.15) can be directly solved by solvers with primal-dual interior-point algorithms designed specifically for cone programming, e.g., SeDuMi [99], [110], SDPT3 [98], [104], or MOSEK [111]. However, in the practical ANC applications where the number of frequencies of interest is much larger than the order of filters, the number of additionally introduced variables, $\mathbf{x}$, is much larger than the dimension of $\mathbf{w}$, which enlarges the problem size significantly. Also, the definition of cone programming, Eq. (2.50), shows that no free variables (i.e., the variables that are not in any conic constraints) are allowed. However, $\mathbf{w}$ in Eq. (3.15) is a set of free variables. Although redundant constraints can be used to convert free variables to variables constrained by redundant conic constraints, numerical behavior may be degraded due to these additional redundant con-

straints [104], [110]. In a previous study, Zhuang and Liu also demonstrated the numerical stability issue associated with the free variables in ANC applications [60].

In a four-input-two-output ANC system with filter length 128, the number of free variables $\mathbf{w}$ in Eq. (3.15) is 1024, and such a large number of free variables can cause numerical instability. Thus, the direct use of Eq. (3.15) may not converge to a satisfactory filter coefficients solution or even fail to give a solution [60] and these numerical issues will be demonstrated in the simulation results section (Section 3.5.5).

As a physical interpretation, the free variables in ANC application come from the fact that most of the constraints on filter design are applied in the frequency domain instead of directly on the filter coefficients. By using the standard procedure, redundant variables and constraints have to be introduced, which, although equivalent in theory, causes numerical stability problems in practice. In the next section, an improved formulation is proposed to eliminate those redundant variables and constraints to prevent numerical instability.

3.2.2 Proposed conic formulation using the duality properties

The problem structure of Eq. (3.15) can be further exploited and simplified. The goal of the proposed formulation in this section is to eliminate the free variables and reduce the problem formulation dimension because they both contribute to the numerical stability issues.

First, $\mathbf{c}_x$ in Eq. (3.15) has only one non-zero element because only t_0 appears in the objective function. One introduced a new dummy variable w_{dum} that always equals t_0 can be appended to the end of $\mathbf{w}$. After this regrouping, Eq. (3.15) can then be reformulated equivalently as:

$$\begin{aligned} \underset{\tilde{\mathbf{w}},\ \mathbf{x}}{\text{minimize}} \quad & (\tilde{\mathbf{c}}_w)^{\mathrm{T}}\tilde{\mathbf{w}} \\ \text{subject to} \quad & \begin{bmatrix} \tilde{\mathbf{A}} & \tilde{\mathbf{B}} \end{bmatrix} \begin{bmatrix} \tilde{\mathbf{w}} \\ \mathbf{x} \end{bmatrix} = \tilde{\mathbf{b}} \\ & \tilde{\mathbf{w}} \in \mathbf{R}^{N_r N_s N_t + 1} \\ & \mathbf{x} \in K, \end{aligned} \tag{3.16}$$

where,

$$\tilde{\mathbf{w}} = \begin{bmatrix} \mathbf{w} \\ w_{dum} \end{bmatrix}, \quad \tilde{\mathbf{c}}_w = \begin{bmatrix} \mathbf{c}_w \\ 1 \end{bmatrix}, \quad \tilde{\mathbf{b}} = \begin{bmatrix} 0 \\ \mathbf{b} \end{bmatrix}, \quad \tilde{\mathbf{A}} = \begin{bmatrix} \mathbf{0} & -1 \\ \mathbf{A} & \mathbf{0} \end{bmatrix}, \quad \tilde{\mathbf{B}} = \begin{bmatrix} 1 & \mathbf{0} \\ & \mathbf{B} \end{bmatrix}.$$

Reformulation to Eq. (3.16) has two benefits compared with Eq. (3.15):

- Variables that are constrained by cones no longer appear in the objective function directly, which is a key step to allow simplification described later in this section.
- The added one row, $[1 \quad \mathbf{0}]$, to $\mathbf{B}$, makes $\tilde{\mathbf{B}}$ a square block diagonal matrix with each block being square. Thus, an inversion is possible for matrix $\tilde{\mathbf{B}}$ and this is another key step in the following derivations.

It can be further noticed that all blocks in $\tilde{\mathbf{B}}$ are invertible and well-conditioned which suggests that $\tilde{\mathbf{B}}$ is always invertible and well-conditioned. As shown in Appendix A.4, the analytical expressions of the inversion of $\tilde{\mathbf{B}}$ can be derived so calculating $\tilde{\mathbf{B}}^{-1}\tilde{\mathbf{A}}$ and $\tilde{\mathbf{B}}^{-1}\tilde{\mathbf{b}}$ does not require extra computational effort (see Appendix A.4 for detail).

By multiplying the inverse of $\tilde{\mathbf{B}}$ to both sides of the equality constraints, Eq. (3.16) can be formulated as:

$$\begin{aligned} \underset{\tilde{\mathbf{w}},\ \mathbf{x}}{\text{minimize}} \quad & (\tilde{\mathbf{c}}_w)^{\mathrm{T}}\tilde{\mathbf{w}} \\ \text{subject to} \quad & \begin{bmatrix} \tilde{\mathbf{B}}^{-1}\tilde{\mathbf{A}} & \mathbf{I} \end{bmatrix} \begin{bmatrix} \tilde{\mathbf{w}} \\ \mathbf{x} \end{bmatrix} = \tilde{\mathbf{B}}^{-1}\tilde{\mathbf{b}} \\ & \tilde{\mathbf{w}} \in \mathbf{R}^{N_r N_s N_t + 1} \\ & \mathbf{x} \in K. \end{aligned} \tag{3.17}$$

Note that the cones in Eq. (3.17) (i.e., the SOCs and PSDCs) are all self-dual cones [99], thus, the cone K in Eq. (3.17) is a self-dual cone. As reviewed in Section 2.3, the dual cone of the cone K in Eq. (3.17) will still be K. So the dual problem of Eq. (3.17) is (note that a negative sign is added to the objective function to change the dual problem from "maximize" to "minimize"):

$$
\begin{aligned}
\underset{\mathbf{y},\ \mathbf{z}_1,\ \mathbf{z}_2}{\text{minimize}} \quad & -(\tilde{\mathbf{B}}^{-1}\tilde{\mathbf{b}})^{\mathrm{T}}\mathbf{y} \\
\text{subject to} \quad & \begin{bmatrix} \left(\tilde{\mathbf{B}}^{-1}\tilde{\mathbf{A}}\right)^{\mathrm{T}} \\ \mathbf{I} \end{bmatrix} \mathbf{y} + \begin{bmatrix} \mathbf{z}_1 \\ \mathbf{z}_2 \end{bmatrix} = \begin{bmatrix} \tilde{\mathbf{c}}_w \\ \mathbf{0} \end{bmatrix} \\
& \mathbf{y} \in \mathbf{R}^m \\
& \mathbf{z}_1 = \mathbf{0} \\
& \mathbf{z}_2 \in K,
\end{aligned}
\tag{3.18}
$$

where, $\mathbf{y}$, $\mathbf{z}_1$, and $\mathbf{z}_2$ are the dual variables associated with equality constraints, free variables $\tilde{\mathbf{w}}$, and conic constraints respectively in Eq. (3.17); and m is the row number of $\tilde{\mathbf{B}}$. From the lower portion of the equality constraints in Eq. (3.18), it can be derived that $\mathbf{y} = -\mathbf{z}_2$ (This is the direct result of the first benefit mentioned earlier). And by further substitute $\mathbf{z}_1 = \mathbf{0}$ back into the equality constraints, Eq. (3.18) can be simplified by eliminating $\mathbf{z}_1$ and $\mathbf{z}_2$:

$$
\begin{aligned}
\underset{-\mathbf{y}}{\text{minimize}} \quad & (\tilde{\mathbf{B}}^{-1}\tilde{\mathbf{b}})^{\mathrm{T}}(-\mathbf{y}) \\
\text{subject to} \quad & \left(\tilde{\mathbf{B}}^{-1}\tilde{\mathbf{A}}\right)^{\mathrm{T}}(-\mathbf{y}) = -\tilde{\mathbf{c}}_w \\
& (-\mathbf{y}) \in K.
\end{aligned}
\tag{3.19}
$$

This formulation Eq. (3.19) is the proposed simplified formulation. Because the dimension of the problem is greatly reduced and no free variables are involved in this formulation, numerical stability can be significantly improved when standard cone programming algorithms are used to solved this problem.

3.2.3 Obtaining filter coefficients from the proposed conic formulation

Equation (3.19) does not have filter coefficients as its variables explicitly. Instead, the filter coefficients are the dual variables associated with equality constraints of Eq. (3.19) if Eq. (3.19) is treated as a standard primal form with $(-\mathbf{y})$ as primal variables. When primal-dual interior-point algorithms are used for this simplified problem (Eq. (3.19)), the dual variables can be obtained without extra computational effort because the dual solution is calculated along with the primal solution [99], [104], [109], [110]. This means that, although

the problem formulated in Eq. (3.19) is not directly based on ANC filter coefficients, the optimal filter coefficients are indeed direct results from common numerical cone programming algorithms.

To show the relationship between filter coefficients $\tilde{\mathbf{w}}$ and the proposed formulation Eq. (3.19), rewrite Eq. (3.17) as:

$$\begin{aligned} \underset{\tilde{\mathbf{w}},\ \mathbf{x}}{\text{maximize}} \quad & (-\tilde{\mathbf{c}}_w)^{\mathrm{T}}\tilde{\mathbf{w}} \\ \text{subject to} \quad & \left(\left(\tilde{\mathbf{B}}^{-1}\tilde{\mathbf{A}}\right)^{\mathrm{T}}\right)^{\mathrm{T}}\tilde{\mathbf{w}} + \mathbf{x} = \tilde{\mathbf{B}}^{-1}\tilde{\mathbf{b}} \\ & \tilde{\mathbf{w}} \in \mathbf{R}^{N_r N_s N_t + 1} \\ & \mathbf{x} \in K. \end{aligned} \tag{3.20}$$

Eq. (3.20) fits a standard dual form (of another primal problem), where $\tilde{\mathbf{w}}$ and $\mathbf{x}$ are the dual variables associated with equality and conic constraints in that primal problem respectively. Then it is easy to obtain the associated primal form as [99], [104], [109], [110]:

$$\begin{aligned} \underset{\mathbf{s}}{\text{minimize}} \quad & (\tilde{\mathbf{B}}^{-1}\tilde{\mathbf{b}})^{\mathrm{T}}\mathbf{s} \\ \text{subject to} \quad & \left(\tilde{\mathbf{B}}^{-1}\tilde{\mathbf{A}}\right)^{\mathrm{T}}\mathbf{s} = -\tilde{\mathbf{c}}_w \\ & \mathbf{s} \in K, \end{aligned} \tag{3.21}$$

where $\mathbf{s}$ is the primal variables associated with the equality constraints in Eq. (3.20). By a change of variable $\mathbf{s} = -\mathbf{y}$, it can be shown that Eq. (3.19) and Eq. (3.21) are exactly the same. This derivation shows the relationship between ANC filter coefficients and the dual variables clearer, compared with the derivation in Section 3.2.2. When Eq. (3.21) (or Eq. (3.19)) is treated as a primal form and solved by common cone programming algorithms, the optimal dual variables associated with equality constraints in Eq. (3.21) (or Eq. (3.19)) will be the optimal ANC filter coefficients. Because of the primal-dual properties of common cone programming algorithms, obtaining the optimal dual variables does not cause any extra computations compared with only obtaining the optimal primal variables [99], [104], [109], [110].

A flowchart showing the procedure of implementing the proposed method (referred to as the "proposed CP" method) and the conventional cone programming formulation (referred to as the "conventional CP" method) is given in Fig. 3.1. Because of the use of the primal-dual interior-point algorithm, the optimal primal and dual solutions are obtained simultaneously. Thus, using the proposed formulation does not complicate the method implementation procedure.

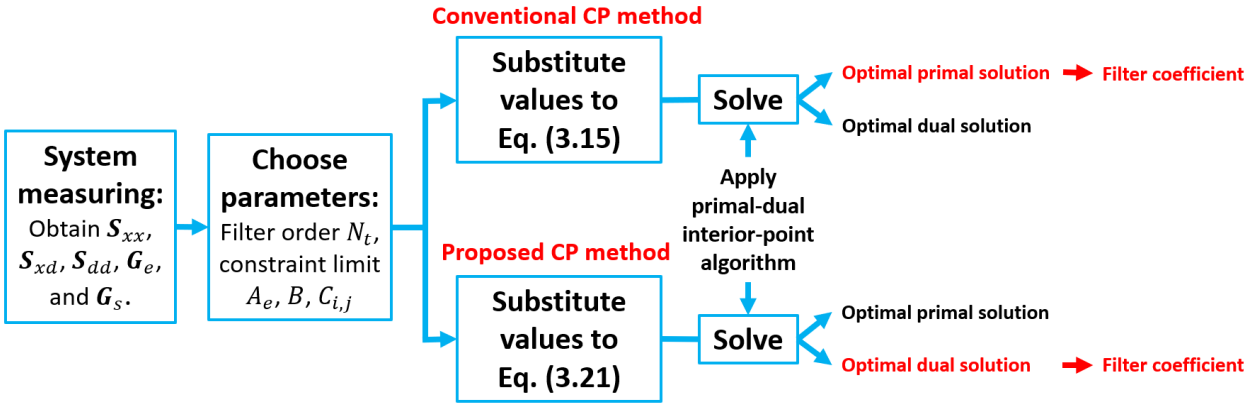


Figure 3.1. A flow chart showing the procedure of implementing the conventional CP method (conic formulation using standard procedure) and the proposed CP method.

3.2.4 Analysis of the proposed conic formulation

To explain why Eq. (3.19) or Eq. (3.21) (i.e., proposed CP method) is a preferable way to calculate the optimal ANC filter coefficients compared with using Eq. (3.15) (i.e., conventional CP method), the dimensions of the two problem formulations are compared in Table 3.1. The numbers of both variables and constraints are considered because, when solving the primal problem using primal-dual interior-point algorithms, the dual problem is solved at the same time as the primal problem. The dimension of the dual problem variables is determined by the number of constraints for the primal problem [99], [104], [109], [110]. m is the summation of the dimensions of all cones which is usually much larger than $N_r N_s N_t$.

In the column labeled "Conventional" in Table 3.1, there are two possible dimensions because of different treatments of free variables, $\mathbf{w}$ (i.e., the free variables can be either placed

Table 3.1. Comparison of problem dimensions using different conic formulations.

	Conventional Lorentz cones	Conventional Non-negative variables	Proposed
Primal Variables	$m + N_r N_s N_t + 1$	$m + 2N_r N_s N_t$	m
Equality constraints	m	m	$N_r N_s N_t + 1$
Inequality constraints	$m + N_r N_s N_t + 1$	$m + 2N_r N_s N_t$	m

inside a Lorentz cone or converted into the difference of two non-negative variables). By comparing the problem dimension of two different methods, it is obvious that the proposed CP method has a much smaller dimension than the conventional CP method (e.g., for one of the cases in the simulation results in Section 3.5.5, m is around 2×10^4 while $N_r N_s N_t$ is around 10^3). So the optimization problem obtained by the conventional CP method has redundant constraint information and large sparse patterns which may not be well exploited by the standard algorithms in solvers. The existence of free variables, $\mathbf{w}$ in the conventional CP method, may also compromise the numerical behavior [60], [99], [104], [109], [110], those free variables are eliminated if the proposed conic formulation is used. Experimentally measured data will be used to illustrate that using the proposed CP method has better numerical behavior and higher computational efficiency compared with using the conventional CP method in Section 3.5.5.

3.3 Constraint Modifications for the Warmstarting Strategy

In many ANC applications, a reasonable guess of the optimal filter coefficients may be obtainable. A good example is that, in commercial product design, some product models are variations of previous models, or a specific product is a variation of the prototype product due to the batch manufacture process error. In these cases, if the optimal filter coefficients of one product are known, it can be used as an initial guess when solving the optimal filter coefficients for other products. On the other hand, when the constrained optimization method is applied to time-varying applications, the optimization problem associated with the current adaption iteration can be treated as a perturbed problem with respect to that

of a previous adaption iteration. The optimal solutions of two adaptation iterations should be close to each other so the previous optimal solution can be used to obtain a warm-start initial point for the current iteration.

The strategy proposed by Skajaa [103] (reviewed in Section 2.3.3) is adopted to warmstart the ANC filter design problem. Their method is mainly used for LP and SOC programming. However, the proposed formulation contains PSDCs reformulated from the stability and robustness constraints. Thus, it is necessary to relax the stability and robustness constraints into SOC. Two different relaxations are proposed to relax the PSDCs to SOCs. In the following derivation, although the PSDC is relaxed to SOC, it is achieved by replacing the original stability or robust constraint function with a more restrictive function.

First, robust stability constraints Eq. (3.8) and Eq. (3.13) are satisfied if the following holds:

$$\|\mathbf{W}_x(f_k)\hat{\mathbf{G}}_s(f_k)\|_2 \leq \min\{1-\epsilon_s, 1/B(f_k)\}. \tag{3.22}$$

A relatively very conservative relaxation is to consider that max-norm of an arbitrary $m \times n$ matrix $\mathbf{M}$ satisfies:

$$\|\mathbf{M}\|_2 \leq \sqrt{mn}\|\mathbf{M}\|_{\max}. \tag{3.23}$$

So,

$$\|\mathbf{W}_x(f_k)\hat{\mathbf{G}}_s(f_k)\|_2 \leq \|\mathbf{W}_x(f_k)\|_2\|\hat{\mathbf{G}}_s(f_k)\|_2 \leq \sqrt{N_rN_s}\|\mathbf{W}_x(f_k)\|_{\max}\|\hat{\mathbf{G}}_s(f_k)\|_2. \tag{3.24}$$

Thus, Eq. (3.22) can be relaxed as:

$$\sqrt{N_rN_s}\|\mathbf{W}_x(f_k)\|_{\max}\|\hat{\mathbf{G}}_s(f_k)\|_2 \leq \min\{1-\epsilon_s, 1/B(f_k)\}. \tag{3.25}$$

So the following constraint (Eq. (3.26)), which can be formulated equivalently to a SOC, can be used to replace Eq. (3.8) and Eq. (3.13):

$$\|\mathbf{W}_x(f_k)\|_{\max} \leq \frac{\min\{1-\epsilon_s, 1/B(f_k)\}}{\sqrt{N_rN_s}\|\hat{\mathbf{G}}_s(f_k)\|_2}. \tag{3.26}$$

Note that the Eq. (3.26) essentially means the magnitude of each element in matrix $\mathbf{W}_x(f_k)$ is less than some constants which can be reformulated into SOC in a similar way to the response magnitude constraint demonstrated in Appendix A.2.

Alternatively, a less conservative relaxation is to consider the Frobenius norm properties:

$$\|\mathbf{W}_x(f_k)\hat{\mathbf{G}}_s(f_k)\|_2 \leq \|\mathbf{W}_x(f_k)\hat{\mathbf{G}}_s(f_k)\|_F, \tag{3.27}$$

where,

$$\|\mathbf{W}_x(f_k)\hat{\mathbf{G}}_s(f_k)\|_F = \sqrt{\mathrm{tr}\left(\hat{\mathbf{G}}_s(f_k)^{\mathrm{H}}\mathbf{W}_x(f_k)^{\mathrm{H}}\mathbf{W}_x(f_k)\hat{\mathbf{G}}_s(f_k)\right)}. \tag{3.28}$$

Thus, the following constraint (Eq. (3.29)), which can also be formulated equivalently to a SOC, can be used to replace Eq. (3.8) and Eq. (3.13) as well:

$$\mathrm{tr}\left(\hat{\mathbf{G}}_s(f_k)^{\mathrm{H}}\mathbf{W}_x(f_k)^{\mathrm{H}}\mathbf{W}_x(f_k)\hat{\mathbf{G}}_s(f_k)\right) \leq \min\{(1-\epsilon_s)^2, 1/B(f_k)^2\}. \tag{3.29}$$

Note that the Eq. (3.29) can be reformulated to a standard convex quadratic function using derivations shown in Appendix A.1 simply by replacing $\mathbf{G}_{\mathrm{e}}$ by $\hat{\mathbf{G}}_s^{\mathrm{T}}$ and set $\mathbf{S}_{xx}$ to an identity matrix. Then it can be formulated into a SOC in a similar way demonstrated in Appendix A.2.

The ANC performance results using these two proposed relaxation methods, Eq. (3.26) and Eq. (3.29), will be compared in the Section 3.5.6.

3.4 Singular Vector Filtering Method for the Noise Amplification Constraint

In some practical cases, the effect of the acoustic feedback path is small. For example, when accelerometers are used as reference sensors, the sound produced by secondary speakers does not have a high impact on the accelerometers. In earphone applications where the earphone is designed to fit tightly in the ear, it is hard for sound to propagate from the interior of the earphone to the reference microphone on the exterior of an earphone. Another case is when the reference microphones are relatively far away from secondary speakers. In those applications, the frequency response of the acoustic feedback path has a small magnitude

such that the robust stability constraint can usually be satisfied even for a Wiener filter. If the output power of control filters is not a limitation in those applications, then the noise amplification (disturbance enhancement) constraint will be the dominant constraint. In this case, although the previously proposed conic formulation can still be used, another simpler approach is proposed here to prevent noise amplification in filter design.

In the previous study, Liu et al. demonstrated that a singular value decomposition (SVD) based method can be used to extract independent sound field components [26]. Inspired by that work, Wang et al. proposed another time-domain treatment for noise amplification where a truncated SVD method is applied [114]. SVD was first applied to the auto-correlation matrix of filtered-reference signals, and the singular values and singular vectors that contribute to the enhancement phenomenon were removed to mitigate the noise amplification. Their results showed that this method can effectively mitigate the enhancement phenomenon. However, some of the removed singular values and singular vectors, although responsible for the enhancement in certain frequency bands, may contribute to the noise control performance in other desired frequency bands. Thus, such a direct truncation will affect the noise control performance. To further reduce this effect, a filtering method is proposed in this section. Instead of a direct truncation, a filtering process was introduced to replace the singular vectors contributing to the noise amplification with a set of new singular vectors whose frequency responses are attenuated in the frequency band where noise amplification occurs, while the frequency responses in other frequency bands are unchanged.

The truncated singular value decomposition method is first reviewed in this section. To investigate the noise amplification phenomenon resulting from the mutual correlation of multichannel reference signals, Wang et al. [114] applied SVD to the auto-correlation matrix $\mathbf{A}_{w\mathrm{i}}$ in Eq. (2.1), which results in

$$\mathbf{A}_{w\mathrm{i}} = \mathbf{U}\boldsymbol{\Sigma}\mathbf{U}^{\mathrm{T}} = \begin{bmatrix} \mathbf{u}_1 & \dots & \mathbf{u}_{N_r N_s N_t} \end{bmatrix} \begin{bmatrix} \sigma_1 & \dots & 0 \\ \vdots & \ddots & \vdots \\ 0 & \dots & \sigma_{N_r N_s N_t} \end{bmatrix} \begin{bmatrix} \mathbf{u}_1^{\mathrm{T}} \\ \vdots \\ \mathbf{u}_{N_r N_s N_t}^{\mathrm{T}} \end{bmatrix}. \tag{3.30}$$

Then, the optimal Wiener filter solution in Eq. (2.2) can be rewritten as

$$\mathbf{w}_{wi,opt} = -\sum_{k=1}^{N_r N_s N_t} \left(\sigma_k^{-1}\mathbf{u}_k^{\mathrm{T}}\mathbf{b}\right)\mathbf{u}_k. \tag{3.31}$$

The optimal filter $\mathbf{w}_{wi,opt}$ can be considered as a linear combination of the singular vectors, $\mathbf{u}_k$, each of which represents a multi-channel FIR filter with N_r outputs, N_s inputs, and N_t filter coefficients. Some $\sigma_k^{-1}\mathbf{u}_k^{\mathrm{T}}\mathbf{b}$ may have a large value which will cause the noise amplification. To mitigate this noise amplification, Wang et al. [114] truncated the singular values and the associated singular vectors, after some index l, to form a modified filter:

$$\mathbf{w}_{wi,0} = -\sum_{k=1}^{l} \left(\sigma_k^{-1}\mathbf{u}_k^{\mathrm{T}}\mathbf{b}\right)\mathbf{u}_k. \tag{3.32}$$

Then $\mathbf{w}_{wi,0}$ will be used to replace $\mathbf{w}_{wi,opt}$ as the control filter. It was demonstrated that this method could mitigate the enhancement if l is chosen appropriately [114]. However, the discarded singular values and vectors also contribute to the noise control performance at other frequency bands, thus such a direct truncation will negatively affect the overall noise control performance.

To reduce this impact on the noise control performance in desired frequency bands, a filtering method, instead of truncation, is proposed. Firstly, the original singular vector representation of the optimal Wiener filter, Eq. (3.31), can be divided into three groups:

$$\mathbf{w}_{wi,opt} = \mathbf{w}_{wi,0} + \sum_{k=l+1}^{m} \mathbf{w}_{wi,k} + \sum_{k=m+1}^{N_r N_s N_t} \mathbf{w}_{wi,k}, \tag{3.33}$$

where $\mathbf{w}_{wi,0}$ is defined in Eq. (3.32), which are the singular vectors with no noise amplification contributions, and $\mathbf{w}_{wi,k}$ is the component in the subspace spanned by the singular vectors contributing to noise amplification in certain bands (i.e., the component that is removed in the truncation method), which is expressed as:

$$\mathbf{w}_{wi,k} = -\left(\sigma_k^{-1}\mathbf{u}_k^{\mathrm{T}}\mathbf{b}\right)\mathbf{u}_k = \begin{bmatrix} w_{k,1,1,0} & \dots & w_{k,1,N_r,0} & \dots & w_{k,N_s,N_r,0} & \dots & w_{k,N_s,N_r,N_t-1} \end{bmatrix}^{\mathrm{T}} \tag{3.34}$$

The index m in Equation Eq. (3.33) suggests that from index $l+1$ to m, the singular vector contains responses that contribute to both the noise amplification and the noise control performance. However, after index m, the singular vectors contain responses that cause the noise amplification only (thus, they should be always truncated). It is noted that $\mathbf{w}_{wi,k}$ can be rearranged to $N_s N_r$ filters $\mathbf{w}_{wi,k,i,j}$ with a filter length of N_t for each input-output channel pair. The frequency response of $\mathbf{w}_{wi,k,i,j}$ can be evaluated appropriately at N_f frequency points:

$$\mathbf{W}_{wi,k,i,j} = \mathbf{F}_M \mathbf{w}_{wi,k,i,j}, \tag{3.35}$$

where $\mathbf{F}_M$ is

$$\mathbf{F}_M = \begin{bmatrix} \mathbf{F}_z(f_1) & \mathbf{F}_z(f_2) & \dots & \mathbf{F}_z(f_{N_f}) \end{bmatrix}^{\mathrm{T}},$$

and $\mathbf{F}_z(f)$ is defined in Eq. (2.9); i and j represent the indices of different input and output channels of the multichannel filter $\mathbf{w}_{wi,k}$. As mentioned earlier, although $\mathbf{w}_{wi,k}$ is responsible for the enhancement phenomenon in some frequency bands, it also contributes to active noise control performance in other bands, thus a direct removal of $\mathbf{w}_{wi,k}$ will inevitably sacrifice the noise control performance. It is proposed that a suitably designed band-stop filter can be applied to each channel pair of $\mathbf{W}_{wi,k,i,j}$ to obtain a new filter, $\tilde{\mathbf{W}}_{wi,k,i,j}$, such that the stopbands of the designed filter cover the frequency bands where noise amplification phenomenon occurs if the original $\mathbf{W}_{wi,k,i,j}$ were used (see Fig. 3.2 for an intuitive illustration. Note that Fig. 3.2 is not presenting actual results but to illustrate the process.). In this way, $\tilde{\mathbf{W}}_{wi,k,i,j}$ can be treated as a filtered version of $\mathbf{W}_{wi,k,i,j}$), thus the proposed method is referred to as singular vector filtering method.

Unlike conventional band-stop filters, the band-stop filter used here should ideally produce no change in either magnitude or phase in the pass-band. Thus, instead of using conventional band-stop filter design methods, the FIR filter coefficients (denoted as $\mathbf{v}_{wi,k,i,j}$) representing the filtered filter $\tilde{\mathbf{W}}_{wi,k,i,j}$)) with the same filter length as $\mathbf{w}_{wi,k}$ are obtained by solving the following optimization problem:

$$\mathbf{v}_{wi,k,i,j} = \underset{\mathbf{v}_{wi,k,i,j}}{\operatorname{argmin}} \|\mathbf{F}_M \mathbf{v}_{wi,k,i,j} - \tilde{\mathbf{W}}_{wi,k,i,j}\|_2^2 = \mathrm{Re}\{\mathbf{F}_M^{\mathrm{H}} \mathbf{F}_M\}^{-1} \mathrm{Re}\{\mathbf{F}_M^{\mathrm{H}} \tilde{\mathbf{W}}_{wi,k,i,j}\}. \tag{3.36}$$

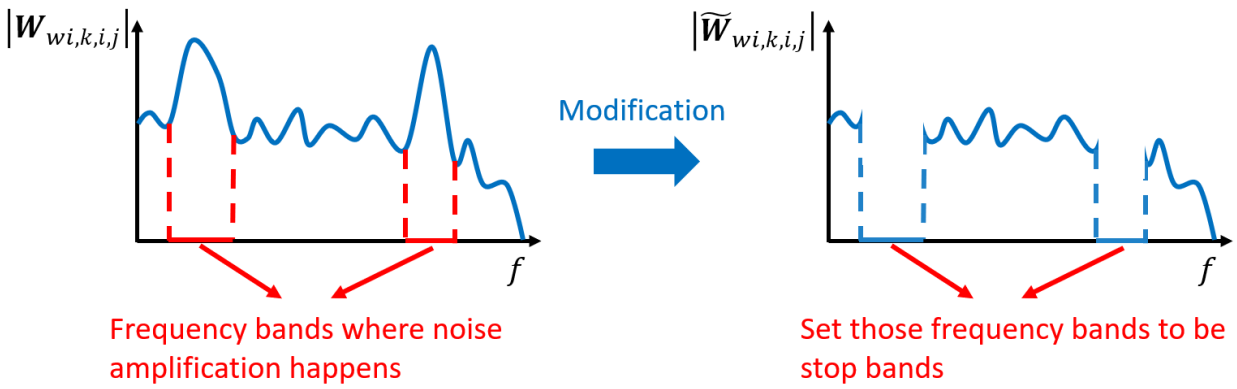


Figure 3.2. An intuitive illustration of the modification from original frequency responses of singular vectors to the modified frequency responses that are to be fitted.

It is noted that the existence of real part operation in Eq. (3.36) is because the desired $\mathbf{v}_{wi,k,i,j}$ should be a real vector. Since the frequency response $\tilde{\mathbf{W}}_{wi,k,i,j}$ is small in the frequency bands where noise amplification occurs and is the same as $\mathbf{W}_{wi,k,i,j}$ in other frequency bands, the filter $\mathbf{v}_{wi,k,i,j}$ will not have enhancement problem while preserving the noise control performance at other frequency bands as much as possible. Also, the $\mathbf{v}_{wi,k,i,j}$ obtained from optimization will not have the impractical sharp transition in the frequency responses as $\tilde{\mathbf{W}}_{wi,k,i,j}$. Then, $\mathbf{v}_{wi,k,i,j}$ can be rearranged to get:

$$\mathbf{v}_{wi,k} = \begin{bmatrix} v_{k,1,1,0} & \cdots & v_{k,1,N_r,0} & \cdots & v_{k,N_s,N_r,0} & \cdots & v_{k,N_s,N_r,N_t-1} \end{bmatrix}^{\mathrm{T}} \tag{3.37}$$

Finally, the modified filter by singular vector filtering method is:

$$\mathbf{w}_{wi,sep} = \mathbf{w}_{wi,0} + \sum_{k=l+1}^{m} \mathbf{v}_{wi,k}, \tag{3.38}$$

where $\mathbf{w}_{wi,sep}$ can be used to replace $\mathbf{w}_{wi,opt}$ as control filters for the active noise control system.

However, if $\mathbf{v}_{wi,k,i,j}$ is to be obtained separately for each i, j pair and for each index k, the optimization problem specified in Eq. (3.36) will need to be solved for $N_r N_s(m-l)$ times,

which involves a significant calculation effort if $N_r N_s m$ is large and l is small. This process can be simplified if $\mathbf{v}_{wi,k,i,j}$ are obtained after summation over k. In usual ANC practices, the frequency bands where noise amplification occurs are found to be similar for each $\mathbf{W}_{wi,k,i,j}$, this suggests that the same band-stop filter can be applied to all $\mathbf{W}_{wi,k,i,j}$. Thus, in order to simplify the proposed filtering process, $\mathbf{w}_{wi,k,i,j}$ can be added first, then calculated for its frequency response:

$$\mathbf{W}_{wi,sum,i,j} = \mathbf{F}_M \left(\sum_{k=l+1}^{m} \mathbf{w}_{wi,k,i,j} \right), \tag{3.39}$$

The frequency responses of those band-stop filters can be multiplied by the frequency response $\mathbf{W}_{wi,sum,i,j}$ to obtain $\tilde{\mathbf{W}}_{wi,sum,i,j}$ such that the stopbands cover all the frequency bands where noise amplification occurs (a similar process as that in Fig. 3.2). Then the second term in Eq. (3.38) can be calculated by a single step:

$$\mathbf{v}_{wi,sum,i,j} = \underset{\mathbf{v}_{wi,sum,i,j}}{\operatorname{argmin}} \|\mathbf{F}_M \mathbf{v}_{wi,sum,i,j} - \tilde{\mathbf{W}}_{wi,sum,i,j}\|_2^2 = \operatorname{Re}\{\mathbf{F}_M^{\mathrm{H}} \mathbf{F}_M\}^{-1} \operatorname{Re}\{\mathbf{F}_M^{\mathrm{H}} \tilde{\mathbf{W}}_{wi,sum,i,j}\}. \tag{3.40}$$

Using similar way in Eq. (3.37) to rearrange $\mathbf{v}_{wi,sum,i,j}$ to get $\mathbf{v}_{wi,sum}$, then we have:

$$\mathbf{w}_{wi,sum} = \mathbf{w}_{wi,0} + \mathbf{v}_{wi,sum}, \tag{3.41}$$

where $\mathbf{w}_{wi,sum}$ can be used to replace $\mathbf{w}_{wi,opt}$ as control filters. Using this method, i.e., filtering after summation, the Eq. (3.40) only needs to be computed for $N_r N_s$ times, which is much more computationally efficient than repetitively solving Eq. (3.36) for different k indices. In Section 3.5.7, results obtained by filtering after summation, i.e., Eq. (3.41), and by filtering separately, i.e., Eq. (3.38), will also be illustrated to be the same.

3.5 Experimental Results and Discussions

3.5.1 Description of the experimental setup

An experiment was carried out to investigate the proposed methods, which is an ANC system installed on the wind channel of a central air handling system. There are two speakers used as secondary sources, four reference microphones, and four error microphones. The

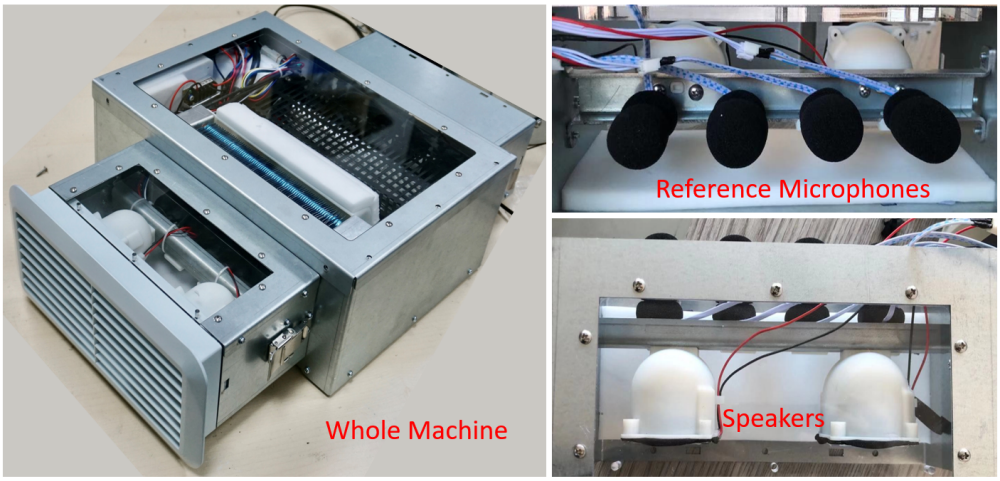


Figure 3.3. The picture of the experimental setup and individual components.

experimental setup is shown in Fig. 3.3. The key dimensions of the components are shown in Fig. 3.4. A non-adaptive controller is designed and implemented in this chapter using measured system characteristics under a nominal operating condition. In this practical application, the constraints discussed earlier are all required especially for the robust stability constraint considering the strong acoustic feedback path.

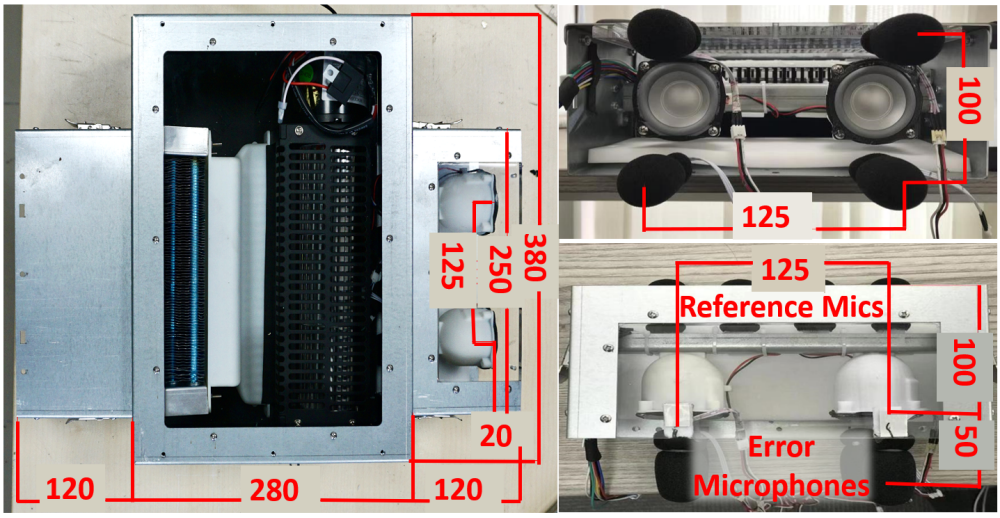


Figure 3.4. The dimensions in the experiment setup (unit: mm).

The cross-spectral matrix, $\mathbf{S}_{xd}$, was measured when the air handling unit is operating. The frequency response matrix, $\mathbf{G}_{\mathrm{e}}$, was measured when the unit is deactivated and the loudspeakers are excited by white noise signals provided by external signal generators. When acquiring measurement data, the sampling rate of the data acquisition system is 48 kHz. Two million measurement points for each channel were acquired for calculating the correlation matrices and frequency responses, where a hamming window of 48000 points is used for averaging with fifty percent overlapping (in total 83 times averages).

Different numbers of channels will be selected to investigate the ANC performance dependence on channel counts. For convenience, the terminology "$xN_ryN_szN_{\mathrm{e}}$ case" is used in this section to denote a study case with x reference microphones, y control speakers, and z error microphones.

3.5.2 Comparison between the regularization parameter method and the proposed conic method

The noise control performance of constrained control filters designed by the regularization parameter method and the proposed conic method is compared in this part. "Regularization parameter method" refers to the method using Eq. (2.2), and "proposed conic method" refers to the proposed cone programming formulation Eq. (3.21) as shown in Fig. 3.1.

Noise amplification and robust stability constraint are particularly focused on. For the regularization parameter method, the parameter β in Eq. (2.2) is gradually increased from zero to an appropriate value such that all constraints are satisfied. For the proposed conic method, constraints are directly specified in the conic formulation Eq. (3.21) (i.e., plug in values into expressions explained in Eq. (3.14)) and no parameter tuning is needed. This also indicates that using the proposed conic method is more convenient for a wide range of applications since no additional tuning efforts from users are required.

In Fig. 3.5 (a) and (c), "ANC OFF" denotes the original noise power spectral density (PSD) averaged among all the error microphones when the ANC system is not activated. "Normalized PSD" is the PSD normalized by the total noise power at the "ANC OFF" case. The stability constraint function values (i.e., the maximum real part of the eigenvalues of open loop responses matrix $-\mathbf{W}_x(f_k)\hat{\mathbf{G}}_s(f_k)$) is shown in Fig. 3.5 (b) and (d). Thus, when

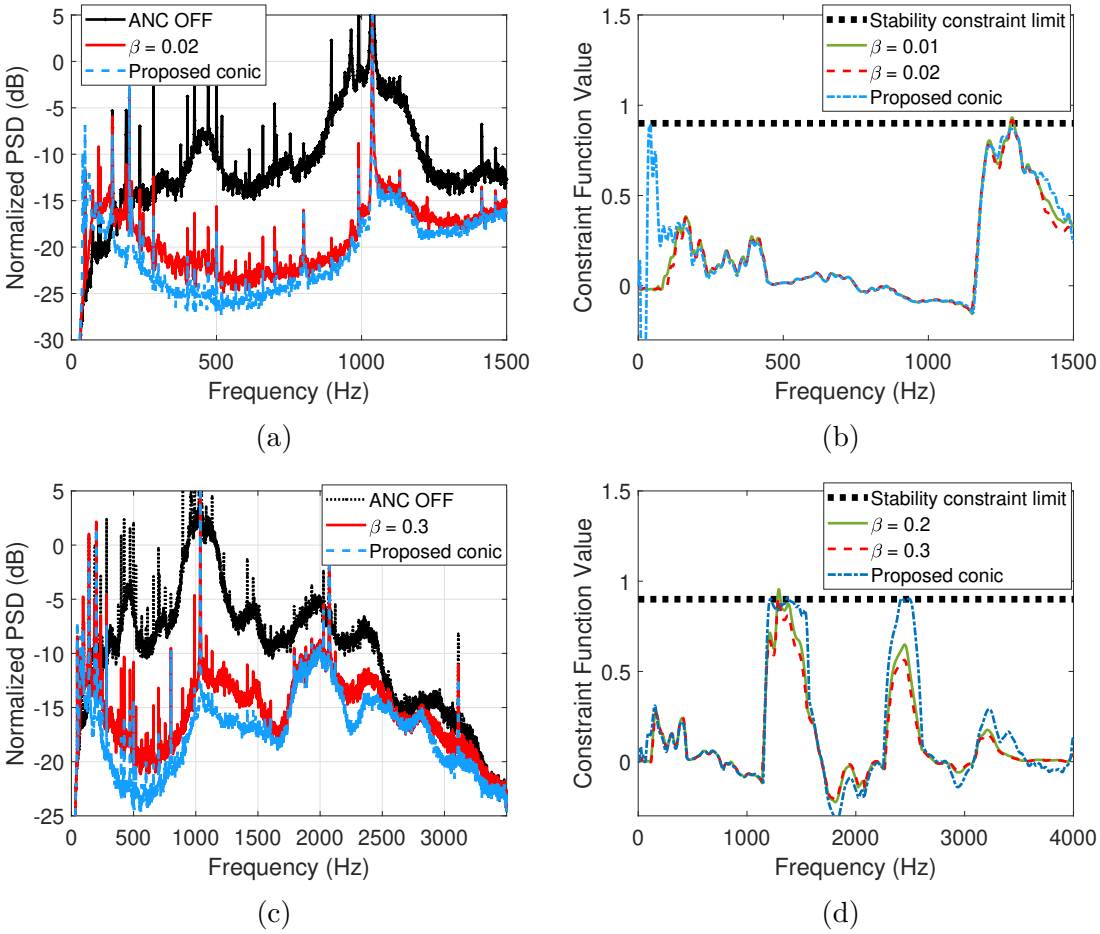


Figure 3.5. The comparison of the regularization parameters method and the proposed conic method using an FIR order of 128 in each control filter channel in a $4N_r2N_s4N_e$ system for (a) noise control performance and (b) stability behavior at 3000 Hz sampling rate, (c) noise control performance and (d) stability behavior at 8000 Hz sampling rate.

they are all smaller than 1 across all frequencies, the control filters are considered to be stable. The stability constraint limit (black dot line) is set to 0.9 to ensure strict stability (i.e., $\epsilon_s = 0.1$).

In Fig. 3.5 (b) and (d), when β is higher than or equal to 0.02 (or 0.3) at a 3 kHz (or 8 kHz) sampling rate, the stability constraint is satisfied (i.e., the open loop frequency response is below the stability constraint limit). The control filter design by the proposed conic method is also stable. By comparing the open loop frequency response of filters designed by the

regularization parameter method and the proposed conic method, there are some frequency bands where the filter designed by the regularization method is noticeably lower than (farther away from the constraint limit) that designed by the proposed conic method. This suggests an over satisfaction of stability constraint when the regularization parameter method is used, which can lead to a degradation of ANC performance. This negative influence on ANC performance can be seen in the results shown in Fig. 3.5 (a) and (c).

Overall, it is clear that, if a strong acoustic feedback path exists and stability constraints need to be satisfied, the proposed conic method can achieve better noise control performance than the traditional regularization parameter method.

3.5.3 Comparison between the traditional constrained optimization method and the proposed conic method

The computational efficiency of the traditional constrained optimization method using Eq. (2.17) and the proposed conic method using Eq. (3.21) as shown in Fig. 3.1 are compared.

In this comparison study, the sampling rate is set to 8000 Hz, and the desired noise deduction frequency range is specified to be from 100 Hz to 3400 Hz. In this range, a 4 Hz interval was used in calculating the total power of error signals, i.e., $N_f = 826$ in the objective functions in Eq. (2.17) and Eq. (3.14). Also, a 20 Hz interval was used in the noise amplification constraints (limited to a maximum amplification of 3 dB); a 30 Hz interval was used in the stability constraints; a 50 Hz interval was used in robustness constraints. There are 81 frequency points in filter response magnitude constraints that covers the frequency band of below 100 Hz and above 3400 Hz to improve the numerical performance and satisfy the speaker linear response requirement. In the filter design process, the computing platform used in current work is a personal computer with an Intel(R) Core(TM) i7-7700 CPU @ 3.60 GHz, and the numerical algorithms are implemented in a Matlab platform installed on Windows 10 64-bit operating system.

The computational time required to solve the optimization problems is listed in Table 3.2. It is noted that, in the $4N_r2N_s4N_e$ case, no computational time is presented for the traditional constrained optimization formulation when the length of the FIR ANC filter in each channel is larger than or equal to 32 because the required computational time for the

Table 3.2. Comparison of the computational time using the traditional constrained optimization methods and the proposed conic method.

System	Filter length N_t	Traditional constrained optimization	Proposed conic
$2N_r2N_s2N_e$	4	1.78×10^2 s	1.22 s
$2N_r2N_s2N_e$	8	4.79×10^3 s	1.42 s
$2N_r2N_s2N_e$	16	1.75×10^4 s	1.38 s
$2N_r2N_s2N_e$	32	3.37×10^4 s	2.43 s
$4N_r2N_s4N_e$	4	1.37×10^3 s	1.58 s
$4N_r2N_s4N_e$	8	3.24×10^4 s	2.08 s
$4N_r2N_s4N_e$	16	9.52×10^4 s	2.26 s
$4N_r2N_s4N_e$	32		6.17 s
$4N_r2N_s4N_e$	64		22.58 s
$4N_r2N_s4N_e$	128		94.44 s

traditional method is over several days. It is shown in Table 3.2 that, compared with the traditional method, the proposed conic formulation has significantly higher computational efficiency. Even for relatively low filter lengths (e.g., a length of 16), the computational time is reduced from tens of hours to several seconds. If a high filter length is used to obtain a reasonable ANC performance in practice, e.g., a length 64 or 128, where solving the traditional constrained optimization formulation is impractical, the computation using the proposed conic formulation only takes less than half a minute for the filter length of 64 and less than 2 minutes for the filter length of 128.

Even for a long FIR length ($N_t = 128$) and high channel counts (8 channels), the proposed conic method can still be updated within two minutes, which suggests that the proposed conic method can be applied to much wider practical applications. For example, with a continuous repeating of the filter design optimization process and updating the filter coefficients based on the most recent measurement of reference and error signals, the proposed conic method can be applied to an adaptive active noise control of a variable speed air handling unit that pairs with a variable speed air conditioner. For variable speed HVAC equipment, equipment speed is usually not changed within several minutes (more often, not even in half an hour) due to the slow change in indoor and outdoor environments. Thus, if the calculation of

the filter design process can be accomplished in minutes, it can be implemented in such a practical adaptive control application. However, if the traditional constrained optimization formulation is employed, even for a short length ($N_t = 16$), it takes more than one day to update all control filters once which cannot follow the time-varying changing of the equipment operating condition.

Another practical advantage brought by the improvement of computational efficiency is that, even for a non-adaptive ANC system, it can accelerate the product development cycle in the commercialization of this ANC technique. Many product prototypes need to be developed in the whole product development cycle and each prototype involves different design parameters, such as geometry, sensor/transducer locations, etc. Thus, there will be a large number of engineering iterations and the filter design problem will be solved multiple times. Also, if the selective fixed-filter ANC [44] is used, a large set of filters need to be designed offline. The improvement of computational efficiency brought by the proposed conic method can significantly reduce the cost of time and resources in these ANC applications.

Besides significant improvement in computational time, the proposed conic method is also more reliable compared with the traditional constrained optimization method. Firstly, because the proposed conic method uses a convex formulation, a global optimal solution can always be found. When the primal-dual interior-point method is used to solve this convex formulation, the non-differential constraints can be processed in a reliable way and the duality gap provides a reliable criterion for convergence [96]. Due to the non-differentiable constraint functions in ANC formulation, the gradient can only be estimated by the finite difference method if algorithms similar to SQP are used, thus, there are potential numerical instability risks associated with this method. Moreover, sometimes, SQP does not converge even to a local minimum solution before it terminates at a sufficiently large maximum iteration, or a sufficiently small step length, which could require further user intervention in actual implementation.

The case where both the traditional constrained optimization method and the proposed conic method converge to satisfactory results is shown in Fig. 3.6 (a) and (b). It is shown that the proposed method can achieve a noise control performance similar to the traditional method, which suggests that the replacement of the non-convex stability constraint Eq. (2.15)

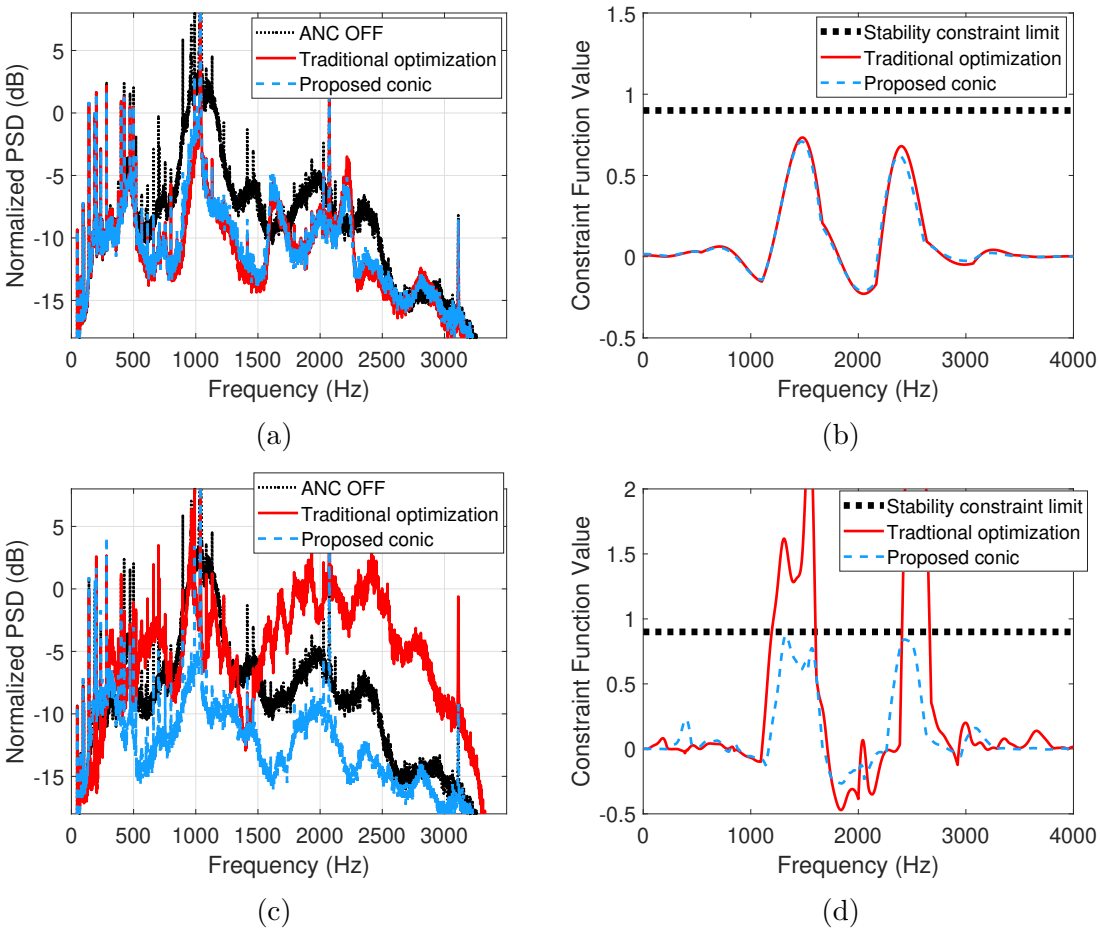


Figure 3.6. The comparison of the traditional constrained optimization method and the proposed conic method of $4N_r2N_s4N_e$ case in 8000 Hz sampling rate for (a) noise control performance and (b) stability behavior of FIR length of 8 in each channel, (c) noise control performance and (d) stability behavior of FIR length of 16 in each channel.

in the traditional formulation with a more restrictive convex stability constraint Eq. (3.8) does not produce any noticeable influence on the final noise control performance. This confirms that the use of the stability constraint relaxation approach in the convexification process Section 3.1.1 is appropriate.

The advantage of the proposed conic method is significant when the case becomes more complicated, e.g., when the order of the FIR filter in each channel becomes higher. Figure3.6 (c) and (d) present a case when the traditional formulation solved by SQP is not

satisfactory. In this case, the final step size of SQP is smaller than 10^{-6} which is usually considered as an achievement of a converged solution, however, when compared with the resulting performance of the proposed method, it is obvious that the solution is far away from its optimal filter solution. The traditional constrained optimization method does not have satisfactory noise control performance and the stability constraint is not satisfied. In contrast, the proposed conic method still achieves satisfactory noise control performance and satisfies the required constraints. In fact, the proposed method can still achieve satisfactory noise control performance while satisfying constraints for even higher filter lengths (32, 64, and 128), which is shown in Fig. 3.7.

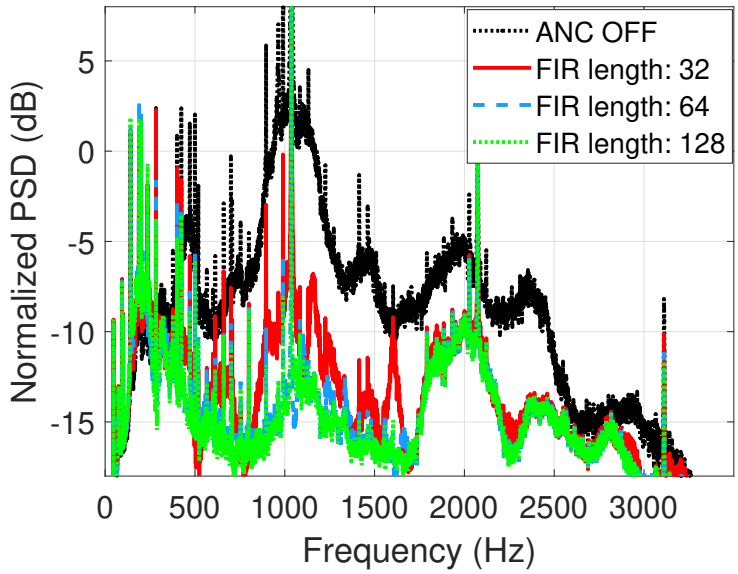


Figure 3.7. Comparison of ANC performance in the "$4N_r2N_s4N_e$" system with different choices of filter lengths N_t designed by the proposed conic method.

3.5.4 Other characteristics of the proposed conic method

It is pointed out in section 3.1.2 that the proposed formulation will result in a problem complexity that is independent of the number of frequency points used in the objective function. To confirm this, the set of data for a $4N_r2N_s4N_e$ configuration was used to test the required time for the proposed method when the frequency resolution in the objective

function varies. In this test, the FIR filter length is chosen to be 128. The results are listed in Table 3.3. Instead of showing the total time required for solving the optimization problem, Table 3.3 shows two parts of the total time separately. The column "Solving time" denotes the time spent in solving the cone programming problem reformulated from the convex optimization formulation described in Eq. (3.21). It is demonstrated that as the number of frequency points used in the objective function increases, the time required for solving the optimization problem remains relatively the same. "Constructing time" is the preprocessing time required for processing measured data to be in the proposed conic form. It is reasonable that the constructing time increases with the increase of frequency resolution used in the objective function (i.e., more data is used). The practical advantage of this property is that the choice of frequency interval for objective function can be sufficiently small to ensure the overall performance without increasing the solving time significantly.

Table 3.3. Computational time of different numbers of frequency points used in the objective function by using the proposed conic method when FIR filter length is 128.

Number of frequencies	Solving time	Constructing time
195	84.61 s	3.37 s
413	84.10 s	4.76 s
826	87.07 s	7.38 s
1651	84.08 s	12.76 s
3302	84.56 s	23.55 s

The number of iterations of more choices of filter lengths with the same set of constraints is listed in Table 3.4. In practice, the number of iterations usually does not change significantly with the increase of problem size and is usually within 100 iterations [96]. This can be demonstrated from results in Table 3.4 that the required iterations are not changing significantly with the increase of problem size. The increase in required solving time with the increase in problem size is mainly from the increase in the calculation time in each iteration. This relatively fixed number of iterations in the numerical solving process is also one important reason why the proposed method is more reliable. The small number of iterations makes the convergence time more predictable. From a practical point of view, there is a

fixed adaptation rate if this method is used in adaptive control via continuous repeating of the filter design process. Thus, it is easy to judge the practical applicability of the proposed method for a specific situation where the time-varying rate of signal characteristics can be estimated.

Table 3.4. Required iterations of different filter lengths of the "$4N_r2N_s4N_e$" system when using proposed method.

filter length N_t	Iterations
4	28
8	28
16	18
32	20
64	22
128	22

3.5.5 Comparison between the conventional conic formulation and the proposed conic formulation using duality

The numerical behavior of the conventional conic formulation, Eq. (3.15), and the proposed conic formulation using duality, Eq. (3.19) or (3.21), is compared in this part. The sampling frequency f_s is 7 kHz and the desired noise attenuation band is from 100 Hz to 3400 Hz. In the attenuation band, a 3 Hz interval was used in expressing the total power of error signals, an 8 Hz interval was used in noise amplification constraints (limited to a maximum of 3 dB amplification), and different frequency intervals (i.e., different number of frequency-dependent constraints) were used for in stability and robustness constraints as different cases. Outside the attenuation band, 68 frequencies were used in filter response magnitude constraints. Two solvers, SeDuMi [99], [110] and SDPT3 [98], [104], were used to implement different variants of primal-dual interior-point algorithms to have a more general conclusion. The experimental data were already scaled properly before using algorithms to solve.

For typical primal-dual interior-point algorithms designed for cone programming, numerical issues may occur when the solution is sufficiently close to the optimal solution or the

boundary of constraints [99], [104], [112]. In practical algorithms, one of the stopping criteria is the optimal duality gap which measures the difference in values between optimal primal and dual objective functions. As reviewed in Section 2.3, the duality gap converges to zero when the current solution is approaching the optimal solution [109], [110]. Both solvers will stop iterating when the duality gap is smaller than a certain threshold or when numerical issues occur, e.g., the generated step length becomes sufficiently small before reaching an optimal point. By setting a small duality gap threshold, the numerical stability of different formulating methods can be compared by comparing the duality gap right before a numerical issue occurs.

The numerical issues usually occur when positive semidefinite cones, i.e., stability and robustness constraints, exist [60]. So three different numbers (56, 83, and 111) of equally spaced frequencies for stability and robustness constraints (applied at the same frequencies) are used as different cases, i.e., the frequency intervals are 60 Hz, 40 Hz, and 30 Hz respectively. For each case, different FIR filter lengths, N_t, are also used to compare the numerical behavior in different problem dimensions.

The duality gap before numerical issues occur for different cases, filter lengths, methods, and solvers are shown in Fig. 3.8. These plots show that for both solvers, the proposed conic formulation always has a smaller final duality gap (i.e., more numerically stable) than the conventional formulation, especially if using solver SeDuMi for high-order FIR filters. When the conventional conic formulation is used for higher order FIR filters, it is possible that a reasonable solution cannot be obtained by SeDuMi since some duality gap in these plots can only reach around 1×10^{-3}. The results also demonstrated that the solver SDPT3 is usually more numerically stable compared with SeDuMi when the same formulating method is used.

To confirm that such a small duality gap is indeed needed, Fig. 3.9 shows the comparison of ANC performance of 96-point FIR filters when 111 frequencies (30 Hz frequency interval) for stability and robustness constraints are used. In Fig. 3.9, the performance of ANC filters solved by using the conventional conic formulation and SeDuMi, which has a duality gap of 2.04×10^{-6}, is obviously worse than other combinations whose duality gaps are all less than 10^{-8}. This confirms that using the conventional conic formulation may not give a satisfactory result if the solver SeDuMi is used and the problem dimension is large. Although when the

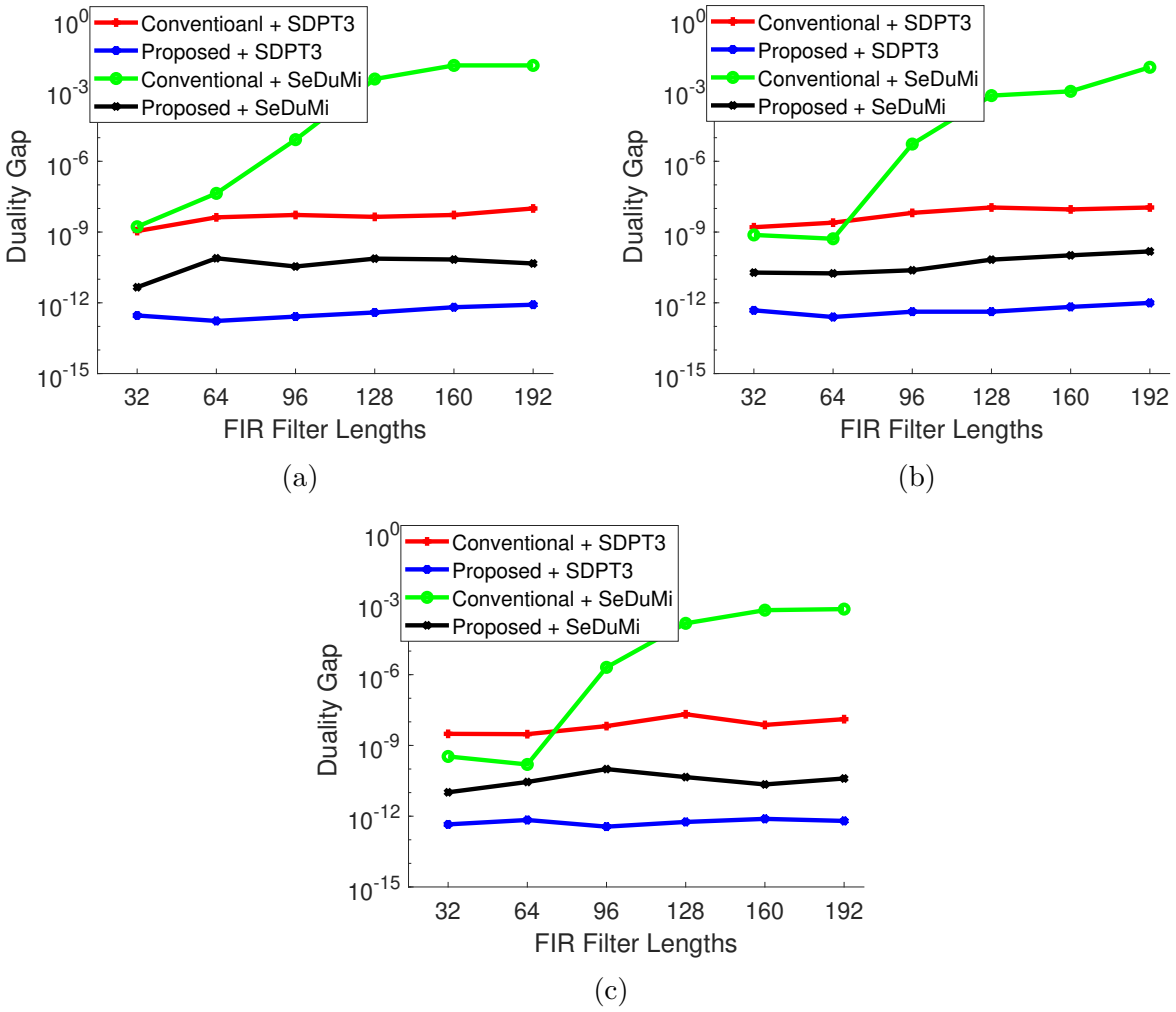


Figure 3.8. The duality gap before numerical issues occur when using (a) 56 frequencies (60 Hz frequency interval), (b) 83 frequencies (40 Hz frequency interval), and (c) 111 frequencies (30 Hz frequency interval) for stability and robustness constraints.

solver SDPT3 is used, the conventional conic formulation can give an accurate solution, it is still less numerically stable than the proposed conic formulation and it will be shown shortly that using SeDuMi is preferred in terms of efficiency.

Besides numerical stability, computational efficiency should also be investigated for the two formulating methods. The computational time for different combinations of filter lengths, methods, and solvers are shown in Fig. 3.10. It is noted that for the combination of the conventional conic formulation and SeDuMi, the results only show filter length at 32 and 64

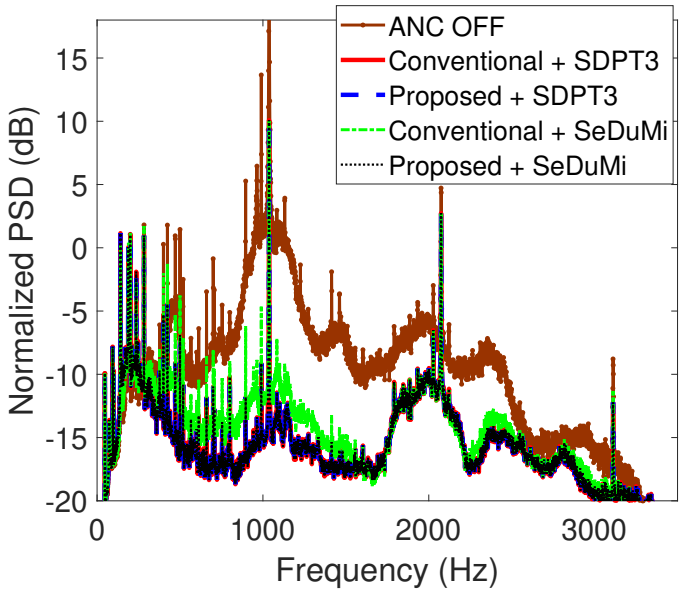


Figure 3.9. The comparison of ANC performance using 96-point FIR filters when 111 frequencies (30 Hz frequency interval) are used for the stability and robustness constraints.

because the algorithm cannot give an accurate enough solution for higher order FIR filters. In Fig. 3.10, results demonstrated that for both solvers, the proposed conic formulation is much more computationally efficient than the conventional conic formulation, especially when the solver SDPT3 is used. The results also show that using solver the SeDuMi is more computationally efficient than using the solver SDPT3 (computational time was reduced by two orders). But the use of SeDuMi is only possible when the proposed conic formulation is used.

In conclusion, the proposed conic formulation using the duality property is more numerically stable and computationally efficient compared with the conventional formulation in both solvers. SeDuMi is preferred because of its higher computational efficiency. And the solver SeDuMi can give accurate enough results (low duality gap) only when the proposed conic formulation is used, which further demonstrates the importance of the proposed conic formulation. If in some cases where the optimal solution needs to be extremely accurate, i.e., a very small duality gap is required, then the combination of the proposed conic formulation

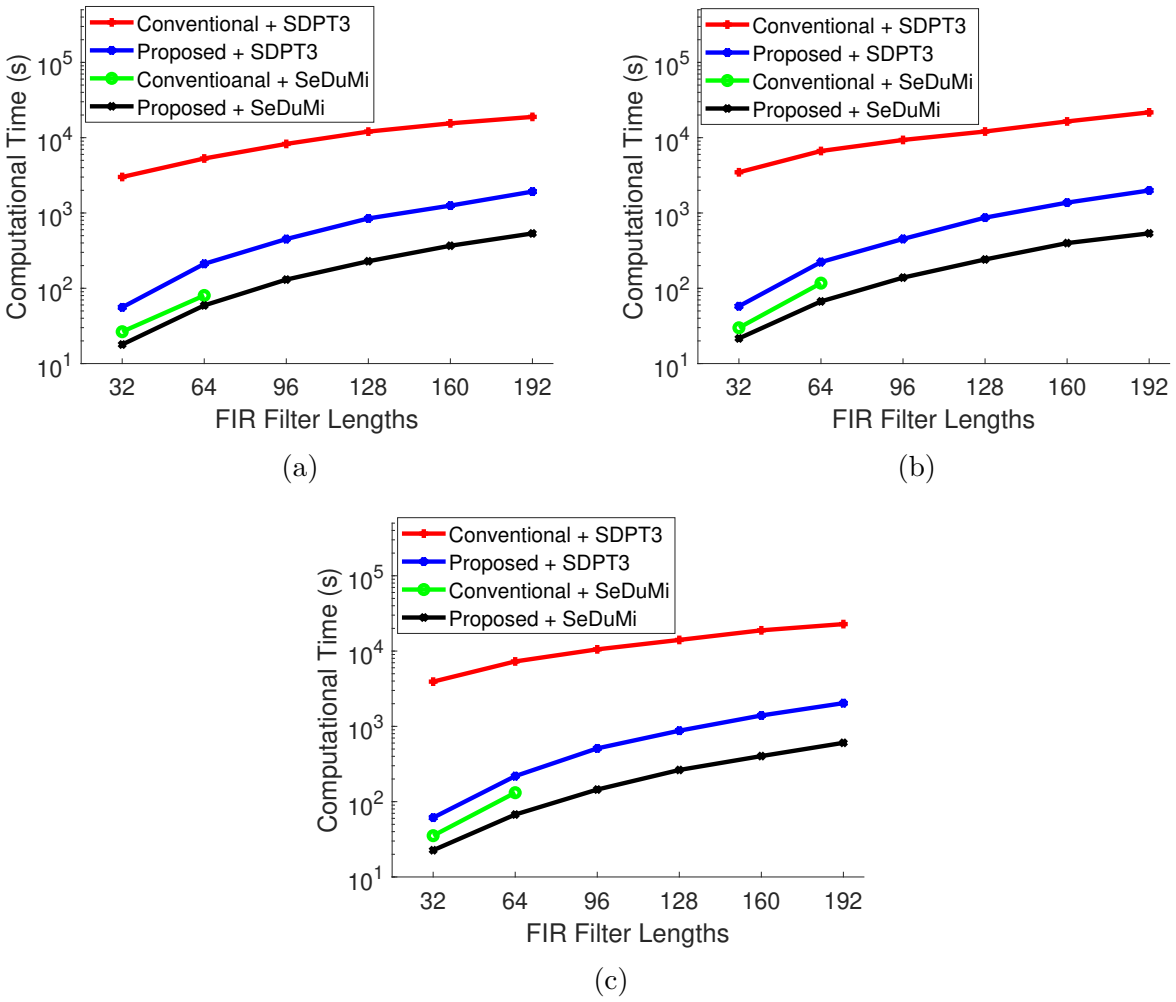


Figure 3.10. The computational time when using (a) 56 frequencies (60 Hz frequency interval), (b) 83 frequencies (40 Hz frequency interval), and (c) 111 frequencies (30 Hz frequency interval) for stability and robustness constraints.

and the solver SDPT3 can be chosen to solve the problem to have a higher accuracy by sacrificing the efficiency.

3.5.6 Investigation of the warmstarting strategy

The noise control performance was first compared using different proposed relaxation methods: (1) using the original PSDCs (Eq. (3.8) and Eq. (3.13)); (2) using the proposed constraint relaxation via the maximum norm (Eq. (3.26)), which is referred to as "Mod-

Max" in figures; (3) and using the proposed constraint relaxation via the Frobenius norm (Eq. (3.29)) which is referred to as "Mod-Fro". In this part, the used sampling rate is 4 kHz.

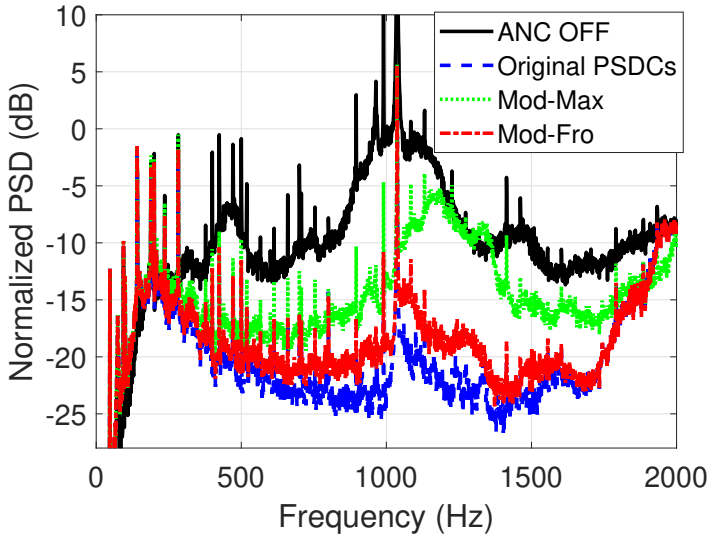


Figure 3.11. The comparison of noise control performance between the originally used PSDCs robust stability constraints, relaxed SOC robust stability constraints using the maximum norm, and relaxed SOC robust stability constraints using the Frobenius norm.

The noise control performance comparison is shown in Fig. 3.11, the comparison of the value of $\max\left(\lambda\left(\frac{\mathbf{A}_s(f_k)+\mathbf{A}_s(f_k)^{\mathrm{H}}}{2}\right)\right)$ is shown in Fig. 3.12. The ϵ_s is set to be 0.01, thus the value should be less than 0.99 to be considered stable. It can be observed from Fig. 3.11 that, compared with the proposed relaxed constraint via the maximum norm, the proposed relaxed constraint via the Frobenius norm has a much better noise control performance especially from 1.2 kHz to 1.5 kHz. This result can be confirmed from Fig. 3.12. All three methods have stable filter design results because the values of all three methods are less than 0.99. Compared with the original PSDCs which are very close to 0.99, the proposed relaxed constraint via the Frobenius norm is closer to 0.99 and the proposed relaxed constraint via the maximum norm is much less than 0.99. This demonstrated that the proposed relaxed constraint via the maximum norm is a more conservative relaxation compared with the proposed relaxed constraint via the Frobenius norm. Therefore, in the investigation of the

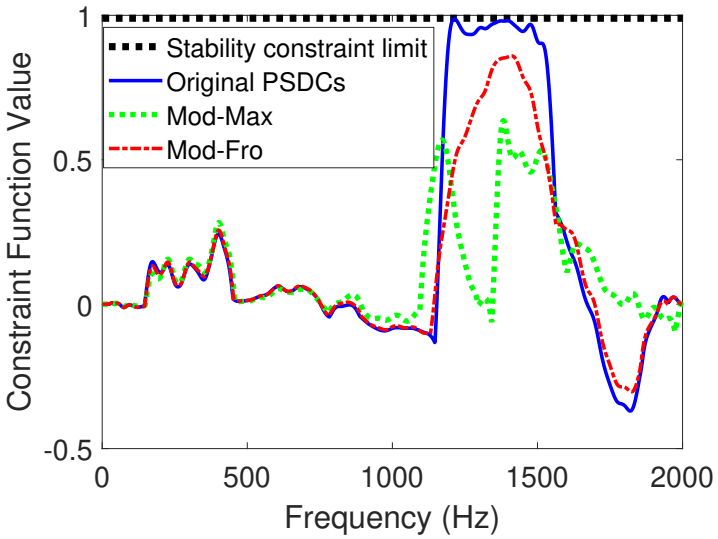


Figure 3.12. The comparison of the value of stability constraint function values when using the originally used PSDCs robust stability constraints, relaxed SOC robust stability constraints using the maximum norm, and relaxed SOC robust stability constraints using the Frobenius norm. The ϵ_s is set to be 0.01 and thus the value should be less than 0.99 to be considered stable.

warmstarting performance, the proposed relaxed constraint via the Frobenius norm will be used for the SOC only case.

To investigate the warmstarting method performance, a series of perturbed problems were generated from the measured reference signal. Three types of perturbation are considered: (a) perturbation of reference signal $\mathbf{S}_{xx}$; (b) perturbation of secondary path responses $\mathbf{G}_{\mathrm{e}}$; and (c) perturbation of acoustical feedback path responses $\mathbf{G}_s$. The perturbed system responses for those three cases are generated using equations:

$$\begin{aligned}
\mathbf{S}_{xx}^{new} &= \mathbf{S}_{xx} \odot \left(\mathbf{E}_{N_r,N_r} + \frac{\eta}{2} \left(\mathbf{P}_{N_r,N_r} + \mathbf{P}_{N_r,N_r}^{\mathrm{T}} \right) \right) \\
\mathbf{G}_{\mathrm{e}}^{new} &= \mathbf{G}_{\mathrm{e}} \odot \left(\mathbf{E}_{N_{\mathrm{e}},N_s} + \eta \mathbf{P}_{N_{\mathrm{e}},N_s} \right) \\
\mathbf{G}_{s}^{new} &= \mathbf{G}_{s} \odot \left(\mathbf{E}_{N_r,N_s} + \eta \mathbf{P}_{N_r,N_s} \right)
\end{aligned} \tag{3.42}$$

where $\mathbf{S}_{xx}^{new}$, $\mathbf{G}_{\mathrm{e}}^{new}$, and $\mathbf{G}_{s}^{new}$ denote the cross-spectral density matrix of the reference signal, secondary path response matrices, and acoustical feedback path response matrices in the

perturbed problems for three different cases, respectively; $\mathbf{S}_{xx}$, $\mathbf{G}_{\mathrm{e}}$, and $\mathbf{G}_s$ are measured from the experimental setup; $\odot$ denotes the Hadamard product (element-wise product). $\mathbf{E}_{m,n}$ denotes an m-by-n matrix with all elements being 1. $\mathbf{P}_{m,n}$ is an m-by-n matrix with each element generated from a standard Gaussian process. η denotes the perturbation ratio as a measure of how much the problem is changed. It is noted that, the representation of perturbation in $\mathbf{S}_{xx}^{new}$ is different from that in $\mathbf{G}_{\mathrm{e}}^{new}$ and $\mathbf{G}_s^{new}$ because $\mathbf{S}_{xx}^{new}$ should always be positive semidefinite. Thus, the perturbation for $\mathbf{S}_{xx}^{new}$ should be symmetric.

In this part, three different η values are used: 0.1%, 1%, and 5% to investigate the warmstarting performance under different perturbation levels. Two different ANC formulations were investigated: (1) the original convex formulation Eq. (3.14) (eventually becomes Eq. (3.21) after reformulation) which is denoted as mixed SOC and PSDCs case; and (2) the problem using proposed relaxation method via the Frobenius norm, i.e., Eq. (3.8) and Eq. (3.13) are replaced by Eq. (3.29) (denoted as SOC only case). Seven different values of warm ratio γ in Eq. (2.54) are used: 0.8, 0.9, 0.99, 0.999, 0.9999, 0.99999, and 0.999999. For each perturbation type, perturbation ratio, formulation, and warm ratio combination, 10 different perturbed problems are generated randomly, and the number of iterations needed to solve the filter design optimization problems is compared. It is noted that the number of iterations is used instead of the solving time because the computation time for each iteration in similar problems is usually the same 3.5.4 while the total solving time may be affected by the number of cores or threads used in computers.

The warmstarting performance is compared in Fig. 3.13. Those figures show the mean and standard deviation of the iteration ratio, i.e., the ratio of the number of iterations using the warmstarting method to the number of iterations using the cold start method. When the proposed relaxation method was used (Fig. 3.13 (a) (c) (e)), the warmstarting method can effectively reduce the required number of iterations using a wide range of warm ratios. However, if the proposed relaxation method is not applied to convert PSDCs into SOC (Fig. 3.13 (b) (d) (f)), the warmstarting method cannot have satisfactory results (the iterations ratios are around 1 or even larger than 1). This demonstrated that the proposed relaxation method 2 is essential to ensure the warmstarting method can work properly.

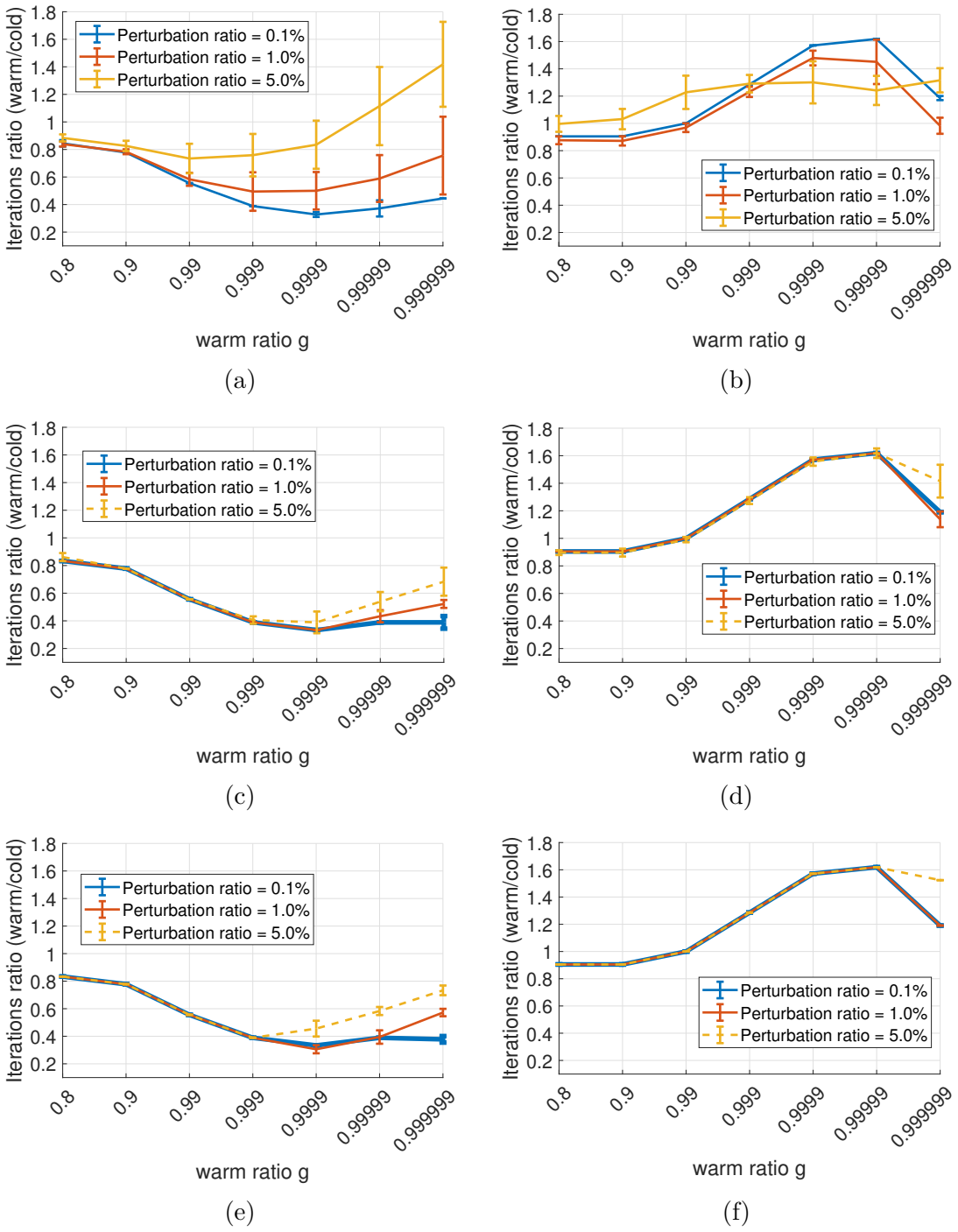


Figure 3.13. The comparison of the warmstart performance when perturbing $\mathbf{S}_{xx}$ using (a) SOCs only formulation, (b) mixed SOCs and PSDCs formulation; perturbing $\mathbf{G}_{\mathrm{e}}$ using (c) SOCs only formulation, (d) mixed SOCs and PSDCs formulation; perturbing $\mathbf{G}_s$ using (e) SOCs only formulation, (f) mixed SOCs and PSDCs formulation.

It is shown in Fig. 3.13 as expected that the smaller the perturbation ratio is (i.e., the more similar the new problem is to the original problem), the better the warmstarting method performs. When the perturbation ratio is about 0.1%, using a warmstarting ratio of 0.999 requires less than 40% of cold start iterations to solve all SOC only cases, which significantly reduces the required computational effort of designing the ANC filter. Even at a relatively high perturbation ratio (5%), the warmstarting method can still require less than 40% of cold start iterations for changing the secondary path $\mathbf{G}_e$ and the acoustic feedback path $\mathbf{G}_s$ cases and require less than 80% of the iterations for changing the primary signal spectral cases. Figure 3.13 also shows that when the warm ratio is too close to 1 (e.g., larger than 0.9999), the resulted initial points are too close to the boundaries and the required iterations are actually increasing with the increase of warm ratio γ. The warm ratio higher than 0.999999 is not shown because it will then be highly likely outside the boundaries of constraint functions and cannot be used as an initial point.

Another conclusion from Fig. 3.13 is that the standard deviation of iteration ratios is also small for most cases when an appropriate warm ratio is used such as 0.999. In some small perturbation cases (e.g., 0.1% or 1%), the reduction ratio is almost the same for randomly generated 10 cases, so the standard deviation is approximately 0 as shown in Fig. 3.13. This means that the warmstarting method is relatively reliable for different problems with similar environmental settings. This finding also confirms the conclusions in Section 3.5.4 that the required iteration is insensitive to the variation in data sets if they are from similar environmental settings. This result further demonstrates the importance of the proposed warmstarting strategies because the reduction in iterations cannot be achieved by simple methods such as data set tuning while the proposed warmstarting strategy can effectively and reliably achieve this reduction in iteration numbers. It is noted that the ANC performance will not be affected by using the warmstarting method compared with using the cold start method because the ANC filter design formulation is convex.

3.5.7 Investigation of the singular vector filtering method

The experimental setup in this section is different from the previous sections. A similar setup to the works of Wang et al. [114] is used and shown in Fig. 3.14. The ANC system consists of two reference microphones (i.e., $N_r = 2$), four error microphones (i.e., $N_e = 4$), two loudspeakers as secondary sources (i.e., $N_s = 2$), and two loudspeakers as primary noise sources. All microphones and speakers were placed symmetrically on both sides with respect to the dummys head. When acquiring measurement data, the sampling rate of the data acquisition system was set to 24 kHz with proper anti-aliasing filters. Two million sampling points (around 83 seconds) for each channel were acquired for calculating the correlation matrices. A hamming window of 24000 points is used for averaging with fifty percent overlapping (165 times averages) to compute the cross-spectral matrix first. Then the correlation function is computed by inverse Fourier transform on corresponding terms in the cross-spectral matrix. After measuring the secondary path responses, an appropriate delay is added to the secondary path representing the total time delay in the electronic controller due to ADC, processing time, DC removal high pass filters, anti-aliasing, and reconstruction filters. The sampling frequency of the control filter was chosen to be 2000 Hz. The length of the FIR filter for each channel is 128. Thus, there are 512 singular vectors in total after decomposing matrix $\mathbf{A}_{wi}$.

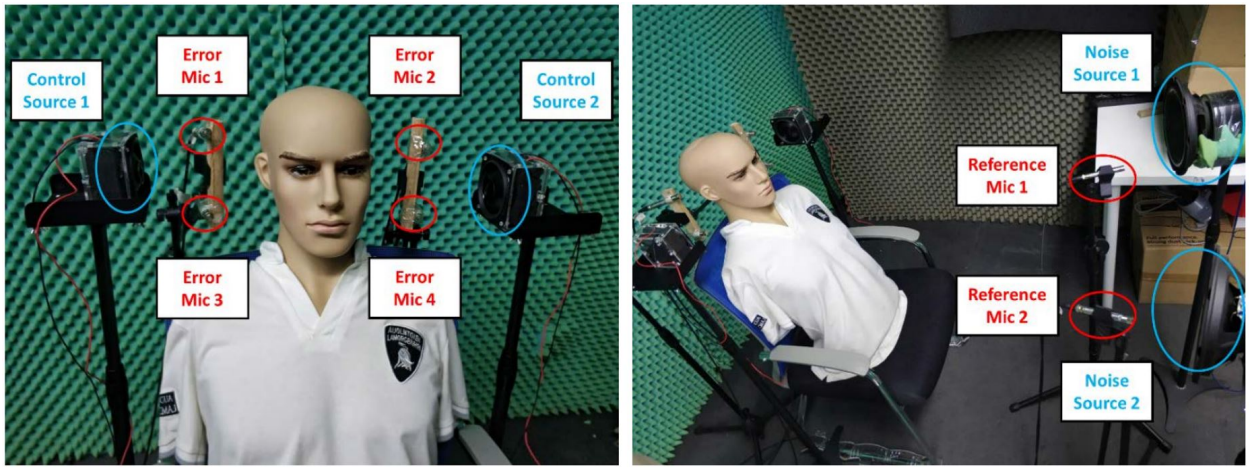


Figure 3.14. The experimental setup for investigating the singular vector filtering method.

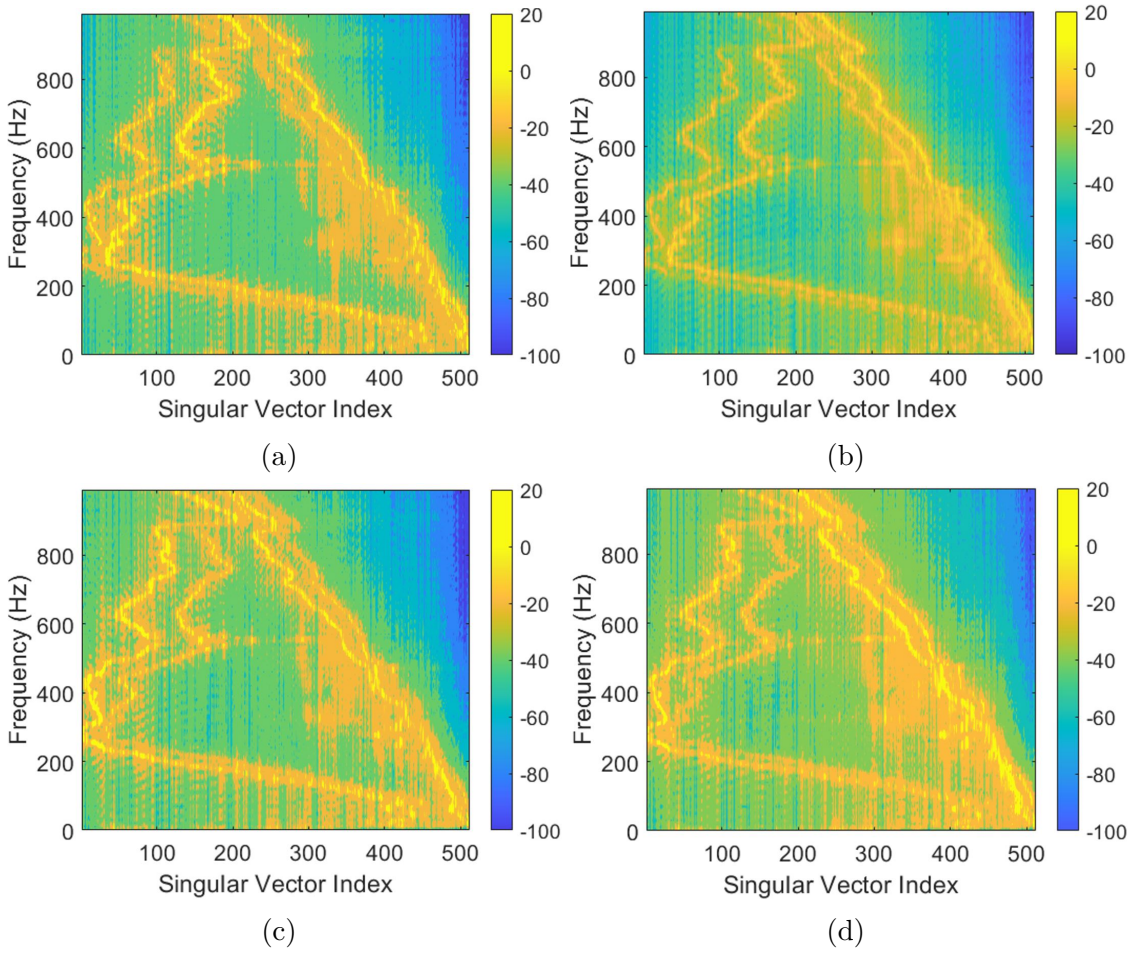


Figure 3.15. Frequency responses of singular vectors of auto-correlation matrix associated with (a) the 1st input and 1st output channel, (b) the 2nd input and 1st output channel, (c) the 1st input and 2nd output channel, and (d) the 2nd input and 2nd output channel.

The results presented in this section are based on offline simulations using experimentally measured data in the setup described above. The frequency responses of singular vectors are shown in Fig. 3.15. Because there are two reference microphones and two control speakers, i.e., 4 channel pairs, there are in total 4 plots denoted from (a) to (d) in Fig. 3.15. The singular vector index denotes the index for singular vectors associated with singular values sorted from large to small.

The comparison of noise control performance is shown in Fig. 3.16. "Wiener filter" denotes the result when the ANC system is operating using $\mathbf{w}_{wi,opt}$ in Eq. (2.2). "Truncated SVD method" denotes the result when the ANC system is operating using $\mathbf{w}_{wi,0}$ in Eq. (3.32)).

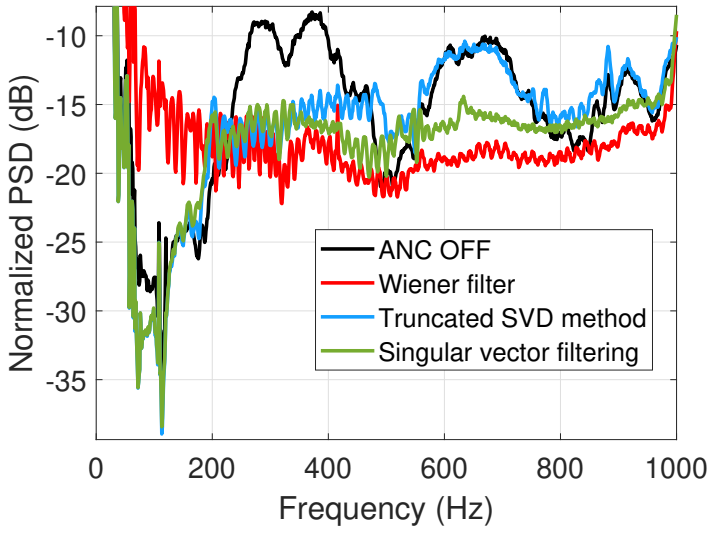


Figure 3.16. Comparison of averaged sound pressure at the error microphones for truncated SVD method and proposed singular vector filtering method.

"Singular vector filtering" denotes the result when the ANC system is operating using $\mathbf{w}_{wi,sum}$ in Eq. (3.41)). By comparing "Wiener filter" and "ANC OFF", it is obvious that the noise amplification phenomenon occurs at frequencies below 200 Hz. It is also noted that the Wiener filter can result in a reasonable ANC performance above 200 Hz. From Fig. 3.15, the singular vectors above index 120 are considered to have a large magnitude of frequency responses where noise amplification occurs below 200 Hz. So, the stopbands of band-stop filters used in the current work are specified to cover those three frequency ranges and l in Eq. (3.32)) is chosen to be 120. The index m is chosen to be 350 because some trials show that the responses above index 350 only contribute to noise amplification. On the other hand, frequency responses corresponding to singular vectors (shown in Fig. 3.15) indeed show that, although the singular vectors from index 120 to 350 have strong responses below 200 Hz where noise amplification occurs, some of them also have strong responses at frequency range above 200 Hz, which may be important contributors to the noise control performance. Thus, truncating them will negatively affect the noise control performance at those frequency ranges. After applying the truncated SVD method and singular vector filtering method,

from Fig. 3.16, it can be seen that both "Truncated SVD method" and "Singular vector filtering method" can mitigate the noise amplification effectively. Although the singular vector filtering method also sacrifices a certain level of noise control performance compared with the Wiener filter, this proposed method can still have a better noise control performance compared with the truncated SVD method in the frequency bands where no enhancement occurs when the Wiener filter is used (in this example, 400 Hz to 800 Hz).

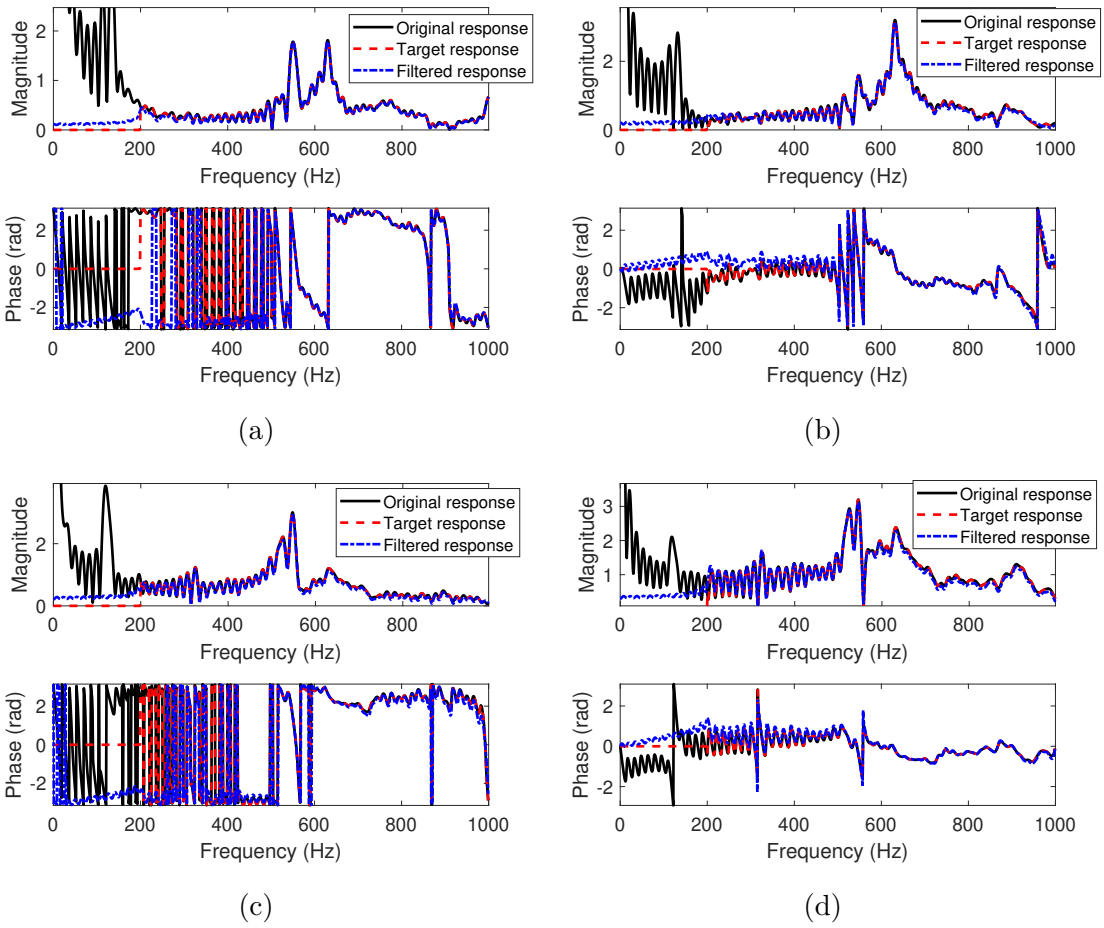


Figure 3.17. Comparison of total frequency responses of singular vectors indexed from 120 to 350 for the original response, target response, and filtered response associated with: (a) the 1st input and 1st output channel, (b) the 2nd input and 1st output channel, (c) the 1st input and 2nd output channel, and (d) the 2nd input and 2nd output channel.

To better demonstrate the proposed singular vector filtering method, Fig. 3.17 shows the frequency responses of the sum of singular vectors from index 120 to index 350. "Orig-

inal responses" denotes the frequency responses of those singular vectors from the Wiener filter $\mathbf{w}_{wi,opt}$, i.e., the $\mathbf{W}_{wi,sum,i,j}$; "Target responses" denotes $\tilde{\mathbf{W}}_{wi,sum,i,j}$, the direct modified frequency responses; "Filtered responses" denotes the final frequency responses after fitting, i.e., the frequency responses of $\mathbf{v}_{wi,sum}$. From Fig. 3.17, it can be observed that the proposed method can fit a $\mathbf{v}_{wi,sum}$ that closely matches the original frequency responses at frequency band where no noise amplification occurs, i.e., above 200 Hz, while attenuating the frequency responses below 200 Hz where noise amplification occurs.

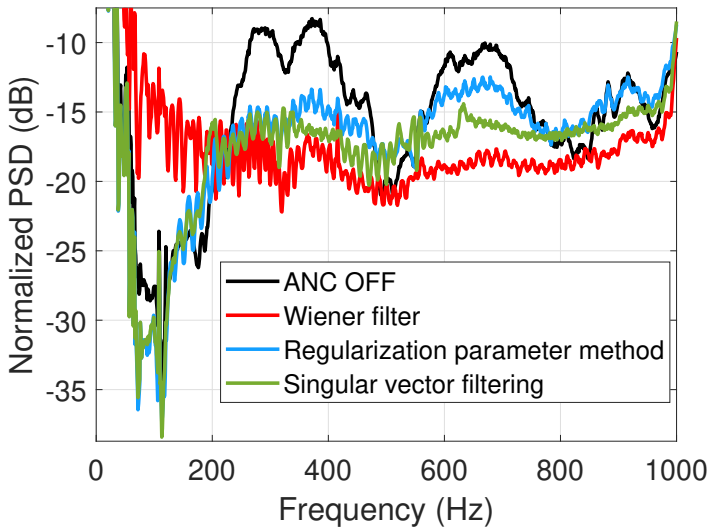


Figure 3.18. Comparison of averaged sound pressure at the error microphones for regularization method and proposed singular vector filtering method.

As mentioned in the previous sections, the regularization method, i.e., Eq. (2.7), can also mitigate noise amplification. Thus, the comparison of the performance of the regularization method and singular vector filtering method is shown in Fig. 3.18. The regularization parameter is tuned and adjusted such that it is around the minimum value that can mitigate the noise amplification to the desired level. From Fig. 3.18, the proposed singular vector filtering method can have a better noise control performance compared with the regularization parameter method.

The performance of two different singular vector filtering methods mentioned are compared in Fig. 3.19. "Singular vector filtering separate" denotes the result when the ANC

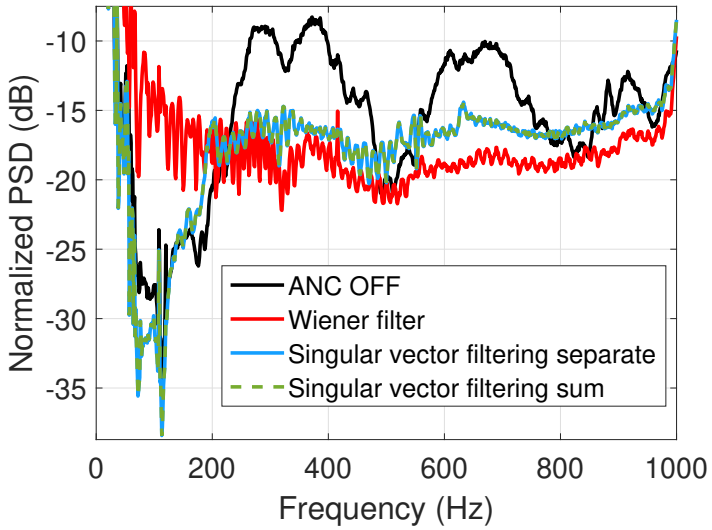


Figure 3.19. Comparison of averaged sound pressure at the error microphones for two different singular vector filtering methods.

system is operating using $\mathbf{w}_{wi,sep}$ in Eq. (3.38), i.e., filtering each filter separately. "Singular vector filtering method sum" denotes the result when the ANC system is operating using $\mathbf{w}_{wi,sum}$ in Eq. (3.41), i.e., filtering after summation. It can be seen that the performance has no obvious difference between these two methods. However, the calculation of $\mathbf{w}_{wi,sum}$ is much more computationally efficient, so using the singular vector filtering method in Eq. (3.41) is preferable in practice.

3.6 Summary

In this chapter, firstly a convex formulation for designing constrained optimal multichannel ANC filter is proposed. The traditional H_2/H_∞ framework is relaxed to a convex problem by replacing the non-convex stability constraint function with its convex upper bound. It is proved that using this upper bound is also less conservative compared with other convex stability constraints used in previous studies. The objective function and other constraint functions are greatly simplified to commonly used standard convex function formulations such that they can be reformulated to a standard conventional conic formulation. Then the

well-conditioned problem structure and sparsity pattern are exploited via dual formulation techniques. General cone programming solvers that implement primal-dual interior-point algorithms can be used to solve the proposed conic formulation.

Compared with the commonly used regularization parameter method to ensure the satisfaction of constraints, the proposed method can achieve better noise control performance, especially when the ANC system is complicated (i.e., systems with multiple channels, strong acoustic feedback path, high sampling rate, etc.). It was demonstrated that when dealing with complicated systems with practical product design considerations (e.g., an air-handling system in air conditioners), this proposed conic formulation will produce better non-adaptive noise control performance over regularization parameters method based algorithm, e.g., leaky LMS algorithm.

Compared with the traditional constrained optimization method, the proposed conic formulation is convex, which means a global minimum can always be found. The proposed method is more reliable since the required number of iterations in the numerical solving process is relatively small and is relatively independent of the filter length chosen in the filter design formulation. Finer frequency resolution in the cost function can also be chosen without significantly increasing the required solving time. With all these benefits, the proposed method allows the use of this constrained optimization method for a wider range of practical applications. It was also demonstrated that the proposed conic method can significantly reduce the computational time from the order of days to seconds, which, in principle, allows the constrained optimization method to be implemented in adaptive control applications through a continuous repeating of the optimal filter design process if the time-varying rate of the system signal characteristics is on the order of minutes. Even for non-adaptive filter design applications, the computation time reduction brought by the proposed method can also significantly accelerate the product development cycle, if this ANC technique is implemented in a commercialized product, since many product prototypes need to be developed to optimize various product design parameters, and the use of the proposed method can reduce the performance evaluation time for each product prototype.

Compared with the conventional conic formulation, the proposed conic formulation using duality techniques is more numerically stable and computationally efficient. Also, the exper-

imental result shows that solver SeDuMi is usually more computationally efficient, but less numerically stable than solver SDPT3. However, the numerical stability is usually sufficient when using SeDuMi if the proposed conic formulation is used. So, the combination of the proposed conic formulation and solver SeDuMi is preferable to be used to solve the multi-channel ANC filter design problem. If in some cases where extreme accuracy is required, i.e., a very small duality gap is needed, then the combination of the proposed simplified form and solver SDPT3 can be chosen to solve the problem to achieve higher accuracy by sacrificing the efficiency. The improvement of numerical stability and computational efficiency brought by the proposed conic formulation is also an important step to potentially realize constrained adaptive control for ANC systems with multiple types of constraints by a continuous redesign procedure.

The warmstarting strategies for the proposed conic formulation are also investigated. First, two relaxation methods are proposed to convert the original ANC design problem (i.e., mixed PSDCs and SOCs problem) to a SOC only problem. Results show that the relaxation of stability and robustness constraints using the Frobenius norm properties has a better noise control performance compared with the relaxation of stability and robustness constraints using maximum norm properties. It was demonstrated that it is essential to apply the proposed relaxation methods to the original ANC problem if the warmstarting method is to be applied. With an appropriate chosen warm ratio, less than 40% iterations are required using the warmstarting method compared with the cold start method. As long as the proposed relaxation method is applied, the warmstarting method can achieve better efficiency compared with using the cold start point for a wide range of warm ratios. These results demonstrated that the used warmstarting method combined with the proposed constraint relaxation can be used effectively and reliably in ANC applications. Practically, this is helpful for commercial product development that involves designing ANC filters in similar but different environmental setups.

The proposed conic formulation can be used for all discussed constraints. But when only the noise amplification (the disturbance enhancement) constraint is required, an alternative method, the singular vector filtering method, can be used. SVD is applied to the auto-correlation matrix of filtered-reference signals and the singular vectors are divided into

different groups. The group that contributes to both the noise control performance and noise amplification is replaced by a new set of filters. The results showed that the proposed singular vector filtering method can mitigate noise amplification and achieve better noise control performance compared with using either the singular vector filtering method or the regularization parameter method. Two different singular vector filtering methods were compared, i.e., filtering each singular vector in the second group separately or filtering after summing up those singular vectors. The results demonstrated that those two different approaches produce the same noise control performance if the disturbance occurs at similar frequency bands for each singular vector. Thus, filtering after summation is preferable because it is more computationally efficient than filtering separately while having similar noise control performance.

4. ACTIVE SOUND CONTROL APPLICATIONS USING THE PROPOSED CONIC FORMULATION

The proposed conic formulation in Chapter 3, including the proposed techniques in convex formulation Eq. (3.14) and its final conic formulation Eq. (3.21), will be applied to various ASC applications in this chapter. The proposed conic method, primarily designed for non-adaptive ANC applications in Chapter 3, will demonstrate its effectiveness in addressing more diverse and expansive ASC scenarios.

4.1 Adaptive Constrained Active Noise Control Filter Design Method

The improvements in numerical efficiency, stability, and reliability brought by the proposed conic formulation, make this non-adaptive filter design approach possible to be applied to time-varying environments by solving the constrained optimization problem continuously using updated system responses.

4.1.1 Control system description

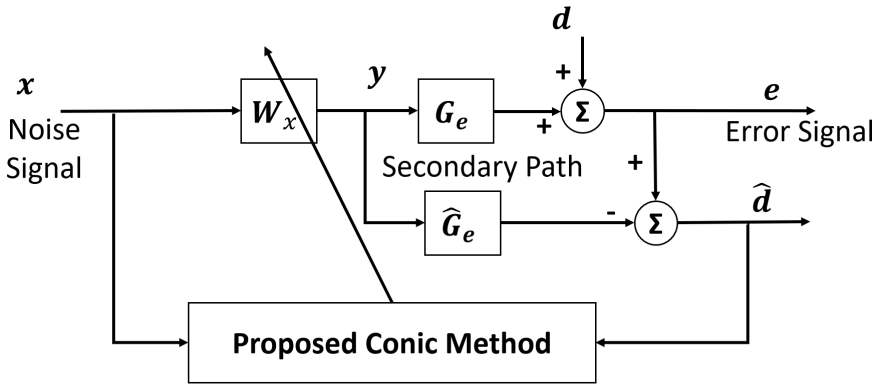


Figure 4.1. Block diagram of the proposed multi-channel adaptive constrained ANC filter design method.

The block diagram of the proposed adaptive constrained multi-channel ANC filter design method is shown in Figure 4.1 when $\hat{\mathbf{G}}_s$ is assumed to be a perfect model in the nominal operating condition (and omitted from the block diagram for brevity). Similar to the leaky

FxLMS method, an estimate of the secondary path, $\hat{\mathbf{G}}_e$, is also required in the real-time implementation to obtain an estimate of the disturbance signal $\hat{\mathbf{d}}$ so that the cross-spectral density matrix of $\mathbf{x}$ and $\mathbf{d}$ can be estimated during the real-time operation.

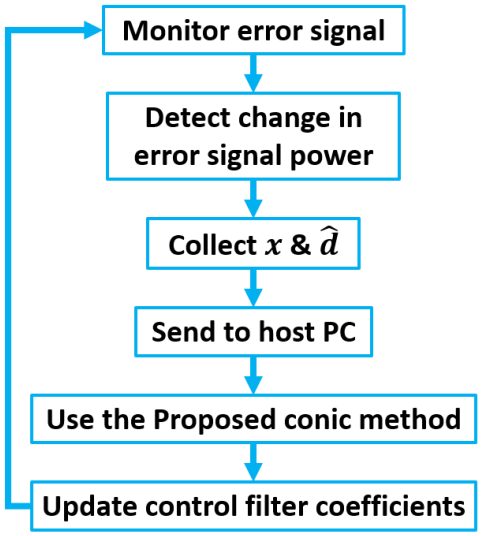


Figure 4.2. A flowchart of the proposed multi-channel adaptive constrained ANC filter design method.

The flowchart of the proposed method is shown in Figure 4.2. When the change of the error signal power exceeds a prescribed threshold, it indicates a change occurs in system response or environment characteristics, the signals $\mathbf{x}$ and $\hat{\mathbf{d}}$ can then be collected for a short period (e.g., 10 seconds) of time and are used to compute updated system responses. Then the proposed conic formulation in Chapter 3 can be used to compute the optimal ANC filter coefficients using the updated system responses. By continuously implementing this procedure, the optimal ANC filter coefficients under practical constraints can be updated in a time-varying environment.

4.1.2 Experimental results and discussions

A multi-channel ANC system was constructed in an anechoic chamber to investigate the ANC performance and related system characteristics of the proposed method. The experiment setup is shown in Figure 4.3. Two speakers were used as primary noise sources and

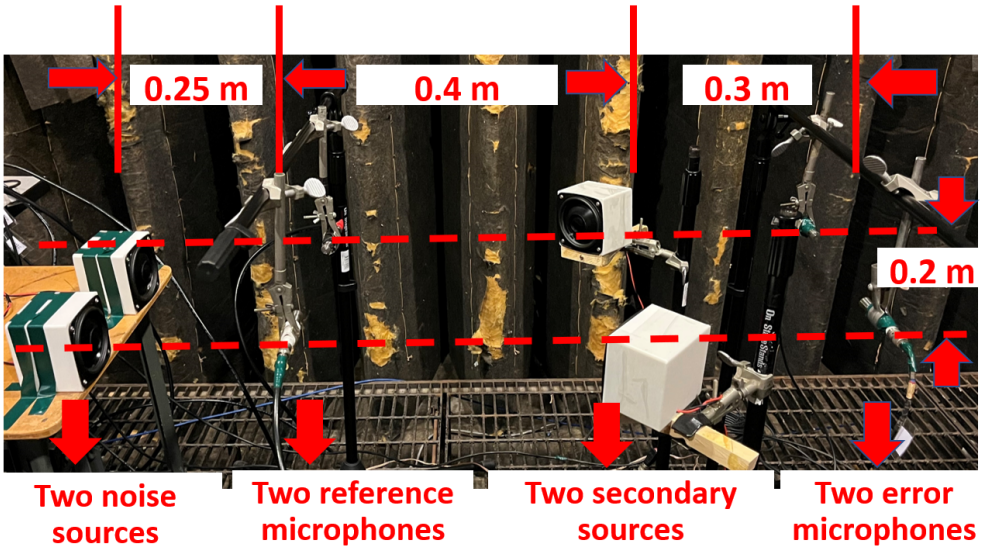
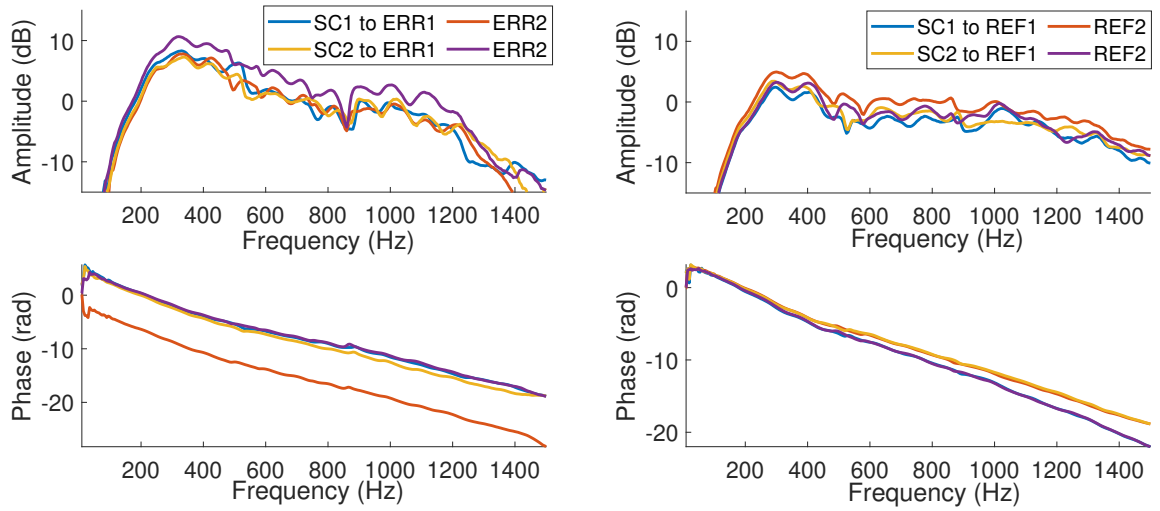


Figure 4.3. A picture of the experimental setup.

two speakers as secondary sources (control sources, i.e., $N_s = 2$). Two reference microphones ($N_r = 2$) and two error microphones ($N_e = 2$) were used. The key dimensions between components are also shown in Figure 4.3. The data acquisition and control algorithm was implemented using dSPACE MicroLabBox (MLBX_1302T). A high sampling rate (9 kHz) was used in the data acquisition process to reduce the electronic delay in the signal paths. After appropriately designed anti-aliasing and reconstruction filters, the measured signal is downsampled to 3 kHz which is the controller operation sampling rate. The desired noise control band was from 100 Hz to 1.4 kHz. In each channel, the filter lengths of ANC control filters, estimated secondary paths, and the estimated acoustic feedback paths were all chosen to be 64, i.e., $N_t = 64$.

The measured frequency responses of the secondary paths $\mathbf{G}_e$ and the acoustic feedback paths $\mathbf{G}_s$ are shown in Figure 4.4. From Figure 4.4, the amplitudes of the acoustic feedback paths' frequency responses are approximately in the same order as those of the secondary paths. This demonstrates that the acoustic feedback paths are strong and the unconstrained optimal ANC filter may cause an unstable closed loop $\mathbf{W}_x(f_k)\hat{\mathbf{G}}_s(f_k)$. In practice, stability constraints should be considered by either using the proposed constraint Eq. 3.8 and



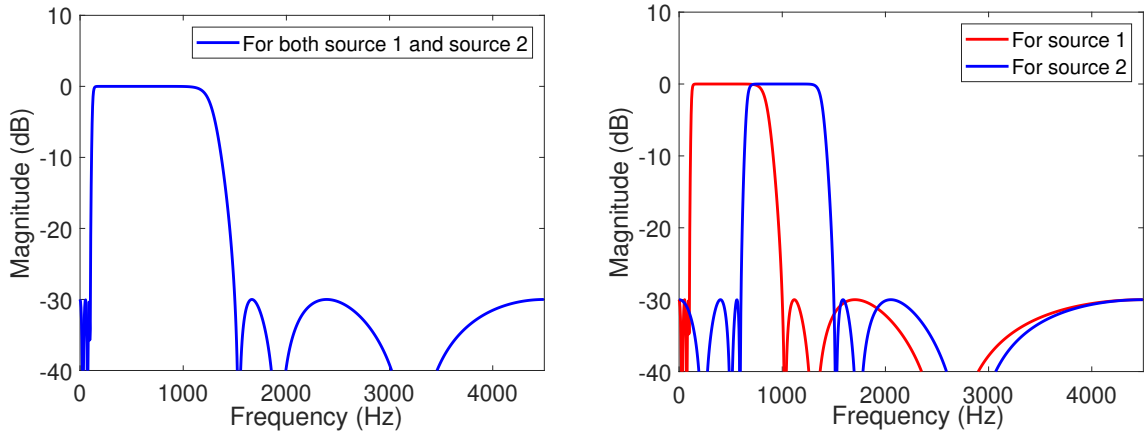
(a) (b)

Figure 4.4. The measured frequency responses of (a) secondary paths $\mathbf{G}_e$, and (b) acoustic feedback paths $\mathbf{G}_s$. "SC1" and "SC2" represent two control speakers; "ERR1" and "ERR2" represent two error microphones; "REF1" and "REF2" represent two reference microphones.

reformulated as the proposed conic formulation or tuning the leakage factor β in the leaky FxLMS method Eq. 2.8.

To create a time-varying environment in the experiment, two types of input signals for primary noise speakers were generated with different frequency spectral characteristics. First, two independent white noise signals were generated digitally and then they were filtered by different digital filters as the input signals for the noise source speakers. The frequency response magnitudes of the two types of digital filters are shown in Figure 4.5. Thus, there were two types of primary noise signal characteristics: (a) full-band case: both noise source speakers play independent noise signals from 100 Hz to 1450 Hz; (b) half-band case: one noise source speaker plays noise signal from 100 Hz to 950 Hz and another noise source speaker plays noise signal from 600 Hz to 1450 Hz. During the experiment, the noise signals can be switched from the full-band case to the half-band case to create a time-varying environment.

When using the leaky FxLMS method, the leakage factor β was tuned to be the smallest value that still produces a stable controller, which was 1×10^{-5} in this experiment. The



(a) (b)

Figure 4.5. The designed frequency responses of (a) full-band case: digital filter passband is from 100 Hz to 1450 Hz, and (b) half-band case: one digital filter passband is from 100 Hz to 950 Hz and another digital filter passband is from 600 Hz to 1450 Hz.

step length α was tuned to be the largest value that still satisfies the convergence of the algorithm, which was 0.1 in this experiment. Thus, in the experiment, the traditional leaky FxLMS was tuned to result in the best achievable ANC performance.

When implementing the proposed conic method, a 5 Hz frequency resolution was used in the filter design formulations (i.e., Eq. 3.21). To choose an appropriate updating interval for the proposed method, the approximate problem solution time for the conic formulation in this experimental setup is required. Thus, 100 cases using the same problem dimension in this experimental setup were first generated with random variations based on measured system responses and then tested in MATLAB R2021a in the host PC (CPU: 11th Gen Intel(R) Core(TM) i7-1185G7 @ 3.00GHz 1.80 GHz; RAM 32 GB; 64-bit operating system). The mean value and 3-sigma limit (99.7%) of the required computational time (in total CPU time summing across all threads) is 5.0 ± 1.8 seconds for solving the cone-programming-based ANC filter design problem, and 0.19 ± 0.16 seconds for computing the system responses spectra from collected data. Thus, in this experimental setup, 10 seconds were used for data collection to include sufficient data to compute the system response spectra, and 10 seconds were used for filter coefficient computation to allow sufficient time in solving the

proposed cone-programming-based ANC design formulation and updating the ANC filter in the controller.

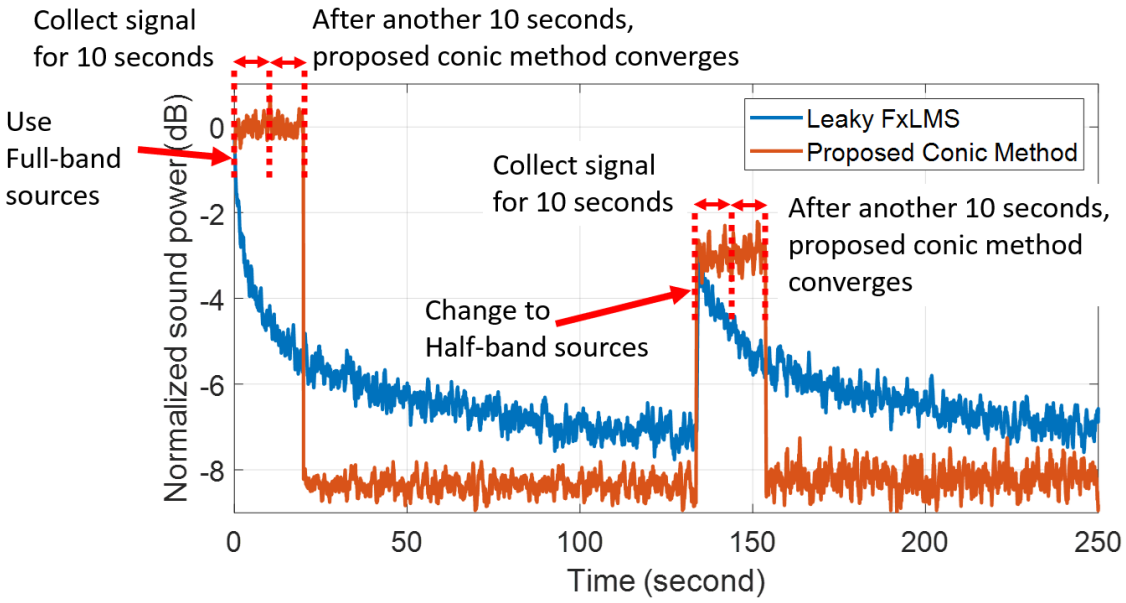


Figure 4.6. The comparison of ANC performance in the time domain using the traditional leaky FxLMS method and the proposed conic method. The power is normalized by the total error signal power at full-band noise sources case without using an ANC system.

The comparison of ANC performance in the time domain using the traditional leaky FxLMS method and the proposed method is shown in Figure 4.6. The full-band case was first used to drive the primary noise source speakers, the traditional FxLMS method started to update its filter coefficients and the noise power began to decrease. For the proposed conic method, immediately after the system changed from a deactivated state to an operating state, 10 seconds were used for collecting signals and another 10 seconds were used for computing the optimal filter coefficients. After the filter coefficients in the controller were updated using the computed optimal filter coefficients, the noise power using the proposed conic method immediately reached the optimal power level. Thus, the convergence time using the proposed method (in the current work, it is defined as the time from the moment when a change in system or environment characteristics occurs to the moment when the optimal

control performance is achieved) is 20 seconds in this experimental setup. However, the convergence time is more than 120 seconds for the traditional leaky FxLMS method.

When both methods converge for the full-band case, the noise source speakers will switch to the half-band case which causes a significant increase in the residual noise power level, because the current filter coefficients are not optimal after the change of primary noise signal characteristics. A similar process started again where the filter coefficients were updated by using both methods. Note that due to the limit in the data communication capability between the host PC and the controller, the ANC performance using the proposed method is measured separately for different stages and plotted in the same figure (i.e., the code loading period when updating the filter coefficients is truncated from the figure to match the time indices because the device will be temporarily shut off while loading the code). This implementation won't affect the conclusion because the proposed method is essentially stationary in each stage.

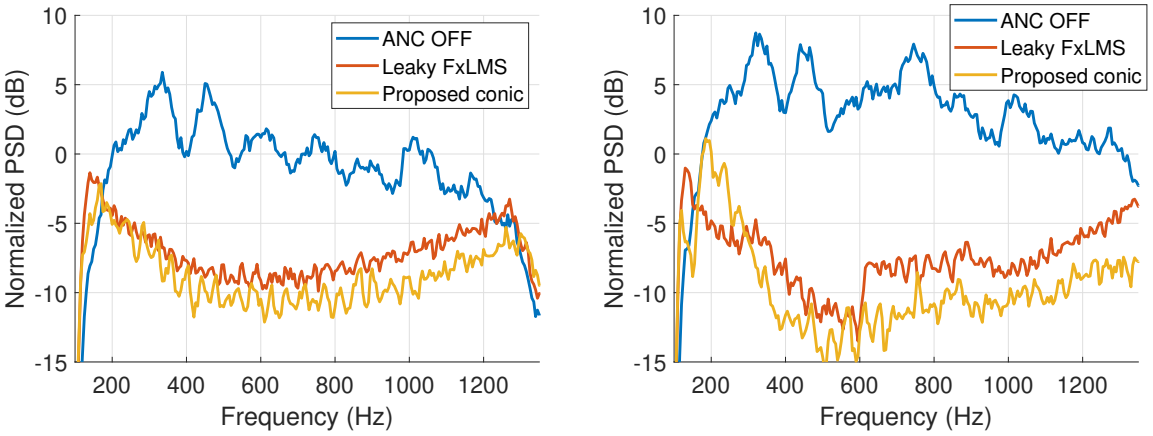


Figure 4.7. The comparison of steady-state ANC performance in the frequency domain when both the traditional leaky FxLMS and the proposed conic method converge for (a) full-band case, and (b) half-band case.

To better compare the steady state ANC performance, Figure 4.7 shows the ANC performance in the frequency domain when both the traditional leaky FxLMS and the proposed method converge for (a) full-band case, and (b) half-band case. Figure 4.6 and Figure 4.7

demonstrate that the proposed method has a faster convergence rate and better steady-state ANC performance compared with the traditional FxLMS method.

4.2 A Constrained Room Equalization Filter Design Method

In general, the purpose of room response equalization is to design equalization filters for loudspeakers to produce the desired sound at particular locations or regions in a given room environment. Unlike the usual room response equalization scenarios that use psychoacoustic effects to simplify the design process [12], [115]–[119], the focus of this section centers on the precise reproduction of sound fields for psychoacoustic subjective testing purposes. For an accurate assessment of human perception of sound, it is crucial to reproduce the sound field with accuracy, rather than solely reproducing the acoustic features previously deemed important.

A playback system for headphone-free psychoacoustic subjective test [120], [121] is considered in this section. To ensure that the sounds being evaluated by subjects are not altered, it is crucial to accurately reproduce all sound signal features, including content over a broad frequency range. Those psychoacoustic experiments are usually performed in a room that is configured to mimic the real environment where the target sound is heard (e.g., an office or factory environment depending on the purpose of the subjective test) [120]–[124]. A remote hidden loudspeaker away from the subject instead of a headphone is used to minimize any potential influence of equipment appearance on the results of psychoacoustic tests. However, this approach presents challenges due to the low-frequency room modes present in large rooms. Consequently, the equalization filter impulse response must have a long time span. Furthermore, the required high sampling frequency to reproduce sound over the full audible frequency range also necessitates a large number of coefficients for the designed equalization filters, especially when using an FIR filter structure. Another challenge of designing such equalization filters for subjective tests is that some response constraints may be needed in practical applications. For example, the loudspeaker should perform in its linear response range and the equalization filter should preserve the natural roll-off of loudspeakers at low

and high frequencies [12], [125], [126]. Some subjective tests may also require the spectrum power at certain frequency bands to be limited or accurate within a certain small error range.

The frequency domain deconvolution (FDD) method, initially proposed by Kulp [127], is commonly used for high-order constrained filter design applications mentioned above. This method involves obtaining the reciprocal of the room responses in the frequency domain and then applying the fast inverse discrete Fourier transform, which is numerically efficient even for high-order cases. Constraining the filter responses in the frequency domain can also be convenient in the frequency domain. However, the FDD method may result in excessive gains and long impulse responses [12], [128]. Regularization parameters can be added to reduce the impulse responses [129], [130] which may sacrifice the sound reproduction accuracy in the low-frequency content. It is later demonstrated in Section. 4.2.4 and 4.2.5 that the use of FDD may cause significant large errors in the low-frequency range.

The least-squares optimization method [12], [126], [131]–[135] is another viable approach for such accurate room equalization applications, as it typically yields an optimal equalization filter in terms of sound reproduction accuracy. However, the computational load will be high. In this section, an efficient constrained equalization filter design approach is derived by extending the proposed conic formulation in Chapter 3 which is essentially a type of least-squares optimization method. A reduced-order technique via sub-band methods is also proposed to further reduce the computational loads.

4.2.1 Control system description

The system block diagram of a typical room equalization filter design is shown in Fig. 4.8 (a). In the diagram, x denotes the original signal to be reproduced at the desired location. W is the designed equalization filter. y is the output of the filter. G_e is the system response between the speaker and the listening location. d denotes the desired signal which is obtained by delaying x by $m\Delta$, where Δ is the sampling interval of the original signal. This delay $m\Delta$ is added to ensure a satisfactory sound field reproduction performance when using a causal equalization filter W. $G_e\, y$ is the sound signal at the listening location which should

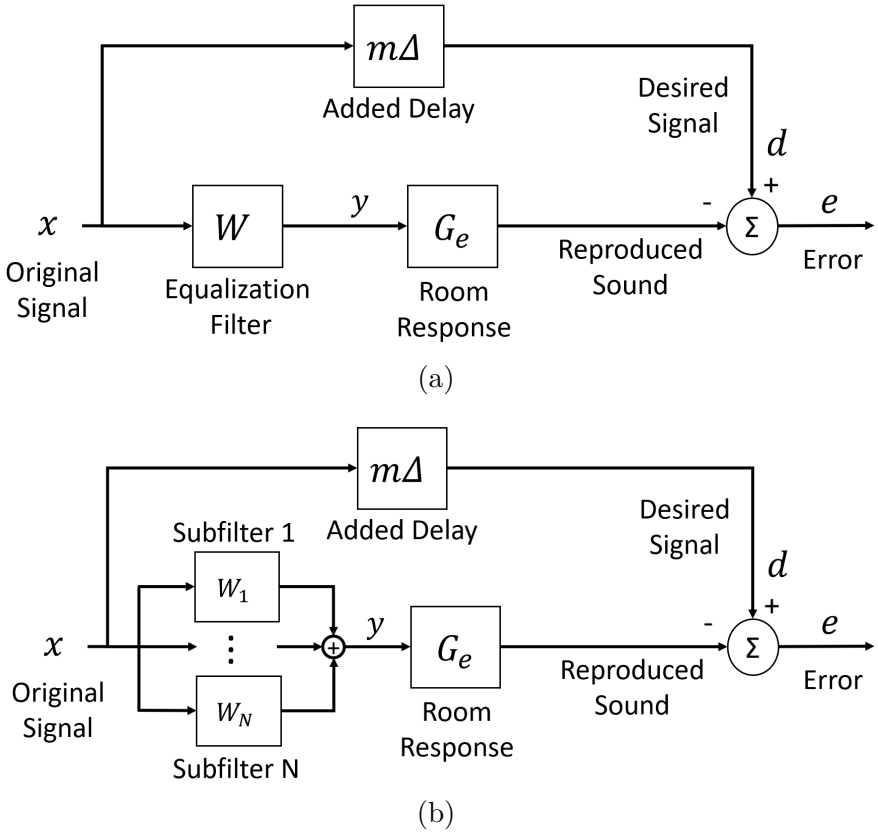


Figure 4.8. Block diagram for designing constrained equalization filter (a) in a full band filter structure, (b) in a subfilters structure.

be close to the desired signal d. Thus, the power of the error e should be minimized in this design problem.

Compared with the ANC block diagram Fig. 2.1 (b), the block diagram in Fig. 4.8 (a) has the same structure if the room response is treated as the secondary path. In the ANC application, d is a disturbance noise from the primary noise sources. In the room equalization filter design, d is just a delayed version of the reference signal x to represent the desired reproduced sound. Thus, in ANC applications, d is present in the physical setup as the primary noise. However, d is added to the room equalization filter design diagram for design purposes and it does not present in the physical setup.

To ensure the formulated design optimization problem is a convex problem such that a global optimal equalization filter W can be obtained, an FIR filter is used as the equalization

filter structure. However, the number of coefficients of this designed FIR filter, i.e., the design parameters, may be large because the required sampling rate is high and the impulse response is long. To reduce the computational load in the design phase, a subband filters technique can be used which is shown in Fig. 4.8 (b). The meanings of symbols in Fig. 4.8 (b) are similar to Fig. 4.8 (a). Although, it is noted that, if the subband filters are to be implemented in real-time filtering, the system response G_e should also include the analysis filter bank and synthesis filter bank effect.

4.2.2 The efficient room equalization filter design formulation

The equalization problem design problem can be formulated in a similar way as in the ANC problems. The frequency response at frequency f_k of the equalization filter W in Fig. 4.8 (a) can be expressed in the same way as in Eq. (2.9):

$$W(f_k) = \mathbf{F}_z(f_k, f_s, N_t)^{\mathrm{T}}\mathbf{w}, \tag{4.1}$$

where W here is the room equalization filter, and the other notations are the same as in Eq. (2.9). Note that $\mathbf{F}_z(f_k, f_s, N_t)$ is the same to $\mathbf{F}_z$ in Eq. (2.9) but with a more flexible notation for later usage:

$$\mathbf{F}_z(f_k, f_s, N_t) = \begin{bmatrix} 1 & \mathrm{e}^{-\mathrm{j}2\pi f \frac{1}{f_s}} & \mathrm{e}^{-\mathrm{j}2\pi f \frac{2}{f_s}} & \dots & \mathrm{e}^{-\mathrm{j}2\pi f \frac{N_t-1}{f_s}} \end{bmatrix}^{\mathrm{T}} \tag{4.2}$$

For the subfilters design in Fig. 4.8 (b), the total frequency response of all subfilters, $\tilde{W}(f_k)$, can be expressed as

$$\tilde{W}(f_k) = \sum_{i=1}^{N} W_i(f_k) = \sum_{i=1}^{N} \begin{bmatrix} 1 & \mathrm{e}^{\frac{-\mathrm{j}2\pi f_k}{f_{s_i}}} & \dots & \mathrm{e}^{\frac{-\mathrm{j}2\pi f_k (N_{t_i}-1)}{f_{s_i}}} \end{bmatrix} \mathbf{w}_i, \tag{4.3}$$

where w_i is the coefficients of the i-th subfilter, and f_{s_i} is the sampling frequency of i-th subfilter. It is noted that the Eq. (4.3) can be rearranged to

$$\tilde{W}(f_k) = \tilde{\mathbf{F}}_z(f_k)^{\mathrm{T}}\tilde{\mathbf{w}}, \tag{4.4}$$

where

$$\tilde{\mathbf{F}}_z(f_k) = \begin{bmatrix} \mathbf{F}_z(f_k, f_{s_1}, N_{t_1}) \\ \dots \\ \mathbf{F}_z(f_k, f_{s_N}, N_{t_N}) \end{bmatrix}, \qquad \tilde{\mathbf{w}} = \begin{bmatrix} \mathbf{w}_1 \\ \dots \\ \mathbf{w}_N \end{bmatrix},$$

and N_{t_i} is the number of coefficients of i-th subfilter. By comparing Eq. (4.1) and Eq. (4.4), it is obvious that designing subfilters in Fig. 4.8 (b) is equivalent to designing one filter in Fig. 4.8 (a) using a modified Fourier transform, i.e., $\tilde{F}(f_k)$. Then, the constrained optimization method used in designing ASC filters can be applied to design the equalization subfilters. In this section, only one channel is considered. The proposed method can be extended to the multi-channel case conveniently since, as shown below, the derivation is similar to the multi-channel ASC method in Chapter 3.

Similar to derivations in Section 2.1.4, the objective function $J_0(\tilde{w})$ is specified to minimize the total power of error signal $\mathrm{e}(n)$ cross all desired frequencies:

$$J(\tilde{\mathbf{w}}) = \sum_{k=1}^{N_f} J(f_k), \tag{4.5}$$

where $J(f_k)$ is the expected power of reproduction error at k-th frequency f_k. Similar to Eq. (2.12), $J(f_k)$ can be expressed as

$$\begin{aligned} J(f_k) &= \mathrm{E}\left(|\mathrm{e}(f_k)|^2\right) \\ &= \mathrm{E}\left(|d(f_k) - G_e\, y(f_k)|^2\right) \end{aligned} \tag{4.6}$$

Similar to the Eq. (2.14), a constraint can be applied on the amplitude of the equalization filter response, $\tilde{W}(f_k)$:

$$|\tilde{W}(f_k)| \leq \tilde{C}(f_k), \tag{4.7}$$

or subfilters responses, $W_\mathrm{i}(f_k)$:

$$|W_\mathrm{i}(f_k)| \leq C_i(f_k), \tag{4.8}$$

where $\tilde{C}(f_k)$ and $C_\mathrm{i}(f_k)$ are some nonnegative constants. The constraint on the filter response can ensure that the loudspeaker always operates in its linear response range. Also, the

magnitude of the frequency response of each subfilter should be limited around the cutoff frequency if those subfilters are to be implemented in real-time filtering.

Similar to the Eq. (2.13)„ a constraint on the allowed maximum error can be applied to enforce the sound field reproduction performance being achieved to some certain level

$$J(f_k) \leq A_{\mathrm{e}}(f_k) S_{xx}(f_k). \tag{4.9}$$

where $A_{\mathrm{e}}(f_k)$ is a nonnegative constant to ensure that the power of the error is less than some predefined threshold. This constraint is useful when a certain frequency band is of particular interest such that the sound field reproduction performance should be achieved to some certain degree. It is noted that if the desired sound field reproduction performance cannot be achieved by the causal FIR equalization filter, this constraint will lead to an infeasible optimization problem.

By using Eq. (4.5) as the objective function, Eq. (4.7) (4.8) (4.9) as the constraints, the convex optimization for designing the room equalization filter (subfilters) using the H_2/H_∞ formulation can be written as

$$\begin{aligned} \underset{\tilde{w}}{\text{minimize}} \quad & \sum_{k=1}^{N_f} J(f_k) \\ \text{subject to} \quad & |\tilde{W}(f_k)| \leq \tilde{C}(f_k), \quad \text{for all } f_k \\ & |W_i(f_k)| \leq C_i(f_k), \ \text{for all } f_k \text{ and } i \\ & J(f_k) \leq A_{\mathrm{e}}(f_k) S_{xx}(f_k), \quad \text{for all } f_k. \end{aligned} \tag{4.10}$$

Similar to the derivations given in the proposed conic formulation in Chapter 3 (i.e., from Eq. (2.17) to Eq. (3.21)), Eq. (4.10) can be reformulated as a proposed conic form and solved by primal-dual interior-point method solvers such as SDPT3 [98], [108], [109], SeDuMi [99], [110], or MOSEK [111].

4.2.3 A reduced order technique

Although the proposed conic method can solve the optimization Eq. (4.10) efficiently, the computational load can still be significant if the designed equalization filter has a large number of coefficients due to high sampling frequency and long impulse response. In the case of long impulse response due to room responses, a reduced order technique is proposed in this section to reduce the design parameters.

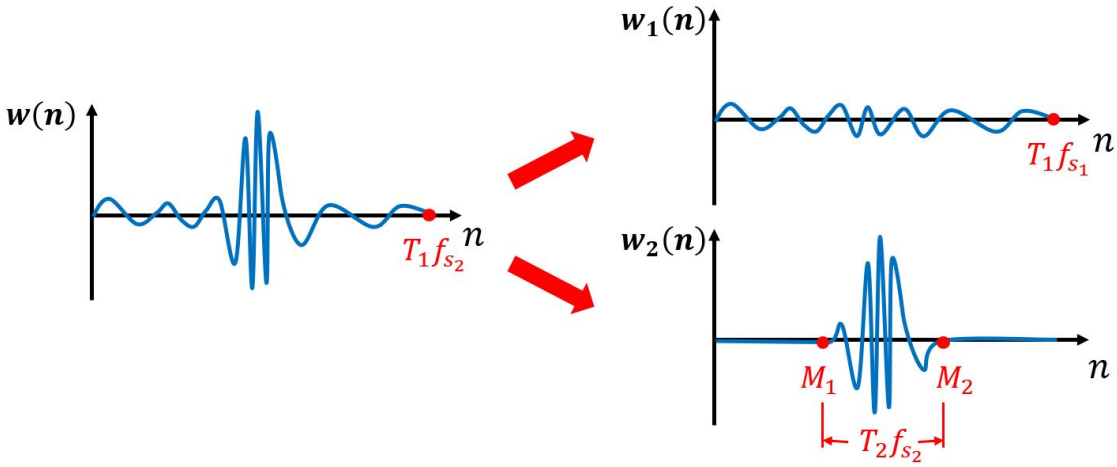


Figure 4.9. An illustration of dividing an equalization filter into two subfilters with different impulse response lengths and sampling frequencies.

In large room sound reproduction applications, although the desired equalization filter has a long impulse response and high sampling frequency, the higher frequency information is usually concentrated in a short time span. This implies that, if the equalization filter to be designed includes several sub-band filters, only subfilters at low frequencies (which are to equalize the room response features that are dominated by low-frequency room modes) have long impulse response times, while the subfilters in high-frequency sub-bands may only have a short impulse response time length. Order reduction can then be achieved by using a low sampling rate for low-frequency subfilters that have long response times, while a high sampling rate for high-frequency subfilters with short response time length.

An illustration of the above-mentioned reduced order method is shown in Fig. 4.9, where $\mathbf{w}(n)$ represents the desired full band equalization filter whose length is T_1 and a high sam-

pling frequency, f_{s_2}, has to be used to effectively reproduce the high-frequency content; $\mathbf{w}_1(n)$ represents a subfilter that has a longer length T_1 but with a lower sampling frequency f_{s_1}, and $\mathbf{w}_2(n)$ represents a subfilter that has a shorter length T_2 and higher sampling frequency f_{s_2}. It is also noted that if the loudspeaker is at a distant location from the listening location, the high-frequency subfilter $\mathbf{w}_2(n)$ may exhibit a pure time delay behavior due to the large added delay (i.e., $m\Delta$ in Fig. 4.8), which, in Fig. 4.9, corresponds to the zero response in impulse response before the time M_1. The parameter M_1 can be estimated to be the difference of added delay ($m\Delta$ in Fig. 4.8) and the time for sound propagating from the loudspeaker to the listening location. Once the time delay M_1 is estimated, there is no need to have undetermined filter coefficients in $\mathbf{w}_2(n)$ before M_1, which is an additional order reduction. Due to the existence of low-frequency room modes in a relatively large room, $T_1 \gg T_2$ and $f_{s_1} \ll f_{s_2}$, this then suggests that the required number of design parameters for a sub-band structure, $T_1 f_{s_1} + T_2 f_{s_2}$, is much smaller than that for a full band filter structure, $T_1 f_{s_2}$.

The implementation of this reduced-order technique is convenient if the proposed conic formulation is used. For example, when implementing the reduced-order technique for the case in Fig. 4.9, the only formulation that needs modification is the Fourier transform vector $\mathbf{F}_z(f_k, f_{s_2}, T_1 f_{s_2})$ associated with the subfilter $\mathbf{w}_2(n)$. More specifically, the Fourier transform vector $\mathbf{F}_z(f_k, f_{s_2}, T_1 f_{s_2})$ should be modified to a reduced-order Fourier transform vector $\mathbf{F}_r(f_k, f_{s_2}, M_1, M_2)$:

$$\mathbf{F}_r(f_k, f_{s_2}, M_1, M_2) = \left[\mathrm{e}^{\frac{-\mathrm{j}2\pi f_k M_1}{f_{s_2}}} \quad \dots \quad \mathrm{e}^{\frac{-\mathrm{j}2\pi f_k M_2}{f_{s_2}}} \right]^{\mathrm{T}}, \tag{4.11}$$

which is mathematically equivalent to assuming the impulse response for the subfilter $\mathbf{w}_2(n)$ before time M_1/f_{s_2} is zero. Thus, the designed parameters can be significantly reduced to reduce the computational load and avoid potential numerical instability issues for large-scale optimization problems.

4.2.4 Simulation results and discussions

To investigate the proposed filter design approach. Rooms of two different sizes (denoted as "small room" and "large room") are simulated using the image sources method. The

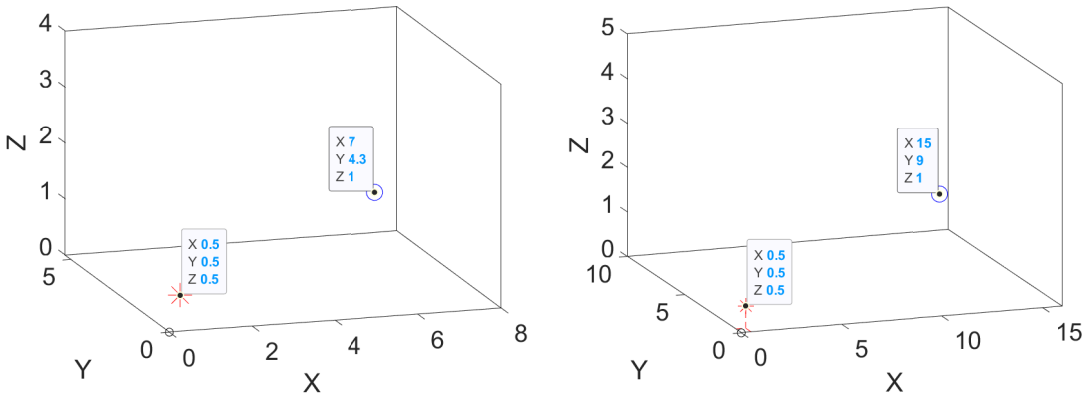


Figure 4.10. An illustration of setups for simulating (a) the small room and (b) the large room. The stars represent the source and the circles represent the listening location. (Unit: meters)

dimensions of the simulated small room are 8 meters in length, 5.3 meters in width, and 4 meters in height. And the dimensions of the simulated large room are 16 meters in length, 10 meters in width, and 5 meters in height. In both rooms, the reflection coefficients of each surface are obtained by assuming the floor is carpeted on concrete and all other surfaces are acoustic tiles on rigid surfaces [136]. The speaker is assumed to be a monopole positioned at a corner 0.5 meters away from the floor and the other two surfaces. The listening location is assumed to be 1 meter in height and 1 meter away from both surfaces. The illustration of setups for the two simulated rooms is shown in Fig. 4.10.

The impulse responses and the frequency responses of the paths from the speaker input to the listening location in two simulated rooms are shown in Fig. 4.11. A point-wise smoothing was implemented with a moving Hann window which covers a one-third octave band centered on the frequency [121], [137]. From Fig. 4.11 (a) (c), the high-frequency content is concentrated in a narrow time-domain region while the low-frequency content spreads out over a long time span. This is one of the key motivations in the proposed reduced-order technique using sub-band design. In the frequency response, "True responses" demonstrates the actual simulated results while the "Used responses" demonstrates the responses used to design filters. The only difference between the "True responses" and the "Used responses"

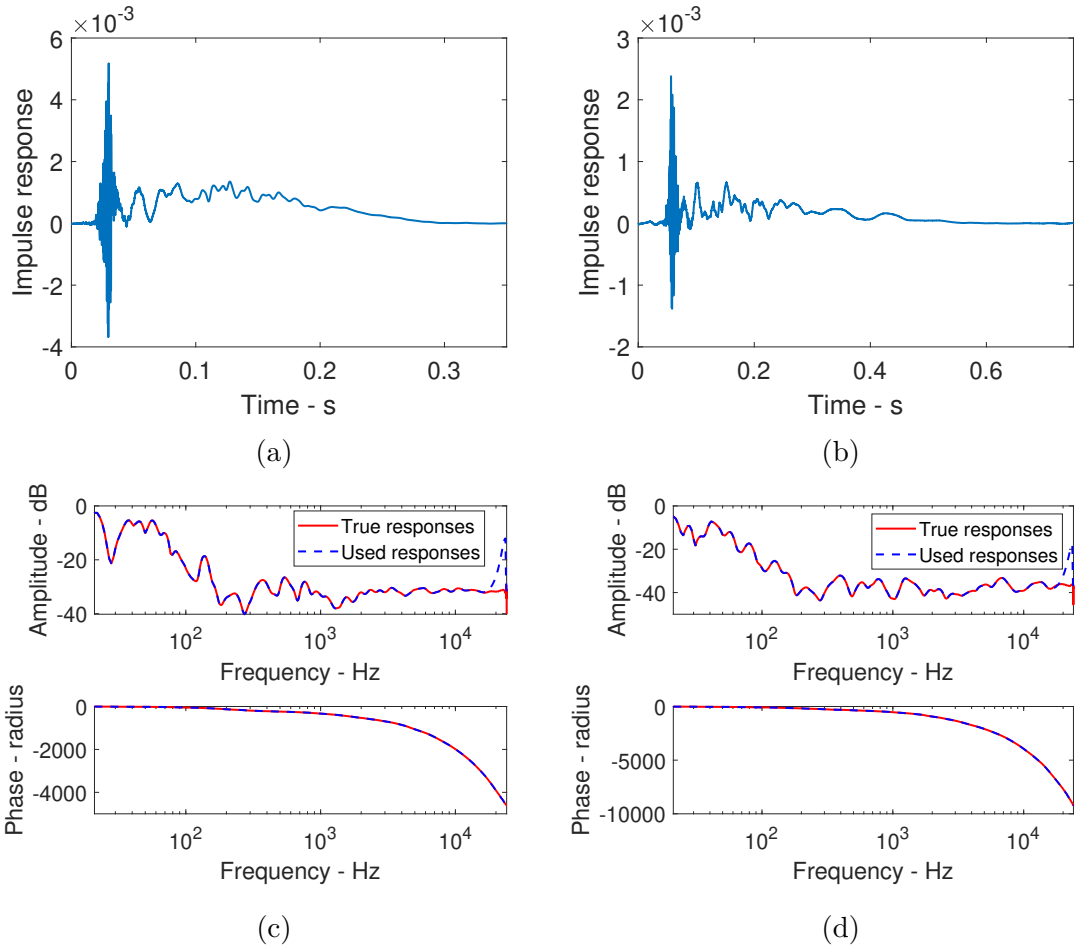


Figure 4.11. Impulse responses and frequency responses of the room response (the path from the speaker input to the listening location). (a): impulse responses in the small room case; (b): impulse responses in the large room case; (c): frequency responses in the small room case; (d): frequency responses in the large room case.

is that the "Used responses" have higher responses towards the cut-off frequency to give a better roll-off in the designed equalization filter.

To design the equalization filters, the sampling rate for the full-band filter is 48 kHz, and the sampling rates for the two subfilters are 2.4 kHz and 48 kHz for all simulated room cases. The test signal is white noise. The delay added is 0.3125 s (i.e., $m = 15000$) in the small room case and 0.2625 s (i.e., $m = 12600$) in the large room case for both methods. The high-sampling-rate subfilter W_2 starts at 0.25 s (i.e., M_1 in Fig. 4.9 is 12000)

Table 4.1. Comparison of the number of design parameters using the traditional least-squares optimization method and the proposed method in small room case.

	Traditional Method	Proposed Method	
		Subfilter 1	Subfilter 2
Time length (s)	0.5	0.5	0.05
Sampling rate (kHz)	48	2.4	48
Filter order	24000	1200	2400

Table 4.2. Comparison of the number of design parameters using the traditional least-squares optimization method and the proposed method in large room case.

	Traditional Method	Proposed Method	
		Subfilter 1	Subfilter 2
Time length (s)	0.9	0.9	0.06
Sampling rate (kHz)	48	2.4	48
Filter order	43200	2160	2880

for the small room case and starts at 0.16 s ($M_1 = 7680$). Frequency response magnitudes are constrained to prevent excessively large amplification at very low and high frequencies. The filter orders using the proposed reduced-order technique and traditional least-squares optimization methods are compared in Table 4.1 and Table 4.2. From the tables, the total number of filter orders is reduced from 24000 to 1200+2400 = 3600 (i.e., 85% reduction or around 6.5 times smaller) in the small room case and from 43200 to 2160+2880 = 5040 (i.e., 88.3% reduction or around 8.5 times smaller) in the large room case. This significant reduction in the number of design parameters can reduce the filter design solution time by several orders of magnitude (in this application, the solution time is reduced from days to below half an hour).

The designed equalization filter using the traditional FDD method and the proposed method is compared in Fig. 4.12. The designed two subfilters using the proposed method are also shown in Fig. 4.12 (a) (b). Although the designed equalization filters are similar using the two approaches over a wide range of frequencies, the proposed method has a

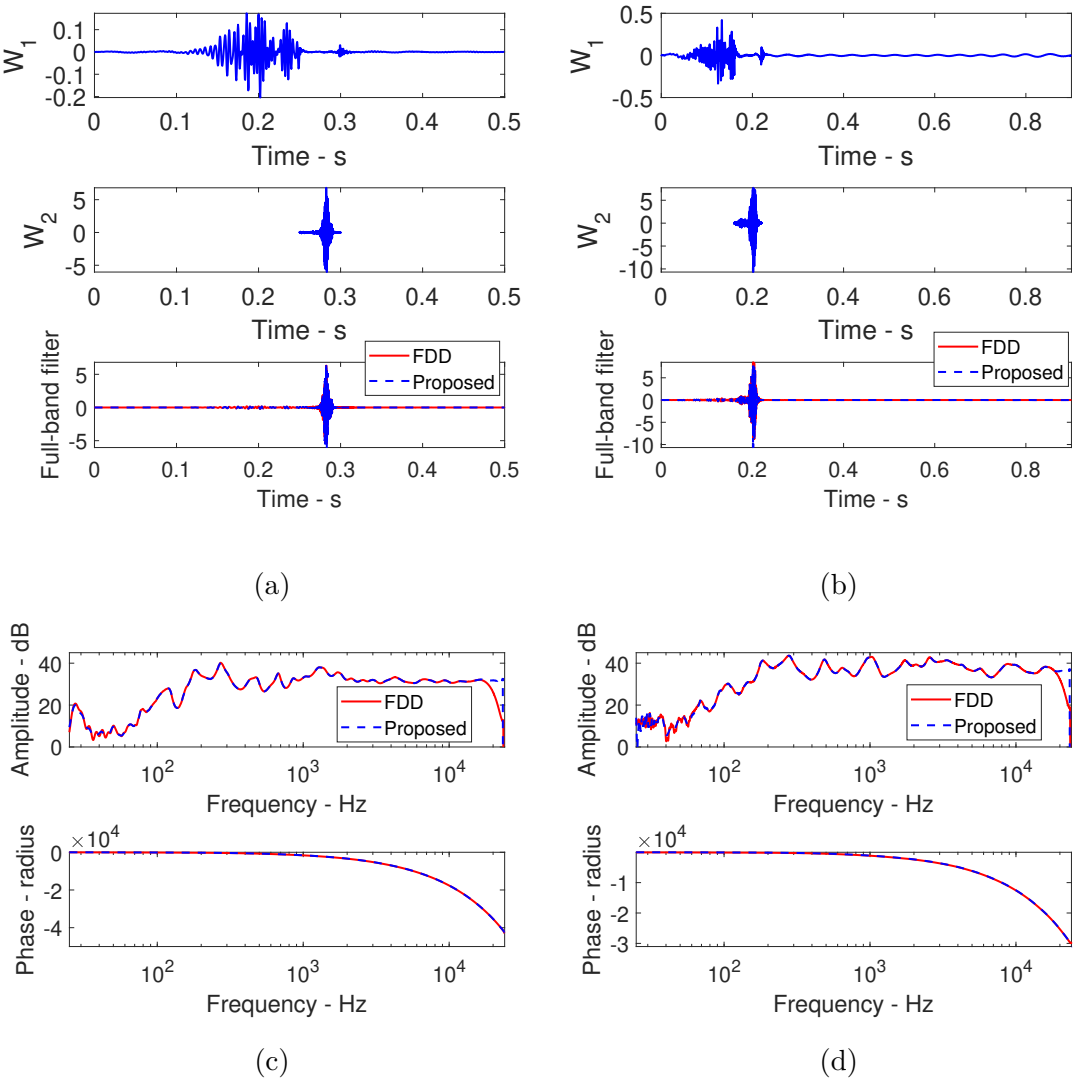


Figure 4.12. The comparison of the designed equalization filter using the frequency-domain deconvolution (denoted as "FDD" in the plot) and the proposed method in time and frequency domain. (a): time domain for the small room case; (b): time domain for the large room case; (c): frequency domain for the small room case; (d): frequency domain for the large room case.

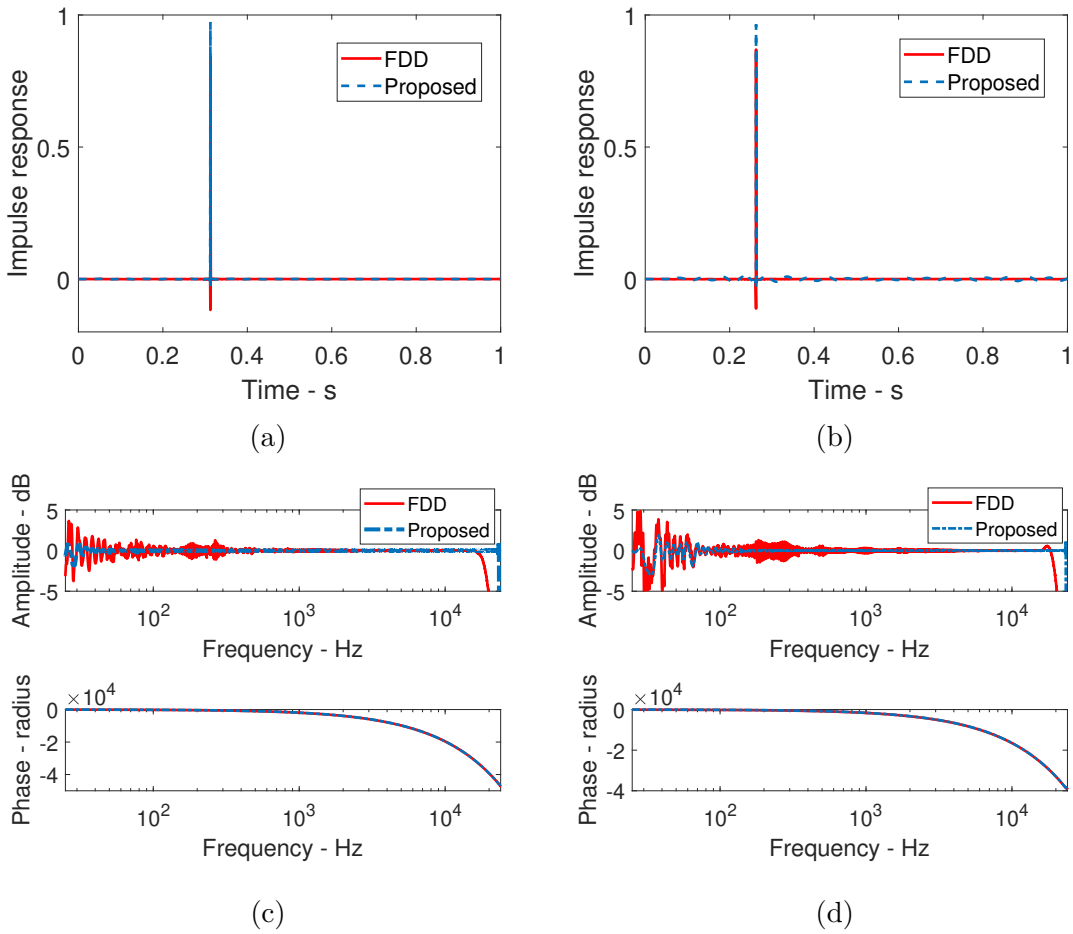


Figure 4.13. The comparison of the convolution result of impulse responses and the multiplication of frequency responses of the designed equalization filters and room responses using the frequency-domain deconvolution (denoted as "FDD" in the plot) and the proposed method. (a): impulse responses in the small room case; (b): impulse responses in the large room case; (c): frequency responses in the small room case; (d): frequency responses in the large room case.

significantly better equalization performance at the low-frequency range which is shown in Fig. 4.13. In Fig. 4.13 (c) (d), the frequency responses after combining the designed equalization filters with the room responses are demonstrated. Ideally, it should be 0 dB across the audible frequency range. The equalization performance using the FDD has larger variations compared with the proposed method because the proposed method gives the

optimal equalization filters for the same equalization filter length. The simulated reproduced sound power spectral density (PSD) is also shown Fig. 4.14.

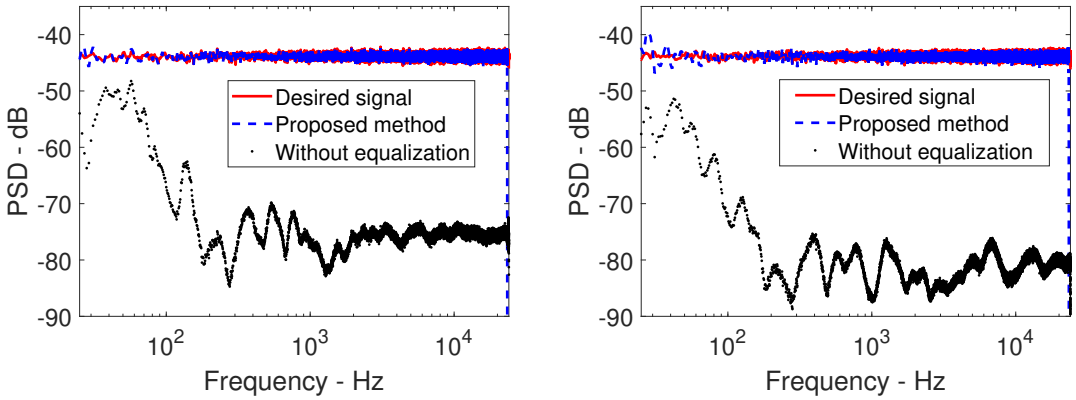
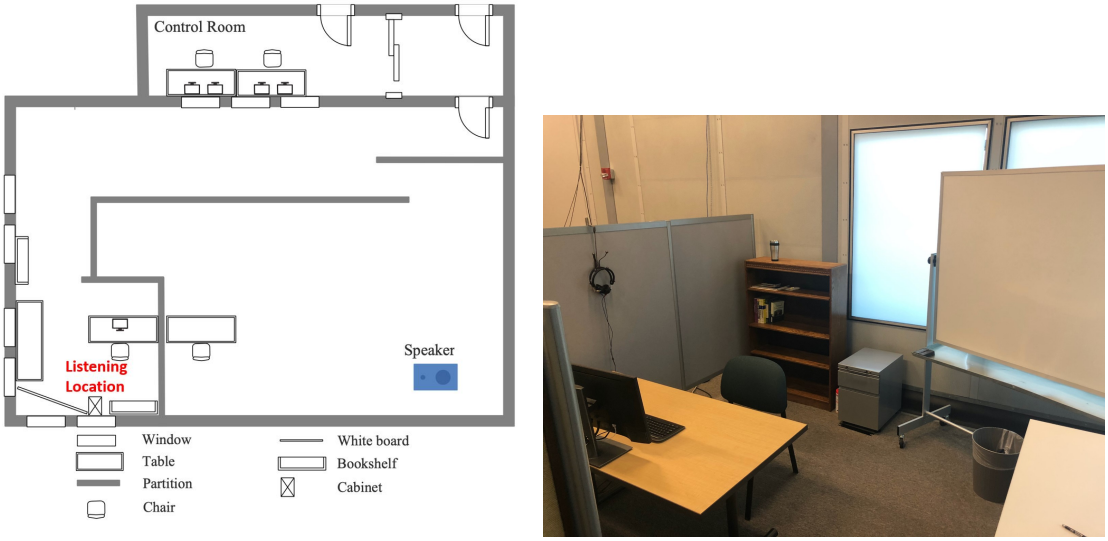


Figure 4.14. Comparison of power spectral density (PSD) of reproduced signal and desired signal at listening location for simulated (a) small room and (b) large room cases.

4.2.5 Experimental results and discussions

In this section, the proposed equalization filter design approach is applied to a sound playback system for a psychoacoustic subjective test in an actual large room, which requires the sound clip being tested to be reproduced accurately for a wide frequency band at the listening location [121].

Since the objective of this particular psychoacoustic test is to evaluate office noise, an office mock-up was set up to create a natural testing environment for subjects. The prefiltered sound clip is played by a hidden distant speaker and the desired sound should be reproduced at the listening location. Hidden loudspeakers are used to ensure that the sound evaluation is not influenced by the subjects' perceived cue that sound is artificially generated by an audio system. The dimensions of the room are 13.1 meters in length, 8.5 meters in width, and 6.7 meters in height. Figure 4.15 (a) shows the layout of the experimental setup including the listening location and the speaker location, and Figure 4.15 (b) shows a picture of the listening location. Because there is sound scattering and absorption from multiple objects,

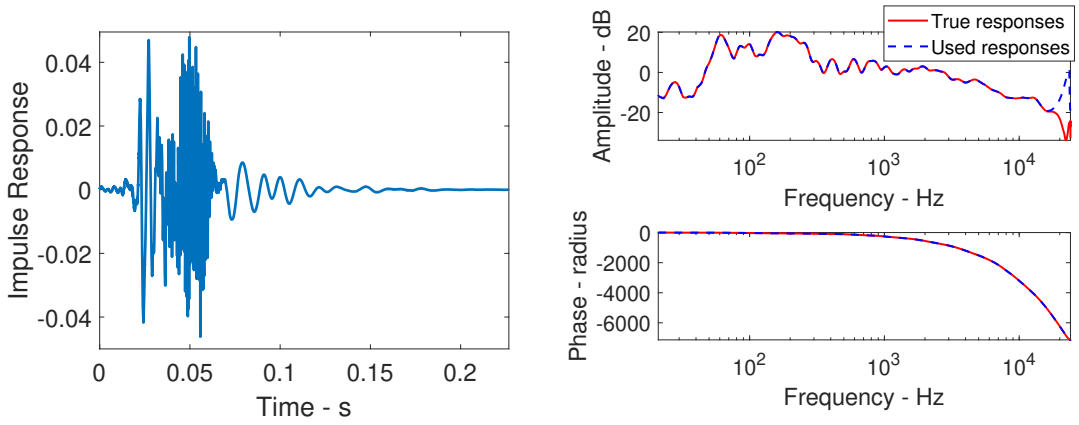


(a) (b)

Figure 4.15. (a) Layout of the experimental setup, (b) picture of the listening location.

such as the partitions and tables, the sound field reproduction is more complicated compared with that in an empty room if an accurate sound field reproduction performance is required. Since the listening location is fixed in the room and it is not likely to have a large variation in subjects' head position and orientation, the requirement of reproducing the sound at a particular location is considered to be sufficient for this application. Also, no artificial head or torso is involved in measurement related to the sound reproduction system, since the binaural effect will occur naturally due to head and torso scattering when a subject is sitting at the listening location in the reproduced sound field.

The playback system that produced the filtered sound clip consists of a LynxONE sound card, a Furman SP20AB amplifier, and a loudspeaker (ALTEC N1201-8A). The frequency response function from the computer output signal to sound pressure at the listening location was measured and a complex smoothing process [121], [137] was then applied. More details on the experimental setup can be referred to the Chapter 4 in Song's previous work [121]. The measured impulse response and the frequency response of the paths from the speaker input to the listening location in this room setup are shown in Fig. 4.16. From Fig. 4.16 (a), it is clear that the high-frequency content is concentrated in a narrow time span while



(a) (b)

Figure 4.16. (a) Impulse responses and (b) frequency responses of the room response (the path from the speaker input to the listening location).

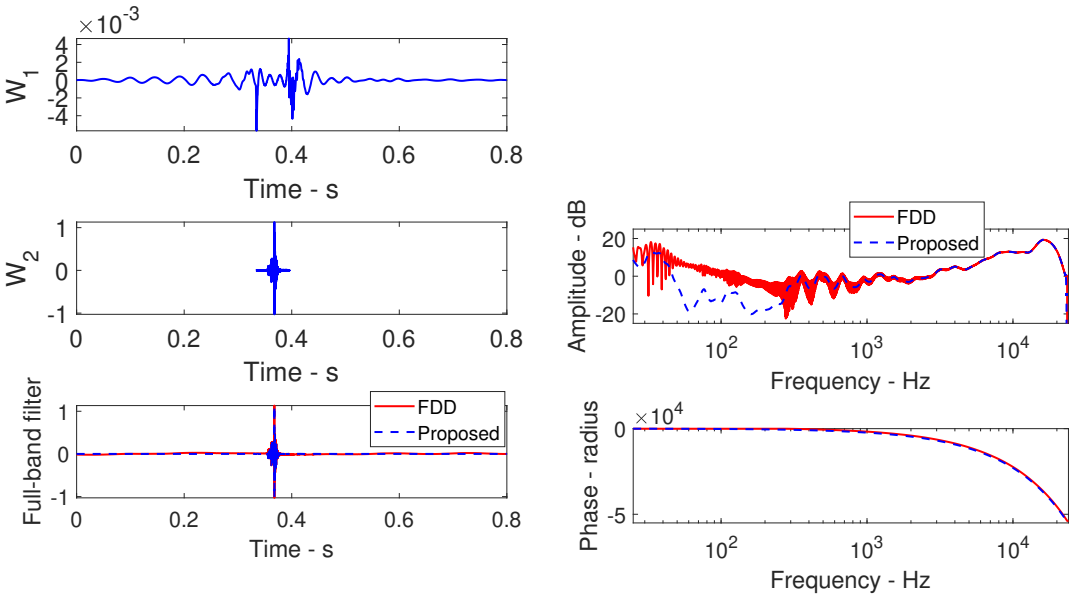
the low-frequency content spreads over a wide time span. Similar to the simulation case, the modified response ("Used responses") is used in the design phase instead of the "True responses" to get a better roll-off towards the cut-off frequency.

Table 4.3. Comparison of the number of design parameters using the traditional least-squares optimization method and the proposed method in the experimental setup.

	Traditional Method	Proposed Method	
		Subfilter 1	Subfilter 2
Time length (s)	0.8	0.8	0.0628
Sampling rate (kHz)	48	2.4	48
Filter order	38400	1920	3000

To design the equalization filters, the sampling rate for the full-band filter is 48 kHz, and the sampling rates for the two subfilters are 2.4 kHz and 48 kHz. The desired sound clip was an ambient broadband noise measured in an office space. The delay added is 0.4167 s (i.e., $m = 20000$) for both methods. The high-sampling-rate subfilter W_2 starts at 0.33 s (i.e., M_1 in Fig. 4.9 is 16000). Frequency response magnitudes are constrained to prevent excessively large amplification at very low and high frequencies. The filter orders using the proposed reduced-order technique and traditional least-squares optimization methods are

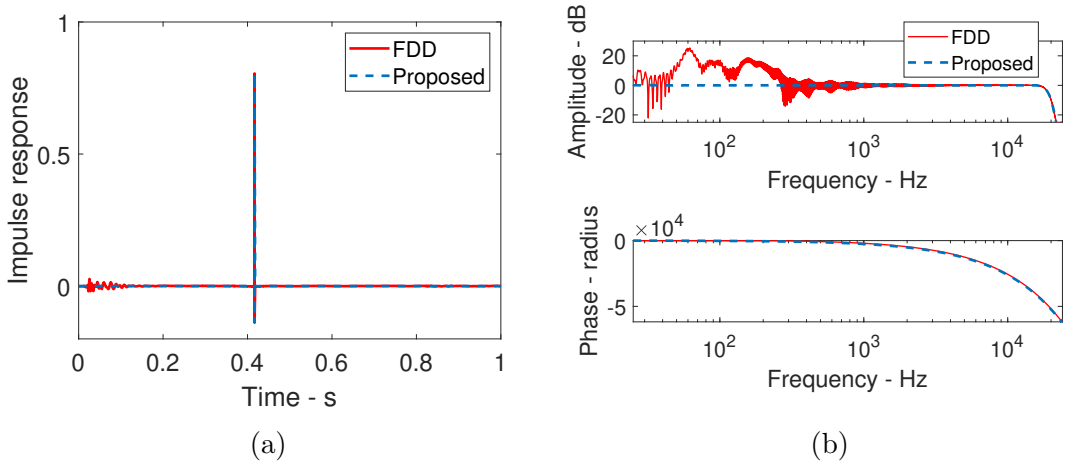
compared in Table 4.3. From the tables, the total number of filter orders is reduced from 38400 to 1920+3000 = 4920 (i.e., 87.2% reduction or around 8 times smaller). Similar to the simulated room cases, this significant reduction in the number of design parameters can reduce the filter design solution time by several orders of magnitude from days to below half an hour.



(a) (b)

Figure 4.17. The comparison of the designed equalization filter using the frequency-domain deconvolution (denoted as "FDD" in the plot) and the proposed method in (a) time and (b) frequency domain.

The designed equalization filter using the traditional FDD method and the proposed method is compared in Fig. 4.17. For this complicated room environment, the difference in the designed equalization filters in the frequency domain is more obvious compared with the simulated room cases in Fig. 4.12. In Fig. 4.18, the impulse responses and frequency responses after combining the designed equalization filters with the room responses are demonstrated. The complicated room environment setup further increases the required filter length which makes the FDD method perform worse. Also, the complicated real-life noise in office setup has large power level variations across the audible frequencies. Compared with the FDD method, the use of the proposed method inherently adds higher weightings to frequencies



(a) (b)

Figure 4.18. The comparison of (a) the convolution result of impulse responses and (b) the multiplication of frequency responses of the designed equalization filters and room responses using the frequency-domain deconvolution (denoted as "FDD" in the plot) and the proposed method.

having higher desired sound power. The proposed method has very small variations around 0 dB across the audible frequency range (within 2 dB variations). However, the FDD method may have variations up to 20 dB which is not suitable for this psychoacoustic testing.

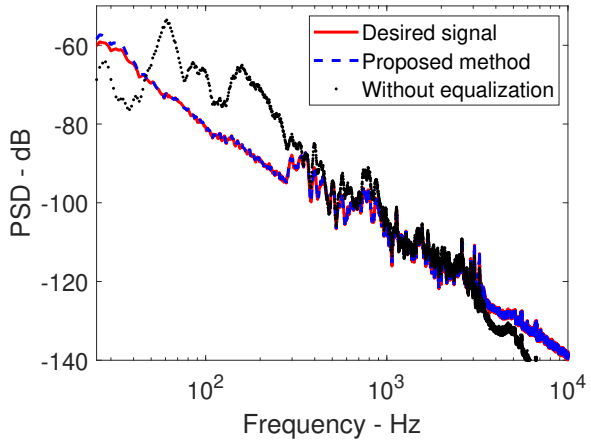


Figure 4.19. Comparison of simulated power spectral density (PSD) of reproduced signal and desired signal at the listening location.

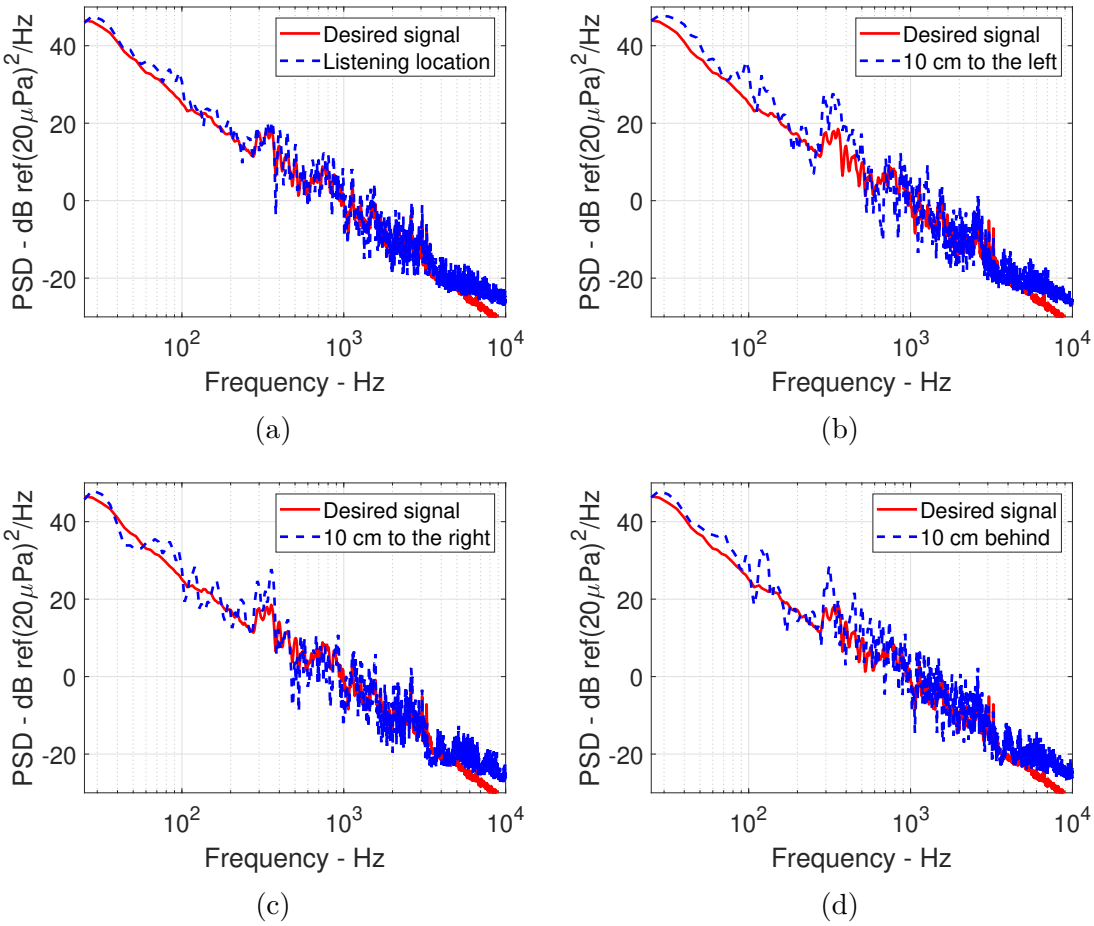


Figure 4.20. Comparison of experimentally measured sound pressure level (SPL) of reproduced signal and desired signal at (a) listening location and location 10 cm to the (b) left of, (c) right of, and (d) behind the listening location.

The simulated sound reproduction performance is shown in Fig. 4.19 and the experimentally measured sound reproduction performance is shown in Fig. 4.20 (a). In Fig. 4.19, compared with the reproduced signal without using an equalization filter, the reproduced signal after using the equalization filter designed by the proposed method is much closer to the desired signal. To further confirm the sound field reproduction performance, the sound pressure level (SPL) of the desired signal and the reproduced signal measured in the experiment are compared in Fig. 4.20 (a). In the experiment, the reproduced signal after using the equalization filter designed by the proposed method is still close to the desired signal. Thus, the sound field reproduction performance of using the proposed equalization filter design

method is experimentally validated. To show the spatial variations of the reproduced sound signal using the proposed method, the measured SPL at three locations 10 cm to the left of, to the right of, and behind the listening location (i.e., the location where measurement was conducted) are shown in Fig. 4.20 (c) (d). Given that human subjects are seated in front of a table, 10 cm can be considered a relatively large distance for the purpose of this study, as head movement is typically limited. In Fig. 4.20 (c) (d), the equalization performance is still satisfactory for a wide range of frequencies except for some spikes and notches due to the change of low-frequency room modes which is typical for a least-squares optimization-based local sound field reproduction method.

4.3 A Constrained Optimal Hear-Through Filter Design Approach for Earphones

When wearing an earphone, the signal characteristics can be altered when sound from the outside environment transmits through the earphone to the ear canal. This makes the person wearing an earphone hears an unnatural environment sound. A hear-through filter is usually implemented to process the sound signals measured by the microphones at the exterior side of an earphone so that appropriate sound can be reproduced by the earphone speaker to create a more natural hearing experience. A well-performing hear-through function, also referred to as ambient mode or transparent mode of an earphone, allows one to hear the ambient sound more clearly and realistically while wearing an earphone. The hear-through filter can also be an important technique in achieving better augmented reality audio performance [138]–[140].

Various approaches have been proposed to design a hear-through filter in previous literature. They can be classified into two categories: design of a direct inverse filter design, and filter design using an ANC structure. For the direct inverse filter approach, a hear-through filter can be designed by flattening the attenuation curve caused by the earphone and (or) the ear canal, e.g., the allpass filter design [141]. However, a certain level of ambient sound will usually be transmitted into the ear canal as leakage through the earphone which deteriorates the performance of the hear-through filter and causes a comb-filtering effect [140], [142], i.e., the resulting sound signal will be oscillating in the spectrum due to the different delay

between reproduced sound and leakage sound. The hear-through filter can also be designed by using an ANC structure, e.g., the use of LMS based algorithm [138], and directional hear-through design can also be incorporated [143]. Since an ANC filter can cancel the sound leakage, the comb-filtering effect can, in principle, be attenuated. However, some practical limitations of designed hear-through filters have not been considered in previous studies yet, e.g., the instability issues caused by the acoustic feedback path reviewed in Section 2.1.4. This is more important for earphones that are designed not to fully cover the ear.

In this section, a hear-through filter design approach is proposed based on the proposed conic method in Chapter 3. Instead of considering the attenuation of sound leakage into the ear canal and the reproduction of ambient sound separately, the proposed method formulates them as a single optimization problem such that the hear-through filter can be optimized while the leakage sound is attenuated at the same time. The robust stability and hear-through filter response amplitude limitation are also considered.

4.3.1 Control system description

The system block diagram of the proposed hear-through filter structure is shown in Fig. 4.21 (a) whose symbols have the same meaning as in a typical ANC system diagram Fig. 2.1 (a). More specifically, x is the incoming ambient sound signal from the environment measured at the reference sensor location. d denotes the ambient sound that transmits around and through the earphone to the ear canal. Note that e includes both the leakage sound and the reproduced sound at the error sensor location. $\tilde{x}$ is the signal of x with an application dependent delay. The total power of $\tilde{\mathrm{e}}$ is to be minimized in the hear-through filter design process, i.e., the reproduced sound in the ear canal should resemble a delayed ambient signal x. The added delay $D = \mathrm{e}^{-\mathrm{j}2\pi f\delta}$ is due to the physical limitation that, by adding an electronic system and filtering process, an additional delay will be inevitably introduced. An advantage of this filter design structure is that the expected delay of reproduced sound can be controlled easily to satisfy particular requirements in applications such as the creation of a spatial impression of sound for augmented reality. One channel is considered in this section, but since the method is proposed based on the derivation of the proposed multi-channel

conic method in Chapter 3, the extension to multi-channel is straightforward which can be referred to reference [144].

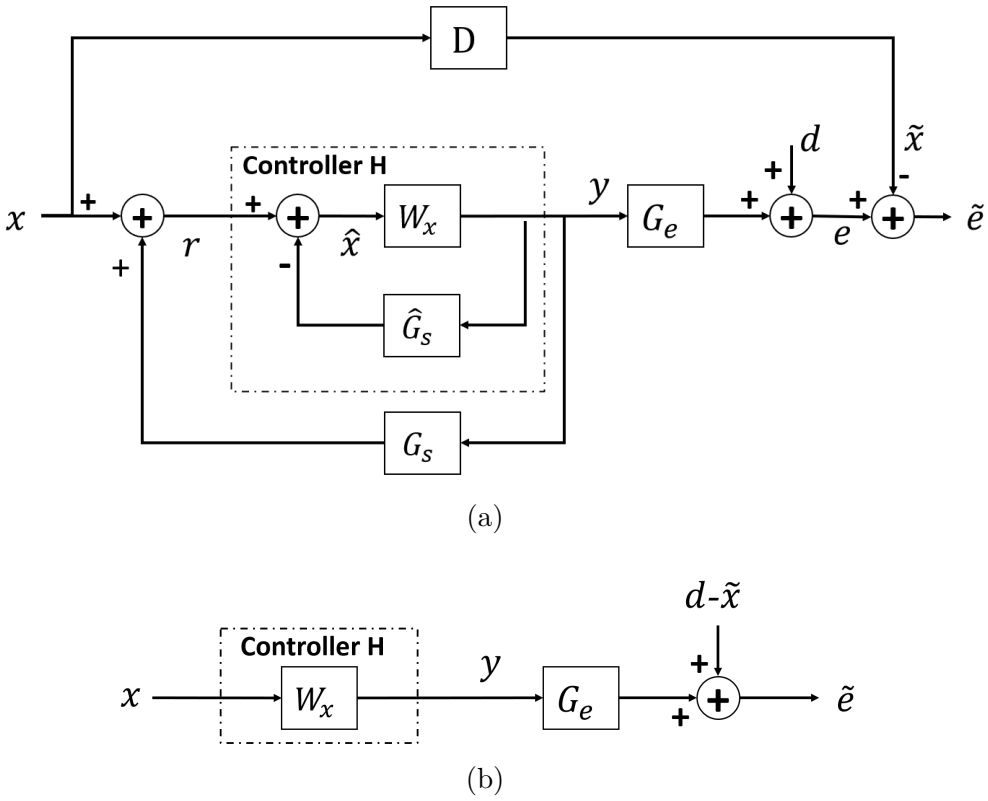


Figure 4.21. Block diagram of a hear-through filter structure: (a) system with an acoustic feedback path and an internal model control structure, (b) an equivalent feedforward system when assuming a perfect cancellation of the acoustic feedback path effect.

Similar to Fig. 2.1 (b), when $\hat{G}_s$ is assumed to be a perfect model, i.e., $\hat{G}_s = G_s$, this system becomes Fig. 4.21 (b). Compared with Fig. 2.1 (b), the only difference is that the disturbance signal d in Fig. 2.1 (b) is changed to $d - \tilde{x}$. Thus, the filter design process, including the constraints considerations, is exactly the same as derived in the proposed conic method in Chapter 3 with a change of variable from $d(f)$ to $d(f) - \mathrm{e}^{-\mathrm{j}2\pi f\delta}x(f)$.

4.3.2 Experimental results and discussions

To investigate the proposed method for designing a hear-through filter. An earphone is used in an experiment to collect the required system response data. There are one reference

microphone and one speaker in the earphone. The error microphone used in this experiment is in an artificial ear (Hangzhou Aihua AWA6162 (IEC711)). The pictures of the earphone mounted on the artificial ear are shown in Fig. 4.22. It is noted that a non-adaptive controller is implemented in the current work using nominal system characteristics $\mathbf{G}_e$ measured using the setup shown in Fig. 4.22.

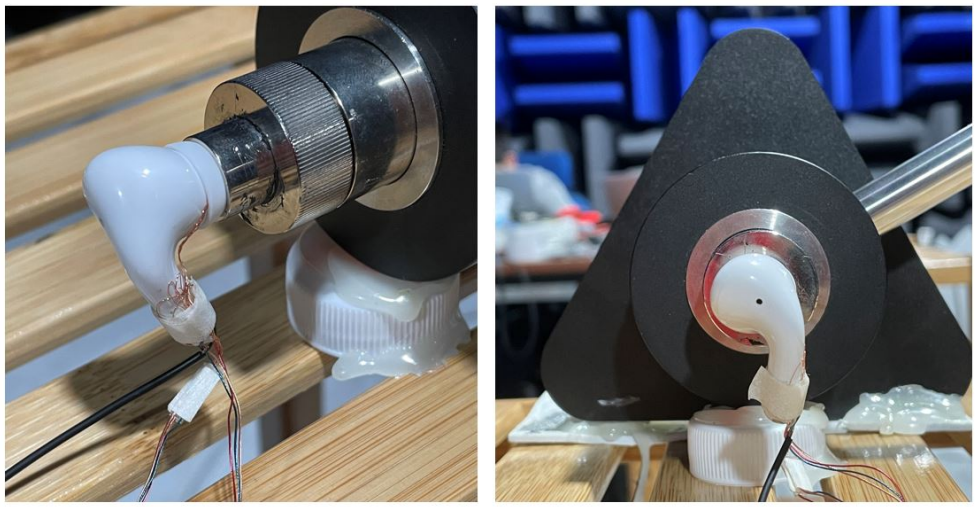
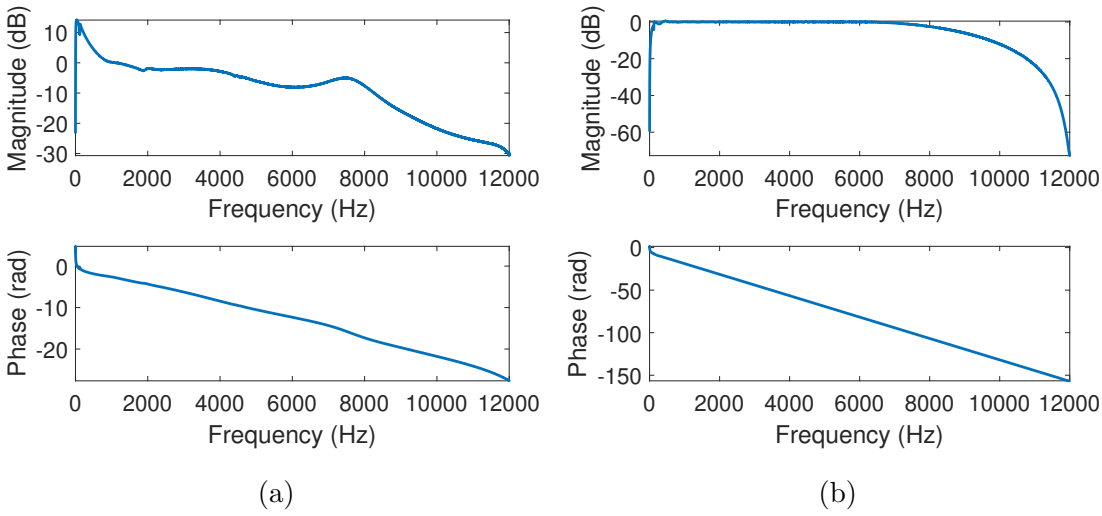


Figure 4.22. Pictures of the earphone mounted on AWA6162 (IEC711) for experimental data collection.

When acquiring measurement data, the sampling rate of the data acquisition system was set to 48000 Hz to prevent aliasing. Two million sampling points (about 42 seconds) for each channel were acquired for calculating the $\mathbf{G}_e$. A hamming window of 48000 points (1 second) is used for averaging with fifty percent overlapping (83 times averages). The length of the designed hear-through FIR filter is 128. The sampling rate for the hear-through filter is 24000 Hz. The desired hear-through band is below 6000 Hz.

As mentioned in the introduction, if a direct inverse filter design approach is being used to flatten the response of $\mathbf{G}_e$, there will be a comb-filtering effect due to the sum of leakage sound and reproduced sound. However, if the proposed method is used, it will reproduce the desired sound field while attenuating the leakage sound. Thus, the comb-filtering effect should be alleviated. To demonstrate this effect, the performance of using the direct inverse filtering

design approach and the proposed method is compared. In this simulation, the secondary path measured using the earphone in the previous section is used. The reference sound signal and leakage sound signal are generated in simulation to compare the performance of different methods. x is a white noise processed by a low-pass filter with a cut-off frequency of 6000 Hz. The leakage sound signal, d is around 6 dB lower than the ambient sound signal at the reference microphone, x, and has a 1 ms lag with respect to x. The desired sound $\tilde{x}$ has a 2 ms lag with respect to x, i.e., $\delta = 2 \times 10^{-3} s$. So there is a relative delay between the desired reproduced sound and the leakage sound.

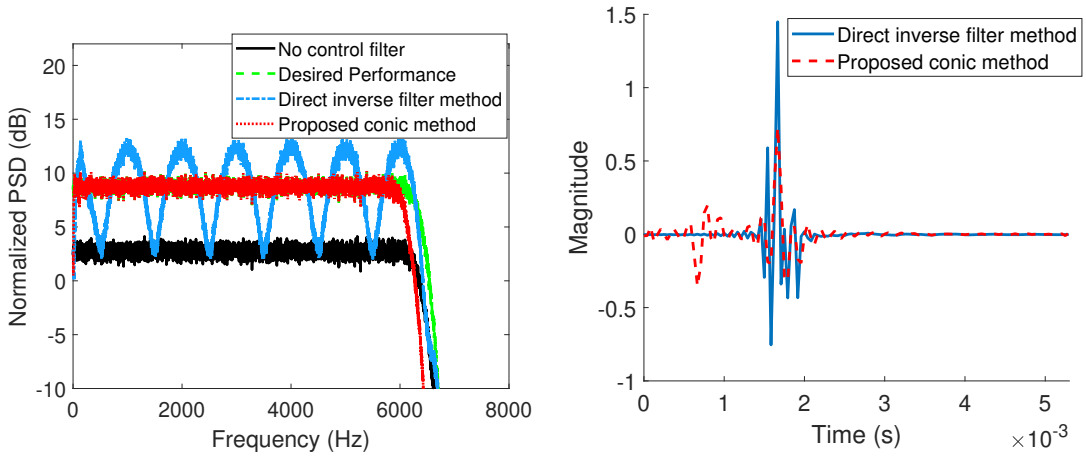


(a) (b)

Figure 4.23. Frequency response of (a) G_{e}, (b) $G_{\mathrm{e}}W_x$, where W_x is designed using direct inverse filter method.

The frequency response of measured G_{e} is shown in Fig. 4.23 (a) which includes the attenuation due to earphone speaker unit response and the ear canal's acoustic response. Fig. 4.23 (b) shows the frequency response of $G_{\mathrm{e}}W_x$, where W_x is designed by using the direct inverse filter method (i.e., performing a least square estimation to fit $\frac{1}{G_{\mathrm{e}}}$). Figure 4.23 (b) demonstrates that the designed hear-through filter can flatten the attenuation curve caused by earphones and ear canals. However, as observed from Fig. 4.24 (a), due to the leakage sound around and through earphones, the contribution of the leakage sound and the reproduced sound leads to a comb-filtering effect in the total sound field, when a direct inverse filter method is used. On the other hand, the proposed method does not have the

comb-filtering effect as shown in Fig. 4.24 (a). By checking the impulse response of filters designed by two methods (shown in Fig. 4.24 (b)), the filter designed by the proposed method has a significant response before 10^{-3} s. This is the filter response that actively reduces the leakage sound, since leakage sound has a 1 ms delay with respect to the ambient sound signal while the reproduced sound requires a 2 ms delay compared with ambient sound at the reference microphone. This result shows that the proposed method can significantly alleviate the comb-filtering effect by attenuating the leakage sound.

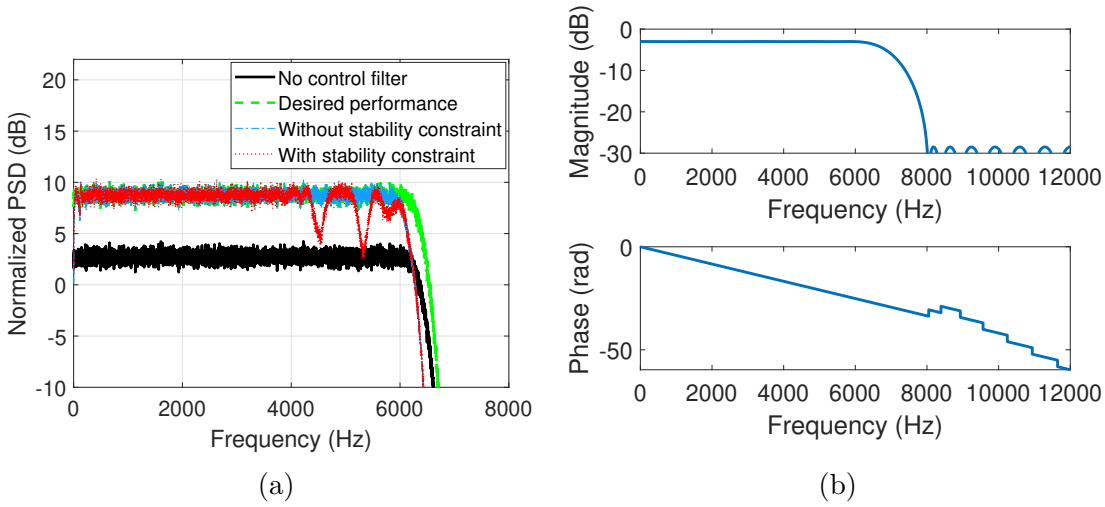


(a) (b)

Figure 4.24. Comparison of (a) hear-through performance in normalized PSD, and (b) impulse response for direct inverse filter design method and the proposed conic method.

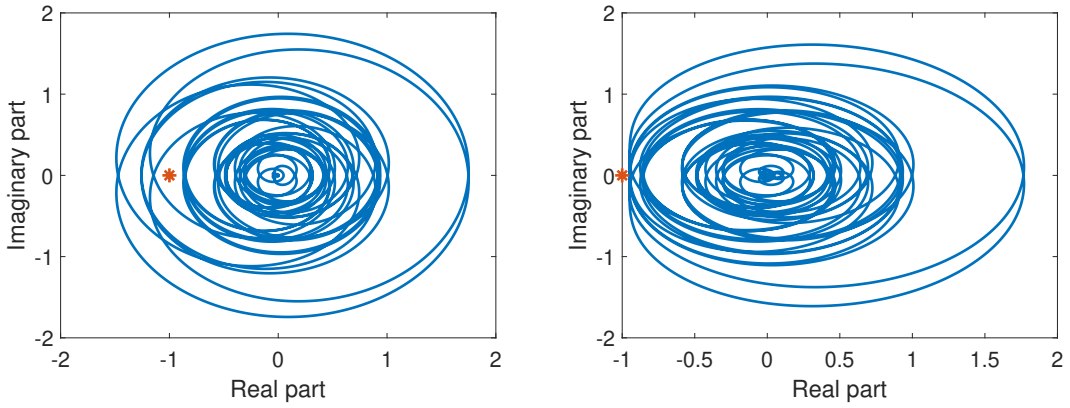
Another advantage of the proposed method is the capability of applying multiple constraints to satisfy practical industrial requirements. In this section, the capability of constraining the designed hear-through filter is investigated. Firstly, since the desired hear-through band is below 6000 Hz, the magnitude of the hear-through filter response is constrained above 6000 Hz as shown in Fig. 4.25 (a). Then stability constraint is focused on in this study. In this simulation, the acoustic feedback path G_s is assumed to have a low-pass type frequency response with 3 dB attenuation in the passband which is shown in Fig. 4.25 (b). Fig. 4.26 shows the Nyquist plot of the designed control system's open loop response, i.e., $W_x G_s$. It is clear that if the stability constraint is not applied, the control system is unstable as shown in Fig. 4.26 (a). When the stability constraint is applied, the control system

becomes stable as shown in Fig. 4.26 (b). Fig. 4.25 (a) also shows that adding stability constraint will sacrifice the hear-through performance near the cut-off frequency of the designed hear-through filter. The hear-through performance below 4000 Hz is still satisfactory.



(a) (b)

Figure 4.25. (a) Comparison of hear-through filter performance with and without applying stability constraint. (b) The frequency response of G_s.



(a) (b)

Figure 4.26. The Nyquist plot (i.e., the frequency response of open loop $W_x G_s$) for hear-through filter W_x designed (a) without applying stability constraint, and (b) with stability constraints.

4.4 Summary

In this chapter, an adaptive multi-channel filter design approach is proposed for ANC applications under controller stability constraints. The optimal ANC filter coefficients are updated by solving a previously proposed conic formulation continuously using the updated system response measurements. Compared with the traditional leaky FxLMS method, the proposed method has a faster convergence rate and better steady-state ANC performance. The proposed method can be suitable for ANC applications where signal characteristics rapidly change from one steady state to another different steady state: e.g., equipment speeds are switched among some predetermined values during the operation of rotating machinery; or when various products share the same host server in multi-task applications that the control filter coefficients can be updated in a short time using the powerful server without adding too much marginal cost: e.g., the smart home/office application.

The proposed conic formulation is also modified to efficiently design a room equalization filter. Either the design of a full band equalization filter or the design of multiple subfilters can be formulated in a similar way by using this conic method. Multiple subband filters can be designed simultaneously by solving one convex optimization problem such that the total sound field reproduction performance can be optimal. Constraints on the frequency responses of each subband filter and the total equalization filter effect can be specified in a convenient way. A reduced order technique by using the subband filters can also be conveniently applied to the proposed method to reduce the number of design parameters. The proposed method was investigated in simulated room cases and an experiment with a playback system for psychoacoustic subjective tests. Results show that, by using the proposed method, the desired sound signal can be reproduced at the required location successfully. Compared with the traditional least-squares optimization methods, the use of a reduced-order technique can result in a satisfactory sound field reproduction performance while reducing the number of required design parameters significantly. This reduction in the number of design parameters can reduce the computational time from the order of days to within half an hour. Compared with the traditional frequency domain deconvolution methods, the proposed method has a better sound reproduction accuracy at the low-frequency range. The sound reproduction

performance is also measured at locations 10 cm to the left of, to the right of, and behind the listening location (measuring location) to demonstrate the spatial robustness of the proposed method.

The proposed conic formulation can also be used to design the hear-through filter for earphones with a simple change of variables. The proposed design method can attenuate the leakage sound and alleviate the comb-filtering effect. The robust stability constraint required by the existence of the acoustic feedback path can be applied. The results show that compared with the direct inverse filter design approach, the proposed method can effectively attenuate the comb-filtering effect. The applied filter magnitude constraint and stability constraint can ensure the corresponding practical requirements are satisfied. This proposed method can also be extended to multi-channel cases [144].

5. EFFICIENT ACTIVE SOUND CONTROL FILTER IMPLEMENTATION APPROACHES

The previous two chapters focus on the filter design method. In this chapter, filter implementation methods will be focused on. The high sampling rate can bring various benefits to the control filter performance, but it also leads to implementation challenges due to its high real-time computational requirements. Two methods, i.e., the delayless polyphase structure and the IIR filter fitting method, are proposed in this chapter to target the implementation challenges brought by high sampling rate systems.

5.1 Delayless Polyphase Method for Efficient Filter Implementation at High Sampling Rate

As discussed in Section 1.3.2, increasing the sampling rate of the digital system can reduce electronic delay, which is crucial to ANC applications targeting broadband noises. Although polyphase structure can be used to reduce the real-time computational load brought by a higher sampling rate, it will introduce additional delay into the signal paths, which limits its application in ANC applications. So far, the multi-rate techniques with polyphase structures were usually applied in the filter adaption process instead of the real-time filtering process, e.g., the subband ANC method [64], [76].

In this section, a delayless polyphase real-time ANC filter implementation method without the need for additional lowpass filters is proposed. The key step involves a new method to decompose an ANC filter into two multiplicative causal filters both of which have lowpass frequency response shapes at high frequencies. More specifically, the proposed method uses the fact that, for high sampling rate ANC systems, the frequency responses of the designed ANC filter should be attenuated to prevent noise amplification outside the desired noise control band (usually the desired noise control band is at low frequencies). The ANC filter's attenuation at higher frequencies can be used as an anti-aliasing and reconstruction filter if the proposed causal filter decomposition is applied. Then, a polyphase filter structure can be implemented without additional anti-aliasing and reconstruction filters (thus, it is named delayless polyphase implementation in this section). By using the proposed delayless

polyphase method, an ANC system can be operated at a sampling rate much higher than the desired frequency band. Compared with traditional direct filter implementation, the associated real-time computation requirement using the proposed method only increases linearly with the sampling rate instead of quadratically. When the ANC system is operated at a high sampling rate, the introduced electronic delay will be lower, and better noise control performance can be achieved. Experiments are implemented to confirm the improvement of real-time computations and noise control performance compared with various traditional implementations.

5.1.1 Delayless polyphase implementation structure

In this section, the discussion is based on single-channel ANC systems. The extension of the proposed method to multi-channel systems is trivial since the proposed method can be applied channel by channel independently. Also, the review of traditional polyphase implementation structure can be referred to in Section 2.2.1. The proposed delayless polyphase method will base on this traditional version and it can be applied directly to the real-time filtering process to reduce the real-time computations without introducing additional delay caused by additional digital anti-aliasing and reconstruction filters. The proposed method is stated as the following.

The purpose is to use a polyphase structure to reduce the real-time computation load to implement the ANC filter, $W_x(z)$, that is designed at a high sampling rate $f_H = Mf_L$ where M is the decimation factor when a multi-rate system is used to implement this filter. The desired noise control band is below $f_L/2$. In the filter design process (using a high sampling rate f_H), the response of $W_x(z)$ at frequencies above $f_L/2$ can be arbitrary as long as it provides sufficient attenuation to prevent noise amplification outside the desired noise control frequency band. In this way, the ANC filter $W_x(z)$ can actually perform as a lowpass filter with cut-off frequency at $f_L/2$. An ANC filter that satisfies the above-mentioned requirements can be designed by the constrained optimization method formulated using the proposed conic method in Chapter 3. After the FIR filter $W_x(z)$ is designed, it can be decomposed as:

$$W_x(\mathrm{e}^{\mathrm{j}2\pi f}) = A(\mathrm{j}2\pi f)B(\mathrm{j}2\pi f), \quad \text{for } f < f_L/2, \tag{5.1}$$

where the responses of both $A(z)$ and $B(z)$ provide sufficient attenuation above $f_L/2$ (the approach to finding such a pair of $A(z)$ and $B(z)$ is discussed in the Section 5.1.2). Then $A(z)$ and $B(z)$ can be used to replace the two lowpass filters, $H(z)$, in Fig. 2.3 (a) and there is no need to have $W_x(z)$.

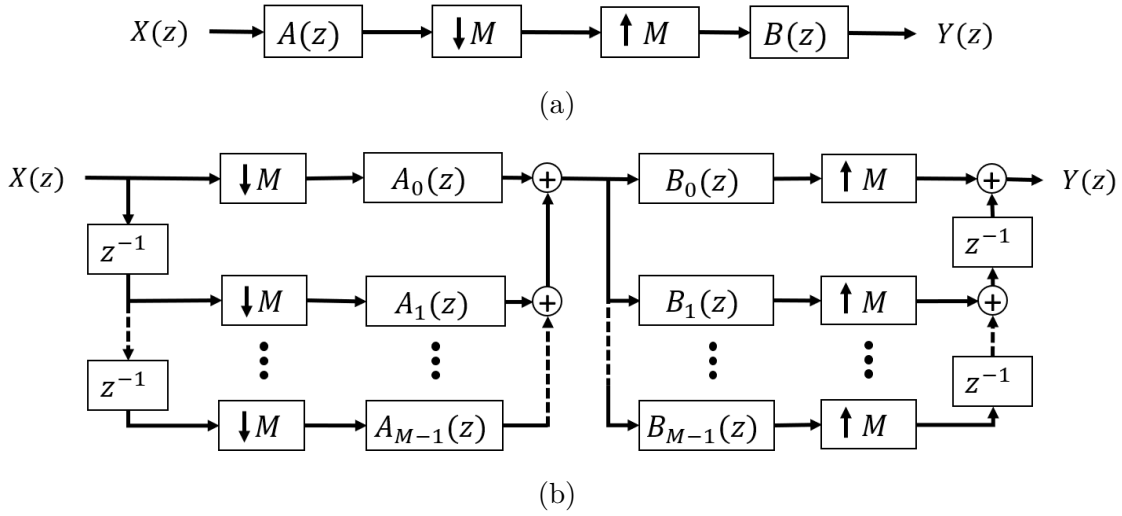


Figure 5.1. Block diagrams of (a) a proposed ANC filter structure that $H(z)$ is replaced by $A(z)$ and $B(z)$ and no $W_x(z)$ is required, (b) a proposed ANC filter structure after applying polyphase filter structures.

A demonstration of this concept is shown in Fig. 5.1 (a). Similarly as in the traditional polyphase implementation, $A(z)$ and $B(z)$ can be expressed as:

$$\begin{aligned} A(z) &= a_0 + a_1 z^{-1} + a_2 z^{-2} + \ \ldots \ + a_{L_a-1} z^{-L_a+1}, \\ B(z) &= b_0 + b_1 z^{-1} + b_2 z^{-2} + \ \ldots \ + b_{L_b-1} z^{-L_b+1}. \end{aligned} \tag{5.2}$$

Then, let $P_a = L_a/M$ and $P_b = L_b/M$ (P_a and P_b are integers), $A_m(z)$ and $B_m(z)$ can be defined as:

$$\begin{aligned} A_m(z) &= \sum_{n=0}^{P_a-1} a_{nM+m} z^{-n}, \\ B_m(z) &= \sum_{n=0}^{P_b-1} b_{nM+m} z^{-n}. \end{aligned} \tag{5.3}$$

By the first and second noble identities [93], if $X(z)$ in Fig. 5.1 (a) and (b) are the same, $Y(z)$ will also be the same. Fig. 5.1 (b) is the proposed delayless polyphase implementation. Obviously,

$$Y(e^{j2\pi f}) = B(e^{j2\pi f})A(e^{j2\pi f})X(e^{j2\pi f}) = W_x(e^{j2\pi f})X(e^{j2\pi f}), \quad \text{for } f < f_L/2. \tag{5.4}$$

Thus, $A(z)$ and $B(z)$ can then perform both as the control filters in the lower frequency band (desired noise control band) and as the lowpass filters in the higher frequency band. No additional delay is introduced when using the proposed delayless polyphase implementation since no additional lowpass filters are added. The real-time computations are also significantly reduced because the downsampling is operated before implementing filters and the upsampling is operated after using the filters.

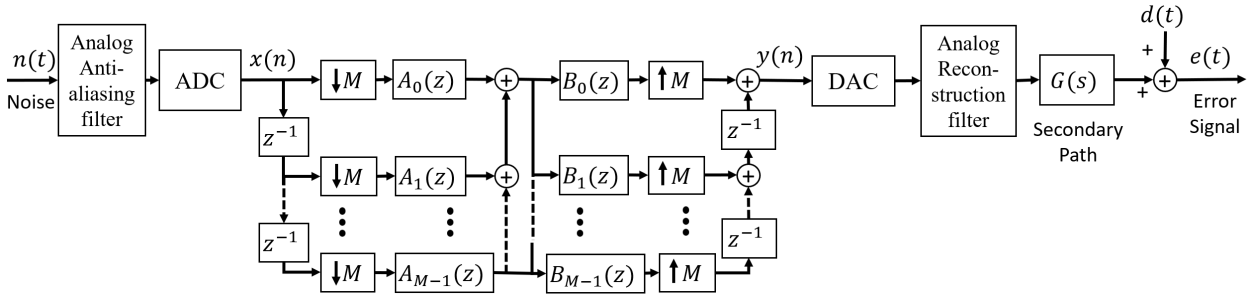


Figure 5.2. Block diagram of the ANC controllers when using the proposed delayless polyphase implementation.

The use of the proposed delayless polyphase implementation in ANC applications is then shown in Fig. 5.2. The delay introduced by the analog anti-aliasing and reconstruction filters, ADC, and DAC can be significantly reduced by using a high sampling rate for $X(z)$ and $Y(z)$. The real-time computations are also significantly reduced because all digital filters are applied after the downsampling operation and before the upsampling operation. And no additional delay is introduced because there is no need for additional digital anti-aliasing and reconstruction filters.

The comparison of real-time computations for various methods is listed in Table 5.1. When the low sampling rate method is used, the introduced delay will be high due to high

Table 5.1. A comparison of real-time multiplications per second for different traditional methods and the proposed method.

Methods	Low f_s method	High f_s method, original IRD	High f_s method, shorter IRD	Proposed method
Sampling Rate	f_L	Mf_L	Mf_L	Mf_L
IRD	T	T	T/M	θT
Filter Order	Tf_L	MTf_L	Tf_L	θMTf_L
Real-time Multiplications	Tf_L^2	$M^2Tf_L^2$	MTf_L^2	θMTf_L^2
Real-time Computational Complexity	$\mathcal{O}(1)$	$\mathcal{O}(M^2)$	$\mathcal{O}(M)$	$\mathcal{O}(M)$
Delay	High	Low	Low	Low

delay in anti-aliasing and reconstruction filters, ADC, and DAC [43], [75], although the real-time multiplications per second will be relatively lower, i.e., the product of multiplications per sampling interval and sampling intervals per second: $Tf_L \times f_L = Tf_L^2$, where T is the effective time lengths (i.e., the IRD) and f_L is the low sampling rate. To reduce the introduced delay, the sampling rate can be increased to Mf_L (M is an integer larger than 1) by redesigning the ANC filter using a higher sampling rate with constraints on the responses' magnitude above the desired noise control band using constrained optimization methods such as the convex conic formulation [36], [58]. And the IRD T should be kept the same since the noise signal and transfer path are essentially analog (a direct implementation of this high sampling rate filter is referred to as the high sampling rate method). However, if the high sampling rate method is used, it increases the number of multiplications required per second to $T(Mf_L)^2 = M^2Tf_L^2$, which is a quadratic growth with respect to M. To mitigate such a significant increase in computation load, the filter's IRD, T, can be shortened (e.g., shortened T to T/M), this method is referred to as the high sampling rate method using shorter IRD in the current work. In this method, the real-time multiplications per second are increased to MTf_L^2, which is a linear growth of sampling rate but the noise control performance is negatively impacted due to the shorter filter response time. By using the proposed method,

suppose the total IRD of designed $A(z)$ and $B(z)$ is θT, where θ, depending on the filter decomposition method (introduced in Section 5.1.2), can be chosen to be 1 or sometimes slightly larger than 1 in practice. The real-time multiplications of the proposed method are then $\theta M T f_L^2$, which is also a linear growth of sampling rate, and the filter length is not shortened (i.e., the noise control performance is not degraded).

5.1.2 Causal filter decomposition method

A key step of the proposed delayless polyphase implementation described in the previous subsection is to find a pair of suitable multiplicative decomposition of the designed ANC control filter $W_x(z)$ into two causal filters $A(z)$ and $B(z)$. There are three challenges in finding such a pair of filters:

1. The order of $W_x(z)$ is usually very high (e.g., several hundred) because the control filter is designed using a high sampling rate, this makes the dimension of the filter decomposition problem very high as well, which is not solvable by "brutal force" optimization approach (particle swarm optimization, genetic algorithm, etc.) within a practical computational time constraint. For example, for an ANC filter of order 300, there may be $\frac{1}{2}C(300, 150) = \frac{300!}{2\times 150!\times(300-150)!} \approx 4.7 \times 10^{88}$ local minimums, which makes the global minimum (or a usable local minimum) difficult to be found.

2. The response of both $A(z)$ and $B(z)$ should have sufficient attenuation in frequency response above f_L to remove the need for anti-aliasing and reconstruction filters in traditional polyphase applications. Without this attenuation requirement, the decomposition of $W_x(z)$ into $A(z)$ and $B(z)$ can be achieved by simply obtaining the zeros of $W_x(z)$ and splitting the zeros into two groups for $A(z)$ and $B(z)$ (although the high order still poses numerical difficulties in the root-finding process [86]). This high-frequency response constraint also significantly increases the computational complexity if a "brutal force" optimization method is used to solve $A(z)$ and $B(z)$ from $W_x(z)$.

3. Both $A(z)$ and $B(z)$ must be causal so they can be implemented in a real-time delay-sensitive system such as an ANC system. Thus, simple frequency-domain fitting meth-

ods, such as fitting the square-rooted frequency responses of $W_x(z)$, cannot be used, because the causality of the resulting filters cannot be guaranteed.

To overcome the three challenges motioned above, a filter decomposition method is proposed as the following. Assume the required attenuation for the stop bands of $A(z)$ and $B(z)$ is K dB and the designed ANC filter $W_x(z)$ reaches $2K$ dB attenuation in the stop band, i.e.,

$$20\log_{10}|W_x(e^{j2\pi f})| < -2K, \quad \text{for } f > f_L/2. \tag{5.5}$$

Firstly, a minimum-phase lowpass filter $A(z)$ can be designed with a cut-off frequency $f_L/2$ where the stop band has K dB attenuation with stop band ripples around δ_s dB, i.e.,

$$-K - \delta_s < 20\log_{10}|A(e^{j2\pi f})| < -K + \delta_s, \quad \text{for } f > f_L/2. \tag{5.6}$$

Because $A(z)$ is a minimum-phase filter, $\frac{1}{A(z)}$ will also be a minimum-phase filter, i.e., $\frac{1}{A(z)}$ will be causal and stable. Since $W_x(z)$ is a designed FIR filter for ANC application, $W_x(z)$ is always stable (having zeros only) and causal. Thus, $\frac{W_x(z)}{A(z)}$ will be causal and stable and a causal filter $B(z)$ can be fitted to have similar frequency responses as $\frac{W_x(z)}{A(z)}$, e.g., using least square approximation. Obviously,

$$20\log_{10}|B(e^{j2\pi f})| \approx 20\log_{10}|\frac{W_x(e^{j2\pi f})}{A(e^{j2\pi f})}| < -K + \delta_s, \quad \text{for } f > f_L/2. \tag{5.7}$$

Thus, both $A(z)$ and $B(z)$ are attenuated as required above $f_L/2$ if ripple δ_s is chosen to be small enough. Also, $A(e^{j2\pi f})B(e^{j2\pi f}) \approx W_x(e^{j2\pi f})$ for $f < f_L/2$. So the proposed filter decomposition method can give a pair of suitable $A(z)$ and $B(z)$ for the proposed delayless polyphase implementation in the previous section.

Figure 5.3 is a flow chart showing the procedure of using three traditional methods (i.e., the low sampling rate method, high sampling rate method using the original IRD, and shorter IRD) and using the proposed delayless polyphase implementation along with the proposed causal filter decomposition method. When using traditional methods, only either less computational time or better noise control performance can be achieved. However, if

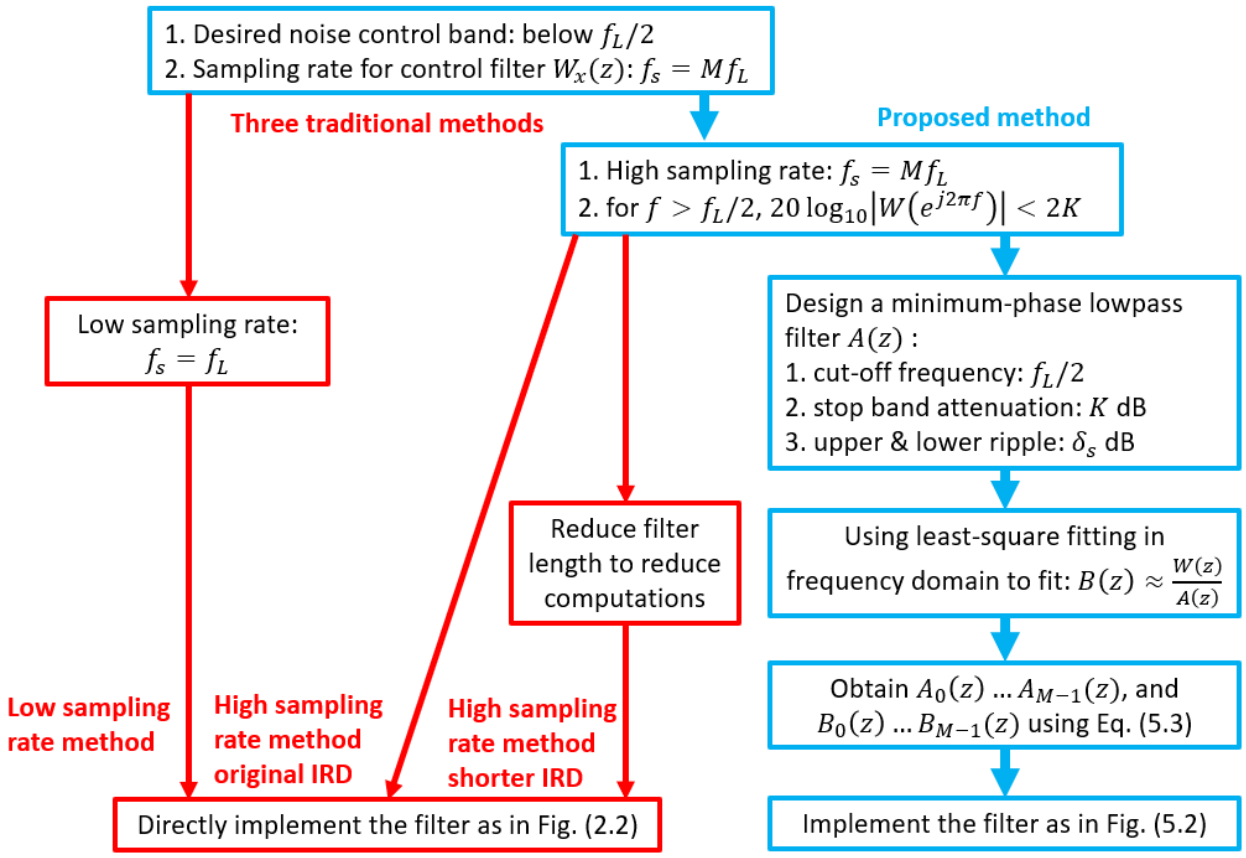


Figure 5.3. A flow chart showing the traditional filter implementation methods and the proposed ANC filter implementation method using delayless polyphase implementation.

the proposed implementation is used, both advantages of less real-time computations and better noise control performance can be achieved.

5.1.3 Experimental results and discussions

To investigate the performance of the proposed delayless polyphase implementation in ANC application, an installed single-channel ANC system is shown in Fig. 5.4. Since the proposed method can be applied channel by channel, a single-channel ANC system is sufficient to investigate the performance of the proposed method. The primary noise source is a speaker that plays a low-pass filtered white noise whose cut-off frequency is 9 kHz. The de-

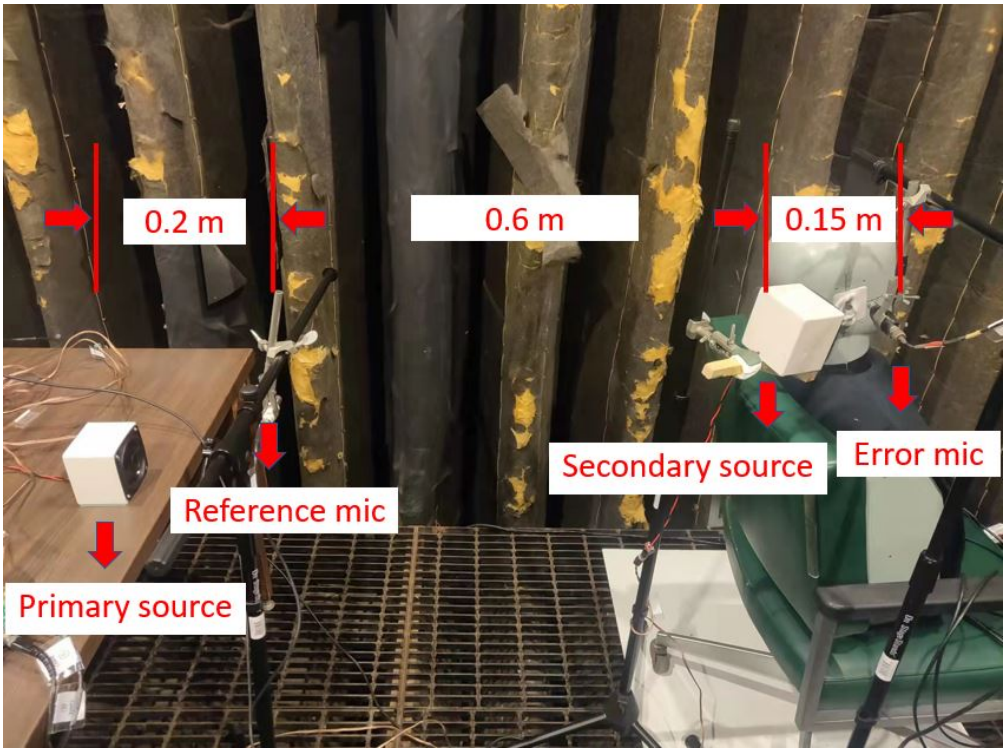


Figure 5.4. A picture of the experimental setup.

sired noise control frequency band is below $f_L/2 = 2$ kHz (i.e., $f_L = 4$ kHz). Since the highest frequency component of the noise source signal (9 kHz) is much higher than the desired noise control frequency band (which is a very common case for most practical ANC applications), anti-aliasing filters are usually needed to prevent aliasing. The secondary source is another speaker that produces the desired sound signal to cancel the noise at the error microphone position. The relative difference in distance between the reference microphone and the error microphone and the secondary source and the error microphone is approximately 0.6 meters, which means the introduced electronic delay (including the delay in anti-aliasing and reconstruction filters) should be at least less than 1.8 ms if a broadband noise control performance is desired.

In this experimental setup, to more accurately set the control variables in high and low sampling rate cases, digital anti-aliasing and reconstruction filter, instead of analog filters, are implemented using a 20 kHz sampling rate. The 20 kHz sampling rate is more than

twice of 9 kHz so the digital filter can be used to simulate analog anti-aliasing filters with better control over the parameters. For both 4 kHz and 20 kHz sampling rates, 1 dB ripple is allowed at the passband, and 30 dB attenuation is required for the stopband. A minimum order Butterworth filter [145] is designed as the anti-aliasing and reconstruction filter. The total electronic delay for desired noise control band including group delay of anti-aliasing and reconstruction filter, and one-sample delay for the processing in controllers is shown in Fig. 5.5. From Fig. 5.5, the introduced electronic delay when using a low sampling rate (4 kHz) is higher than 10 ms, which is much higher than the high sampling rate case (the delay introduced in 20 kHz sampling rate case is less than 1 ms).

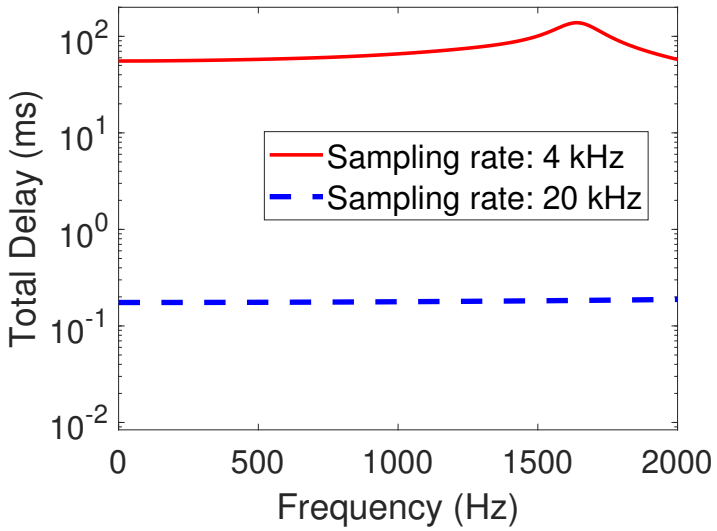
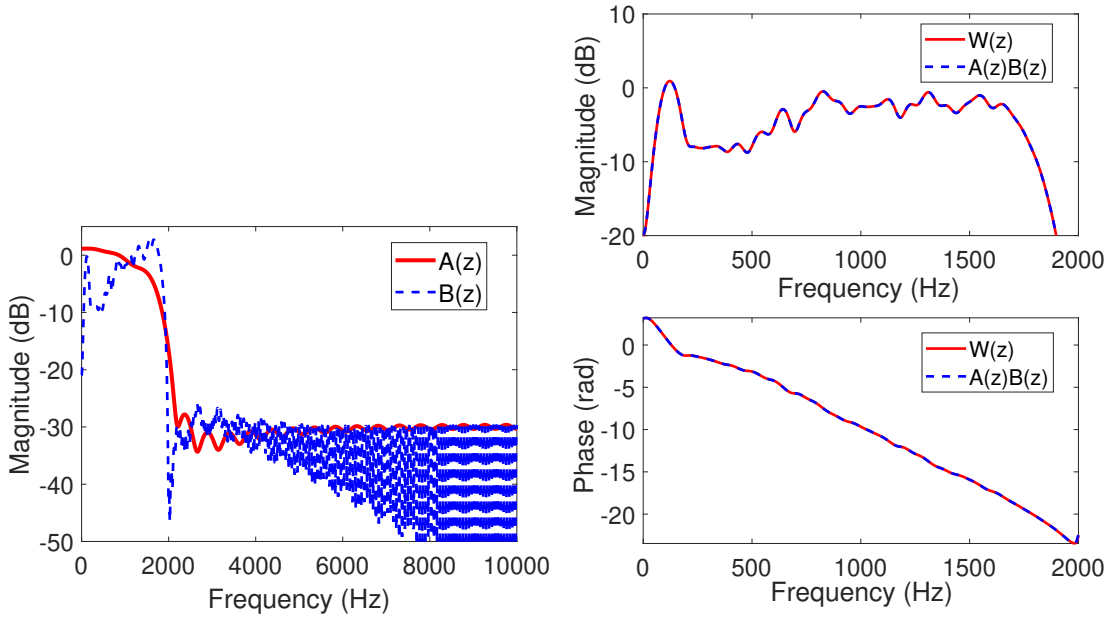


Figure 5.5. The total electronic delay including group delay of anti-aliasing and reconstruction filter, and one-sample delay for the processing in controllers for two different sampling rate.

The noise control performance of using various traditional methods that directly implement the ANC filter as in Fig. 2.2 and the proposed method that implements the filter as in Fig. 5.2 are compared. For the high sampling rate case, since the designed filter response should be attenuated for at least 2K dB (in this experimental setup, K = 30), the optimal ANC filter $W_x(z)$ is designed by the proposed conic method in Chapter 3. Two different choices of IRD (15 ms and 3 ms) are used to design the ANC FIR filter. When IRD T is 15 ms, the number of FIR ANC filter coefficients is 60 if the sampling rate is 4 kHz. However,

the number of FIR filter coefficients reaches 300 if the sampling rate is 20 kHz which is significantly larger than 60 (i.e., $M = 5$). For the 20 kHz sampling rate, if the filter IRD is reduced to 3 ms, the FIR ANC filter length is then the same as the 15 ms IRD in a low sampling rate case.



(a) (b)

Figure 5.6. (a) Magnitude of the frequency responses of $A(z)$ and $B(z)$ for the whole frequency band to show they are well attenuated above 2 kHz, (b) comparison of magnitude and phase of the frequency responses of $W_x(z)$ and $A(z)B(z)$ for the desired noise control frequency band (below 2 kHz).

To use the proposed method, two subfilters $A(z)$ (filter order 40) and $B(z)$ (filter order 300) are obtained by using the proposed filter decomposition method. Thus, $\theta = 1.13$ in this case. Their frequency responses are shown in Fig. 5.6. From Fig. 5.6(a), the designed $A(z)$ and $B(z)$ using the proposed filter decomposition method are well attenuated (30 dB attenuation) above 2 kHz, which means that they can be used as anti-aliasing and reconstruction filters. From Fig. 5.6(b), clearly $A(e^{j2\pi f})B(e^{j2\pi f}) \approx W_x(e^{j2\pi f})$ below 2 kHz, which means that the decomposed $A(z)$ and $B(z)$ together can achieve similar noise control performance compared with using $W_x(z)$ in the desired noise control band (below 2 kHz).

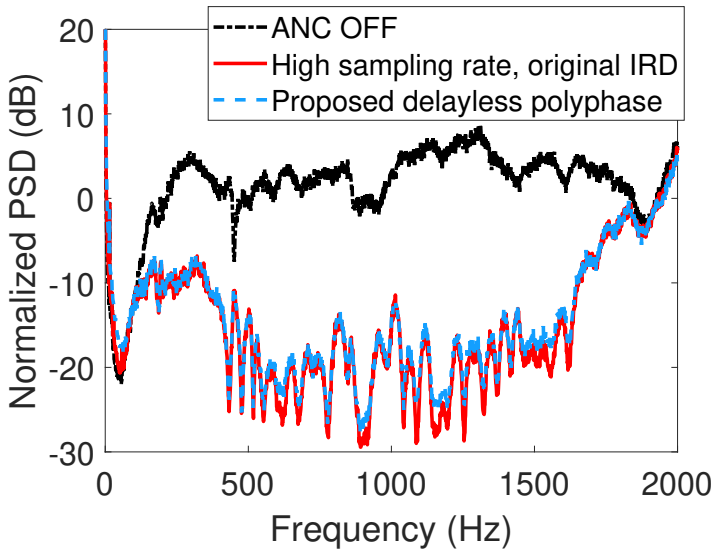


Figure 5.7. The comparison of noise control performance for traditionally used high sampling rate method using the original IRD and the proposed delayless polyphase implementation method at the desired noise control frequency band.

Figure 5.7 confirms that the noise control performance of using the proposed method is not sacrificed compared with using the traditional high sampling rate method using the original IRD. It is noted that the traditional high sampling rate method using the original IRD requires 300 multiplications for each sampling interval (20 kHz), while the proposed delayless polyphase method only requires $(40+300)/5 = 68$ multiplications for each sampling interval (also in 20 kHz) which reduces the real-time multiplications to only 23% of the traditional high sampling rate methods. Thus, compared with the traditional high sampling rate method, the proposed method uses much less real-time computations and has almost the same noise control performance. A comparison of real-time multiplications per second for different traditional methods and the proposed method in this experimental setup is shown in Table 5.2.

In Fig. 5.8, when using approximately the same real-time computations as the proposed method (i.e., effectively around 60 or 68 multiplications at 20 kHz rate), the noise control performance of the proposed method is better than that of the traditional method 2 (i.e.,

Table 5.2. A comparison of real-time multiplications per second for different traditional methods and the proposed method in the experimental setup.

Methods	Low f_s method	High f_s method, original IRD	High f_s method, shorter IRD	Proposed method
Sampling Rate f_s	4 kHz	20 kHz	20 kHz	20 kHz
IRD	15 ms	15 ms	3 ms	16.95 ms
Filter Order	60	300	60	340
Real-time Multiplications	240 k	6000 k	1200 k	1360 k
Delay	$>$ 10 ms	$<$ 1 ms	$<$ 1 ms	$<$ 1 ms

the high sampling rate for 3 ms IRD) or low sampling rate method for 15 ms. In Fig. 5.8, the traditionally used high sampling rate method using shorter IRD has worse noise control performance compared with the proposed method because it uses only a 3 ms IRD which is much shorter compared with around 15 ms. The traditionally used low sampling rate method has almost no noise control performance because, at such a low sampling rate, the introduced electronic delay is too high as already shown in Fig. 5.5.

The experimental result section confirms that, compared with the low sampling rate method, all two traditional high sampling rate methods and the proposed method can achieve better noise control performance because the use of a high sampling rate reduces introduced electronic delay. Compared with the traditional high sampling rate method using the original IRD, i.e., high sampling rate with filter order increases accordingly, the proposed method increases real-time computations linearly while the traditional high sampling rate method using the original IRD increases real-time computations quadratically. In this experimental setup, since the sampling rate is increased by 5, the proposed method reduces to around one-fifth of the multiplications compared with the traditional high sampling rate method using the original IRD. Compared with the traditional high sampling rate method using shorter IRD, i.e., high sampling rate with shortened filter length, the proposed method has much better noise control performance while keeping similar required real-time computations.

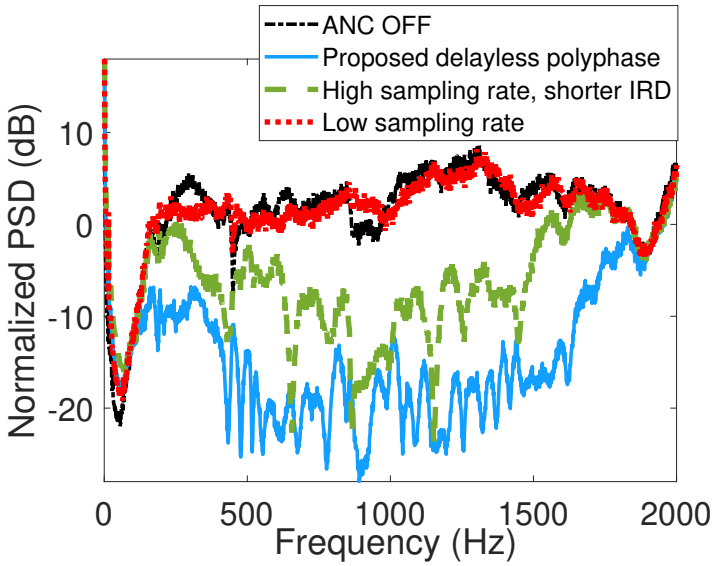


Figure 5.8. The comparison of noise control performance for the traditional high sampling rate method using shorter IRD, the low sampling rate method, and the proposed delayless polyphase implementation method at the desired noise control frequency band.

5.2 A Stable IIR Filter Fitting Method for High-Order Active Sound Control

As discussed in Section 1.3.2, a stable IIR approximation approach for high sampling rate ANC applications should be developed so the benefits of both FIR and IIR filter structures can be combined by using an IIR filter structure to fit pre-designed FIR filter coefficients or the desired frequency responses.

In this section, to fit a stable IIR filter for ANC applications, the IIR filter approximation method proposed by Brandenstein and Unbehauen [94], [95] is adopted. Improvements are proposed based on their method to make it applicable in ANC applications. An ANC system installed on a commercial earphone prototype is used to investigate the performance of the proposed method.

5.2.1 Improvements in weighted least-square approximation method

The IIR filter approximation method proposed by Brandenstein and Unbehauen (referred to as the BU's method in this section) is reviewed in Section 2.2.2. Some improvements were made to the BU's method such that it is more suitable for practical ANC applications. For simplicity, these improvements on BU's method are referred to as the "proposed method" in this section.

When using the iteration process in Section 2.2.2, the approximation error norm $E^{(k)}$ does not always converge to the minimum value, especially for some maximum phase FIR filters with high order (larger than 50) [94]. In ANC applications, the order of the FIR filter is usually larger than 50, which makes this issue more serious. Since this phenomenon occurs when the matrix $A^{(k)}$ is ill-conditioned [94], one improvement is proposed as follows. If ${A^{(k)}}^{\mathrm{T}}A^{(k)}$ is near singular at the current iteration, then a gradient descent is applied to continue solving $Q(z)$. More specifically, the goal of solving Eq. (2.29) is to minimize

$$\begin{aligned} J(q^{(k)}) &= \|A^{(k)}q^{(k)} - b^{(k)}\|_2^2 \\ &= {q^{(k)}}^{\mathrm{T}}{A^{(k)}}^{\mathrm{T}}A^{(k)}q^{(k)} - 2{b^{(k)}}^{\mathrm{T}}A^{(k)}q^{(k)} + {b^{(k)}}^{\mathrm{T}}b^{(k)}. \end{aligned} \tag{5.8}$$

Thus, $\hat{g}$, an estimation of gradient of function $J(q^{(k)})$ can be obtained by using $q^{(k-1)}$

$$\hat{g} = 2{A^{(k)}}^{\mathrm{T}}A^{(k)}q^{(k-1)} - 2{A^{(k)}}^{\mathrm{T}}b^{(k)}. \tag{5.9}$$

The approximated $q^{(k)}$ can then be obtained by

$$q^{(k)} = q^{(k-1)} - \alpha\hat{g}, \tag{5.10}$$

where $\alpha < 1$ is the step length such that $Q^{(k)}(z)$ is stable and can have a smaller approximation error norm compared with $Q^{(k)}(z-1)$. Repeat this process until some prescribed convergence criteria are satisfied, e.g., step length, norm of gradient, etc.

The selection of maximum phase weighting function $G(z)$ also needs to be considered. In ANC applications, the required weighting function is usually in the form of $|W(\mathrm{e}^{-\mathrm{j}\Omega})|$. For

simplicity, a linear-phase FIR filter with real coefficients can be easily designed to have the magnitude $\sqrt{|W(\mathrm{e}^{-\mathrm{j}\Omega})|}$ such that $W(\mathrm{e}^{-\mathrm{j}\Omega}) = W(\mathrm{e}^{\mathrm{j}\Omega})$ is satisfied. Because of the linear phase, the coefficients of this designed filter will be symmetric such that a spectral factorization can be applied to the coefficients sequence of this FIR filter to obtain a minimum phase decomposition. After flipping the coefficients of decomposed minimum phase filter, the maximum phase counterpart $G(z)$ can be obtained.

Since the signal used in ANC controller is usually in the discrete format, the computation of c(n) and b(n) in Eq. (2.36) and (2.37) is done by FFT and IFFT after a sufficiently large zero padding.

In summary, the whole proposed process of fitting an FIR filter using an IIR filter structure is presented in Algorithm 1, 2, 3.

Algorithm 1 Finding an appropriate weighting function

Require: Desired weighting curve $|W(\mathrm{e}^{\mathrm{j}\Omega})|$ in the frequency domain; the order of weighting function K

- Designed a linear phase filter coefficients $W_z = \begin{bmatrix} w_0 & w_1 & \dots & w_{2K} \end{bmatrix}^{\mathrm{T}}$ that has frequency magnitude $\sqrt{|W(\mathrm{e}^{\mathrm{j}\Omega})|}$
- (E.g., using Parks-McClellan or least-square optimal FIR filter design).
- Apply spectral factorization to W_z to obtain a minimum phase decomposition $G_{min} = \begin{bmatrix} \tilde{g}_0 & \tilde{g}_1 & \dots & \tilde{g}_K \end{bmatrix}^{\mathrm{T}}$.
- The maximum phase weighting function is $G = \mathrm{flip}(G_{min}) = \begin{bmatrix} \tilde{g}_K & \tilde{g}_{K-1} & \dots & \tilde{g}_0 \end{bmatrix}^{\mathrm{T}}$.

return The weighting function $G = \begin{bmatrix} g_0 & g_1 & \dots & g_K \end{bmatrix}^{\mathrm{T}}$

5.2.2 Experimental results and discussions

To investigate the fitting performance and its effect on the noise control performance of the proposed method, an earphone is used to collect the system response data. For this earphone, there is one microphone used as the reference sensor and one speaker used as the noise control speaker. The error microphone used in this experiment that measured the

Algorithm 2 Finding the optimal IIR filter denominator coefficients

Require: FIR filter coefficients $F = \begin{bmatrix} f_0 & f_1 & \dots & f_L \end{bmatrix}^{\mathrm{T}}$; the order of IIR numerator M and denominator N; the weighting function $G = \begin{bmatrix} g_0 & g_1 & \dots & g_K \end{bmatrix}^{\mathrm{T}}$ in Algorithm 1.

Let $X = \text{flip}(\text{convolution}(\text{G},\text{F}))$, $\quad Q^{(0)} = \begin{bmatrix} 1 & 0 & \dots & 0 \end{bmatrix}^{\mathrm{T}}$

for $k \leftarrow 1$ to max iteration **do**

$x^{(k)} \leftarrow$ Filtering sequence X using IIR filter with numerator 1 and denominator coefficients $Q^{(k-1)}$, keep the first $L + N - M$ points.

Construct $A^{(k)}$, $b^{(k)}$ using Eq. (2.30), (2.31)

if condition number of ${A^{(k)}}^{\mathrm{T}} A^{(k)}$ is small **then**

$Q^{(k)}(2{:}\text{end}) \leftarrow \text{flip}(({A^{(k)}}^{\mathrm{T}} A^{(k)})^{-1} {A^{(k)}}^{\mathrm{T}} b^{(k)})$

else

Compute the gradient descent direction:

$\hat{g}^{(k)} \leftarrow 2{A^{(k)}}^{\mathrm{T}} A^{(k)} \text{flip}(Q^{(k-1)}(2:\text{end})) - 2{A^{(k)}}^{\mathrm{T}} b^{(k)}$

len $\leftarrow 1$

while STOP $==$ 1 **do** $Q^{(k)}_{temp}(1) \leftarrow 1$

$Q^{(k)}_{temp}(2:end) \leftarrow Q^{(k-1)} -$ len $\times$ flip$(\hat{g}^{(k)})$

$E_{temp} \leftarrow$ Filtering X using IIR filter with numerator coefficients flip$(Q^{(k)}_{temp})$ and denominator coefficients $Q^{(k)}_{temp}$, compute the 2-norm of first $L + N - M$ points.

if E_{temp} less than $E^{(k-1)}$ and $Q^{(k)}_{temp}$ is stable **then**

$Q^{(k)} \leftarrow Q^{(k)}_{temp}$

STOP $\leftarrow 0$, break the loop.

else

Reduce len

end if

end while

end if

$E^{(k-1)} \leftarrow$ Filtering X using IIR filter with numerator coefficients flip$(Q^{(k)})$ and denominator coefficients $Q^{(k)}$, compute the 2-norm of first $L + N - M$ points

if Stopping criterion satisfied **then**

Break the loop

else

Do nothing

end if

end for

return Fitted IIR denominator $Q = \begin{bmatrix} q_0 & q_1 & \dots & q_N \end{bmatrix}^{\mathrm{T}}$

noise control performance is in an artificial ear shown in Fig. 5.9. The used artificial ear is Hangzhou Aihua AWA6162 (IEC711).

Algorithm 3 Finding the optimal IIR filter numerator coefficients

Require: FIR filter coefficients $F = \begin{bmatrix} f_0 & f_1 & \dots & f_L \end{bmatrix}^{\mathrm{T}}$, the order of IIR numerator M, the weighting function $G = \begin{bmatrix} g_0 & g_1 & \dots & g_K \end{bmatrix}^{\mathrm{T}}$ in Algorithm 1, IIR denominator $Q = \begin{bmatrix} q_0 & q_1 & \dots & q_N \end{bmatrix}^{\mathrm{T}}$ in Algorithm 2.
$S_W \leftarrow$ square of the magnitude of FFT of the sufficiently zero-padded sequence G
$S_Q \leftarrow$ FFT of sufficiently zero-padded sequence Q
$S_F \leftarrow$ FFT of sufficiently zero-padded sequence F
$c \leftarrow$ IFFT of S_W pointwise divided by the square of magnitude of S_Q, truncate to $M+1$ points
$b \leftarrow$ IFFT of S_W pointwise multiplied by S_F and then pointwise divided by the complex conjugate of S_Q, truncate to $M+1$ points
$C_p \leftarrow$ construct a square real symmetric Toeplitz matrix using c as the first row
$P \leftarrow$ solve $C_p P = b$, Toeplitz properties can be applied
return Fitted IIR numerator $P = \begin{bmatrix} p_0 & p_1 & \dots & p_M \end{bmatrix}^{\mathrm{T}}$



Figure 5.9. A picture of the experimental setup showing an earphone mounted on an artificial ear for experimental data collection.

The broadband noise control performance was considered in this section. Because of the limited dimension of the earphone, the delay in the signal path introduced by the electronic devices and anti-aliasing/reconstruction filters should be sufficiently small to achieve broadband noise control performance. Thus, the sampling rate of the data acquisition system

and the noise control system was set to 48 kHz. Although the sampling rate is high (48 kHz), the desired noise control band is set from 50 Hz to 3 kHz for practical considerations. When measuring and computing the system responses, two million sampling points (about 42 seconds) were acquired and a hamming window of 48000 points (around 1 second) is used for averaging with 50% overlap. The frequency responses of the measured secondary path are shown in Fig. 5.10.

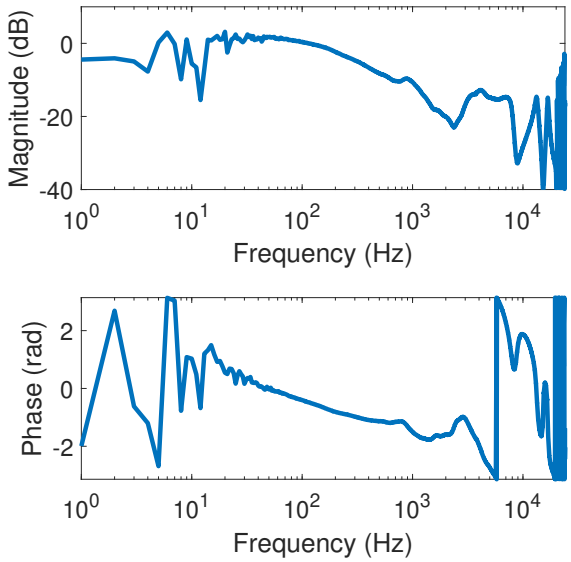


Figure 5.10. The frequency responses of measured secondary path $\mathbf{G}_e$. The reference value for the dB scale is 1.

Because the sampling rate is 48 kHz which is much higher than the desired noise control band (50 Hz to 3 kHz), some constraints such as the filter responses amplitude constraints or the noise amplification constraints should be applied to prevent the amplification of the high-frequency noises outside desired noise control frequency band. Thus, the ANC filter is designed by the proposed conic method in Chapter 3.

Since the FIR filter is not required to be implemented in real-time, a sufficiently large order should be chosen. The nominal noise control performance using the designed FIR filter with different orders is shown in Fig. 5.11. Figure 5.11 (a) shows the designed FIR filter can achieve satisfactory noise control performance in desired noise control frequency band and does not amplify noises outside the desired noise control frequency band. Figure 5.11

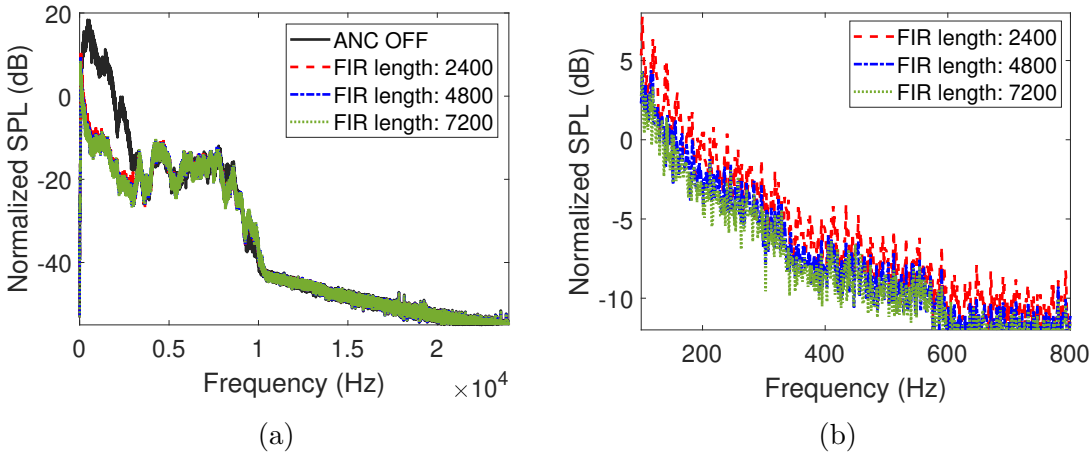
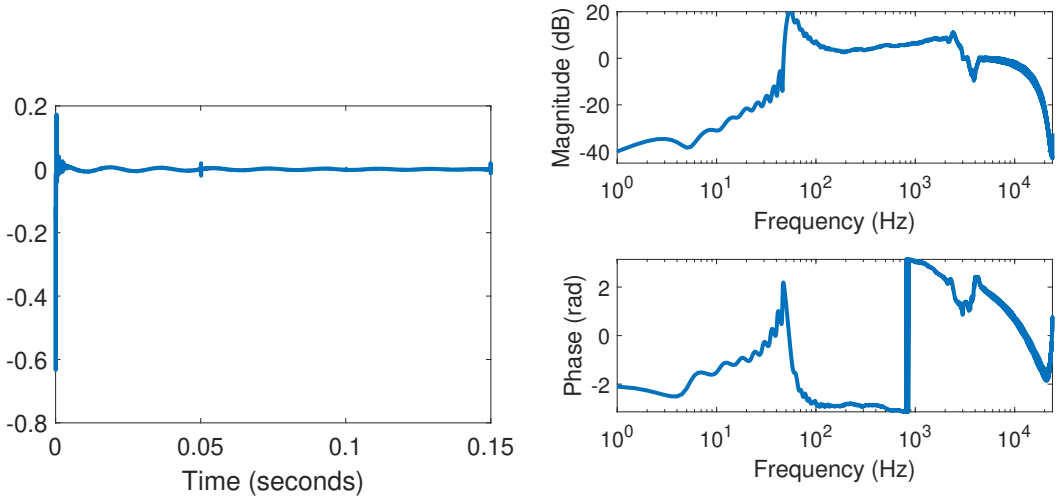


Figure 5.11. The nominal noise control performance of designed noise control filter using FIR filter structure with different filter lengths: (a) showing the full frequency band: from 0 Hz to 24 kHz; (b) showing the zoomed-in frequency band: from 100 Hz to 800 Hz.

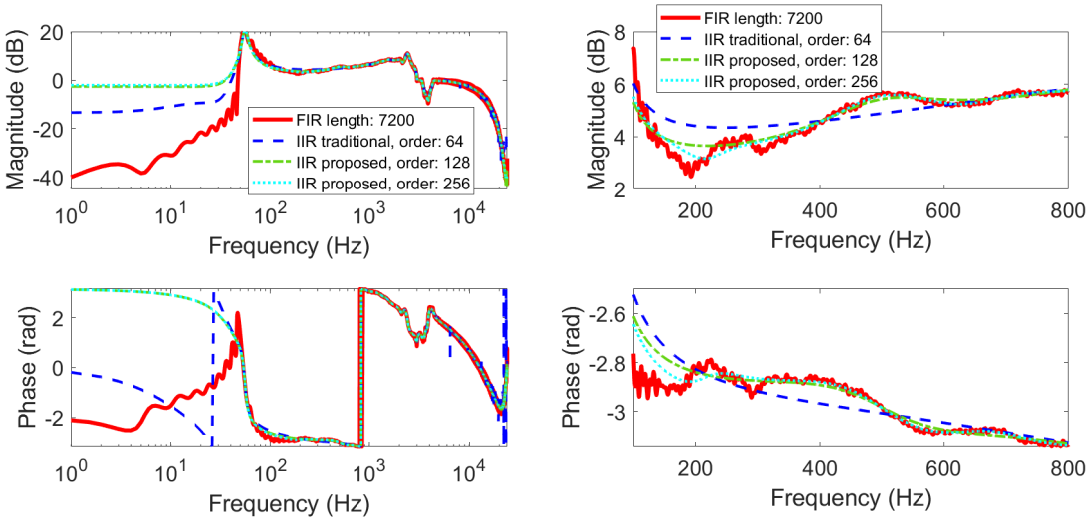
(b) demonstrates that a large filter length (7200) is needed because, compared with using 2400 and 4800 coefficients, using 7200 coefficients (equivalently to 0.15 seconds IRD) can still improve the noise control performance, especially around the lower frequency band (3-4 dB better than 2400 coefficients case and around 1 dB better than 4800 coefficients case). Since the improvement from using 4800 coefficients to using 7200 coefficients is not significant, 7200 coefficients are considered sufficient for this ANC application. The impulse response and frequency response of the designed FIR filter using 7200 coefficients are shown in Fig. 5.12.

Although using 7200 coefficients can achieve satisfactory noise control performance at the desired frequency band without amplifying noises outside the frequency band, the real-time computational requirement is significant if a 7200-point FIR filter is implemented at a 48 kHz sampling rate. Thus, IIR filter structure should be used to fit the responses of this 7200-point FIR filter. The order of the numerator polynomial was set to be equal to the order of the denominator polynomial. Because the desired noise control (50 Hz to 3 kHz) is relatively narrow compared with the full band, 100 times higher weighting is applied to frequencies below 3 kHz to ensure an accurate fitting in the desired noise control band.



(a) (b)

Figure 5.12. The (a) impulse response and the (b) frequency response of designed optimal control filter using FIR filter structure using 7200 time-domain coefficients



(a) (b)

Figure 5.13. The comparison of pre-designed FIR filter frequency responses and the fitted IIR filter frequency responses using different methods and filter orders: (a) showing the full frequency band: from 0 Hz to 24 kHz; (b) showing the zoomed-in frequency band: from 100 Hz to 800 Hz.

When using the traditional method, if the order of the IIR filter is chosen to be higher than 64, the algorithm cannot converge to a stable IIR filter. However, the proposed method can successfully fit the frequency responses using the IIR filter with higher orders (e.g., 128 or 256). The comparison of pre-designed FIR filter frequency responses and the fitted IIR filter frequency responses using different methods and filter orders are shown in Fig. 5.13 (a). Figure 5.13 (a) shows all methods and filter orders can achieve satisfactory overall fitting accuracy for the whole frequency band, especially at higher frequencies. A zoomed-in frequency band from 100 Hz to 800 Hz is shown in Fig. 5.13 (b) to have a clearer comparison of the fitting accuracy. It demonstrated that during this relatively lower frequency range, the IIR filter fitted using the proposed method has a much better fitting accuracy compared with that using the traditional method because the proposed method enables a higher-order stable IIR filter to be fitted.

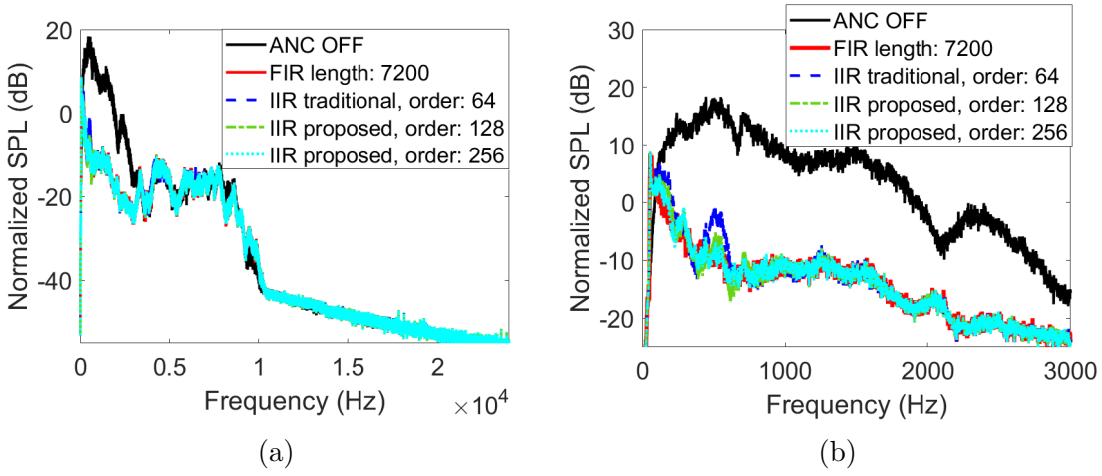


Figure 5.14. The comparison of nominal noise control performance using the traditional method and the proposed method: (a) showing the full frequency band: from 0 Hz to 24 kHz; (b) showing the desired noise control frequency band: from 0 Hz to 3 kHz.

The comparison of nominal noise control performance using the traditional method and the proposed method is shown in Fig. 5.14 for the full frequency band and the desired noise control band. The zoomed-in frequency band from 100 Hz to 800 Hz is also shown in Fig. 5.15. This demonstrated that the proposed method can achieve a better noise control

performance compared with the traditional method, especially for certain frequency bands: e.g., 3-5 dB better from 400 Hz to 600 Hz.

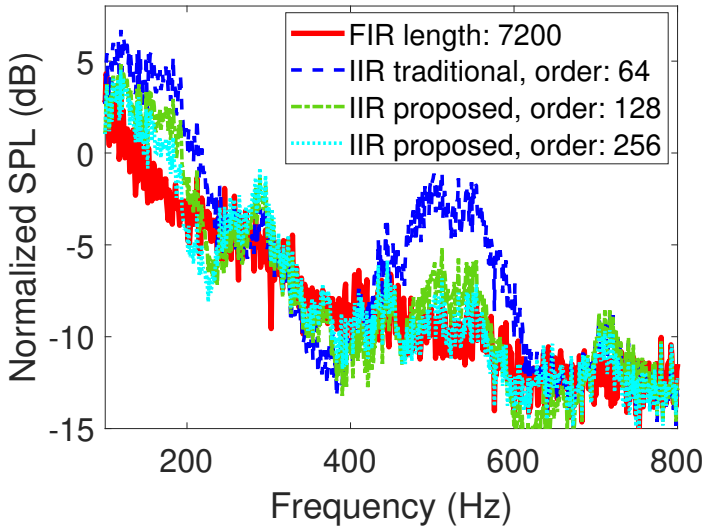


Figure 5.15. Zoomed-in frequency band: from 100 Hz to 800 Hz for the comparison of nominal noise control performance using the traditional method and the proposed method..

5.3 Summary

In this chapter, a delayless polyphase implementation and the associated multiplicative causal filter decomposition method are proposed. The proposed method uses the property that the frequency response of a high sampling rate ANC filter should be attenuated outside the desired noise control band to prevent noise amplification. Thus, the high sampling rate ANC filter can be decomposed into two multiplicative causal sub-filters by the proposed causal filter decomposition method using a minimum-phase low-pass filter design. The two causal sub-filters can then perform as both control filters and anti-aliasing and reconstruction filters so polyphase implementation can be used to reduce the real-time computations without introducing an additional delay. By using the proposed methods, the real-time computations only increase with the sampling rate linearly instead of quadratically compared with the traditional high sampling rate method. The experimental result confirms that the proposed structure can achieve the same noise control performance while reducing the

real-time multiplications to only 23% of the required multiplications using the traditional method. After using the proposed method, less electronic delay is introduced to the ANC system and the noise control performance can be significantly improved. A smaller physical dimension of the broadband ANC system is also possible with the proposed method since the reduced electronic delay allows a closer distance between reference microphones, secondary speakers, and the desired noise control region.

A stable IIR fitting approach in high-order ANC applications is also proposed by improving Brandenstein and Unbehauen's method [94], [95] such that the stability of the designed IIR filter can be guaranteed without implementing root-finding. A gradient-based searching method is proposed in addition to the original solving approach in BU's method such that the convergence can be guaranteed which is more applicable in practical applications. Practical approaches to obtain the required maximum phase weighting function and compute the optimal IIR filter numerator coefficients are also proposed. An ANC system installed on a commercial earphone prototype is used to investigate the performance of the proposed method. The result shows that the proposed improved IIR filter approximation method can achieve better fitting accuracy and noise control performance compared with the traditional IIR fitting approach. Besides the fitting of the noise control filter, the proposed method can also be used for fitting secondary paths and acoustic feedback paths to further reduce the real-time computations in both non-adaptive and adaptive ANC applications.

6. SUMMARY

In this dissertation, to efficiently design multi-channel constrained ANC filters, the traditional constrained optimization method based on the H_2/H_∞ formulation is convexified and reformulated into a conic formulation. Results show that the proposed conic method can produce better noise control performance than the regularization parameter method. Compared with the traditional constrained optimization method, the proposed method is more reliable and the computation time can be reduced by several orders of magnitude (from the order of days to seconds). Compared with the conventional cone programming formulation procedure, the proposed conic form using duality properties improves both numerical stability and computational efficiency. The proposed conic method also brings various other benefits: e.g., the frequency resolution can be increased in the cost function without increasing solution time, the required iteration number is relatively predictable, etc. A robust stability constraint modification is also proposed to allow a warmstarting strategy to be applied to the proposed conic method. Results show that using the warmstarting method requires less than 40% iterations compared with using cold-start approaches in 0.1% perturbation.

The proposed conic method can satisfy multiple types of constraints simultaneously. When only the noise amplification constraint is required, another simpler method, the singular vector filtering method, is proposed, which filters the singular vectors obtained by applying SVD to the auto-correlation matrix of filtered-reference signals. Results show that the proposed singular vector filtering method can effectively attenuate the noise amplification and achieve better noise control performance compared with the regularization parameter method and truncated singular value method.

Besides the ANC application, the proposed conic formulation can be extended to various other ASC applications. Because of the improved numerical efficiency and stability brought by the proposed conic method, the time-varying noise signals can be actively controlled by a continuous redesign of the optimal ANC filter coefficients using the proposed conic method. Results show that the proposed conic method in time-varying environments can achieve a faster convergence rate and better steady-state noise control performance compared with the commonly used leaky FxLMS method. The proposed conic method is also extended to

design the room equalization filter with a proposed order reduction technique, especially for accurate wide-band sound reproduction. Results show that the proposed room equalization filter design method can achieve better sound reproduction performance compared with the common frequency-domain deconvolution method. It is also more numerically efficient compared with traditional least-squares optimization methods. The hear-through filter design is also shown to have the same control diagram with a change of variables compared with the ANC filter design. Thus, the proposed conic method can be directly applied to design hear-through filters. Results show that when using the proposed conic method, satisfactory hear-through performance can be achieved without the comb-filtering effect and the controller can be stable when the acoustic feedback path is strong.

Besides efficient filter design methods, efficient filter implementation methods are also developed. A delayless polyphase implementation structure and the associated causal filter decomposition method are proposed for delay-sensitive applications. Compared with the traditional high sampling rate method, the real-time computational complexity is improved from quadratic to linear using the proposed method. The specific result shows that the proposed method can achieve the same noise control performance while reducing the real-time multiplications to only 23% of the required multiplications using the traditional method. Since less delay is introduced by using the proposed method, better noise control performance can be achieved (or smaller physical dimension can be possible)) compared with other traditional methods with similar computational requirements. A stable IIR filter fitting method is also developed to further reduce the real-time computations. No pole placements are involved in the proposed method. Thus, it is more suitable when high-order systems are used.

In summary, efficient filter design and implementation methods are proposed in this dissertation that targets various current challenges in ASC applications. Results demonstrate their effectiveness. Although the ANC application is focused, the proposed method is also shown to be applicable to various different ASC applications.

REFERENCES

[1] J. Cheer, "Active sound control in the automotive interior," *Future Interior Concepts*, pp. 53–69, 2021.

[2] Y. Kajikawa, W.-S. Gan, and S. M. Kuo, "Recent advances on active noise control: Open issues and innovative applications," *APSIPA Transactions on Signal and Information Processing*, vol. 1, 2012.

[3] W. Chen, C. Lu, Z. Liu, H. Williams, and L. Xie, "A computationally efficient active sound quality control algorithm using local secondary-path estimation for vehicle interior noise," *Mechanical Systems and Signal Processing*, vol. 168, p. 108 698, 2022.

[4] L. P. de Oliveira, K. Janssens, P. Gajdatsy, *et al.*, "Active sound quality control of engine induced cavity noise," *Mechanical systems and signal processing*, vol. 23, no. 2, pp. 476–488, 2009.

[5] S. M. Kuo, R. K. Yenduri, and A. Gupta, "Frequency-domain delayless active sound quality control algorithm," *Journal of Sound and Vibration*, vol. 318, no. 4-5, pp. 715–724, 2008.

[6] S. M. Kuo, A. Gupta, and S. Mallu, "Development of adaptive algorithm for active sound quality control," *Journal of Sound and Vibration*, vol. 299, no. 1-2, pp. 12–21, 2007.

[7] F. Rumsey, *Spatial audio*. Taylor & Francis, 2012.

[8] Y. Zhuang and Y. Liu, "A constrained optimal hear-through filter design approach for earphones," in *INTER-NOISE and NOISE-CON Congress and Conference Proceedings*, Institute of Noise Control Engineering, vol. 263, 2021, pp. 1329–1337.

[9] C.-R. Huang, C.-Y. Chang, and S. M. Kuo, "Time-shift modeling-based hear-through system for in-ear headphones," *IEEE Transactions on Consumer Electronics*, vol. 68, no. 3, pp. 273–280, 2022.

[10] F. Denk, H. Schepker, S. Doclo, and B. Kollmeier, "Acoustic transparency in hearablestechnical evaluation," *Journal of the Audio Engineering Society*, vol. 68, no. 7/8, pp. 508–521, 2020.

[11] C.-R. Huang, C.-Y. Chang, and S. M. Kuo, "Development of active hear-through equalization algorithm for earphones," in *2021 Asia-Pacific Signal and Information Processing Association Annual Summit and Conference (APSIPA ASC)*, IEEE, 2021, pp. 1197–1201.

[12] S. Cecchi, A. Carini, and S. Spors, "Room response equalizationa review," *Applied Sciences*, vol. 8, no. 1, p. 16, 2017.

[13] P. Lueg, "Process of silencing sound oscillations," *US patent 2043416*, 1936.

[14] H. F. Olson and E. G. May, "Electronic sound absorber," *The Journal of the Acoustical Society of America*, vol. 25, no. 6, pp. 1130–1136, 1953.

[15] W. B. Conover, "Fighting noise with noise," *Noise control*, vol. 2, no. 2, pp. 78–92, 1956.

[16] M. Jessel and G. Mangiante, "Active sound absorbers in an air duct," *Journal of sound and vibration*, vol. 23, no. 3, pp. 383–390, 1972.

[17] G. Mangiante, "Active sound absorption," *The Journal of the Acoustical Society of America*, vol. 61, no. 6, pp. 1516–1523, 1977.

[18] S. J. Elliott and P. A. Nelson, "Active noise control," *IEEE signal processing magazine*, vol. 10, no. 4, pp. 12–35, 1993.

[19] X. Shen, D. Shi, W.-S. Gan, and S. Peksi, "Adaptive-gain algorithm on the fixed filters applied for active noise control headphone," *Mechanical Systems and Signal Processing*, vol. 169, p. 108 641, 2022.

[20] F. An and B. Liu, "Cascade biquad controller design for feedforward active noise control headphones considering incident noise from multiple directions," *Applied Acoustics*, vol. 185, p. 108 430, 2022.

[21] S. M. Kuo, S. Mitra, and W.-S. Gan, "Active noise control system for headphone applications," *IEEE Transactions on Control Systems Technology*, vol. 14, no. 2, pp. 331–335, 2006.

[22] Z. Zhang, M. Wu, L. Yin, *et al.*, "Robust parallel virtual sensing method for feedback active noise control in a headrest," *Mechanical Systems and Signal Processing*, vol. 178, p. 109 293, 2022.

[23] C.-Y. Chang, C.-T. Chuang, S. M. Kuo, and C.-H. Lin, "Multi-functional active noise control system on headrest of airplane seat," *Mechanical Systems and Signal Processing*, vol. 167, p. 108 552, 2022.

[24] J. Bean, N. Schiller, and C. Fuller, "Numerical modeling of an active headrest," in *INTER-NOISE and NOISE-CON Congress and Conference Proceedings*, Institute of Noise Control Engineering, vol. 255, 2017, pp. 4065–4075.

[25] Y. Liu and J. Liu, "The stochastic domain design of a real-time controller for an active noise control headrest based on finite element analysis," in *INTER-NOISE and NOISE-CON Congress and Conference Proceedings*, Institute of Noise Control Engineering, vol. 255, 2017, pp. 488–499.

[26] Y. Liu, S. Wang, and X. Wang, "A generalized spatial filtering method in broadband active noise control based on independent sound field component analysis," in *INTER-NOISE and NOISE-CON Congress and Conference Proceedings*, Institute of Noise Control Engineering, vol. 255, 2017, pp. 476–487.

[27] B. Rafaely and S. J. Elliott, "H_2 / H_∞ active control of sound in a headrest: Design and implementation," *IEEE Transactions on control systems technology*, vol. 7, no. 1, pp. 79–84, 1999.

[28] P. N. Samarasinghe, W. Zhang, and T. D. Abhayapala, "Recent advances in active noise control inside automobile cabins: Toward quieter cars," *IEEE Signal Processing Magazine*, vol. 33, no. 6, pp. 61–73, 2016.

[29] J. Cheer and S. J. Elliott, "Multichannel control systems for the attenuation of interior road noise in vehicles," *Mechanical Systems and Signal Processing*, vol. 60, pp. 753–769, 2015.

[30] I. Dimino, C. Colangeli, J. Cuenca, P. Vitiello, and M. Barbarino, "Active noise control for aircraft cabin seats," *Applied Sciences*, vol. 12, no. 11, p. 5610, 2022.

[31] C. R. Fuller, S. Snyder, C. Hansen, and R. Silcox, "Active control of interior noise in model aircraft fuselages using piezoceramic actuators," *AIAA journal*, vol. 30, no. 11, pp. 2613–2617, 1992.

[32] S. Elliot, P. Nelson, I. Stothers, and C. Boucher, "In-flight experiments on the active control of propeller-induced cabin noise," *Journal of Sound and Vibration*, vol. 140, no. 2, pp. 219–238, 1990.

[33] R. Castañé-Selga and R. S. S. Peña, "Active noise hybrid time-varying control for motorcycle helmets," *IEEE Transactions on control systems technology*, vol. 18, no. 3, pp. 602–612, 2009.

[34] R. M. Reddy, I. M. Panahi, and R. Briggs, "Hybrid fxrls-fxnlms adaptive algorithm for active noise control in fmri application," *IEEE Transactions on Control Systems Technology*, vol. 19, no. 2, pp. 474–480, 2010.

[35] M. McJury, R. Stewart, D. Crawford, and E. Toma, "The use of active noise control (anc) to reduce acoustic noise generated during mri scanning: Some initial results," *Magnetic resonance imaging*, vol. 15, no. 3, pp. 319–322, 1997.

[36] Y. Zhuang and Y. Liu, "Constrained optimal filter design for multi-channel active noise control via convex optimization," *The Journal of the Acoustical Society of America*, vol. 150, no. 4, pp. 2888–2899, 2021.

[37] B. Lam, D. Shi, W.-S. Gan, S. J. Elliott, and M. Nishimura, "Active control of broadband sound through the open aperture of a full-sized domestic window," *Scientific reports*, vol. 10, no. 1, pp. 1–7, 2020.

[38] X. Qiu, J. Lu, and J. Pan, "A new era for applications of active noise control," in *INTER-NOISE and NOISE-CON Congress and Conference Proceedings*, Institute of Noise Control Engineering, vol. 249, 2014, pp. 1254–1263.

[39] B. Kwon and Y. Park, "Interior noise control with an active window system," *Applied Acoustics*, vol. 74, no. 5, pp. 647–652, 2013.

[40] S. J. Elliott, P. Joseph, A. Bullmore, and P. A. Nelson, "Active cancellation at a point in a pure tone diffuse sound field," *Journal of sound and vibration*, vol. 120, no. 1, pp. 183–189, 1988.

[41] J. Garcia-Bonito, S. Elliott, and M. Bonilha, "Active cancellation of pressure at a point in a pure tone diffracted diffuse sound field," *Journal of sound and vibration*, vol. 201, no. 1, pp. 43–65, 1997.

[42] B. M. Faber and S. D. Sommerfeldt, "Global active control of energy density in a mock tractor cabin.," *Noise control engineering journal*, vol. 54, no. 3, 2006.

[43] M. R. Bai, Y. Lin, and J. Lai, "Reduction of electronic delay in active noise control systemsa multirate signal processing approach," *The Journal of the Acoustical Society of America*, vol. 111, no. 2, pp. 916–924, 2002.

[44] D. Shi, W.-S. Gan, B. Lam, and S. Wen, "Feedforward selective fixed-filter active noise control: Algorithm and implementation," *IEEE/ACM Transactions on Audio, Speech, and Language Processing*, vol. 28, pp. 1479–1492, 2020.

[45] Y. Zhuang and Y. Liu, "An adaptive constrained multi-channel active noise control filter design approach using convex cone optimization," in *INTER-NOISE and NOISE-CON Congress and Conference Proceedings*, Institute of Noise Control Engineering, vol. 266, 2023, pp. 510–521.

[46] S. Elliott, "Signal processing for active control," in (Signal Processing and its Applications), Signal Processing and its Applications. London: Academic Press, 2001, ch. 6, pp. 271–327, ISBN: 978-0-12-237085-4. DOI: https://doi.org/10.1016/B978-012237085-4/50008-9. [Online]. Available: http://www.sciencedirect.com/science/article/pii/B9780122370854500089.

[47] F. An, Y. Cao, M. Wu, H. Sun, B. Liu, and J. Yang, "Robust wiener controller design with acoustic feedback for active noise control systems," *The Journal of the Acoustical Society of America*, vol. 145, no. 4, EL291–EL296, 2019.

[48] L. Wu, X. Qiu, and Y. Guo, "A simplified adaptive feedback active noise control system," *Applied Acoustics*, vol. 81, pp. 40–46, 2014.

[49] D. Shi, W.-S. Gan, B. Lam, and X. Shen, "Comb-partitioned frequency-domain constraint adaptive algorithm for active noise control," *Signal Processing*, p. 108 222, 2021.

[50] D. Shi, W.-S. Gan, B. Lam, S. Wen, and X. Shen, "Optimal output-constrained active noise control based on inverse adaptive modeling leak factor estimate," *IEEE/ACM Transactions on Audio, Speech, and Language Processing*, vol. 29, pp. 1256–1269, 2021.

[51] J. C. Bermudez and M. H. Costa, "Optimum leakage factor for the MOV-LMS algorithm in nonlinear modeling and control systems," in *2002 IEEE International Conference on Acoustics, Speech, and Signal Processing*, IEEE, vol. 2, 2002, pp. II–1393.

[52] W. J. Kozacky and T. Ogunfunmi, "An active noise control algorithm with gain and power constraints on the adaptive filter," *EURASIP Journal on Advances in Signal Processing*, vol. 2013, no. 1, pp. 1–12, 2013.

[53] W. J. Kozacky and T. Ogunfunmi, "A cascaded IIR-FIR adaptive ANC system with output power constraints," *Signal processing*, vol. 94, pp. 456–464, 2014.

[54] C. Zhou, H. Zou, and X. Qiu, "A frequency band constrained filtered–x least mean square algorithm for feedback active control systems," *The Journal of the Acoustical Society of America*, vol. 148, no. 4, pp. 1947–1951, 2020.

[55] L. Wu, X. Qiu, and Y. Guo, "A generalized leaky fxlms algorithm for tuning the waterbed effect of feedback active noise control systems," *Mechanical Systems and Signal Processing*, vol. 106, pp. 13–23, 2018.

[56] Y. Zhuang, X. Wang, and Y. Liu, "Singular vector filtering method for mitigation of disturbance enhancement in multichannel active noise control systems," *Noise Control Engineering Journal*, vol. 69, no. 5, pp. 451–459, 2021.

[57] Y. Zhuang, Y. Liu, and X. Wang, "Singular vector filtering method for disturbance enhancement mitigation in active noise control systems," in *INTER-NOISE and NOISE-CON Congress and Conference Proceedings*, Institute of Noise Control Engineering, vol. 262, 2020, pp. 333–341.

[58] Y. Zhuang and Y. Liu, "A numerically stable constrained optimal filter design method for multichannel active noise control using dual conic formulation," *The Journal of the Acoustical Society of America*, vol. 152, no. 4, pp. 2169–2182, 2022.

[59] Y. Zhuang and Y. Liu, "Study on the cone programming reformulation of active noise control filter design in the frequency domain," in *INTER-NOISE and NOISE-CON Congress and Conference Proceedings*, Institute of Noise Control Engineering, vol. 260, 2019, pp. 126–136.

[60] Y. Zhuang and Y. Liu, "Development and application of dual form conic formulation of multichannel active noise control filter design problem in frequency domain," in *INTER-NOISE and NOISE-CON Congress and Conference Proceedings*, Institute of Noise Control Engineering, vol. 261, 2020, pp. 676–687.

[61] M. Bai and S. Elliott, "Preconditioning multichannel adaptive filtering algorithms using evd-and svd-based signal prewhitening and system decoupling," *Journal of sound and vibration*, vol. 270, no. 4-5, pp. 639–655, 2004.

[62] Y. Wang, Y. Zhuang, and Y. Liu, "Design of causal preconditioning filters for adaptive filtering algorithms in real-time multi-channel active noise control applications," in *INTER-NOISE and NOISE-CON Congress and Conference Proceedings*, Institute of Noise Control Engineering, vol. 265, 2023, pp. 2038–2045.

[63] B. Widrow and S. D. Stearns, "Adaptive signal processing, englewood cliffs, nj, 545 prentice-hall," *Inc*, vol. 491, p. 1, 1985.

[64] D. R. Morgan and J. C. Thi, "A delayless subband adaptive filter architecture," *IEEE transactions on signal processing*, vol. 43, no. 8, pp. 1819–1830, 1995.

[65] S. Elliott, "Signal processing for active control," in (Signal Processing and its Applications), Signal Processing and its Applications. London: Academic Press, 2001, ch. 5, pp. 233–270, ISBN: 978-0-12-237085-4. DOI: https://doi.org/10.1016/B978-012237085-4/50007-7. [Online]. Available: http://www.sciencedirect.com/science/article/pii/B9780122370854500077.

[66] P. Loiseau, P. Chevrel, M. Yagoubi, and J.-M. Duffal, "Investigating achievable performances for robust broadband active noise control in an enclosure," *IEEE Transactions on Control Systems Technology*, vol. 27, no. 1, pp. 426–433, 2017.

[67] M. Paweczyk, "Feedback control of acoustic noise at desired locations," *Zeszyty Naukowe. Automatyka/Politechnika lkaska*, pp. 1–182, 2005.

[68] M. Paweczyk, "Active noise control-a review of control-related problems," *Archives of Acoustics*, vol. 33, no. 4, pp. 509–520, 2008.

[69] L. Paul, C. Philippe, Y. Mohamed, and D. Jean-Marc, "Broadband active noise control design through nonsmooth H_∞ synthesis," *IFAC-PapersOnLine*, vol. 48, no. 14, pp. 396–401, 2015.

[70] P. Titterton and J. A. Olkin, "A practical method for constrained-optimization controller design: H_2 Or H_∞ optimization with multiple H_2 and/or H_∞ constraints," in *Conference Record of The Twenty-Ninth Asilomar Conference on Signals, Systems and Computers*, IEEE, vol. 2, 1995, pp. 1265–1269.

[71] P. A. Lopes and J. A. B. Gerald, "Low delay short word length sigma delta active noise control," *IEEE Transactions on Circuits and Systems I: Regular Papers*, vol. 68, no. 9, pp. 3746–3757, 2021.

[72] P. A. Lopes, "Low-delay and low-cost sigma-delta adaptive controller for active noise control," *Circuits, Systems, and Signal Processing*, pp. 1–12, 2022.

[73] N. Krishnamurthy, M. Mansour, and R. Cole, "Implementation challenges for feedback active noise cancellation," in *2012 IEEE International Conference on Acoustics, Speech and Signal Processing (ICASSP)*, IEEE, 2012, pp. 1649–1652.

[74] B. Lam, W.-S. Gan, D. Shi, M. Nishimura, and S. Elliott, "Ten questions concerning active noise control in the built environment," *Building and Environment*, vol. 200, p. 107 928, 2021.

[75] P. Nelson and S. Elliott, "Active control of sound," in ACADEMIC PRESS INC., 1994, ch. 6.13, pp. 194–195.

[76] S. J. Park, J. H. Yun, Y. C. Park, and D. H. Youn, "A delayless subband active noise control system for wideband noise control," *IEEE transactions on speech and audio processing*, vol. 9, no. 8, pp. 892–899, 2001.

[77] G. Long, Y. Wang, and T. C. Lim, "Optimal parametric design of delayless subband active noise control system based on genetic algorithm optimization," *Journal of Vibration and Control*, p. 10 775 463 211 001 625, 2021.

[78] J. Cheer and S. Daley, "An investigation of delayless subband adaptive filtering for multi-input multi-output active noise control applications," *IEEE/ACM Transactions on Audio, Speech, and Language Processing*, vol. 25, no. 2, pp. 359–373, 2016.

[79] N. K. Rout, D. P. Das, and G. Panda, "Computationally efficient algorithm for high sampling-frequency operation of active noise control," *Mechanical Systems and Signal Processing*, vol. 56, pp. 302–319, 2015.

[80] T. W. Parks and C. S. Burrus, *Digital filter design*. Wiley-Interscience, 1987.

[81] K. Steiglitz and L. McBride, "A technique for the identification of linear systems," *IEEE Transactions on Automatic Control*, vol. 10, no. 4, pp. 461–464, 1965.

[82] L. Ljung, "System identification-theory for the user 2nd edition ptr prentice-hall," *Upper Saddle River, NJ*, 1999.

[83] E. Levy, "Complex-curve fitting," *IRE transactions on automatic control*, no. 1, pp. 37–43, 1959.

[84] J. E. Dennis Jr, *Rb schnabel numerical methods for unconstrained optimization and nonlinear equations*, 1983.

[85] D. Calvetti and L. Reichel, "On the evaluation of polynomial coefficients," *Numerical Algorithms*, vol. 33, pp. 153–161, 2003.

[86] G. A. Sitton, C. S. Burrus, J. W. Fox, and S. Treitel, "Factoring very-high-degree polynomials," *IEEE Signal Processing Magazine*, vol. 20, no. 6, pp. 27–42, 2003.

[87] Y. Zhuang, G. Song, and Y. Liu, "A sub-band filter design approach for sound field reproduction," *The Journal of the Acoustical Society of America*, vol. 148, no. 4 Supplement, pp. 2793–2793, Oct. 2020.

[88] Y. Zhuang and Y. Liu, "Delayless polyphase implementation of filters in active noise control systems," *The Journal of the Acoustical Society of America*, vol. 150, no. 4 Supplement, A154–A154, Oct. 2021.

[89] Y. Zhuang, Z. Mo, and Y. Liu, "Warmstarting the constrained optimal filter design problem for active noise control systems in conic formulation," in *INTER-NOISE and NOISE-CON Congress and Conference Proceedings*, Institute of Noise Control Engineering, vol. 264, 2022, pp. 259–269.

[90] Y. Zhuang and Y. Liu, "A constrained adaptive active noise control filter design method via online convex optimization," *The Journal of the Acoustical Society of America*, vol. 152, no. 4 Supplement, A98–A98, Oct. 2022.

[91] X. Qiu and C. H. Hansen, "A study of time-domain fxlms algorithms with control output constraint," *The Journal of the Acoustical Society of America*, vol. 109, no. 6, pp. 2815–2823, 2001.

[92] S. Elliott, "Signal processing for active control," in (Signal Processing and its Applications), Signal Processing and its Applications. London: Academic Press, 2001, ch. 3, pp. 103–175, ISBN: 978-0-12-237085-4. DOI: https://doi.org/10.1016/B978-012237085-4/50005-3. [Online]. Available: https://www.sciencedirect.com/science/article/pii/B9780122370854500053.

[93] J. G. Proakis and D. G. Manolakis, "Digital signal processing - principles, algorithms, and applications," in 4th ed. Pearson Prentice Hall, 2007, ch. 11, pp. 750–813.

[94] H. Brandenstein and R. Unbehauen, "Least-squares approximation of fir by iir digital filters," *IEEE Transactions on Signal Processing*, vol. 46, no. 1, pp. 21–30, 1998.

[95] H. Brandenstein and R. Unbehauen, "Weighted least-squares approximation of fir by iir digital filters," *IEEE Transactions on Signal Processing*, vol. 49, no. 3, pp. 558–568, 2001.

[96] S. Boyd and L. Vandenberghe, *Convex optimization*. Cambridge university press, 2004.

[97] A. Ben-Tal and A. Nemirovski, "Lectures on modern convex optimization," in (MOS-SIAM Series on Optimization), MOS-SIAM Series on Optimization. 2001, ch. 2, pp. 43–77. DOI: 10.1137/1.9780898718829.ch2. eprint: epubs.siam.org/doi/pdf/10.1137/1.9780898718829.ch2. [Online]. Available: epubs.siam.org/doi/abs/10.1137/1.9780898718829.ch2.

[98] R. Tütüncü, K. Toh, and M. Todd, "Sdpt3a matlab software package for semidefinite-quadratic-linear programming, version 3.0," *Web page http://www. math. nus. edu. sg/mattohkc/sdpt3. html*, 2001.

[99] J. F. Sturm, "Implementation of interior point methods for mixed semidefinite and second order cone optimization problems," *Optimization Methods and Software*, vol. 17, no. 6, pp. 1105–1154,

[100] Y. Xia, "An algorithm for perturbed second-order cone programs," Citeseer, Tech. Rep., 2004.

[101] J. Gondzio and A. Grothey, "A new unblocking technique to warmstart interior point methods based on sensitivity analysis," *SIAM Journal on Optimization*, vol. 19, no. 3, pp. 1184–1210, 2008.

[102] A. Skajaa, "The homogeneous interior-point algorithm: Nonsymmetric cones, warmstarting, and applications," 2013.

[103] A. Skajaa, E. D. Andersen, and Y. Ye, "Warmstarting the homogeneous and self-dual interior point method for linear and conic quadratic problems," *Mathematical Programming Computation*, vol. 5, no. 1, pp. 1–25, 2013.

[104] K.-C. Toh, M. J. Todd, and R. H. Tütüncü, "On the implementation and usage of sdpt3–a matlab software package for semidefinite-quadratic-linear programming, version 4.0," in *Handbook on semidefinite, conic and polynomial optimization*, Springer, 2012, pp. 715–754.

[105] K. B. Petersen and M. S. Pedersen, "The matrix cookbook," in Technical Univ. Denmark, Kongens Lyngby, Denmark, Tech. Rep, Vol. 3274, 2012, ch. 10.2, pp. 59–60. [Online]. Available: https://www.math.uwaterloo.ca/~hwolkowi/matrixcookbook.pdf.

[106] M. Grant and S. Boyd, *CVX: Matlab software for disciplined convex programming, version 2.1*, Mar. 2014. [Online]. Available: http://cvxr.com/cvx.

[107] M. Grant and S. Boyd, "Graph implementations for nonsmooth convex programs," in *Recent Advances in Learning and Control*, ser. Lecture Notes in Control and Information Sciences, V. Blondel, S. Boyd, and H. Kimura, Eds., Springer-Verlag Limited, 2008, pp. 95–110. [Online]. Available: http://stanford.edu/~boyd/graph%5C_dcp.html.

[108] K.-C. Toh, M. J. Todd, and R. H. Tütüncü, "SDPT3 a matlab software package for semidefinite programming, version 1.3," *Optimization methods and software*, vol. 11, no. 1-4, pp. 545–581, 1999.

[109] R. H. Tütüncü, K.-C. Toh, and M. J. Todd, "Solving semidefinite-quadratic-linear programs using sdpt3," *Mathematical programming*, vol. 95, no. 2, pp. 189–217, 2003.

[110] J. F. Sturm, "Using sedumi 1.02, a matlab toolbox for optimization over symmetric cones," *Optimization methods and software*, vol. 11, no. 1-4, pp. 625–653, 1999.

[111] M. ApS, *The mosek optimization toolbox for matlab manual. version 9.0.* 2019. [Online]. Available: docs.mosek.com/9.0/toolbox/index.html.

[112] A. Ben-Tal and A. Nemirovski, "Lectures on modern convex optimization," in (MOS-SIAM Series on Optimization), MOS-SIAM Series on Optimization. 2001, ch. 6, pp. 377–442. DOI: 10.1137/1.9780898718829.ch6. eprint: epubs.siam.org/doi/pdf/10.1137/1.9780898718829.ch6. [Online]. Available: epubs.siam.org/doi/abs/10.1137/1.9780898718829.ch6.

[113] M. Grant, S. Boyd, and Y. Ye, "Disciplined convex programming," in *Global Optimization: From Theory to Implementation*, L. Liberti and N. Maculan, Eds. Boston, MA: Springer US, 2006, pp. 155–210, ISBN: 978-0-387-30528-8. DOI: 10.1007/0-387-30528-9_7. [Online]. Available: https://doi.org/10.1007/0-387-30528-9_7.

[114] X. Wang, Y. Liu, and J. S. Bolton, "Truncated singular value decomposition method for mitigating unwanted enhancement in active noise control systems," in *INTER-NOISE and NOISE-CON Congress and Conference Proceedings*, Institute of Noise Control Engineering, vol. 258, 2018, pp. 1831–1841.

[115] A. Maamar, I. Kale, A. Krukowski, and B. Daoud, "Partial equalization of non-minimum-phase impulse responses," *EURASIP Journal on Advances in Signal Processing*, vol. 2006, pp. 1–8, 2006.

[116] J. Durbin, "The fitting of time-series models," *Revue de l'Institut International de Statistique*, pp. 233–244, 1960.

[117] J. Mourjopoulos and M. Paraskevas, "Pole and zero modeling of room transfer functions," *Journal of Sound and Vibration*, vol. 146, no. 2, pp. 281–302, 1991.

[118] A. Carini, S. Cecchi, F. Piazza, I. Omiciuolo, and G. L. Sicuranza, "Multiple position room response equalization in frequency domain," *IEEE transactions on audio, speech, and language processing*, vol. 20, no. 1, pp. 122–135, 2011.

[119] F. E. Toole and S. E. Olive, "The modification of timbre by resonances: Perception and measurement," *Journal of the Audio Engineering Society*, vol. 36, no. 3, pp. 122–142, 1988.

[120] G. Song, P. Davies, and Y. Liu, "Development of metric models to predict annoyance due to tonal office noise," *Science and Technology for the Built Environment*, vol. 28, no. 8, pp. 1054–1068, 2022.

[121] G. Song, *Annoyance thresholds of tones in noise as related to building services equipment*, Dec. 2020. DOI: 10.25394/PGS.13360649.v1.

[122] N. Broner, *Determination of the Relationship Between Low-frequency HVAC Noise and Comfort in Occupied Spaces: Psycho-acoustic Phase*. Vipac Engineers & Scientists Limited, 2004.

[123] J. Lee, J. M. Francis, and L. M. Wang, "How tonality and loudness of noise relate to annoyance and task performance," *Noise Control Engineering Journal*, vol. 65, no. 2, pp. 71–82, 2017.

[124] E. Bowden and L. Wang, "Relating human productivity and annoyance to indoor noise criteria systems: A low frequency analysis," *ASHRAE Transactions*, vol. 111, no. 1, pp. 684–692, 2005.

[125] T. Paatero and M. Karjalainen, "Kautz filters and generalized frequency resolution: Theory and audio applications," *Journal of the Audio Engineering Society*, vol. 51, no. 1/2, pp. 27–44, 2003.

[126] M. Karjalainen and T. Paatero, "Equalization of loudspeaker and room responses using kautz filters: Direct least squares design," *EURASIP Journal on Advances in Signal Processing*, vol. 2007, pp. 1–13, 2006.

[127] B. D. Kulp, "Digital equalization using fourier transform techniques," in *Audio Engineering Society Convention 85*, Audio Engineering Society, 1988.

[128] O. Kirkeby and P. A. Nelson, "Digital filter design for inversion problems in sound reproduction," *Journal of the Audio Engineering Society*, vol. 47, no. 7/8, pp. 583–595, 1999.

[129] O. Kirkeby, P. A. Nelson, H. Hamada, and F. Orduna-Bustamante, "Fast deconvolution of multichannel systems using regularization," *IEEE Transactions on speech and audio processing*, vol. 6, no. 2, pp. 189–194, 1998.

[130] O. Kirkeby, P. Rubak, and A. Farina, "Analysis of ill-conditioning of multi-channel deconvolution problems," in *Proceedings of the 1999 IEEE Workshop on Applications of Signal Processing to Audio and Acoustics. WASPAA'99 (Cat. No. 99TH8452)*, IEEE, 1999, pp. 155–158.

[131] P. A. Nelson, F. Orduna-Bustamante, and H. Hamada, "Multi-channel signal processing techniques in the reproduction of sound," in *Audio Engineering Society Conference: UK 7th Conference: Digital Signal Processing (DSP)*, Audio Engineering Society, 1992.

[132] O. Kirkeby, P. A. Nelson, F. Orduna-Bustamante, and H. Hamada, "Local sound field reproduction using digital signal processing," *The Journal of the Acoustical Society of America*, vol. 100, no. 3, pp. 1584–1593, 1996.

[133] P. M. Clarkson, J. Mourjopoulos, and J. Hammond, "Spectral, phase, and transient equalization for audio systems," *Journal of the Audio Engineering Society*, vol. 33, no. 3, pp. 127–132, 1985.

[134] T. Mei, A. Mertins, and M. Kallinger, "Room impulse response reshaping/shortening based on least mean squares optimizationwith infinity norm constraint," in *2009 16th International Conference on Digital Signal Processing*, IEEE, 2009, pp. 1–6.

[135] M. Kolundija, C. Faller, and M. Vetterli, "Multi-channel low-frequency room equalization using perceptually motivated constrained optimization," in *2012 IEEE International Conference on Acoustics, Speech and Signal Processing (ICASSP)*, Ieee, 2012, pp. 533–536.

[136] L. E. Kinsler, A. R. Frey, A. B. Coppens, and J. V. Sanders, "Fundamentals of acoustics," in 4th ed. John Wiley & Sons, 1999, ch. 12, pp. 333–358.

[137] P. D. Hatziantoniou and J. N. Mourjopoulos, "Generalized fractional-octave smoothing of audio and acoustic responses," *Journal of the Audio Engineering Society*, vol. 48, no. 4, pp. 259–280, 2000.

[138] R. Gupta, R. Ranjan, J. He, and G. Woon-Seng, "On the use of closed-back headphones for active hear-through equalization in augmented reality applications," in *Audio Engineering Society Conference: 2018 AES International Conference on Audio for Virtual and Augmented Reality*, Audio Engineering Society, 2018.

[139] R. Gupta, R. Ranjan, J. He, and W. S. Gan, "Parametric hear through equalization for augmented reality audio," in *ICASSP 2019-2019 IEEE International Conference on Acoustics, Speech and Signal Processing (ICASSP)*, IEEE, 2019, pp. 1587–1591.

[140] J. Rämö and V. Välimäki, "Digital augmented reality audio headset," *Journal of Electrical and Computer Engineering*, vol. 2012, 2012.

[141] J. Rämö and V. Välimäki, "An allpass hear-through headset," in *2014 22nd European Signal Processing Conference (EUSIPCO)*, IEEE, 2014, pp. 1123–1127.

[142] J. Liski, "Adaptive hear-through headset," M.S. thesis, School of Electrical Engineering, Aalto University, 2016.

[143] V. Patel, J. Cheer, and S. Fontana, "Design and implementation of an active noise control headphone with directional hear-through capability," *IEEE Transactions on Consumer Electronics*, vol. 66, no. 1, pp. 32–40, 2019.

[144] J. Kim, Y. Zhuang, and Y. Liu, "A constrained multi-channel hear-through filter design approach using active control formulations," in *INTER-NOISE and NOISE-CON Congress and Conference Proceedings*, Institute of Noise Control Engineering, vol. 266, 2023, pp. 497–509.

[145] L. R. Rabiner and B. Gold, "Theory and application of digital signal processing," *Englewood Cliffs: Prentice-Hall*, 1975.

[146] E. Deadman, N. J. Higham, and R. Ralha, "Blocked schur algorithms for computing the matrix square root," in *International Workshop on Applied Parallel Computing*, Springer, 2012, pp. 171–182.

[147] A. Ben-Tal and A. Nemirovski, "Lectures on modern convex optimization," in (MOS-SIAM Series on Optimization), MOS-SIAM Series on Optimization. 2001, ch. 3, pp. 79–138. DOI: 10.1137/1.9780898718829.ch3. eprint: epubs.siam.org/doi/pdf/10.1137/1.9780898718829.ch3. [Online]. Available: epubs.siam.org/doi/abs/10.1137/1.9780898718829.ch3.

A. DETAILED DERIVATION IN CONVEX AND CONE PROGRAMMING REFORMULATION

The detailed derivations for the proposed conic formulation are presented in this appendix.

A.1 Reformulation of the Objective Function to a Standard Convex Quadratic Function

For brevity, f_k is ignored when simplifying Eq. (2.12). Firstly, the trace of $\mathbf{G}_{\mathrm{e}}\mathbf{W}_x\mathbf{S}_{xx}\mathbf{W}_x^{\mathrm{H}}\mathbf{G}_{\mathrm{e}}^{\mathrm{H}}$ can be expressed as a Frobenius inner product by using the vectorization operator, vec(), which converts a matrix to a vector by stacking the columns [105]:

$$\mathrm{tr}[\mathbf{G}_{\mathrm{e}}\mathbf{W}_x\mathbf{S}_{xx}\mathbf{W}_x^{\mathrm{H}}\mathbf{G}_{\mathrm{e}}^{\mathrm{H}}] = \mathrm{vec}(\mathbf{W}_x^{\mathrm{H}}\mathbf{G}_{\mathrm{e}}^{\mathrm{H}})^{\mathrm{H}}\mathrm{vec}(\mathbf{S}_{xx}\mathbf{W}_x^{\mathrm{H}}\mathbf{G}_{\mathrm{e}}^{\mathrm{H}}). \tag{A.1}$$

Then, use relation: $\mathrm{vec}(\mathbf{AB}) = (\mathbf{I}\otimes\mathbf{A})\mathrm{vec}(\mathbf{B}) = (\mathbf{B}^{\mathrm{T}}\otimes\mathbf{I})\mathrm{vec}(\mathbf{A})$, where $\otimes$ denotes the Kronecker product, Eq. (A.1) can be reformulated as:

$$\mathrm{vec}(\mathbf{W}_x^{\mathrm{T}})^{\mathrm{T}}(\mathbf{G}_{\mathrm{e}}^{\mathrm{T}}\otimes\mathbf{I}_{N_r})(\mathbf{I}_{N_{\mathrm{e}}}\otimes\mathbf{S}_{xx})(\mathbf{G}_{\mathrm{e}}^{*}\otimes\mathbf{I}_{N_r})\mathrm{vec}(\mathbf{W}_x^{\mathrm{H}}). \tag{A.2}$$

Note that Eq. (A.2) can be simplified using the mixed-product property of Kronecker product: $(\mathbf{A}\otimes\mathbf{B})(\mathbf{C}\otimes\mathbf{D}) = (\mathbf{AC})\otimes(\mathbf{BD})$:

$$\mathrm{vec}(\mathbf{W}_x^{\mathrm{T}})^{\mathrm{T}}((\mathbf{G}_{\mathrm{e}}^{\mathrm{H}}\mathbf{G}_{\mathrm{e}})^{\mathrm{T}}\otimes\mathbf{S}_{xx})\mathrm{vec}(\mathbf{W}_x^{\mathrm{H}})\ . \tag{A.3}$$

Since Eq. (A.3) is a scalar, taking a transpose of Eq. (A.3) will result in the same value. Thus, Eq. (A.3) equals to:

$$\mathrm{vec}(\mathbf{W}_x^{\mathrm{T}})^{\mathrm{H}}(\mathbf{G}_{\mathrm{e}}^{\mathrm{H}}\mathbf{G}_{\mathrm{e}}\otimes\mathbf{S}_{xx}^{\mathrm{T}})\mathrm{vec}(\mathbf{W}_x^{\mathrm{T}}). \tag{A.4}$$

If coefficients of control filters are rearranged as the order in $\mathbf{w}$ in Eq. (3.9), then we have:

$$\mathrm{vec}(\mathbf{W}_x^{\mathrm{T}}) = (\mathbf{I}_{N_s}\otimes\mathbf{I}_{N_r}\otimes\mathbf{F}_z^{\mathrm{T}})\mathbf{w}. \tag{A.5}$$

By using Eq. (A.5) and those Kronecker product properties mentioned above, the Eq. (A.4) can be finally simplified as:

$$\mathbf{w}^{\mathrm{T}}\left(\mathbf{G}_{\mathrm{e}}^{\mathrm{H}}\mathbf{G}_{\mathrm{e}}\right)\otimes\mathbf{S}_{xx}^{\mathrm{T}}\otimes\left(\mathbf{F}_{z}^{*}\mathbf{F}_{z}^{\mathrm{T}}\right)\mathbf{w}. \tag{A.6}$$

Since $\mathbf{w}$ is a real-valued vector, Eq. (A.6) can be further simplified as:

$$\mathbf{w}^{\mathrm{T}}\,\mathrm{Re}\Big\{\left(\mathbf{G}_{\mathrm{e}}^{\mathrm{H}}\mathbf{G}_{\mathrm{e}}\right)\otimes\mathbf{S}_{xx}^{\mathrm{T}}\otimes\left(\mathbf{F}_{z}^{*}\mathbf{F}_{z}^{\mathrm{T}}\right)\Big\}\mathbf{w}. \tag{A.7}$$

In a similar way of rearranging Eq. (A.1) to (A.6), we have

$$\mathrm{tr}[\mathbf{G}_{\mathrm{e}}\mathbf{W}_{x}\mathbf{S}_{xd}]=\mathrm{vec}\Big[\left(\mathbf{S}_{xd}\mathbf{G}_{\mathrm{e}}\right)\otimes\mathbf{F}_{z}\Big]^{\mathrm{T}}\mathbf{w}. \tag{A.8}$$

Considering that Eq. (A.8) is a scalar, we have:

$$\mathrm{tr}[\mathbf{G}_{\mathrm{e}}\mathbf{W}_{x}\mathbf{S}_{xd}+\mathbf{S}_{xd}^{\mathrm{H}}\mathbf{W}_{x}^{\mathrm{H}}\mathbf{G}_{\mathrm{e}}^{\mathrm{H}}]=2\,\mathrm{Re}\Big\{\mathrm{vec}\Big[\left(\mathbf{S}_{xd}\mathbf{G}_{\mathrm{e}}\right)\otimes\mathbf{F}_{z}\Big]\Big\}^{\mathrm{T}}\mathbf{w}. \tag{A.9}$$

Then, Eq. (2.12) is simplified to a standard quadratic form in Eq. (3.9).

A.2 Second Order Cone Reformulation

In this appendix, the expressions related to the SOC reformulation, i.e., the $\mathbf{A}_0$, $\mathbf{A}_{1,k}$, $\mathbf{A}_{2,l,k}$, $\mathbf{B}_0$, $\mathbf{B}_{1,k}$, $\mathbf{B}_{2,l,k}$, $\mathbf{b}_0$, $\mathbf{b}_{1,k}$, and $\mathbf{b}_{2,l,k}$ in Eq. (3.15), are derived. For convenience, $v\in K_n^q$ and $v\in K_n^s$ are used to represent all conic relations without assigning a different notation for each conic constraint.

For objective function, a new variable t_0 and a new constraint can be introduced. Minimizing Eq. (3.10) is equivalent to

$$\begin{aligned}\underset{\mathbf{w},t_0}{\text{minimize}}\quad & t_0+\sum_{k=1}^{N_f}\mathbf{b}_J^{\mathrm{T}}(f_k)\,\mathbf{w},\\ \text{subject to}\quad & \|\mathbf{M}_0\mathbf{w}\|_2\le\sqrt{t_0},\end{aligned} \tag{A.10}$$

where the matrix $\mathbf{M}_0$ is a matrix such that $\mathbf{M}_0^{\mathrm{T}}\mathbf{M}_0 = \sum_{k=1}^{N_f} \mathbf{A}_J(f_k)$, which, depending on the rank of the matrix, can be obtained by either a square root of the matrix [146], Cholesky factorization, or full rank factorization using singular value decomposition. Note that, the two sets:

$$\begin{aligned} K &= \{(\mathbf{x}, y_1, y_2) \in \mathbf{R}^n \times \mathbf{R} \times \mathbf{R} \mid y_1, y_2 \geq 0, \sqrt{y_1 y_2} \geq \|\mathbf{x}\|_2\} \\ K &= \{(\mathbf{x}, y_1, y_2) \in \mathbf{R}^n \times \mathbf{R} \times \mathbf{R} \mid \left\| \begin{bmatrix} 2\mathbf{x} \\ y_1 - y_2 \end{bmatrix} \right\|_2 \leq y_1 + y_2\} \end{aligned} \tag{A.11}$$

are equivalent [147]. Thus, Eq. (A.10) can be reformulated equivalently as:

$$\begin{aligned} \underset{\mathbf{w}, t_0}{\text{minimize}} \quad & t_0 + \sum_{k=1}^{N_f} \mathbf{b}_J^{\mathrm{T}}(f_k)\ \mathbf{w} \\ \text{subject to} \quad & \left\| \begin{bmatrix} 2\mathbf{M}_0\mathbf{w} \\ t_0 - 2 \end{bmatrix} \right\|_2 \leq t_0. \end{aligned} \tag{A.12}$$

By introducing a new set of variables $\mathbf{x}_0 \in \mathbf{R}^{N_r N_s N_t + 2}$ and eliminating t_0, Eq. (A.12) can be rearranged as:

$$\begin{aligned} \underset{\mathbf{w}, \mathbf{x}_0}{\text{minimize}} \quad & (\mathbf{c}_w)^{\mathrm{T}}\mathbf{w} + (\mathbf{c}_0)^{\mathrm{T}}\mathbf{x}_0 \\ \text{subject to} \quad & \begin{bmatrix} \mathbf{A}_0 & \mathbf{B}_0 \end{bmatrix} \begin{bmatrix} \mathbf{w} \\ \mathbf{x}_0 \end{bmatrix} = \mathbf{b}_0, \\ & \mathbf{x}_0 \in K_n^q, \end{aligned} \tag{A.13}$$

where $\mathbf{w}$ and $\mathbf{x}_0$ are variables, and the constants $\mathbf{c}_w \in \mathbf{R}^{N_r N_s N_t}$, $\mathbf{c}_0 \in \mathbf{R}^{N_r N_s N_t + 2}$, $\mathbf{b}_0 \in \mathbf{R}^{N_r N_s N_t + 1}$, $\mathbf{A}_0 \in \mathbf{R}^{(N_r N_s N_t + 1) \times (N_r N_s N_t)}$, and $\mathbf{B}_0 \in \mathbf{R}^{(N_r N_s N_t + 1) \times (N_r N_s N_t + 2)}$ are:

$$\begin{aligned} \mathbf{c}_w &= \sum_{k=1}^{N_f} \mathbf{b}_J(f_k), \quad \mathbf{c}_0 = \begin{bmatrix} 1 \\ \mathbf{0} \end{bmatrix}, \quad \mathbf{b}_0 = \begin{bmatrix} \mathbf{0} \\ 2 \end{bmatrix}, \\ \mathbf{A}_0 &= \begin{bmatrix} 2\mathbf{M}_0 \\ \mathbf{0} \end{bmatrix}, \quad \mathbf{B}_0 = \begin{bmatrix} \mathbf{0} & \mathbf{0} & -\mathbf{I}_{N_s N_r N_t} \\ 1 & -1 & \mathbf{0} \end{bmatrix}, \end{aligned}$$

and $\mathbf{0}$ represents a zero matrix with an appropriate dimension.

For the noise amplification (disturbance enhancement) constraint, Eq. (3.11), it is also in a quadratic form, which can be reformulated equivalently in a similar way as:

$$\begin{aligned} & t_{1,k} + \mathbf{b}_J^{\mathrm{T}}(f_k)\ \mathbf{w} + \tilde{c}_J(f_k) = 0. \\ & \|\mathbf{M}_{1,k}\ \mathbf{w}\|_2 \leq \sqrt{t_{1,k}}, \end{aligned} \tag{A.14}$$

where,

$$\mathbf{M}_{1,k} = \left(\mathbf{G}_{\mathrm{e}}^{\mathrm{H}}(f_k)\mathbf{G}_{\mathrm{e}}(f_k)\right)^{\frac{1}{2}} \otimes \left(\mathbf{S}_{xx}^{\mathrm{T}}(f_k)\right)^{\frac{1}{2}} \otimes \mathbf{F}_z^{\mathrm{T}}(f_k),$$

$\left(\mathbf{G}_{\mathrm{e}}^{\mathrm{H}}(f_k)\mathbf{G}_{\mathrm{e}}(f_k)\right)^{\frac{1}{2}}$ and $\left(\mathbf{S}_{xx}^{\mathrm{T}}(f_k)\right)^{\frac{1}{2}}$ is the complex matrix square root of $\mathbf{G}_{\mathrm{e}}^{\mathrm{H}}(f_k)\mathbf{G}_{\mathrm{e}}(f_k)$ and $\mathbf{S}_{xx}^{\mathrm{T}}(f_k)$, which can be obtained by methods discussed in objective function reformulation above.

Equation. (A.14) can be rearranged from complex form to an equivalent real form, then reformulated in a similar way as in the objective function reformulation into:

$$\begin{aligned} & t_{1,k} - 1 + \mathbf{b}_J^{\mathrm{T}}(f_k)\ \mathbf{w} + \tilde{c}_J(f_k) = 0, \\ & \left\| \begin{bmatrix} 2\,\mathrm{Re}(\mathbf{M}_{1,k})\mathbf{w} \\ 2\,\mathrm{Im}(\mathbf{M}_{1,k})\mathbf{w} \\ t_{1,k} - 2 \end{bmatrix} \right\|_2 \leq t_{1,k}, \end{aligned} \tag{A.15}$$

where Im denotes the imaginary part of a complex value. By introducing a new set of variables $\mathbf{x}_{1,k} \in \mathbf{R}^{2N_rN_s+2}$ and eliminating $t_{1,k}$, Eq. (A.15) can be rearranged as:

$$\begin{aligned} & \begin{bmatrix} \mathbf{A}_{1,k} & \mathbf{B}_{1,k} \end{bmatrix} \begin{bmatrix} \mathbf{w} \\ \mathbf{x}_{1,k} \end{bmatrix} = \mathbf{b}_{1,k}, \\ & \mathbf{x}_{1,k} \in K_n^q, \end{aligned} \tag{A.16}$$

for all frequencies f_k, where $\mathbf{w}$ and $\mathbf{x}_{1,k}$ are variables, and the constants $\mathbf{A}_{1,k} \in \mathbf{R}^{(2N_rN_s+2)\times(N_rN_sN_t)}$, $\mathbf{B}_{1,k} \in \mathbf{R}^{(2N_rN_s+2)\times(2N_rN_s+2)}$, and $\mathbf{b}_{1,k} \in \mathbf{R}^{2N_rN_s+2}$ are:

$$\mathbf{A}_{1,k} = \begin{bmatrix} 2\,\mathrm{Re}(\mathbf{M}_{1,k}) \\ 2\,\mathrm{Im}(\mathbf{M}_{1,k}) \\ \mathbf{b}_J^{\mathrm{T}}(f_k) \\ \mathbf{0} \end{bmatrix}, \quad \mathbf{B}_{1,k} = \begin{bmatrix} \mathbf{0} & \mathbf{0} & -\mathbf{I}_{2N_sN_r} \\ 1 & 0 & \mathbf{0} \\ 1 & -1 & \mathbf{0} \end{bmatrix}, \quad \mathbf{b}_{1,k} = \begin{bmatrix} \mathbf{0} \\ 1-\tilde{c}_J(f_k) \\ 2 \end{bmatrix}.$$

For the filter response magnitude constraint Eq. (3.12), it is already in a similar form as a SOC. Note that:

$$\begin{aligned} &\left\|\mathbf{F}_z^{\mathrm{T}}(f_k)\mathbf{w}_{i,j}\right\|_2 \\ =&\left\|\mathbf{e}_l^{\mathrm{T}}\left(\mathbf{I}_{N_r}\otimes\mathbf{I}_{N_s}\otimes\mathbf{F}_z^{\mathrm{T}}(f_k)\right)(\mathbf{P}_r\otimes\mathbf{I}_{N_t})\mathbf{w}\right\|_2 \\ =&\left\|\mathbf{e}_l^{\mathrm{T}}\left(\mathbf{P}_r\otimes\mathbf{F}_z^{\mathrm{T}}(f_k)\right)\mathbf{w}\right\|_2 \end{aligned} \tag{A.17}$$

where $\mathbf{e}_l \in \mathbf{R}^{N_rN_s}$ is a unit vector for selecting information from an individual channel, it has value 1 in the l-th element and 0 in other elements; and sparse matrix $\mathbf{P}_r$ is used to rearrange the sequence of elements in a vector. So the i-th row and j-th column of $\mathbf{P}_r \in \mathbf{R}^{(N_rN_s)\times(N_rN_s)}$ is 1 if $(i,\ j) \in \mathbb{S}_{P_r}$, where

$$\mathbb{S}_{P_r} = \{((r-1)N_s+s, (s-1)N_r+r) \mid 1\le r\le N_r, 1\le s\le N_s, r,s\in\mathbf{Z}\}.$$

Thus, Eq. (3.12) can be converted to an equivalent real-valued SOC formulation:

$$\left\|\begin{bmatrix} \mathbf{e}_l^{\mathrm{T}}\,\mathrm{Re}\left(\mathbf{P}_r\otimes\mathbf{F}_z(f_k)\right) \\ \mathbf{e}_l^{\mathrm{T}}\,\mathrm{Im}\left(\mathbf{P}_r\otimes\mathbf{F}_z(f_k)\right) \end{bmatrix}\mathbf{w}\right\|_2 \le C_{i,j}(f_k), \tag{A.18}$$

for all l and f_k, where $l=(j-1)N_s+i$. By introducing a new set of variables $\mathbf{x}_{2,l,k}\in\mathbf{R}^3$, Eq. (A.18) can be rearranged as:

$$\begin{aligned} &\begin{bmatrix} \mathbf{A}_{2,l,k} & \mathbf{B}_{2,l,k} \end{bmatrix}\begin{bmatrix} \mathbf{w} \\ \mathbf{x}_{2,l,k} \end{bmatrix} = \mathbf{b}_{2,l,k}, \\ &\mathbf{x}_{2,l,k}\in K_n^q, \end{aligned} \tag{A.19}$$

for all frequencies f_k and all l, where $\mathbf{w}$ and $\mathbf{x}_{2,l,k}$ are variables, and the constants, $\mathbf{A}_{2,l,k} \in \mathbf{R}^{3\times(N_r N_s N_t)}$, $\mathbf{B}_{2,l,k} \in \mathbf{R}^{3\times 3}$, and $\mathbf{b}_{2,l,k} \in \mathbf{R}^3$ are:

$$\mathbf{A}_{2,l,k} = \begin{bmatrix} \mathbf{e}_l^{\mathrm{T}} \operatorname{Re}\left(\mathbf{P}_r \otimes \mathbf{F}_z(f_k)\right) \\ \mathbf{e}_l^{\mathrm{T}} \operatorname{Im}\left(\mathbf{P}_r \otimes \mathbf{F}_z(f_k)\right) \\ \mathbf{0} \end{bmatrix}, \quad \mathbf{B}_{2,l,k} = \begin{bmatrix} 0 & -1 & 0 \\ 0 & 0 & -1 \\ 1 & 0 & 0 \end{bmatrix}, \quad \mathbf{b}_{2,l,k} = \begin{bmatrix} 0 \\ 0 \\ C_{\mathrm{i,j}}(f_k) \end{bmatrix}.$$

A.3 Positive Semidefinite Cone Reformulation

In this appendix, the expressions related to the positive semidefinite cone reformulation, i.e., the $\mathbf{A}_{3,k}$, $\mathbf{A}_{4,k}$, $\mathbf{B}_{3,k}$, $\mathbf{B}_{4,k}$, $\mathbf{b}_{3,k}$, and $\mathbf{b}_{4,k}$ in Eq. (3.15), are derived.

Since each element of $\mathbf{A}_s(f_k)$ and $\mathbf{A}_s(f_k)^{\mathrm{H}}$ is a linear function of variables $\mathbf{w}_F$, the stability constraint, Eq. (3.8), can be equivalently reformulated as positive semidefinite cone with respect to the introduced variables as:

$$-\mathbf{A}_s(f_k) - \mathbf{A}_s(f_k)^{\mathrm{H}} + 2(1-\epsilon_s)\mathbf{I}_{N_s} \succeq 0, \tag{A.20}$$

where $\succeq 0$ means the matrix is positive semidefinite, and $\mathbf{I}_{N_s}$ is an N_s by N_s identity matrix.

For the robustness constraint, Eq. (3.13), Schur complement lemma is needed (because the elements of $\mathbf{A}_s(f_k)^{\mathrm{H}}\mathbf{A}_s(f_k)$ are not linear transforms of $\mathbf{w}$) to equivalently convert it to PSDCs [96]:

$$\begin{bmatrix} \frac{1}{B(f_k)}\mathbf{I}_{N_s} & -\mathbf{A}_s(f_k) \\ -\mathbf{A}_s(f_k)^{\mathrm{H}} & \frac{1}{B(f_k)}\mathbf{I}_{N_s} \end{bmatrix} \succeq 0. \tag{A.21}$$

Note that Eqs. (A.20) and (A.21) can be converted into equivalent real forms by using the property that a Hermitian matrix $A \succeq 0$ is equivalently to:

$$\begin{bmatrix} \operatorname{Re}(A) & -\operatorname{Im}(A) \\ \operatorname{Im}(A) & \operatorname{Re}(A) \end{bmatrix} \succeq 0, \tag{A.22}$$

To express matrices in vectors forms, first:

$$\begin{aligned}
&\operatorname{vec}(-\mathbf{A}_s(f_k)) \\
=&\operatorname{vec}\left(\mathbf{W}_x(f_k)\hat{\mathbf{G}}_s(f_k)\right) \\
=&\left(\left(\hat{\mathbf{G}}_s^{\mathrm{T}}(f_k)\otimes\mathbf{I}_{N_s}\right)\mathbf{P}_r\right)\otimes\mathbf{F}_z(f_k)\ \mathbf{w} \\
\triangleq&\left(\mathbf{Q}_k^r+\mathrm{i}\mathbf{Q}_k^{\mathrm{i}}\right)\mathbf{w},
\end{aligned} \tag{A.23}$$

where the last equality is a notation of real and imaginary part of the constant matrices for the use in latter formulations; and $\mathbf{P}_r$ is defined in Eq. (A.17). Similarly,

$$\begin{aligned}
\operatorname{vec}(-\mathbf{A}_s(f_k)^{\mathrm{H}}) &= \left(\mathbf{I}_{N_s}\otimes\hat{\mathbf{G}}_s^{\mathrm{H}}(f_k)\right)\otimes\mathbf{F}_z^*(f_k)\ \mathbf{w} \\
&\triangleq\left(\mathbf{R}_k^r+\mathrm{i}\mathbf{R}_k^{\mathrm{i}}\right)\mathbf{w}.
\end{aligned} \tag{A.24}$$

Thus, let $\mathbf{A}_{3,k}\in\mathbf{R}^{(4N_s^2)\times(N_rN_sN_t)}$ be:

$$\mathbf{A}_{3,k}=\begin{bmatrix}\bar{\mathbf{A}}_{3,k}\\ \mathbf{0}_{2N_s^2}\end{bmatrix},\qquad \bar{\mathbf{A}}_{3,k}=\begin{bmatrix}\mathbf{A}_{3,k,1}^r\\ \mathbf{A}_{3,k,1}^{\mathrm{i}}\\ \vdots\\ \mathbf{A}_{3,k,N_s}^r\\ \mathbf{A}_{3,k,N_s}^{\mathrm{i}}\end{bmatrix},$$

where

$$\begin{aligned}
\mathbf{A}_{3,k,s}^r&=\left[\mathbf{Q}_k^r((s-1)N_s+1:sN_s,:)+\mathbf{R}_k^r((s-1)N_s+1:sN_s,:)\right],\\
\mathbf{A}_{3,k,s}^{\mathrm{i}}&=\left[\mathbf{Q}_k^{\mathrm{i}}((s-1)N_s+1:sN_s,:)+\mathbf{R}_k^{\mathrm{i}}((s-1)N_s+1:sN_s,:)\right],
\end{aligned}$$

and $\mathbf{Q}_k^r(1:N_s,:)$ means the 1st to N_s-th rows of matrix $\mathbf{Q}_k^r$ with all columns (Similar for other notations and the dimension of zero matrices is labeled to prevent confusion); constant matrix $\mathbf{B}_{3,k}\in\mathbf{R}^{(4N_s^2)\times(4N_s^2)}$ is:

$$\mathbf{B}_{3,k}=\begin{bmatrix}-\mathbf{I}_{2N_s^2} & \mathbf{0}\\ \mathbf{I}_{N_s}\otimes\mathbf{P}_s\otimes\mathbf{I}_{N_s} & -\mathbf{I}_{2N_s^2}\end{bmatrix},\qquad \mathbf{P}_s=\begin{bmatrix}0 & -1\\ 1 & 0\end{bmatrix}, \tag{A.25}$$

where $\mathbf{P}_s$ comes from symmetric matrix structure. The i-th element of the sparse vector $\mathbf{b}_{3,k} \in \mathbf{R}^{4N_s^2}$ is $-2(1-\epsilon_s)$ if $i \in \mathbb{S}_{b_3}$, where $\mathbb{S}_{b_3} = \{2N_s(s-1)+s \mid 1 \le s \le N_s, s \in \mathbf{Z}\}$.

The constant matrix $\mathbf{A}_{4,k} \in \mathbf{R}^{(16N_s^2)\times(N_rN_sN_t)}$ is:

$$\mathbf{A}_{4,k} = \begin{bmatrix} \bar{\mathbf{A}}_{4,k} \\ \mathbf{0}_{8N_s^2,N_sN_rN_t} \end{bmatrix}, \bar{\mathbf{A}}_{4,k} = \begin{bmatrix} \mathbf{A}^r_{4,k,\mathbf{R},1} \\ \mathbf{A}^{\mathrm{i}}_{4,k,\mathbf{R},1} \\ \vdots \\ \mathbf{A}^r_{4,k,\mathbf{R},N_s} \\ \mathbf{A}^{\mathrm{i}}_{4,k,\mathbf{R},N_s} \\ \mathbf{A}^r_{4,k,\mathbf{Q},1} \\ \mathbf{A}^{\mathrm{i}}_{4,k,\mathbf{Q},1} \\ \vdots \\ \mathbf{A}^r_{4,k,\mathbf{Q},N_s} \\ \mathbf{A}^{\mathrm{i}}_{4,k,\mathbf{Q},N_s} \end{bmatrix},$$

where

$$\mathbf{A}^r_{4,k,\mathbf{R},s} = \begin{bmatrix} \mathbf{0}_{N_s,N_sN_rN_t} \\ \mathbf{R}^r_k((s-1)N_s+1:sN_s,:) \end{bmatrix}, \mathbf{A}^r_{4,k,\mathbf{Q},s} = \begin{bmatrix} \mathbf{Q}^r_k((s-1)N_s+1:sN_s,:) \\ \mathbf{0}_{N_s,N_sN_rN_t} \end{bmatrix},$$
$$\mathbf{A}^{\mathrm{i}}_{4,k,\mathbf{R},s} = \begin{bmatrix} \mathbf{0}_{N_s,N_sN_rN_t} \\ \mathbf{R}^{\mathrm{i}}_k((s-1)N_s+1:sN_s,:) \end{bmatrix}, \mathbf{A}^{\mathrm{i}}_{4,k,\mathbf{Q},s} = \begin{bmatrix} \mathbf{Q}^{\mathrm{i}}_k((s-1)N_s+1:sN_s,:) \\ \mathbf{0}_{N_s,N_sN_rN_t} \end{bmatrix},$$

constant matrix $\mathbf{B}_{4,k} \in \mathbf{R}^{(16N_s^2)\times(16N_s^2)}$ is:

$$\mathbf{B}_{4,k} = \begin{bmatrix} -\mathbf{I}_{8N_s^2} & \mathbf{0} \\ \mathbf{I}_{2N_s} \otimes \mathbf{P}_s \otimes \mathbf{I}_{2N_s} & -\mathbf{I}_{8N_s^2} \end{bmatrix},$$

and the i-th element of the sparse vector $\mathbf{b}_{4,k} \in \mathbf{R}^{16N_s^2}$ is $-1/B(f_k)$ if i or $(i-4N_s^2-N_s) \in \mathbb{S}_{b_4}$, where $\mathbb{S}_{b_4} = \{4N_s(s-1)+s \mid 1 \le s \le N_s, s \in \mathbf{Z}\}$.

Finally, with the new set of variables $\mathbf{x}_{3,k} \in \mathbf{R}^{4N_s^2}$, Eqs. (A.20) can be equivalently reformulated as:

$$\begin{aligned} &\begin{bmatrix} \mathbf{A}_{3,k} & \mathbf{B}_{3,k} \end{bmatrix} \begin{bmatrix} \mathbf{w} \\ \mathbf{x}_{3,k} \end{bmatrix} = \mathbf{b}_{3,k}, \\ &\mathbf{x}_{3,k} \in K_n^s, \end{aligned} \tag{A.26}$$

for all frequencies f_k. Similar relations can be obtained for Eq. (A.21) as:

$$\begin{aligned} &\begin{bmatrix} \mathbf{A}_{4,k} & \mathbf{B}_{4,k} \end{bmatrix} \begin{bmatrix} \mathbf{w} \\ \mathbf{x}_{4,k} \end{bmatrix} = \mathbf{b}_{4,k}, \\ &\mathbf{x}_{4,k} \in K_n^s, \end{aligned} \tag{A.27}$$

A.4 Analytical Expressions for Matrix Inversions in the Proposed Conic Formulation

In this appendix, the analytical expressions for $\tilde{\mathbf{B}}^{-1}\tilde{\mathbf{A}}$ and $\tilde{\mathbf{B}}^{-1}\tilde{\mathbf{b}}$ in Eq. (3.17) are given. Thus, no numerical inversion is required.

To inverse block diagonal matrix $\tilde{\mathbf{B}}$, only the inverse of each block of $\tilde{\mathbf{B}}$ is needed. The difference between $\tilde{\mathbf{B}}$ and $\mathbf{B}$ is the added row in Eq. (3.16). This added row should be considered in the first block of $\tilde{\mathbf{B}}$, i.e., above the $\mathbf{B}_0$ in Eq. (A.13):

$$\tilde{\mathbf{B}}_0 = \begin{bmatrix} 1 & \mathbf{0} \\ \mathbf{B}_0 \end{bmatrix} = \begin{bmatrix} 1 & 0 & \mathbf{0} \\ \mathbf{0} & \mathbf{0} & -\mathbf{I}_{N_s N_r N_t} \\ 1 & -1 & \mathbf{0} \end{bmatrix}, \tag{A.28}$$

It can be easily seen that the inverse of $\tilde{\mathbf{B}}_0$ is:

$$\tilde{\mathbf{B}}_0^{-1} = \begin{bmatrix} 1 & \mathbf{0} & \mathbf{0} \\ 1 & \mathbf{0} & -1 \\ \mathbf{0} & -\mathbf{I}_{N_s N_r N_t} & \mathbf{0} \end{bmatrix}. \tag{A.29}$$

Similarly, one can easily check that the inverse of each type of block in $\tilde{\mathbf{B}}$ is:

$$\begin{aligned}
\mathbf{B}_{1,k}^{-1} &= \begin{bmatrix} \mathbf{0} & 1 & 0 \\ \mathbf{0} & 1 & -1 \\ -\mathbf{I}_{2N_sN_r} & \mathbf{0} & \mathbf{0} \end{bmatrix}, \qquad \mathbf{B}_{2,l,k}^{-1} = \begin{bmatrix} 0 & 0 & 1 \\ -1 & 0 & 0 \\ 0 & -1 & 0 \end{bmatrix}, \\
\mathbf{B}_{3,k}^{-1} &= \begin{bmatrix} -\mathbf{I}_{2N_s^2} & \mathbf{0} \\ -\mathbf{I}_{N_s} \otimes \mathbf{P}_s \otimes \mathbf{I}_{N_s} & -\mathbf{I}_{2N_s^2} \end{bmatrix}, \\
\mathbf{B}_{4,k}^{-1} &= \begin{bmatrix} -\mathbf{I}_{8N_s^2} & \mathbf{0} \\ -\mathbf{I}_{2N_s} \otimes \mathbf{P}_s \otimes \mathbf{I}_{2N_s} & -\mathbf{I}_{8N_s^2} \end{bmatrix}.
\end{aligned} \tag{A.30}$$

Let $\tilde{\mathbf{A}}_0$ and $\tilde{\mathbf{b}}_0$ be:

$$\tilde{\mathbf{A}}_0 = \begin{bmatrix} \mathbf{0} & -1 \\ 2\mathbf{M}_0 & \mathbf{0} \\ \mathbf{0} & 0 \end{bmatrix}, \qquad \tilde{\mathbf{b}}_0 = \begin{bmatrix} \mathbf{0} \\ 2 \end{bmatrix}. \tag{A.31}$$

Then $\tilde{\mathbf{A}}$ can be seen as vertically concatenating $\tilde{\mathbf{A}}_0$, $\tilde{\mathbf{A}}_{1,k}$, $\tilde{\mathbf{A}}_{2,l,k}$, $\tilde{\mathbf{A}}_{3,k}$, and $\tilde{\mathbf{A}}_{4,k}$ for all k and l. It is noted that $\tilde{\mathbf{A}}_{1,k}$, $\tilde{\mathbf{A}}_{2,l,k}$, $\tilde{\mathbf{A}}_{3,k}$, and $\tilde{\mathbf{A}}_{4,k}$ have one more zero columns to the right compared with $\mathbf{A}_{1,k}$, $\mathbf{A}_{2,l,k}$, $\mathbf{A}_{3,k}$, and $\mathbf{A}_{4,k}$. $\tilde{\mathbf{B}}^{-1}$ can be seen as a sparse block diagonal matrix obtained by diagonally concatenating $\tilde{\mathbf{B}}_0^{-1}$, $\mathbf{B}_{1,k}^{-1}$, $\mathbf{B}_{2,l,k}^{-1}$, $\mathbf{B}_{3,k}^{-1}$, and $\mathbf{B}_{4,k}^{-1}$ for all k and l. Thus, $\tilde{\mathbf{B}}^{-1}\tilde{\mathbf{A}}$ can be seen as vertically concatenating $\tilde{\mathbf{B}}_0^{-1}\tilde{\mathbf{A}}_0$, $\mathbf{B}_{1,k}^{-1}\tilde{\mathbf{A}}_{1,k}$, $\mathbf{B}_{2,l,k}^{-1}\tilde{\mathbf{A}}_{2,l,k}$, $\mathbf{B}_{3,k}^{-1}\tilde{\mathbf{A}}_{3,k}$, and $\mathbf{B}_{4,k}^{-1}\tilde{\mathbf{A}}_{4,k}$ for all k and l. By using the expression of each block of $\tilde{\mathbf{A}}$ and $\tilde{\mathbf{B}}^{-1}$, they can be easily computed as:

$$\tilde{\mathbf{B}}_0^{-1}\tilde{\mathbf{A}}_0 = \begin{bmatrix} \mathbf{0} & -1 \\ \mathbf{0} & -1 \\ -2\mathbf{M}_0 & \mathbf{0} \end{bmatrix}, \qquad \mathbf{B}_{1,k}^{-1}\tilde{\mathbf{A}}_{1,k} = \begin{bmatrix} \mathbf{b}_J^{\mathrm{T}}(f_k) & 0 \\ \mathbf{b}_J^{\mathrm{T}}(f_k) & 0 \\ -2\,\mathrm{Re}(\mathbf{M}_{1,k}) & \mathbf{0} \\ -2\,\mathrm{Im}(\mathbf{M}_{1,k}) & \mathbf{0} \end{bmatrix},$$

$$\mathbf{B}_{2,l,k}^{-1}\mathbf{A}_{2,l,k} = \begin{bmatrix} \mathbf{0} & 0 \\ -\mathbf{e}_l^{\mathrm{T}}\,\mathrm{Re}\left(\mathbf{P}_r \otimes \mathbf{F}_z(f_k)\right) & 0 \\ -\mathbf{e}_l^{\mathrm{T}}\,\mathrm{Im}\left(\mathbf{P}_r \otimes \mathbf{F}_z(f_k)\right) & 0 \end{bmatrix},$$

$$\mathbf{B}_{3,k}^{-1}\tilde{\mathbf{A}}_{3,k} = \begin{bmatrix} -\bar{\mathbf{A}}_{3,k} & \mathbf{0} \\ \mathbf{A}_{3,k,1}^{\mathrm{i}} & \mathbf{0} \\ -\mathbf{A}_{3,k,1}^{r} & \mathbf{0} \\ \vdots & \vdots \\ \mathbf{A}_{3,k,N_s}^{\mathrm{i}} & \mathbf{0} \\ -\mathbf{A}_{3,k,N_s}^{r} & \mathbf{0} \end{bmatrix}, \qquad \mathbf{B}_{4,k}^{-1}\tilde{\mathbf{A}}_{4,k} = \begin{bmatrix} -\bar{\mathbf{A}}_{4,k} & \mathbf{0} \\ \mathbf{A}_{4,k,\mathbf{R},1}^{\mathrm{i}} & \mathbf{0} \\ -\mathbf{A}_{4,k,\mathbf{R},1}^{r} & \mathbf{0} \\ \vdots & \vdots \\ \mathbf{A}_{4,k,\mathbf{R},N_s}^{\mathrm{i}} & \mathbf{0} \\ -\mathbf{A}_{4,k,\mathbf{R},N_s}^{r} & \mathbf{0} \\ \mathbf{A}_{4,k,\mathbf{Q},1}^{\mathrm{i}} & \mathbf{0} \\ -\mathbf{A}_{4,k,\mathbf{Q},1}^{r} & \mathbf{0} \\ \vdots & \vdots \\ \mathbf{A}_{4,k,\mathbf{Q},N_s}^{\mathrm{i}} & \mathbf{0} \\ -\mathbf{A}_{4,k,\mathbf{Q},N_s}^{r} & \mathbf{0} \end{bmatrix}.$$

Similarly, $\tilde{\mathbf{B}}^{-1}\tilde{\mathbf{b}}$ can be seen as vertically concatenating $\tilde{\mathbf{B}}_0^{-1}\tilde{\mathbf{b}}_0$, $\mathbf{B}_{1,k}^{-1}\mathbf{b}_{1,k}$, $\mathbf{B}_{2,l,k}^{-1}\mathbf{b}_{2,l,k}$, $\mathbf{B}_{3,k}^{-1}\mathbf{b}_{3,k}$, $\mathbf{B}_{4,k}^{-1}\mathbf{b}_{4,k}$, and for all k and l. By using the expression of each block of $\tilde{\mathbf{b}}$ and $\tilde{\mathbf{B}}^{-1}$, they can be easily computed as:

$$\tilde{\mathbf{B}}_0^{-1}\tilde{\mathbf{b}}_0 = \begin{bmatrix} 0 \\ -2 \\ \mathbf{0} \end{bmatrix}, \qquad \mathbf{B}_{1,k}^{-1}\mathbf{b}_{1,k} = \begin{bmatrix} 1-\tilde{c}_J(f_k) \\ -1-\tilde{c}_J(f_k) \\ \mathbf{0} \end{bmatrix}, \qquad \mathbf{B}_{2,l,k}^{-1}\mathbf{b}_{2,l,k} = \begin{bmatrix} C_{i,j}(f_k) \\ 0 \\ 0 \end{bmatrix},$$

and the i-th element of the sparse vector $\mathbf{B}_{3,k}^{-1}\mathbf{b}_{3,k}$ is $2(1-\epsilon_s)$ if i or $(i-2N_s^2-N_s) \in \mathbb{S}_{b_3}$; the i-th element of the sparse vector $\mathbf{B}_{4,k}^{-1}\mathbf{b}_{4,k}$ is $1/B(f_k)$ if i, $(i-4N_s^2-N_s)$, $(i-8N_s^2-2N_s)$, or $(i-12N_s^2-3N_s) \in \mathbb{S}_{b_4}$.

Thus, calculating $\tilde{\mathbf{B}}^{-1}\tilde{\mathbf{A}}$ and $\tilde{\mathbf{B}}^{-1}\tilde{\mathbf{b}}$ is merely a rearrange of elements sequence in the matrix and does not require extra computational effort in practice.

VITA

Yongjie Zhuang was born in Fujian Province, China. He graduated from Shanghai Jiao Tong University in 2018 with a BSc in Mechanical Engineering. He was admitted to the School of Mechanical Engineering, Purdue University as an exchange student in August 2017, and was later enrolled as a graduate student in August 2018. During his graduate study, he was advised by Dr. Yangfan Liu and worked on active sound control.

List of awards:

- Ward A. Lambert Graduate Teaching Fellowship, Purdue University (Jan. 2022)
- Hallberg Foundation Award, NOISE-CON 2022 Conference (Jun. 2022)
- Classic Papers in Noise Control Presentation Award, NOISE-CON 2020 Conference (Nov. 2020)
- Student Paper Award, NOISE-CON 2019 Conference (Aug. 2019)
- Michiko So Finegold Award, NOISE-CON 2019 Conference (Aug. 2019)
- Bottomley Research Scholarship, Purdue University (Dec. 2017)
- China National Scholarship (Nov. 2017)

PUBLICATIONS

Peer-Reviewed Journal Publications

1. **Zhuang, Yongjie**, and Yangfan Liu. "A numerically stable constrained optimal filter design method for multichannel active noise control using dual conic formulation." *The Journal of the Acoustical Society of America* 152.4 (2022): 2169-2182. [DOI: 10.1121/10.0014627]

2. **Zhuang, Yongjie**, and Yangfan Liu. "Constrained optimal filter design for multichannel active noise control via convex optimization." *The Journal of the Acoustical Society of America* 150.4 (2021): 2888-2899. [DOI: 10.1121/10.0006738]

3. **Zhuang, Yongjie**, Xuchen Wang, and Yangfan Liu. "Singular vector filtering method for mitigation of disturbance enhancement in multichannel active noise control systems." *Noise Control Engineering Journal* 69.5 (2021): 451-459. [DOI: 10.3397/1/376941]

Conference Papers or Oral Presentations

1. **Zhuang, Yongjie**, and Yangfan Liu. "An adaptive constrained multi-channel active noise control filter design approach using convex cone optimization." Proceedings of Noise-Con 2023, Grand Rapids, Michigan, USA, May 2023, *INTER-NOISE and NOISE-CON Congress and Conference Proceedings*. Vol. 266. No. 2. Institute of Noise Control Engineering, 2023. [Full text, DOI: 10.3397/NC_2023_0074]

2. Kim, Juhyung, **Yongjie Zhuang**, and Yangfan Liu. "A constrained multi-channel hear-through filter design approach using active control formulations." Proceedings of Noise-Con 2023, Grand Rapids, Michigan, USA, May 2023, *INTER-NOISE and NOISE-CON Congress and Conference Proceedings*. Vol. 266. No. 2. Institute of Noise Control Engineering, 2023. [Full text, DOI: 10.3397/NC_2023_0073]

3. **Zhuang, Yongjie**, and Yangfan Liu. "A constrained adaptive active noise control filter design method via online convex optimization." 183rd Meeting of the Acoustical Society of America, Nashville, Tennessee, USA, December 2022, *The Journal of the Acoustical Society of America* 152.4 (2022): A98-A98. [Abstract only, DOI: 10.1121/10.0015669]

4. Kim, Juhyung, **Yongjie Zhuang**, and Yangfan Liu. "A multi-channel hear-through filter design approach and its applications." 183rd Meeting of the Acoustical Society of America, Nashville, Tennessee, USA, December 2022, *The Journal of the Acoustical Society of America* 152.4 (2022): A99-A99. [Abstract only, DOI: 10.1121/10.0015674]

5. Wang, Yiming, **Yongjie Zhuang**, and Yangfan Liu. " Design of causal preconditioning filters for adaptive filtering algorithms in real-time multi-channel active noise control applications." Proceedings of Inter-Noise 2022, Glasgow, Scotland, UK, August 2022, *INTER-NOISE and NOISE-CON Congress and Conference Proceedings*. Vol. 265. No. 5. Institute of Noise Control Engineering, 2022. [Full text, DOI: 10.3397/10.3397/IN_2022_0293]

6. **Zhuang, Yongjie**, Zhuang Mo, and Yangfan Liu. "Warmstarting the constrained optimal filter design problem for active noise control systems in conic formulation." Proceedings of Noise-Con 2022, Lexington, Kentucky, USA, June 2022, *INTER-NOISE and NOISE-CON Congress and Conference Proceedings*. Vol. 264. No. 1. Institute of Noise Control Engineering, 2022. [Full text, DOI: 10.3397/NC-2022-727]

7. **Zhuang, Yongjie**, and Yangfan Liu. "A constrained optimal hear-through filter design approach for earphones." Proceedings of Inter-Noise 2021, Washington DC, USA, August 2021, *INTER-NOISE and NOISE-CON Congress and Conference Proceedings*. Vol. 263. No. 5. Institute of Noise Control Engineering, 2021. [Full text, DOI: 10.3397/IN-2021-1816]

8. **Zhuang, Yongjie**, and Yangfan Liu. "Delayless polyphase implementation of filters in active noise control systems." 181st Meeting of the Acoustical Society of America, Seattle, Washington, USA, November 2021, *The Journal of the Acoustical Society of America* 150.4 (2021): A154-A154. [Abstract only, DOI: 10.1121/10.0007964]

9. **Zhuang, Yongjie**, Yangfan Liu, and Xuchen Wang. "Singular Vector Filtering Method for Disturbance Enhancement Mitigation in Active Noise Control Systems." Proceedings of Noise-Con 2020, virtual event, November 2020, *INTER-NOISE and NOISE-*

CON Congress and Conference Proceedings. Vol. 262. No. 1. Institute of Noise Control Engineering, 2020. [Full text]

10. **Zhuang, Yongjie**, and Yangfan Liu. "Development and application of dual form conic formulation of multichannel active noise control filter design problem in frequency domain." Proceedings of Inter-Noise 2020, virtual event, August 2020, *INTER-NOISE and NOISE-CON Congress and Conference Proceedings*. Vol. 261. No. 6. Institute of Noise Control Engineering, 2020. [Full text]

11. **Zhuang, Yongjie**, and Yangfan Liu. "A sub-band filter design approach for sound field reproduction." 179th Meeting of the Acoustical Society of America, virtual event, December 2020, *The Journal of the Acoustical Society of America* 148.4 (2020): 2793-2793. [Abstract only, DOI: 10.1121/1.5147775]

12. **Zhuang, Yongjie**, and Yangfan Liu. "Study on the cone programming reformulation of active noise control filter design in the frequency domain." Proceedings of Noise-Con 2019, San Diego, California, USA, August 2019, *INTER-NOISE and NOISE-CON Congress and Conference Proceedings*. Vol. 260. No. 1. Institute of Noise Control Engineering, 2019. [Full text]